

“Thermoelectric Characterization Of Functionalized Poly(3,4-ethylenedioxythiophene) And Its Nanocomposites For Device Applications”

Thesis submitted to
Jadavpur University



By

Shilpa Maity

In partial fulfilment of the requirements
for the degree of
Doctor of Philosophy (Ph.D)
In Science


Department of Physics
Jadavpur University
Kolkata-700032

August 2023




CERTIFICATE FROM THE SUPERVISOR(S)

This is to certify that the thesis entitled “**Thermoelectric Characterization Of Functionalized Poly(3,4-ethylenedioxythiophene) And Its Nanocomposites For Device Applications**” Submitted by Smt. **Shilpa Maity** who got her name registered on 18/03/2021 (Index no.: 17/21/Phys./27) for the award of Ph. D. (Science) Degree of Jadavpur University, is absolutely based upon her own work under the supervision of **Prof. Sukhen Das** and **Dr. Krishanu Chatterjee** and that neither this thesis nor any part of it has been submitted for either any degree / diploma or any other academic award anywhere before.


Prof. Sukhen Das
Professor
Department of Physics
Jadavpur University
Kolkata – 700032



Prof. Sukhen Das
Department of Physics,
Jadavpur University
Kolkata - 700 032

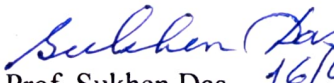

Dr. Krishanu Chatterjee
Associate Professor
Department of Physics
Techno India University, West Bengal
Kolkata- 700091

Dr. Krishanu Chatterjee
Associate Professor
Department of Physics,
Techno India University, West Bengal
Kolkata - 700091




CERTIFICATE OF SIMILARITY CHECK

This is to certify that the plagiarism checking for this thesis authored by Smt. Shilpa Maity has been performed using professional plagiarism prevention software *iThenticate*. According to the report generated after plagiarism checking there is 11% similarity in this thesis, which is in the category “Level 0” (minor similarities) as per the “Promotion of Academic Integrity and Prevention of Plagiarism in Higher Education Institutions Regulations, 2018” of the University Grand Commission (UGC) of India. The common knowledge or coincidental terms upto 10 (ten) consecutive words (as prescribed in the above said UGC Regulation upto 14 (fourteen) terms for such common knowledge or coincidental terms can be excluded) and own works of the candidate published in various peer-reviewed journals (those are attached in the thesis) are excluded from the similarity checking. It is certified that the present thesis submitted by Smt. Shilpa Maity is plagiarism free and has been followed standard norms of academic integrity and scientific ethics.


Prof. Sukhen Das 16/08/2023
Department of Physics,
Jadavpur University,
Kolkata- 700032, India,



Prof. Sukhen Das
Department of Physics,
Jadavpur University
Kolkata - 700 032


Dr. Krishanu Chatterjee 16/08/2023
Department of Physics,
Techno India University, West Bengal,
Kolkata- 700091, India

Dr. Krishanu Chatterjee
Associate Professor
Department of Physics,
Techno India University, West Bengal
Kolkata-700091

DECLARATION

I, hereby, declare that the work embodied in the present thesis has been carried out by me under the supervision of Prof. Sukhen Das, department of physics, Jadavpur University, and Dr. Krishanu Chatterjee, department of physics, Techno India University, India. Neither this thesis nor any part thereof has been submitted for any degree whatsoever.

Shilpa Maity
16/08/2023

Smt. Shilpa Maity

Department of Physics,

Jadavpur University

Kolkata- 700032, India

Dedicated.....

To my family

ACKNOWLEDGEMENTS

“No one achieves success does so without acknowledging the help of others. The wise and confident acknowledge this help with gratitude.”

..... Alfred North Whitehead

My initial steps into the world of research were made in 2017 at Jadavpur University. Currently, my thesis is virtually complete. The fulfilment of my wish is imminent. I have had a lot of ups and downs along with some successes and learning opportunities along my trip. Thinking back to those times makes me emotional right now. I am grateful to God for allowing me to go on this wonderful adventure. I would want to thank everyone who has supported me during my study; without you, it would not have been possible.

*To begin with, I would like to express my profound gratitude to **Prof. Sukhen Das**, my supervisor, for giving me the opportunity to do research and realize my dream. He is really kind to me, and his continual backing has allowed me to work well for all these years.*

*I would like to extend my heartfelt gratitude to **Dr. Krishanu Chatterjee**, an associate professor in the physics department at Techno India University, my co- supervisor, for allowing me to work on this problem and his invaluable advice. I want to thank him especially for allowing me the flexibility to investigate the things that most interested me.*

***Prof. Das** and **Dr. Chatterjee's** consistent enthusiasm and leadership during my employment not only provided a seemingly limitless source of inspirations each morning but also kept me moving forward at the most difficult times. They always functioned as a philosopher and a friend in addition to providing scientific guidance. I appreciate them for allowing me the chance to contribute to leading edge research*

freely and independently as well as for introducing me to previously unknown to me prospective uses of different characterisation. They spent a great deal of effort and their valuable time in educating me on all the pertinent subjects and real-world problems. Additionally, I am appreciative of their scientific advice and subject-specific counsel.

*I would like to convey my sincere thanks to **Professor Papiya Nandy** and **Dr. Ruma Basu** for their insightful counsel and ongoing assistance. They have provided me with a wealth of knowledge and served as an inspiration for all my study.*

*I would like to convey my sincere thanks to **Prof. Dipali Banerjee** of IEST Shibpur, Howrah for warmly giving me permission to work there and utilize its facilities.*

*I would especially want to thank **Dr. Sudip Kumar Ghosh** from the Chemistry Department of Techno India University for his scientific guidance.*

I would like to express my gratitude to my immediate lab colleagues Dr. Shubham Roy, Dr. Dheeraj Mondal and Dr. Souravi Bardhan, as well as Miss Debbethi Bera, who supported me throughout my first few weeks there.

For their supportive attitude during my dissertation study, I truly appreciate my junior colleagues Mr. Debmalaya Sarkar, Miss Namrata Das, Mr. Tanmoy Chakraborty, Miss. Jhilik Roy and Mr. Dhananjay Mondal.

I would also like to express my gratitude to my lab's senior researchers, Dr. Nur Amin Hoque, Mr. Minarul Saikh, Dr. Biplab Paul, Dr. Arpan Kool, Dr. Samtirtha Banerjee, Dr. Farha Khatun, Dr. Tanumoy Debnath, Mr. Soumen Biswas, Miss Bidisha Ghosh, Dr. Santanu Das, Dr. Nayim Sepay and Dr. Dipak Chanda for their suggestions and guidance.

A group of enthusiastic lab juniors is another thing I count as a blessing namely, Miss. Saheli Ghosh, Miss. Jhilik Roy, Mr. Subhojit Dutta, Miss. Aliva Saha, Miss. Suman

Saha, Miss. Neelanjana Bag, Mr. Indrajit Mondal, Miss. Piyali Halder, Mrs. Sanghita Dey, Miss. Manisha Kundu, Miss. Anwesha Mukherjee, Miss. Anuja Chatterjee, Mr. Kishan Gupta, Mr. Souvik Sau, Mr. Anandalal Gayen, Miss. Jaba Roy Chowdhury and all other newcomers, who are responsible for creating a welcoming environment in the lab space.

My junior friends Miss Subhra Rakshit and Mr. Rhitaparna Pal have supported me in pursuing this goal throughout my research career.

I would especially want to thank Mr. Aniket Mondal from Techno India University, Kolkata for his assistance in helping me finish my dissertation work.

*Now it is my chance to express gratitude to everyone who worked behind the scenes to finish my thesis. First and foremost, I want to express my gratitude to my parents, **Mr. Susanta Kumar Maity (Baba)**, **Mrs. Sukla Panda Maity (Ma)**, **Mr. Swarnadeep Maity (Brother)**, **Mrs. Aradhita Deb (Sister-in-law)** who encouraged me to finish my thesis work. Also, I want to express my sincere thanks to my in-laws, Mr. Murari Mohan Bera (father-in-law), **Mrs. Sampa Rani Bera (Mother-in-law)**, and **Mr. Supriya Kumar Bera (Bhai)**, for taking on all the responsibility for all family issues and encouraging me to finish my thesis work. Without their tremendous affection and support, and, I could not have completed this dissertation. I dedicate this dissertation to my family since I will always be grateful to them. I would also want to thank my husband **Mr. Sourav Kumar Bera** for all his support, encouragement, and unwavering love during the writing of this thesis. My son **Adhiraj Bera (Betu)**'s innocent assistance in helping me accomplish my thesis work inspired me to dedicate this dissertation to him.*

Finally, I would like to express my gratitude for the financial assistance received for Project No. DST/WOS-A/PM-73/2019, which is sponsored by DST. The completion of this thesis work would not have been feasible at all without these substantial supports.

Shilpa Maity

ABSTRACT

“Thermoelectric Characterization Of Functionalized Poly(3,4-ethylenedioxythiophene) And Its Nanocomposites For Device Applications”

Submitted by
Shilpa Maity

Index no.: 17/21/Phys./27

The breakthrough invention of conducting polymers (CPs) initiates a new pathway for the researchers to make use of their properties in thermoelectric (TE) applications. They are potential candidates in TE application when combined with inorganic counterparts. Therefore, investigation on the properties and synthesis of hybrid TE materials of conducting polymer and different nanofillers is very important. The present work mainly focused on the synthesis of conducting polymer Poly(3,4ethylenedioxythiophene) (PEDOT) and its hybrid composite along with the study of its structural and electrical properties for TE applications.

In-situ polymerization technique has been employed for the synthesis of PEDOT from its monomer (EDOT) for TE property analysis. The reaction condition and variation of nanofillers in the polymer have been investigated. It is observed that different nanofillers influence the morphology of the material which in turn stimulates the TE properties of the material. Further, the effects of different oxidizing agents on the TE performance of the materials are also noteworthy.

It has been observed that in hybrid composite of tosylate doped PEDOT and SWCNT, with the variation of SWCNT content, there is an increase in the ordered structure, resulting an enhanced electrical conductivity. This is attributed to the increases in the carrier concentration by pushing the Fermi level (E_F) into the conduction band. Though

the thermoelectric power decreases, yet there is an overall increase in power factor that leads to an increment of ZT.

On the other hand, in tosylate doped PEDOT/Graphene hybrid composite a simultaneous hike in room temperature electrical conductivity and thermoelectric power is noted with the increasing graphene content. The increase is due to the increase in the degree of ordered structure enhancing the hopping rate (including hopping distance and activation energy) within the polymer matrix in addition to the increase in the charge carrier mobility. At the same time low thermal conductivity due to the large phonon scattering by the introduction of nanointerfaces increases the figure of merit ZT.

In this study, selenium (Se) was used to functionalize the polymer PEDOT, and its structural and electrical transport characteristics were examined. The addition of Se to the PEDOT matrix was shown to improve the thermoelectric characteristics. We suggest creating connected chains of PEDOT containing Se, which improve the figure of merit by boosting electrical transport but impeding heat transport.

Hence this work reports PEDOT polymer and its hybrid composites are so distinctive that they well thought out to be extremely capable and hopeful TE candidates. Further ease of synthesis and mechanical flexibility of those materials permits various design to be used in device applications. The inimitability of these materials undoubtedly opens a new era of smart materials with the initiation of opportunities in TE domain.

LIST OF PUBLICATIONS

1. **Shilpa Maity**, Subhra Rakshit, Sukhen Das, Krishanu Chatterjee*, *Enhanced thermoelectric performance of template based nanostructured polyaniline*, AIP Conference Proceedings 1832, 110053 (2017)
2. **Shilpa Maity**, Nayim Sepay, Chiranjit Kulsi, Arpan Kool, Sukhen Das, Dipali Banerjee, Krishanu Chatterjee*, *Enhancement of Thermoelectric Performance in Oligomeric PEDOT-SWCNT Nanocomposite via Band Gap Tuning*, Chemistry Select, 3, 2018, 8992-8997
3. **Shilpa Maity**, Chiranjit Kulsi, Shiladitya Banerjee, Sukhen Das, Krishanu Chatterjee*, *Dependence of thermoelectric power and electrical conductivity on structural order of PEDOT-Tos-graphene nanocomposite via charge carrier mobility*, Material Research Express 6, 2019, 105095.
4. **Shilpa Maity**, Salini Datta, Megha Mishra, Shiladitya Banerjee, Sukhen Das, Krishanu Chatterjee*, *Poly(3,4 ethylenedioxythiophene)-tosylate—Its synthesis, properties and various applications*, Polymer for Advanced Technologies. 2020, 1–19.
5. **Shilpa Maity**, Umme Karnij Salma Parvin, Sukhen Das, Krishanu Chatterjee*, *Polymer chalcogenides—new smart materials for thermoelectric applications*, Smart Mater. Struct. 31 (2022) 073001 (20pp).

Co- author Publications

1. Shubham Roy, Kunal Pal, Souravi Bardhan, **Shilpa Maity**, Dipak Kr. Chanda, Saheli Ghosh, Parimal Karmakar, and Sukhen Das*, *Gd(III)-Doped Boehmite Nanoparticle: An Emergent Material for the Fluorescent Sensing of Cr(VI) in Wastewater and Live Cells*, Inorganic Chemistry, 58, 2019, 13, 8369-8378.
2. Sajal Biswas, **Shilpa Maity** and Krishanu Chatterjee*, *Semiconductor to metallic transition of Bismuth Telluride with incorporation of Graphene- Its enhanced thermoelectric properties*, *International Conference on Computer, Electrical & Communication Engineering (ICCECE)*, 2019, pp. 1-4, doi: 10.1109/ICCECE44727.2019.9001902.

LIST OF SEMINARS ATTENDED

1. **103rd Indian Science Congress**, University of Mysore, Mysore, January 3-7, 2016
2. **7th Vidyasagar - Satyendra Nath Bose National Workshop 2016 on Theory and Application of Advanced Materials (TAAM 2016)**, Vidyasagar University, March 15-17, 2016.
3. **Recent Trend in Composite Material 2016**, Jadavpur University, Kolkata, 18th August, 2016.
4. **Frontiers in Modern Physics**, Jogamaya Devi College, Kolkata, November 21-22, 2016.
5. **61st DAE Solid State Physics Symposium**, KIIT University, Bhubaneswar, December 26-30, 2016.
6. **International Conference on Emerging Trends in Chemical Sciences**, Department of Chemistry, Dibrugarh University, February 26 – 28, 2018

LIST OF AWARD /ACHIEVEMENTS

1. 1st position in the eastern zone research convention, **ANVESHAN- 2018**, organized by the Association of Indian Universities (AIU) held on 18-19 Feb 2019, Central University of Jharkhand, Ranchi.
2. 2nd position in National research convention, **ANVESHAN- 2018**, organized by the Association of Indian Universities (AIU) held on 12-14 March 2019, Ganpat University, Gujarat.

LIST OF FIGURES

Chapter 1

Figure 1.1. Schematic diagram of a thermoelectric device..... 2

Chapter 2

Figure 2.1. Schematics depicting the discover of PEDOT..... 12

Figure 2.2. (A) Grazing incidence wide angle X-ray scattering of PEDOT-Tos. (B) After the immersion dedoping procedure with methanol from initial washing to 5 hours of immersion and with Dimethylformamide (DMF) for 1 hour, S(2p) XPS spectra of PEDOT: Tos films were obtained. (C) The PEDOT:Tos molecular structure is depicted with Tos in green and PEDOT in blue..... 13

Figure 2.3. Schematics diagram of various polymerization methods of forming PEDOT-Tos films: (A) The chemical polymerization process. (B) The vapor phase polymerization process. (C) The electrochemical polymerization processes..... 14

Figure 2.4. Photographic images and electricity generation by the touch of fingertips of the flexible PP-PEDOT thermoelectric film. (A) Bending, (B) twisting, and (C) cutting with scissors images of PP-PEDOT films. (D) Electricity generation by fingertip touch at one side with air..... 21

Figure 2.5. (a) Synthesis of PEDOT:PSS passivated Te nanorods, followed by formation of smooth nanocomposite films during solution casting and TEM image showing the crystalline Te nanorod passivated with PEDOT:PSS (b) Schematic illustration of the flexible PEDOT:PSS/ce-MoS₂ thin-films (c) Schematic illustration of

<i>PEDOT:PSS and SWCNTs (d) Sketch of the spin-coating Setup and the diagram of the PEDOT:PSS/ce-MoS₂ heterostructure TE films</i>	<i>23</i>
---	-----------

Figure 2.6. <i>Flow chart of the executed research work.....</i>	<i>25</i>
---	-----------

Chapter 3

Figure 3.1. <i>Schematic diagram of the synthesis process of PEDOT:Tos</i>	<i>29</i>
---	-----------

Figure 3.2. <i>Schematic diagram of the synthesis process of Se-PEDOT composite</i>	<i>31</i>
--	-----------

Figure 3.3. <i>(A) X-ray diffractometer (BRUKER D8 Advance) (B) Principle of X-ray diffraction</i>	<i>33</i>
---	-----------

Figure 3.4. <i>FTIR spectrometer (Shimadzu FTIR-8400S) at Jadavpur university</i>	<i>35</i>
--	-----------

Figure 3.5. <i>Ultraviolet–visible spectroscopy set up (Uv-1800, Shimadzu, Japan)</i>	<i>36</i>
--	-----------

Figure 3.6. <i>Theory of Raman Spectra.....</i>	<i>37</i>
--	-----------

Figure 3.7. <i>Raman Spectroscopy set up (Model no. LabRAM HR).....</i>	<i>38</i>
--	-----------

Figure 3.8. <i>(A) Schematic diagram of a field emission scanning electron microscope (FESEM) (B) FESEM Set up (FEI, INSPECT F50) at Jadavpur University.....</i>	<i>40</i>
--	-----------

Figure 3.9. <i>Thermoelectric measurement setup.....</i>	<i>42</i>
---	-----------

Chapter 4

Figure 4.1. Variation of a) Electrical Conductivity and Thermoelectric Power. b) Carrier concentration and mobility with SWCNT weight fraction..... 50

Figure 4.2. Variation of a) Thermal conductivity and Power factor b) Figure of merit with SWCNT weight fraction..... 51

Figure 4.3. Variation of a) Thermoelectric power and Power factor with electrical conductivity b) Electrical conductivity with number of days..... 53

Figure 4.4. Spectral analysis of the synthesized samples a) XRD b) Uv-vis spectra 54

Figure 4.5. FESEM images a-e) Sample I-V, scale bar 1mm f) Magnified portion of sample V, scale bar 500 nm..... 56

Figure 4.6. a) Probable stereochemistry of the oligomeric bulk material and their HOMO and LUMO b) Energy profile diagram of the PEDOT before and after SWCNT doping..... 58

Chapter 5

Figure 5.1. XRD spectra of the synthesized samples..... 66

Figure 5.2. UV-vis spectra of the synthesized samples..... 67

Figure 5.3. FTIR spectra of the synthesized samples..... 68

Figure 5.4. Raman spectra of all the synthesized samples..... 69

Figure 5.5. FESEM images of (a) graphene and the synthesized samples (b-f) Sample S-I to S-V. Scale bar 1 μ m..... 70

Figure 5.6. (a) Variation of electrical conductivity with percentage graphene weight and (b) temperature dependence of electrical conductivity of all samples..... 72

Figure 5.7. Variation of (a) thermoelectric power and (b) power factor with percentage graphene weight..... 75

Figure 5.8. Variation of thermal conductivity and figure of merit with percentage graphene weight..... 77

Figure 5.9. Schematic representation of polymerization of EDOT and mechanism of formation of nanocomposites 79

Chapter 6

Figure 6.1. XRD analysis of (a) PEDOT (b) various percentage of Se-PEDOT composites 86

Figure 6.2. Raman spectra analysis of PEDOT and all the Se-PEDOT composites 87

Figure 6.3. FESEM images of (A) PEDOT (B) 6% Se-PEDOT composite (C) 20% Se-PEDOT composite (D) 33% Se-PEDOT composite (E) 66% Se-PEDOT composite and (F) 82% Se-PEDOT composite with 10 μ m scale bar..... 88

Figure 6.4. Variation of electrical conductivity and thermoelectric power with Se content..... 89

Figure 6.5. <i>Variation of power factor and thermal conductivity with Se content</i>	
.....	92

Figure 6.6. <i>Variation of figure of merit with Se content</i>	94
--	----

LIST OF TABLES

Table 5.1. Room temperature values of the characteristic Mott temperature (T_0), hopping distance (R_{hop}), activation energy (E_{hop}), carrier concentration (n) and carrier mobility (μ) of the synthesized samples 73

Table 6.1. Carrier concentration and mobility of all the samples 91

CONTENTS

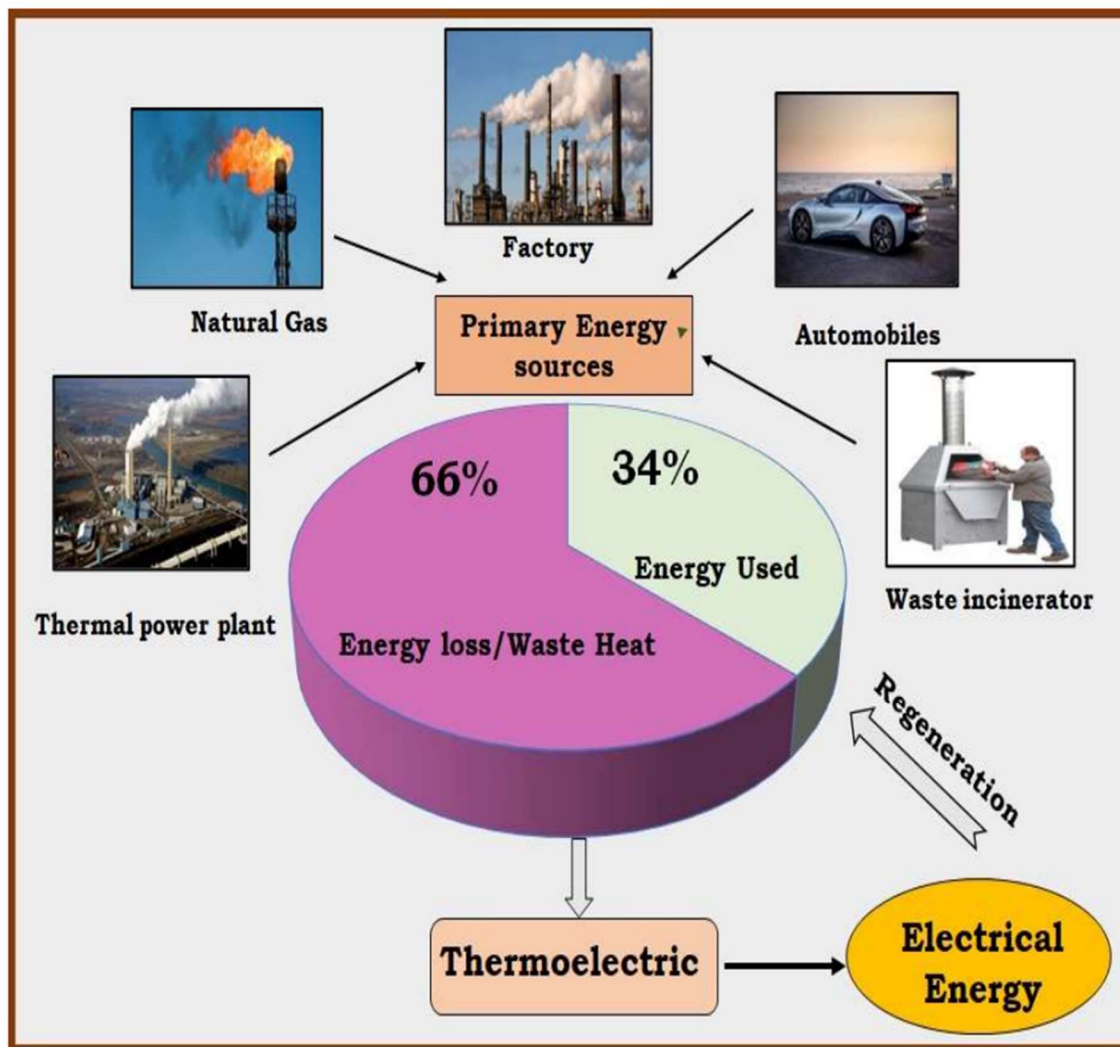
Acknowledgements.....	i
Abstract.....	iv
List of Publications.....	vi
List of Seminar attended.....	viii
List of awards/Achievements.....	ix
List of Figures.....	x
List of Tables.....	xiv
 Chapter 1. Introduction.....	 1
1.1. Overview of Thermoelectricity.....	2
1.1.1. Advantages of Thermoelectric devices.....	3
1.1.2. Application of Thermoelectric.....	3
1.1.3. Basic Thermoelectric parameters.....	4
1.2. Origin of Polymer Thermoelectric.....	6
1.2.1. Concept of Conducting Polymer.....	6
1.3. Composite Thermoelectric.....	8
 Chapter 2. Literature Review.....	 10
2.1. PEDOT as a TE Material.....	11
2.2. Structure and Properties of PEDOT.....	11
2.3. Different Synthesis Methods.....	14
2.3.1. Chemical Polymerization.....	15
2.3.2. Vapor Phase Polymerization.....	17
2.3.3. Electrochemical Polymerization.....	18
2.4. PEDOT for TE application.....	19
2.5. PEDOT Based Composite Materials for TE application.....	22

2.6. Objective of the work.....	25
Chapter 3. Materials and Characterizations.....	26
3.1. Materials.....	28
3.2. Synthesis of PEDOT-Tos.....	28
3.2.1. Synthesis of PEDOT-Tos/ SWCNT Composite.....	30
3.2.2. Synthesis of PEDOT-Tos/Graphene Composite.....	30
3.3. Synthesis of Se-PEDOT.....	31
3.4. Characterization.....	32
3.4.1. X-Ray Diffraction (XRD).....	32
3.4.2. Fourier transform infra-red (FTIR) spectroscopy.....	34
3.4.2. Ultraviolet–visible spectroscopy (UV-vis).....	36
3.4.4. Raman Spectroscopy.....	37
3.4.5. Field Emission Scanning Electron Microscope (FESEM).....	39
3.4.6. Electrical Characterization.....	41
3.4.6.1. Electrical conductivity.....	41
3.4.6.2. Thermoelectric power.....	42
3.4.6.3. Thermal conductivity.....	43
3.5. Accuracy Measurement.....	43
Chapter 4. PEDOT Based CNT Composite System.....	43
4.1. Introduction.....	45
4.2. Enhancement of Thermoelectric Performance in Oligomeric PEDOT-SWCNT Nanocomposite via Band Gap Tuning.....	47
4.2.1. Experimental.....	47
4.2.1.1. Materials Used.....	47
4.2.1.2. Synthesis of PEDOT-Tos.....	47
4.2.1.3 Synthesis of PEDOT-Tos-SWCNT nanocomposite.....	48

4.3. Characterization.....	48
4.4. Results and Discussion.....	49
4.4.1. Electrical Characterization.....	49
4.4.1.1. Electrical Conductivity.....	49
4.4.1.2. Thermoelectric Power.....	50
4.4.1.3. Power Factor.....	51
4.4.1.4. Thermal Conductivity and Figure of merit.....	52
4.4.1.5. Relation between all electrical parameters.....	53
4.4.2. Structural Characterization.....	54
4.4.2.1. X-ray Diffraction (XRD) Analysis.....	54
4.4.2.2. Uv-vis spectroscopy.....	55
4.4.2.3. Field emission scanning electron microscopy (FESEM).....	56
4.4.2.4. Theoretical analysis via DFT.....	57
4.5. Conclusions.....	58
Chapter 5. PEDOT Based Graphene Composite System.....	60
5.1. Introduction.....	61
5.2. Dependence of thermoelectric power and electrical conductivity on structural order of PEDOT-Tos-graphene nanocomposite via charge carrier mobility.....	63
5.2.1. Experimental.....	63
5.2.1.1. Material used.....	63
5.2.1.2. Synthesis of PEDOT-Tos by in situ polymerization.....	63
5.2.1.3. Preparation of PEDOT-Tos/Graphene nanocomposites.....	64
5.3. Characterization.....	64
5.4. Results and discussions.....	65
5.4.1 Spectral Studies.....	65
5.4.2. Structural Characterization.....	70

5.4.3 Electrical characterization.....	71
5.4.4. Thermal Conductivity and figure of merit.....	76
5.5. Proposed mechanism of formation of nanocomposites.....	78
5.6. Conclusion.....	80
Chapter 6. PEDOT Functionalized with Se composite System.....	81
6.1. Introduction.....	82
6.2. PEDOT Functionalized with Se-Optimization of TE application.....	84
6.2.1. Experimental.....	84
6.2.1.1 Material used.....	84
6.2.1.2. Preparation of hybrid composite.....	84
6.2.1.2.1. Synthesis of Poly(3,4-Ethylenedioxythiophene....	84
6.2.1.2.2. Synthesis of hybrid composite of Se-PEDOT.....	85
6.3. Characterization.....	85
6.4. Result and discussion.....	86
6.4.1. Structural Characterization.....	86
6.4.2. Electrical Characterization.....	89
6.5. Conclusion.....	95
Chapter 7. General Conclusion and Future Scope.....	96
7.1. General Conclusion.....	97
7.2. Future Scope.....	98
Chapter 8. References.....	100
8.1 Reference.....	101
Publications Reprint.....	110
Seminar Attended.....	172
Awards or Achievements.....	178

CHAPTER 1: INTRODUCTION



Introduction

1.1. Thermoelectricity: An overview

The combustion of fossil fuels is the primary source of power, which has become more and more essential as civilization has advanced. As a result, the generation of carbon dioxide (CO_2) gas is increasing daily, which has a negative impact on global warming. To solve such issues, research into alternate technologies is necessary. Thermoelectricity is an energy conversion technique that converts thermal energy into electrical energy by using waste heat. [1-3] The approach can be scaled to meet the current energy demand since it is very dependable, has no moving components, and is green. Numerous low- and high-grade waste heat sources, including industries, hot water vapour, biomass waste processing heat, automobile engines, solar radiation (photo-thermoelectric module), household appliances, human body heat, etc., are being used in thermoelectricity.

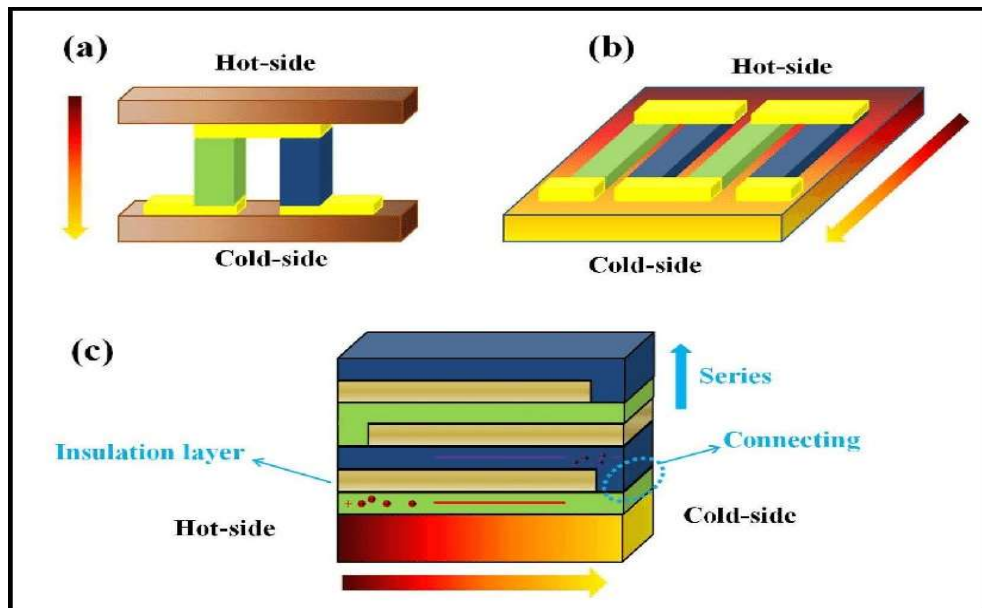


Figure 1.1. Schematic diagram of a thermoelectric device [4]

The operating temperature of a material based on the Seebeck effect can be obtained via thermoelectric devices. Figure 1.1 shows how an ordinary thermoelectric device is made up of an n-number p type and n type thermopiles which are connected electrically in series and thermally coupled in parallel.

1.1.1. Advantages of Thermoelectric device

- Low-maintenance: No moving components and operating fluid
- Prolonged lifespan
- Applicable in deep-sea and zero-gravity environments
- Operation without vibration or noise is preferred in mechanically delicate situations.
- Economic-friendly
- Could flip between heating and refrigeration modes in a dual action mode.
- Low production cost
- Reducing global warming by collecting garbage from commercial and industrial sites as well as from residential regions.

1.1.2. Applications of Thermoelectric

- Electricity generation from waste heat, Thermoelectric coolers- refrigeration, air-conditioning
- Automotive thermoelectric generators-increase fuel efficiency, regenerative braking
- Space applications-radioisotopes thermoelectric generator
- Temperature sensing
- Power plant

- Radio communication

1.1.3. Basic thermoelectric parameters

The dimensionless figure of merit (ZT) expresses the performance of a thermoelectric (TE) material

$$ZT = \frac{\sigma S^2 T}{\kappa} \quad (1.1)$$

where the material's electrical conductivity, Seebeck coefficient, and thermal conductivity are represented by σ , S , and κ respectively, and T is the working temperature.

The maximum conversion efficiency is indicated by a higher ZT value.

The electrical conductivity is described as

$$\sigma = \frac{L}{RA} = \frac{IL}{VA} \quad (1.2)$$

Where L is the length of a sample TE material, R is the resistance, A is the constant cross-sectional area of the sample, I is the current through the sample and V is the applied voltage.

In the presence of a magnetic field, electric charge carriers experience a force in a conductor. An electric field acts in a perpendicular direction to both the current and the magnetic field, Where the magnetic field is applied perpendicular to the electric current in a conductor to produce a voltage. The appearance of this voltage is called the Hall effect. The hall effect can be used to identify the charge carriers. Taking only one type of charge carrier, the Hall voltage for a conductor is defined as

$$V_H = -\frac{IB}{net} \quad (1.3)$$

where e is the elementary charge, t is the plate thickness, B is the magnetic field, I is the electrical current across the plate length, and n is the charge carrier density. Finally, the Hall coefficient is defined as

$$R_H = \frac{E}{jB} = \frac{V_H t}{IB} = -\frac{1}{ne} \quad (1.4)$$

where E is the induced electric field and j is the current density. Once again, it is suitable to express the electrical conductivity as

$$\sigma = ne\mu \quad (1.5)$$

where μ is the carrier mobility and can be calculated from the data of σ and V_H .

The thermal conductivity is generally defined as

$$\kappa = -\frac{QL}{A\Delta T} \quad (1.6)$$

where Q is the rate of heat flow through the sample having a temperature difference ΔT between its two ends with constant cross-sectional area A and length L . The total thermal conductivity expressed as

$$\kappa = \kappa_e + \kappa_l \quad (1.7)$$

Where, κ_e is the electronic contribution of thermal conductivity and κ_l is the lattice component.

For the thermoelectric application, a measurement including both the S (Thermoelectric power) and the σ (electrical conductivity) has been presented as power factor P . It is defined as

$$P = S^2 \sigma \quad (1.8)$$

The parameters S and σ also depend on the carrier concentration (n). The maximum value of n corresponds to maximum power factor giving the highest value of ZT .

There is a common tradeoff between σ and S in a 3D crystalline material. Typically, a rise in S causes a fall in σ , which also reduces κ value. So, in such materials, it is problematic to tune these parameters separately for the enhancement of ZT . Therefore, to improve ZT value and overall, TE performance, various strategies are being adopted along with the establishment of different materials. [5-7]

1.2. Origin of Polymer Thermoelectric

Conducting polymers (CPs) are now considered as promising alternatives for thermoelectric (TE) energy harvesting devices [8]. Without electrical optimization, polymers maintain an inherently low, making this material class suitable for use in device applications. Additionally, compared to their inorganic counterparts, polymers are printable, flexible, and moldable, which has its benefits. But they are characterized by lower TE efficiency in comparison to inorganic TE materials, and thus do not meet the standard ZT value to be used commercially. Tuning the band gaps [9–12], altering the doping [13], and alloying [14,15] with other TE materials are some of the focused methods used to further enhance the TE performance of the CPs. The addition of nanofillers to the polymer matrix is another potential method for improving TE performance.

1.2.1. Concepts of Conducting Polymer (CP)

The π -conjugated structure of conducting polymers is what triggers their electrical and electronic characteristics. The molecular π -orbitals of the polymer backbone atoms are lengthened as a result of the delocalization of their π -orbital electrons along the polymer chain. The polymer's electrical characteristics are stimulated by the delocalization of electrons. Conjugated polymers can remove electrons (p-doping) or add electrons (n-

doping) by the oxidation or reduction processes, respectively. The oxidation levels of the semiconducting polymers are directly linked with the charge carrier concentration, which leads to different and new electronic structures. In the doping process, the electrical charges on the polymer's backbone are stabilized by the addition of the counterions with opposing charges. Due to the doping technique, the bond length around the charge is deformed, developing a charged quasi-state particle known as a polaron. In addition, bipolarons are also observed in some polymers due to the supplementary doping of such systems, which is more effective in energy release than polarons. The development of wider bipolaron bonds to reduce the material's optical band gap and the increase in the number of bipolarons in the material are both caused by the greater dopant concentration. [16-17]. The hopping process, where charge carriers may travel from interchain to intrachain levels of the material, is said to be the mechanism responsible for charge transport in conducting polymers [18,19]. These hopping locations are the prolonged π -systems designed between the chain units, which are naturally conducting. As a result, the doped polymer materials' degree of crystallinity and chain orientation were crucial in enhancing the material's electronic structure and electronic characteristics [19,20]. Long-chained polymers gain from intrachain hopping transport because it increases charge carrier mobility. The interchain transport method might happen naturally along the chain's principal axis, along the direction of the backbone plane, or along the direction of stacking. The density of states (DOS) in CPs determines the number of states that are accessible and used in relation to energy. For disordered polaronic polymers, the Fermi level (E_F) is in the center of the polaron band; for disordered bipolaronic polymers, it is located between the valence band (VB) and the bipolaron band. Additionally, these

polymers can be considered Fermi glasses. The placement of E_F within localized states suggests that charge carriers are localized, and the transport of these carriers between localized states requires temperature-activated hopping. So, the materials where the bipolaronic states are overlapping show a semi-metallic behavior. By enhancing the material's order structure, it is discovered that the behavior of polaronic networks changes from a Fermi glass to a metallic one [18, 20, 21]. The S of a material is comparable with the slope of the density of state (DOS) at the Fermi level, depicted by the Mott's equation given by

$$S \sim \left(\frac{\partial \ln \text{DOS}(E)}{\partial E} \right)_{E_F} \quad (1.9)$$

S is predicted to be low because the doped conducting polymer in the polaronic network has a slope of the DOS at the Fermi level of zero. However, a bipolaronic network exhibits a greater S value than a polaronic network because the DOS at E_F has a steeper slope. A material's density of state will also be significantly influenced by the degrees of order or crystallinity. The DOS can expand and soften close to the band edge with energy alignment, which lowers the DOS's slope at E_F and makes a low value of S observable in the material.

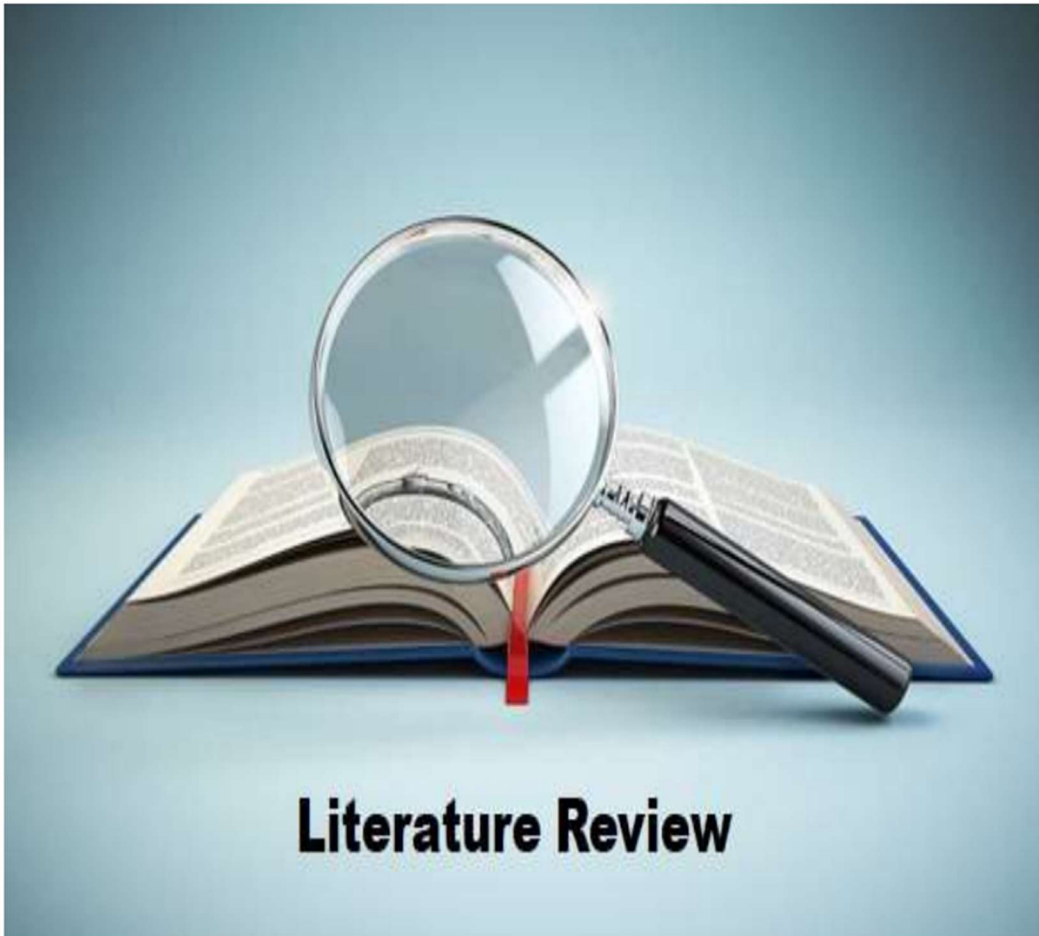
2.1. Composite Thermoelectric

At and near room temperature, the applications for thermoelectricity are very beneficial for energy harvesting [22-24]. The lower TE efficiency of a polymeric material in comparison to inorganic TE material is disadvantageous. However, hybridization with nanofillers like 1D, 2D, etc. materials can enhance their TE efficiency using various strategic material designs. [8, 18, 25]. Thus, one of the promising pathways to improve the TE performance of organic material is by hybridizing it with inorganic TE material.

Further by varying the size of the organic/ inorganic hybrid TE materials, a quantum confinement effect arises which can allow one to improvise the variation of σ and S independently and enhance the power factor ($S^2\sigma$). [26] Using appropriate particle size, preparation procedures, and compositions are other methods for improving the required TE characteristics of the hybrid composite TE material. Moreover, composite materials introduce interfaces within the samples that affect the scattering of phonons rather than electrons. As a result, the lattice contribution of κ may be decreased by selective phonon scattering due to interface reflectivity and relaxation time. [27, 28] Thus, a hybrid composite of organic and inorganic TE materials provides low thermal conductivity and flexibility for energy harvesting. [29] So, the combined effect of quantum confinement introduced by the low dimensionality of the material [30, 31] and the scattering of phonons due to introduction of interfaces play a key role for the enhancement of ZT in such composites. This creates an interest in the field of organic-inorganic composite TEs. [32]

As mentioned before, the Figure of merit (ZT) is used to assess a TE material's performance. In this section, we attempt to concentrate on the practical aspects of measuring the values of all the parameters to characterize the performance of composite TE materials based on polymers for the intended application. As was previously said, the figure of merit of the TE materials is influenced by the electrical conductivity, thermoelectric power, and thermal conductivity. When it comes to these parameters, it has been found that various materials have been utilized as fillers in the polymer matrix to change the values of, S , or, which can then have an impact on the ZT. Usually, the filler concentration in the polymer matrix is varied.

CHAPTER 2: LITERATURE REVIEW



Literature Review

Literature Review

2.1. PEDOT as a TE Material

Because of their instability in air, the first generation of conducting polymers, including polyacetylene, had little commercial success. However, the development of PEDOT has paved the path for improved thermal and air stability in the doped state. Due to its processability in solutions, wide range of conductivities [33], strong electrochemical stability, and thermal stability, PEDOT has gained a lot of interest lately. [34] Also having a very narrow band gap of 1.5 eV, PEDOT may be made transparent by being doped with the tosylate ion to modify the absorption level in the NIR region. Additionally, it is one of the preferred contenders to take the position of ITO in flexible electronics and displays [35] and the TE efficiency may be improved by regulating the oxidation level. [36] Due to these characteristics, PEDOT has a variety of uses, including energy conversion and storage fields. Here, we outline the various methods for synthesizing functionalized PEDOT, as well as its structure and characteristics, and we provide an in-depth report on the development of thermoelectric applications.

2.2. Structure and Properties of PEDOT

The German Bayer Company created PEDOT for the first time in 1988. EDOT is a bicyclic derivative of thiophene that is joined by ethylene and has two alkoxy substituents at the thiophene ring's positions 3 and 4. While the electron-donating oxygen substituents stabilize free radicals and positive electrical charges inside the conjugated backbone, the six-membered ring closure with less steric hindrance increases stability [38]. The most commercially significant CP now is PEDOT due to its superior air and temperature stability, high and other intrinsic features [39].

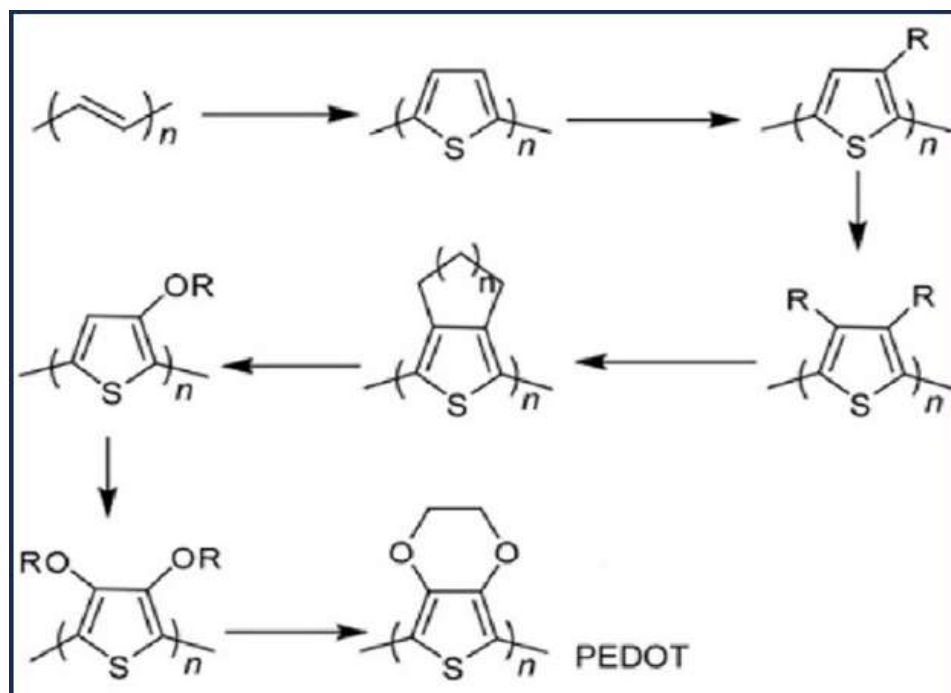


Figure 2.1. Schematics depicting the discover of PEDOT [37]

The process of oxidative polymerizing EDOT to PEDOT basically involves three phases.

(i) Cationic radicals are initially produced by oxidizing EDOT. (ii) After that, two cationic radicals combine to form a dimer. (iii) By oxidizing the dimers and polymerizing them, PEDOT is produced [40]. As a result, it is unavoidable that the oxidant will dope the PEDOT during the polymerization process, and the oxidant's anion will serve as a counter-ion to balance out the positively charged PEDOT.

PEDOT polymers exhibit good electrical conductivity because the electron-donor oxygen group, which is a part of the conjugated backbone chain, balances out free radicals and positive electronic charges. [38] There are few reports on functionalizing PEDOT with inorganic elements.

PEDOT's functionalization with opposing Tosylate (Tos) ions suggests that PEDOT has a more ordered, crystalline structure inside of a haphazard, amorphous matrix (Figure 2A).

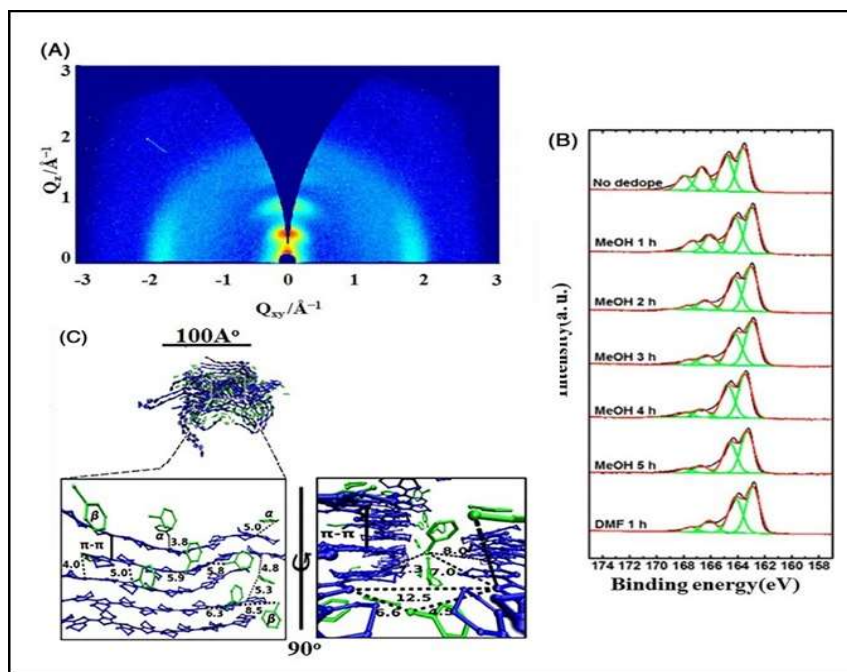


Figure 2.2. (A) Grazing incidence wide angle X-ray scattering of PEDOT-Tos. [41] (B) After the immersion dedoping procedure with methanol from initial washing to 5 hours of immersion and with Dimethylformamide (DMF) for 1 hour, $S(2p)$ XPS spectra of PEDOT: Tos films were obtained. [42] (C) The PEDOT:Tos molecular structure is depicted with Tos in green and PEDOT in blue. [43]

The lamellar stacking of the (100) and (200) planes of PEDOT:Tos is responsible for the small angle diffraction peaks at $Q = 0.45 \text{ \AA}^{-1}$ and $Q = 0.89 \text{ \AA}^{-1}$, while the inter-ring (010) stacking of PEDOT is responsible for the peak at $Q = 1.82 \text{ \AA}^{-1}$. [20, 44-46] As a result, the orthorhombic unit cell structure of PEDOT with the polymer chains extending along the c axis and an axis parallel to the substrate is what is proposed [43]. It suggests that PEDOT-Tos has a lamellar structure, with the tosylate anion [45] occupying an inter-lamella gap between stacked lamellae chains of the polymer. It oversees the rise in crystallinity [47, 48].

2.3. Different Synthesis Methods

PEDOT-Tos has already gained notoriety in the world of conducting polymers due to its exceptional capabilities. It is well known that variations in the synthesis process have an impact on the micro- or nanoscale structures, which in turn have an influence on the application-based characteristics of conducting polymers.

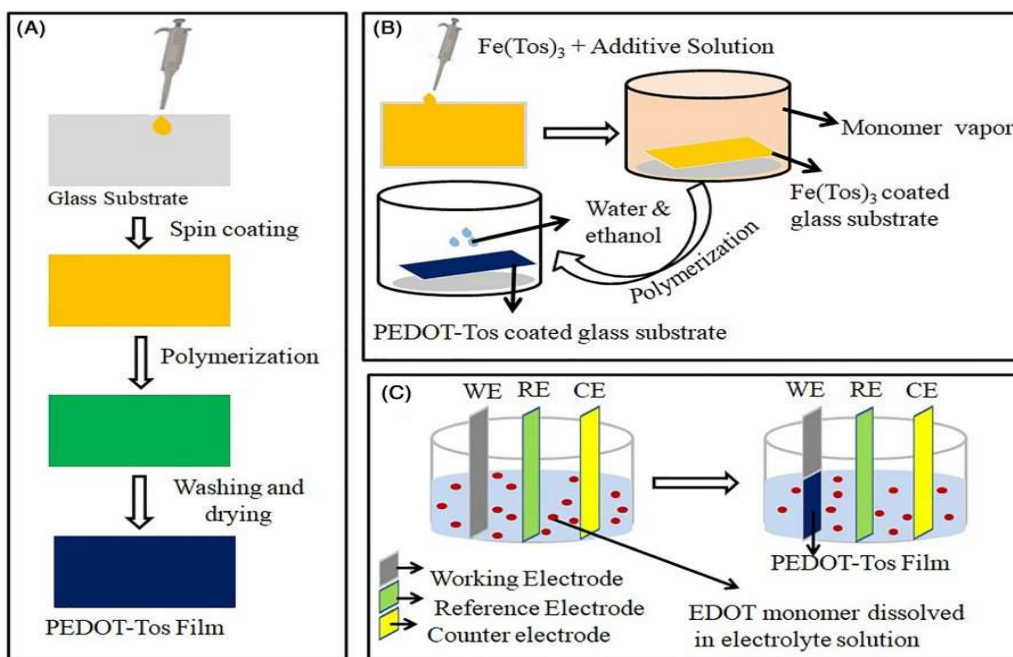


Figure 2.3. Schematics of several PEDOT-Tos film-forming polymerization techniques:
(A) The chemical polymerization process. (B) The vapor phase polymerization process.
(C) The electrochemical polymerization processes. [38]

There have been several attempts to fabricate PEDOT using controlled designs. Figure 2.3 provides a thorough summary of the typical synthesis procedures, which include chemical polymerization, vapour phase polymerization, and electrochemical polymerization.

2.3.1. Chemical Polymerization

Chemical polymerization is one of the efficient processes for making PEDOT on a large scale. This method is rather simple to use. The rate of oxidation of EDOT and the synthesis of polymers with higher molecular weights are easily controlled using the chemical polymerization method. Even though research on PEDOT is currently ongoing, the polymer was first chemically created in 1994 by Leeuw et al. [33]

For the traditional synthesis method, the oxidizing agent iron (III) tris-*p*-toluenesulfonate, imidazole, and the monomer ethylenedioxythiophene (EDOT) were originally dissolved in *n*-butanol. The entire oxidant solution was then filtered via a 0.5 μ m filter. The solution was spin-coated at a speed of 1000 rpm onto pre-washed substrates (typically 5 \times 5 cm) made of glass or plastic, and then baked for five minutes at 110 $^{\circ}$ C (or in a convection oven). Heating triggered the polymerization of the monomer EDOT into PEDOT doped with tosylate. [49, 50] Later, several adjustments to the process were made in order to produce the polymer. Such organic solvents as methanol, ethanol, *n*-butanol, hexanol, and dodecyl benzenesulfonic acid (DBSA), which alter the materials' electrical characteristics, have been used to make PEDOT powders and thin films as well [46, 51]. Significant hydrogen bonding interactions between PEDOT and alcoholic solvents change the samples' molecular ordering. PEDOT thin films were also polymerized with a variety of high boiling point additives, such as acetonitrile (ACN), toluene (Tol), chlorobenzene (CB), dimethylformamide (DMF), dimethyl sulfoxide (DMSO), ethylene glycol (EG), and propylene carbonate (PC), in order to fine-tune the polymer's structure. There have also been reports of the incorporation of co-dopants [Methanesulfonic acid (MSA), 2-naphthalenesulfonic acid (NSA), and *p*-toluenesulfonic acid monohydrate

(PSA)] in the backbone of PEDOT that were dissolved in the oxidant solution prior to mixing it with the monomer solution. Tri-block copolymer and pyridine were both used in the synthesis procedure to further fine-tune the kinetics of the polymerization. [52, 35] Another newly described change is the inclusion of copolymers like polyurethane (PU), polyethylene glycol (PEG), and PEO-b-PPO-b-PEO BCP to the oxidative polymerization process. [42, 53, 54] In order to improve the structural and electrical properties of PEDOT, two different tactics were applied, such as altering the quantities of iron (III) p-toluenesulfonate solution. In addition, reducing agents such tetrakis(dimethylamino) ethylene (TDAE) [36] are used. Vitamin C, or ascorbic acid. [56] The most effective alternative for extending the advantageous effects for practical applications was organic-inorganic hybrid materials. As a result, efforts are currently being made to produce nanocomposites of PEDOT and their inorganic analogues. Copper (II) oxide (CuO) and manganese oxide (Mn₃O₄) nanocomposite thin films [57] and PEDOT were produced by chemical polymerization using varying amounts of their inorganic equivalents. [58] PEDOT-Mn₃O₄ nanocomposite films were altered by esterifying EDOT-methanol and glutaric anhydride to produce a monomer augmented with a glutaryl. The titanium dioxide (TiO₂) nanotubes were covered with layers of PEDOT, which were similarly created using chemical polymerization. A common synthesis process also involved the production of PEDOT using solution-casting chemical polymerization, which was subsequently spun-coated on a variety of substrates, including TiO₂ nanotubes or glass substrates that had been doused with Carbon nanotubes (CNTs). [59] To alter the degree of PEDOT interference with CNTs, a modification in CNT concentration was made.

2.3.2. Vapor Phase Polymerization

In order to expose the oxidizing component to EDOT vapors and start the polymerization process, pyridine is used to create a film over it in the process known as "vapor phase polymerization," or VPP. [60-62] Bottom-up strategies, such as VPP, have an advantage over top-down ones, such as chemical synthesis, since the monomers are stacked up, creating a well-ordered crystalline structure for the polymer.[63] For the PEDOT-Tos structure to be well-ordered, the oxidant film is changed using a variety of techniques. Butanol, polyethylene glycol, and iron (III) p-toluenesulfonate are a few of the copolymers that make up this mixture. [62-65] Spin coating was used to apply poly (ethylene glycol-ran-(propylene glycol)) (PEG-ran-PPG), also known as PEG/PDMS/PEG [66], to a glass surface that had already been prewashed and coated with ITO. The spin-coated glass substrate was then exposed to EDOT vapor for polymerization after allowing the solvent to drain. An alternative procedure involved utilizing a dip coating process to apply an oxidant solution of iron (III) p-toluenesulfonate on both sides of the plasma-treated PVDF sheets. The PVDF flexible film with the oxidant coating was then placed in a VPP chamber and subjected to the vapor of an EDOT monomer to produce a PEDOT-Tos-coated PVDF film for use in subsequent practical applications. To produce PEDOT films using VPP, the triblock polymer PEG-PPG-PEG was also added to the combination of oxidant solution with alcohols [66,68–74], along with other additions such deionized water, DMF, DMSO, or EDTA [76]. This procedure allowed for the gradual polymerization of several layers of PEDOT until the free-standing PEDOT film was created. [77] To regulate the crystallization of PEDOT, the tripolymer PEG-PPG-PEG with additives was utilized. It was essential to further alter

the VPP process such that the films were produced in air rather than a vacuum for the synthesis of the PEDOT-PPP. [78, 79] The substrate in the VPP process has also been altered in order to create a stretchy and flexible PEDOT film under nitrogen flow. [80] A composite film made of aligned carbon nanotubes and PEDOT on PVDF film was also developed using VPP.[81] A porous pellet coated in tantalum pentoxide (Ta_2O_5) was used to create a different composite film called PEDOT/Graphene. On the porous Ta_2O_5 pellet, a FeTos/graphene layer was created, and when exposed to the vapor of the EDOT monomer, a PEDOT/graphene composite film was created. [82] A rGO/CNTs/PEDOT-Tos composite film was also created using straightforward VPP deposition. A CNT and rGo solution-sprayed substrate was evenly coated with an oxidant Iron (III) p-toluene sulfonate hexahydrate ($\text{Fe}(\text{OTs})_3$) solution before being placed into the EDOT vapor chamber for deposition and polymerization under the necessary conditions. [83]

2.3.3. Electrochemical Polymerization

Chemical synthesis or polymerization in the vapor phase While electrochemical polymerization (ECP) uses a voltage to oxidize EDOT rather than an oxidant, which is how EDOT is typically oxidized. A one-compartment, three-electrode cell with a working electrode, $\text{Ag}/\text{Ag}_2\text{Cl}_3$ as a reference electrode, and platinum foil as a counter electrode is the conventional setup for the ECP. The applied potential was ideally between 1.0 and 1.2 V as low polymerization potential made polymer film sticky [84]. A mixture of 3,4-ethylenedioxythiophene and iron (III) tris-p-toluenesulfonate in n-butanol serves as the cell's electrolyte. The working electrode is a polyethylene substrate onto which PEDOT was electropolymerized. [34]

The chemical polymerization method is a simple method for producing PEDOT with a higher molecular weight, but the VPP technique is a different synthesis route with a bottom-up approach that is superior to the chemical polymerization method because it produces well-ordered crystalline polymer structures, which are necessary for the improvement of various PEDOT parameters. One benefit of the electrochemical polymerization strategy is that it does not necessitate the use of a reagent as an oxidant, in contrast to chemical polymerization or the VPP method. In this technique, the voltage is employed to oxidize the EDOT monomer. However, compared to chemical and vapor phase polymerization, the electrochemical polymerization approach requires a more complicated setup.

2.4. PEDOT for TE application

Researchers have used a variety of techniques to raise the PEDOT figure of merit, including lowering the oxidation level, treating with acids and bases, employing additives, including inorganic equivalents, etc. Aqueous vitamin C solution [56], TDAE [36], or different concentrations of iron (III) p-toluenesulfonate hexahydrate with respect to n-butanol [55] have all been found to significantly affect the electrical conductivity and thermoelectric power, which in turn affect the ZT. The power factor may be tuned at a certain oxidation state, according to the reciprocal relationship between electrical conductivity and thermoelectric power with rise in oxidation level for polymers. As a result, TDAE has lowered PEDOT, and it has been noted that at 22% of oxidation level, the power factor achieves its highest value. At this lower degree of oxidation, the polymer's figure of merit (ZT) achieves its maximum value of 0.25 [36] at room temperature with a low intrinsic thermal conductivity of around $0.37 \text{ Wm}^{-1} \text{ K}^{-1}$ since the

thermal conductivity of conducting polymers is independent of their oxidation state. Similarly, the degree of oxidation of PEDOT film has been adjusted using various concentrations of aqueous vitamin C solutions. It has been shown that the ZT value peaks at about 23% of the oxidation level. [56] Changing the concentrations of iron(III) p-toluenesulfonate hexahydrate (1, 10, 20, 40, 60, and 80 wt% with reference to n-butanol) can also alter the degree of oxidation of the conjugated polymer PEDOT. The size of the particle is also influenced by the loading of the oxidant. It was shown that the power factor peaks at around 20% of the oxidation level and then declines as the oxidation level rises. However, it starts to rise once again and reaches its maximum value at 80% of the oxidation level. This is likely because the electrical conductivity rises with the oxidation level. Another method of affecting the thermoelectric characteristics of PEDOT thin films is to subject them to acid and base treatment. When PEDOT films are exposed to acids and bases, it has been shown that the thermoelectric characteristics of the films undergo a similar sort of alteration. A maximum power factor value was attained with pH fluctuation at pH 7. [68] When PEDOT thin films were exposed to co-solvents during the polymerization process, a change in the structure of the films was noticed. There is an enhancement in the power factor due to the increase in the electrical conductivity which is due to the influence of structural change in the PEDOT thin films. [46] The thermoelectric properties of PEDOT are also tuned by the inclusion of nanoparticles in the polymer matrix such as Mn_3O_4 nanoparticle, [57] CuO nanoparticle, [58] carbon nanotubes [59] or graphene. [86.] Nanoparticle inclusion may alter the crystallinity of PEDOT, which in turn may alter the density of state (DoS) slope and the thermoelectric power. All the strategies discussed are geared toward improving the molecular ordered

structure because for PEDOT, an increase in order improves carrier delocalization and orbital overlapping [47], which change the electronic band structure and affect the charge transport properties. As a result, this affects the charge carrier mobility, and a rise in the polymer's electrical and thermoelectric power has been seen, giving rise to a larger value for ZT. This shows that PEDOT has enormous potential for use in the creation and operation of organic thermoelectric devices. [75, 87]

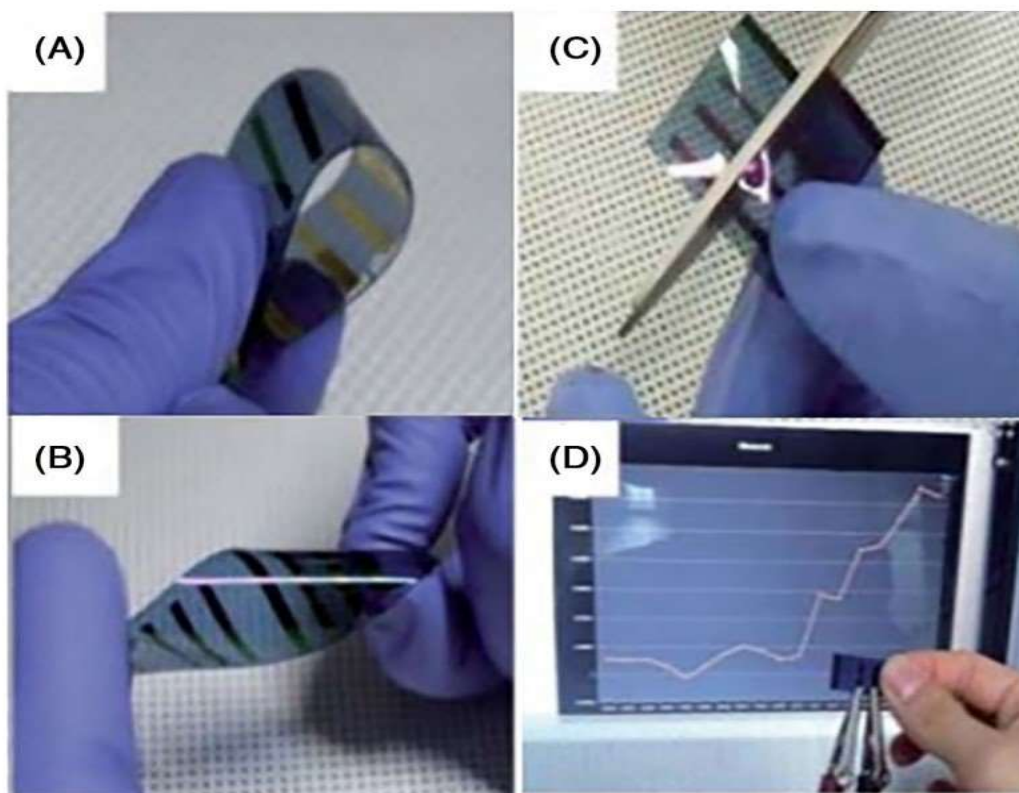


Figure 2.4. The flexible PP-PEDOT thermoelectric film may be touched with the fingertips to produce photographs and power. (A) Bending, (B) twisting, and (C) cutting with scissors images of PP-PEDOT films. (D) Electricity generation by fingertip touch at one side with air.[52]

According to reports, a thermoelectric generator (TEG) may provide a maximum power output of $0.128 \mu\text{W}$ at $\Delta T = 10^\circ\text{C}$ and 26.0 nW cm^{-2} at $\Delta T 9.5 \text{ K}$ when it is made with

PEDOT for the p type legs and TTF-TCNQ/PVC mix or n doped graphene for the n type legs. In order to create thin films on different substrates, Poly(ethylene glycol)-block-poly(propylene glycol)-block-poly(ethylene glycol) triblock copolymer (PEPG) was used as an inhibitor. PEDOT has a good electrical conductivity at an oxidation level of 24.1%. As seen in figure 2.4, an effort was made to construct a flexible thermoelectric device that produces energy with a fingertip touch. The constructed gadget produces a voltage of 8–10 mV by touching it at 27 °C, room temperature. Additionally, composites made of PEDOT are a strong contender for the industrial scale fabrication of thermoelectric generators (TEGs) that are cost-effective. [88] In addition, PEO-b-PPO-b-PEO BCP and Fe(Tos)₃ oxidant mixed PEDOT films from disordered nanostructures rather than ordered nanostructures demonstrated a maximum thermoelectric power of 70 Wm⁻¹ K⁻². This is explained by the fact that oxidants and monomers may move about in disordered nanostructures more easily in terms of mass. [42]

2.5. PEDOT Based Composite Materials for TE application

The intrinsic low S of PEDOT severely hinders the enhancement of TE performance, despite its high σ and low κ values. One of the most promising methods to attain high TE performance is the use of composite materials. It can combine the benefits of phonon boundary scattering, which can be used to restrict phonon transport, interfacial scattering, which can be used to filter out low-energy charge carriers, and potential filler templating, which can be used to organize polymer chains [89].

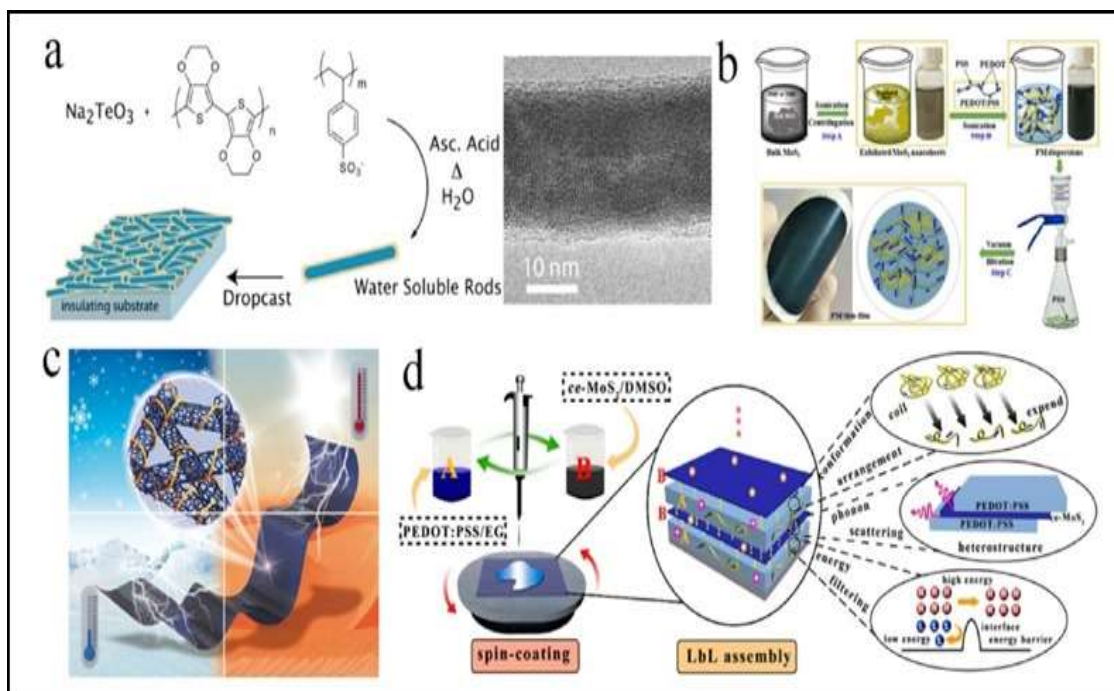


Figure 2.5. (a) PEDOT: PSS-passivated Te nanorod synthesis, solution-casting of smooth nanocomposite films, and TEM image of the crystalline Te nanorod with PEDOT: PSS passivation. PSS. [90](b) Flexible PEDOT: PSS/ce-MoS₂ thin-films are depicted schematically. [91] (c) Schematic representation of SWCNTs and PEDOT:PSS [92] (d) Diagrams of the PEDOT: PSS/ce-MoS₂ heterostructure TE films and the spin-coating setup are shown in the sketch. [93].

Research on various composite materials based on PEDOT with different synthesis technique shown in figure 2.5. The following advantages of PEDOT-based composites result from the high S of inorganic components: (i) When compared to inorganic materials, is greatly decreased in κ value, and this is mostly due to phonon scattering at the composite contact [94]. (ii) PEDOT may effectively link inorganic nanomaterials, achieving excellent contact, as well as operate as a protective layer to stop the oxidation of inorganic materials [90]. (iii) Strong scattering of low-energy carriers at the composite

interface will result in an energy filtering effect, raising the S of PEDOT [95]. (iv) PEDOT-based composites exhibit greater flexibility compared to inorganic materials [96]. Based on the aforementioned benefits, PEDOT-based composite TE materials have been widely researched, such as PbTe/PEDOT:PSS, [97] Bi₂Te₃/PEDOT:PSS, [98-101] Ag₂Te/PEDOT:PSS, [102] Te/PEDOT:PSS, [90, 96] SnTe/PEDOT:PSS, [103, 104] MoS₂/PEDOT:PSS, [91] Au/PEDOT:PSS, [105, 106] etc. Like composite materials, attention has also been paid to materials like PEDOT and graphene, [107, 108] carbon nanotubes [109], CPs [110, 111], and others. Since they have a better carrier mobility than PEDOT, graphene and carbon nanotubes are thought to be among the best options for recombination. There is a $\pi - \pi$ interaction between them that can simultaneously increase σ and S [112] by maintaining the carrier concentration and enhancing the mobility of the carriers in the composite material. Despite the fact that the present PEDOT-based composite materials have shown good TE characteristics like SnTe/PEDOT:PSS (386 W/ m1 K²) [103] and Te/PEDOT:PSS (284 W/ m1 K²) [96], PEDOT:PSS/Se (15 μ W/cmK²) [113] more work still has to be put into the hunt for concurrently improving σ and S . Therefore, a lot of research has already been done on PEDOT, which is functionalized by ionic counters and its inorganic composites. However, no comparable research has been conducted on PEDOT composites made of functionalized inorganic materials.

Thus, we observe that work on functionalization of PEDOT and composites of functionalized PEDOT for TE application are very scanty.

2.6. Objective of the work

The present work mainly focused on the synthesis of PEDOT and its hybrid composite, along with the study of its structural and electrical properties for TE applications.

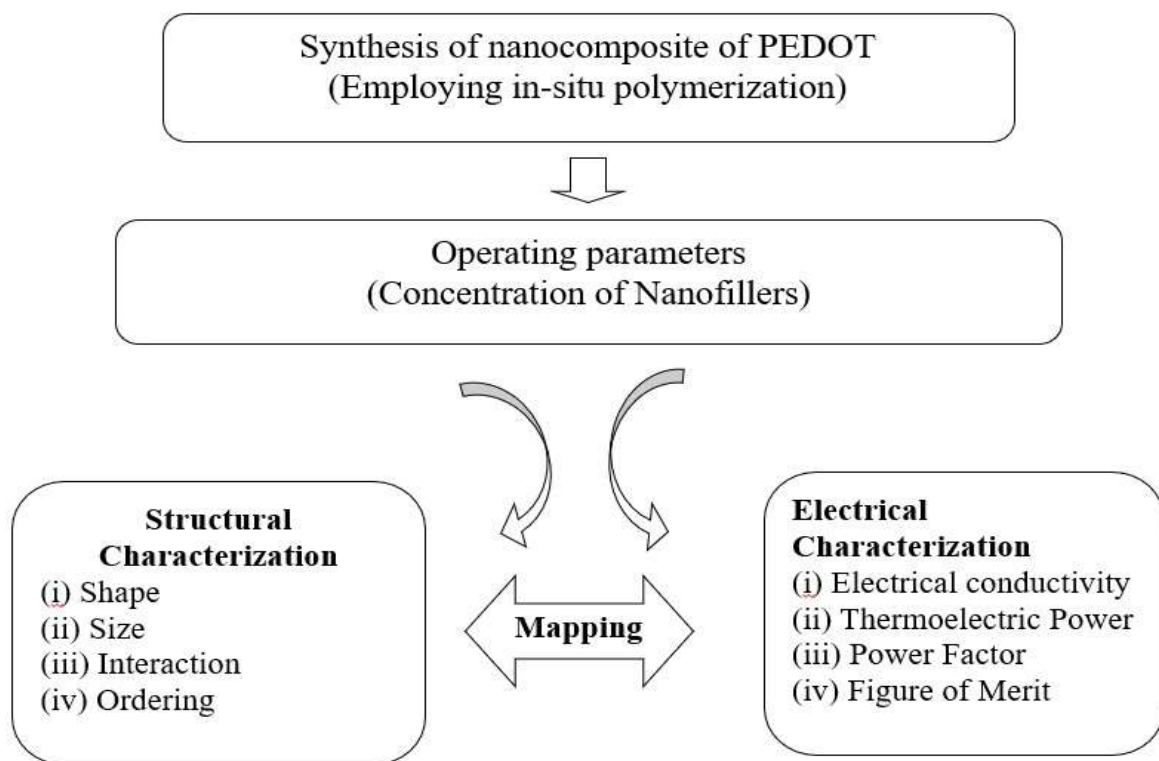


Figure 2.6. Flow chart of the executed research work

The main objective of the present work is the improvement of the structure and TE properties of PEDOT by introducing nanofillers and mapping the properties with the process parameters for device application.

In-situ polymerization techniques have been employed for the synthesis of PEDOT from its monomer (EDOT) for TE property analysis in all cases. The variation of nanofillers in PEDOT has been investigated. It is observed that different nanofillers influence the morphology of the material, which in turn stimulates the TE properties of the material.

Further, the effects of different oxidizing agents on the TE performance of the materials are also noteworthy.

The research demonstrates how strong and promising TE candidates PEDOT and its hybrid composites are. Additionally simple to synthesize and mechanically adaptable, these materials allow for the utilization of a variety of designs in device applications. With the start of potential in the TE field, these materials' uniqueness surely brings in a new age of smart materials.

CHAPTER 3: MATERIALS AND CHARACTERIZATIONS



Materials and Characterizations

In this chapter, sample preparations and experimental characterization techniques for studying of the fabricated materials are presented. Several techniques can be employed to obtain a profound understanding of the physics behind the materials. Different methods starting from spectroscopic techniques to the electrical and thermal characterization are described.

3.1. Materials

3,4-Ethylenedioxythiophene (EDOT) and Pyridine were obtained from Sigma-Aldrich (98%). para toluene sulfonic acid (pTSA) and ammonium peroxydisulfate (APS) were purchased from alfa-aesar. Ferric chloride (FeCl_3) and acetonitrile, n-hexane, butanol, and ethanol were obtained from Merck. Sodium dodecyl sulfate (SDS) was purchased from SRL. Selenium (Se) powder was purchased from RFCL Limited. SWCNT was purchased from US Research Nanomaterials, Inc. Graphene was purchased from Platonic Nanotech Pvt. Ltd. Deionized water was purchased from Hydro Lab, India.

3.2. Synthesis of PEDOT-Tos

A solution was made by dissolving 0.02 mol of FeCl_3 into 25 ml of acetonitrile (solution A) with magnetic stirring in order to synthesize the p-Toluenesulfonic acid (pTSA)-doped PEDOT conducting polymer. Solution B was prepared by dissolving 0.01 mol of EDOT in 15 ml of n-hexane. A third solution, classified as solution C, was made by dissolving 0.02 mol of pTSA in 20 ml of butanol. The entire synthesis process was inhibited using pyridine. A typical approach involved dropping solution A into solution B. Pyridine was added to the mix containing solutions A and B after 15 minutes of

stirring in order to control the polymerization kinetics. The mixture was then stirred continuously for 21 hours at room temperature.

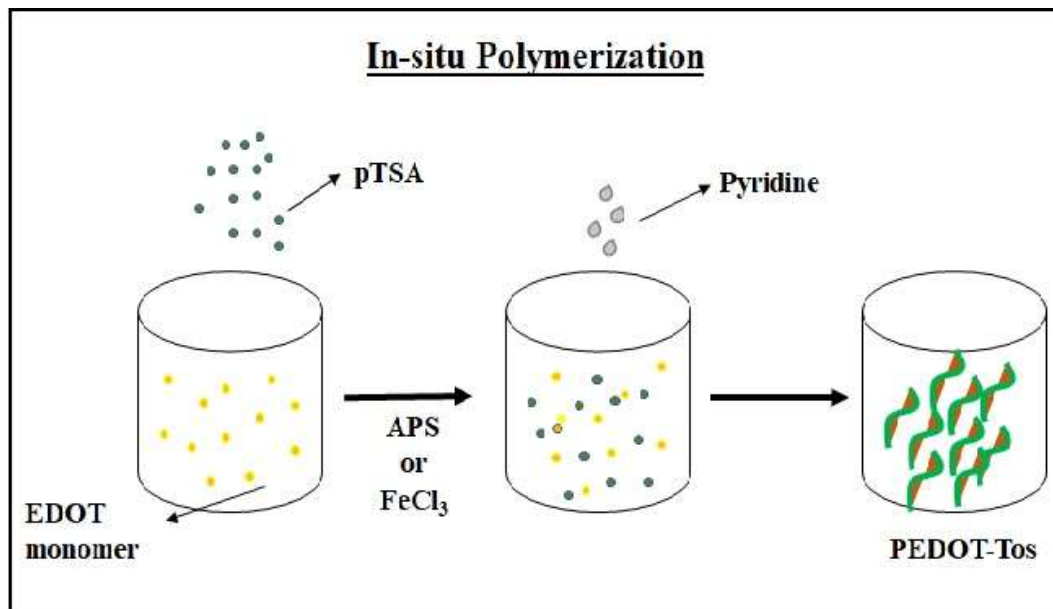


Figure3.1. Schematic diagram of the synthesis process of PEDOT-Tos

The final step was to add Solution C to the resulting mixture, which was then stirred for 3 hours at room temperature. The product was obtained by centrifugation for 5 minutes at 7000 rpm, followed by ethanol and deionized water rinses, and then vacuum drying at 70°C.

PEDOT polymer was also synthesized using APS, as a different oxidizing agent. In this typical synthesis process using in situ polymerization technique, EDOT monomer was polymerized in an aqueous solution of PTSA, using APS as oxidant. A magnetic stirrer was used to mix an aqueous solution containing PTSA (0.04 mol) and EDOT (0.02 mol) for 30 minutes at room temperature. A solution of APS (0.02 mol) in 100 ml of water was prepared. The EDOT monomer aqueous solution was added drop by drop in the

subsequent stages, and the reaction mixture was stirred for 24 hours at room temperature. Indicating PEDOT (doped with PTSA), a dark blue precipitate appeared. After 24 hours, the product was recovered by centrifugation for 5 minutes at 7000 rpm. It was then washed with ethanol and deionized water, in that order, before being dried in a vacuum at 70 °C.

3.2.1. Synthesis of PEDOT-Tos/ SWCNT Composite

Solution A was designed to produce the PEDOT-Tos-SWCNT nanocomposite, as previously mentioned. SWCNT and 0.01 mol of EDOT were added to formulate Solution B, which was then ultrasonically processed for an hour. Drop by drop, Solution A was added to the SWCNT dispersion solution. After 15 minutes, Pyridine was added according to the earlier mentioned procedure, and the mixture was stirred at room temperature for 21 hours. As previously mentioned, the mixture was then supplemented with Solution C and stirred for 3 hours at room temperature. The product was collected by centrifugation for 5 minutes at 7000 rpm, washed with ethanol and deionized water, and then dried under vacuum at 70°C.

3.2.2. Synthesis of PEDOT-Tos/Graphene Composite

For the fabrication of a nanostructured PEDOT-Tos/Graphene nanocomposite doped with PTSA, graphene was added to an aqueous solution that already included pTSA (0.04 mol), which was then ultrasonically processed again for 30 min to further disperse the mixture. After adding EDOT (0.02 mol) to the solution, the mixture was vigorously stirred for 30 minutes. For the immediate fabrication of PEDOT-Tos/Graphene nanocomposites, APS (0.02 mol) was then added to the solution as an oxidant. The reaction mixture was then agitated for 24 hours at room temperature. After

polymerization, the finished product was vacuum dried in an oven at 70 0C for 5 minutes while being centrifuged at 7000 rpm.

3.3. Synthesis of Se-PEDOT

PEDOT polymer was synthesized by the self-accumulated micellar prototype method. In this typical procedure, first SDS (30 mmol) was dissolved in 100 ml of deionized (DI) water, and then FeCl_3 (15 mmol) was mixed with that transparent solution and kept for 1 hour stirring at 50°C. After 1 hour of stirring, the color of the solution turned deep yellow.

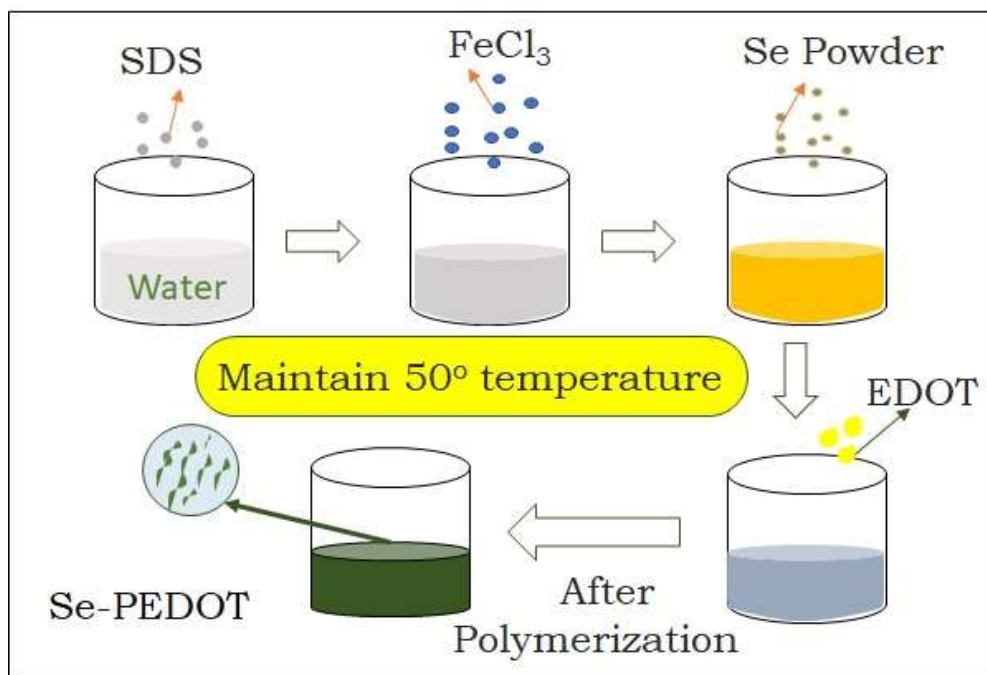


Figure3.2. Schematic diagram of the synthesis process of Se-PEDOT composite

EDOT monomer (7 mmol) was gradually added to the following solution, and at 50°C, the polymerization process was carried out. During the progression of the polymerization process, different weight percentages of ingot selenium nanoparticles were incorporated

and stirred for 1 hour, maintaining 50°C. The samples were centrifuged at 5000 rpm for 5 min. several times. The collected samples were dissolved in ethanol, washed by vacuum filtration, and kept dry at 60°C in vacuum for 24 h.

3.4. Characterization

3.4.1. X-Ray Diffraction (XRD)

A non-destructive method for learning more about the chemical composition and crystallographic structure of solids and thin film materials is X-ray diffraction (XRD). Both qualitative and quantitative evaluations can be performed with X-ray diffraction techniques. When carrying out a qualitative analysis, a specimen's phase or phases are recognized by comparison to a reference pattern or set of standard diffraction data, and the relative proportion of each phase in multiphase specimens is estimated by comparing the peak intensities associated with each identified phase. The quantification of diffraction data entails quantifying the quantities of various phases in multi-phase samples. However, the XRD method has difficulty detecting tiny amounts of dopant or localized flaws. The generation of X-rays occurs when an electrically heated filament, typically tungsten, emits electrons that are then allowed to strike a metal target, the anode, which is cooled with water, and which emits a continuous spectrum of X-rays known as "white" radiation. 'Characteristic' X-rays are the sharp, strong X-ray peaks (K_{α} and K_{β}) superimposed on these white X-rays. Every anode metal has a different wavelength for the K_{α} and K_{β} lines. Typically, copper or molybdenum are utilized as the anodes in X-ray diffraction experiments. The energy of the bombardment electrons knocks away electrons from the innermost K shell, which produces X-rays. This creates vacancies in the K shell which are filled by electrons descending from the shells above.

The energy released when electron from outer shell fills the vacancies in the innermost shell, appears as radiation. The $K\alpha$ radiations occur when the electron from L shell ($n=2$) descend and $K\beta$ radiations occur for the electrons from M shell ($n=3$). For XRD study, it is very important that the wavelength of the wave should be about the same as the repeat distance of the periodic structure for diffraction to occur.

Inter-atomic distances are of the order of a few angstroms. X-rays have wavelengths of the same order and hence they are used to investigate the crystals. The X-ray diffraction facility available at Jadavpur university is shown in Figure3.3. The current work will make advantage of the same.

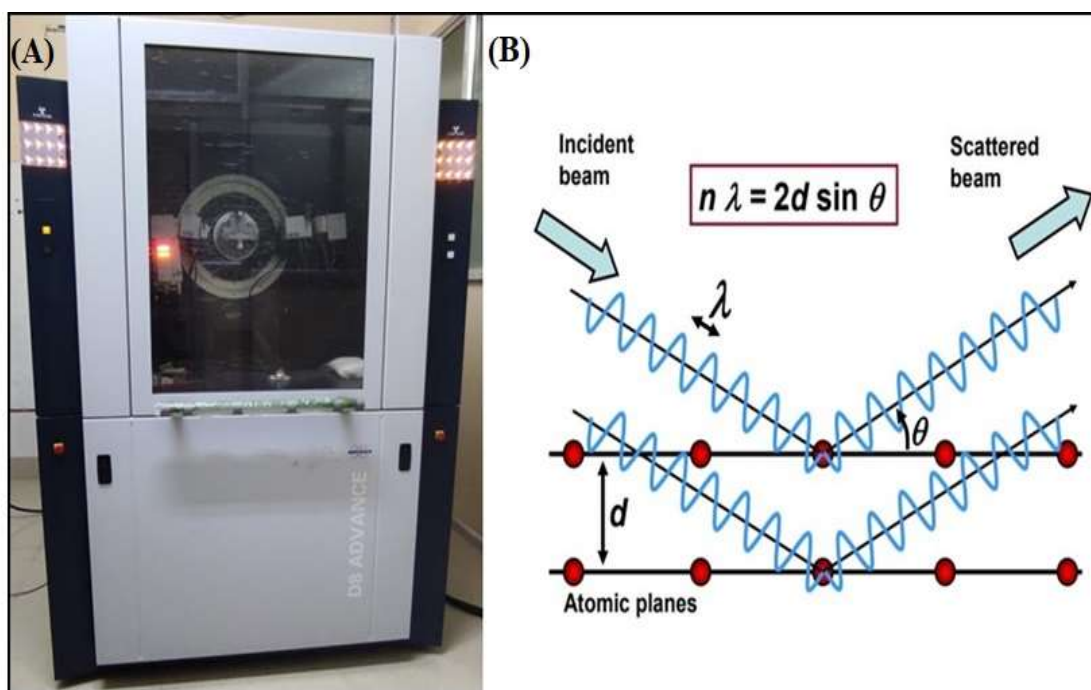


Figure3.3. (A) X-ray diffractometer (BRUKER D8 Advance) (B) Principle of X-ray diffraction [114]

The X-ray diffractometer model was BRUKER D8 Advance with Cu $K\alpha$ radiation ($\lambda = 1.54182 \text{ \AA}$).and 35 kV accelerating voltage. The 2θ range studied for general survey was

5-80 degrees. The 2θ steps and step acquisition time were 0.05° and 0.5° /min respectively. The XRD method is based on diffraction determined by Bragg's law. The law states that when an X-ray beam is incident on a crystal it interacts with the parallel plane of atoms either constructively or destructively depending upon the path difference. Bragg's law is satisfied when the waves interfere constructively and the following condition is met.

$$n\lambda = 2d \sin\theta \quad (3.1)$$

where n = an integer (1, 2, 3... etc.), d is the spacing between atomic planes in the crystalline phase and λ is the X-ray wavelength and θ is the diffraction angle in degrees. The intensity of the diffracted X-ray is measured as a function of the diffraction angle 2θ and the samples orientation. This diffractometer is based on Bragg-Brentano parafocusing diffraction geometry. In this geometry, the X-ray detector is at 2θ and the sample surface is at θ angle to the incident beam. The incident beam, normal to the sample surface, and detector are in the same plane since the diffracted beam always lies in the plane containing the incident beam and normal plane.

3.4.2. Fourier transform infra-red (FTIR) spectroscopy

The sum of the rotational, vibrational, and electronic energy levels can be used to estimate the total internal energy of a molecule. The investigation of interactions in the IR range between matter and electromagnetic fields is known as infrared spectroscopy. The principal chemical vibrations that the EM waves coupled with in this spectral area include. In other words, absorbing IR light can stimulate a molecule to a higher vibrational state. The actual interaction between a certain IR frequency and the molecule

determines the likelihood that it will be absorbed. A frequency will often be significantly absorbed if its photon energy matches the molecule's vibrational energy levels. Therefore, IR spectroscopy is a very potent method that offers fingerprint details about the chemical composition of the sample.



Figure3.4. FTIR spectrometer (Shimadzu FTIR-8400S) at Jadavpur university

The FTIR spectrometer (Model no. Shimadzu FTIR-8400S) being utilized for the present work. In possible vibrational and rotational modes, only molecules with insignificant energy differences may absorb IR. The vibrations or rotations within a molecule must result in a net change in the molecule's dipole moment for it to absorb IR.

The oscillations in the molecule's dipole moment are affected by the alternating electrical field of the radiation (keep in mind that electromagnetic radiation is made up of an oscillating electrical field and an oscillating magnetic field that is perpendicular to one

another). Radiation will be absorbed and influence the amplitude of molecular vibration if its frequency is the same as the molecule's vibrational frequency.

3.4.3. Ultraviolet–visible spectroscopy:

UV spectroscopy, also known as UV-visible spectrophotometry (UV-Vis or UV/Vis), is the study of absorption or reflectance spectra in portions of the ultraviolet and the complete, nearby visible spectrums.



***Figure3.5.** Ultraviolet–visible spectroscopy set up (Uv-1800, Shimadzu, Japan)*

This approach is frequently employed in a wide range of practical and theoretical applications since it is reasonably affordable and simple to apply. The sample must only be a chromophore, which means it must absorb in the UV-Visible range. Together with fluorescence spectroscopy, absorption spectroscopy is useful. Along with the measuring wavelength, parameters like absorbance (A), transmittance (%T), and reflectance (%R) are important. The Uv-vis spectroscopy at Jadavpur University is Uv-1800, Shimadzu, Japan. The same will be used for the present work.

Being chromophores, most molecules and ions absorb energy in the ultraviolet or visible spectrum. A chromophore's electron is stimulated to higher energy molecular orbitals by the photon that was absorbed, creating an excited state. Four potential transition types π -, π^* , n - π^* , σ - σ^* , and n - σ^* —are postulated to exist for organic chromophores. Because they include various electronic states linked to partially filled d orbitals, transition metal complexes are frequently colored (i.e., absorb visible light).

3.4.4. Raman Spectroscopy

An effective method for identifying chemical compounds is Raman spectroscopy. Raman spectroscopy, like other spectroscopic methods, finds specific interactions of light with materials.

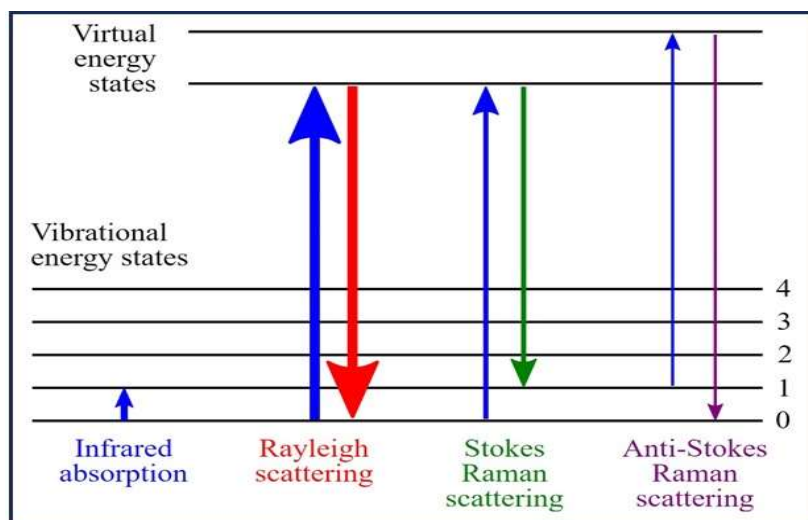


Figure 3.6. Theory of Raman Spectra

Utilizing Stokes and Anti-Stokes scattering (figure 3.6), this method looks at molecule structure. There are several forms of scattering that can happen when light from the visible or near infrared (NIR) ranges interacts with a molecule. A bond's capacity to

exhibit polarizability affects the Raman effect. This gauges how easily a bond will bend under the influence of an electric field. This variable mostly depends on how easily a sample may induce a transient dipole by dislodging the electrons in the connection. The polarizability is also high when there is a high concentration of loosely held electrons in a bond, and the group or molecule will have a strong Raman signal. As a result, Raman is frequently more sensitive to a molecule's molecular structure than it is to a particular functional group as in IR. Contrast this with a molecule's polarity, which measures the separation of electric charge within a molecule. Due to the near proximity of the electrons held by electronegative atoms, polar molecules frequently have very weak Raman signals. The present work will benefit from the Raman spectroscopy (LabRAM HR) facility at Bose Institute, Kolkata.



Figure3.7. Raman Spectroscopy set up (Model no. LabRAM HR)

Raman spectroscopy may reveal details about the chemical compositions of both inorganic and organic materials. Since many electron atoms have numerous loosely

bound electrons, such as metals in coordination compounds, they frequently exhibit Raman activity. Raman can provide details about the metal-ligand link, enabling researchers to understand the make-up, structure, and stability of these complexes. This is especially helpful for metal complexes with low IR vibrational absorption frequencies. The functional groups and fingerprints of organic compounds may be identified using Raman, which is also highly helpful. Since molecules vibrate individually rather than in confined groupings, Raman vibrations are frequently quite unique to a particular molecule. The groups that do show up in Raman spectra contain vibrations that are frequently several bonds strong and generally confined inside the group.

3.4.5. Field Emission Scanning Electron Microscope (FESEM)

Field emission guns are used in FESEM as the electron source. With a suitable detector (energy/wavelength dispersive X-ray spectroscopy), the scanning electron microscope may be utilized for topographical research, microstructural analysis, chemical composition analysis, and elemental mapping. The Jadavpur University's FESEM facility is depicted in Figure 3.8. The current work will make advantage of the same.

The model utilized in this investigation was a FEI, INSPECT F50 with an operating accelerating voltage 10-20kV. A sample surface may be captured in high-resolution photographs using a field emission scanning electron microscope (FESEM).

The sample is exposed to an electron beam with a spot size of a few nanometers, and the incoming electrons interact with the sample's atoms to scatter. Some emission from the surface is the consequence of these scattering mechanisms. The specimen's surface features, size, shape of the features, composition, and crystalline structure are all revealed by the electron beam's interaction with the sample.

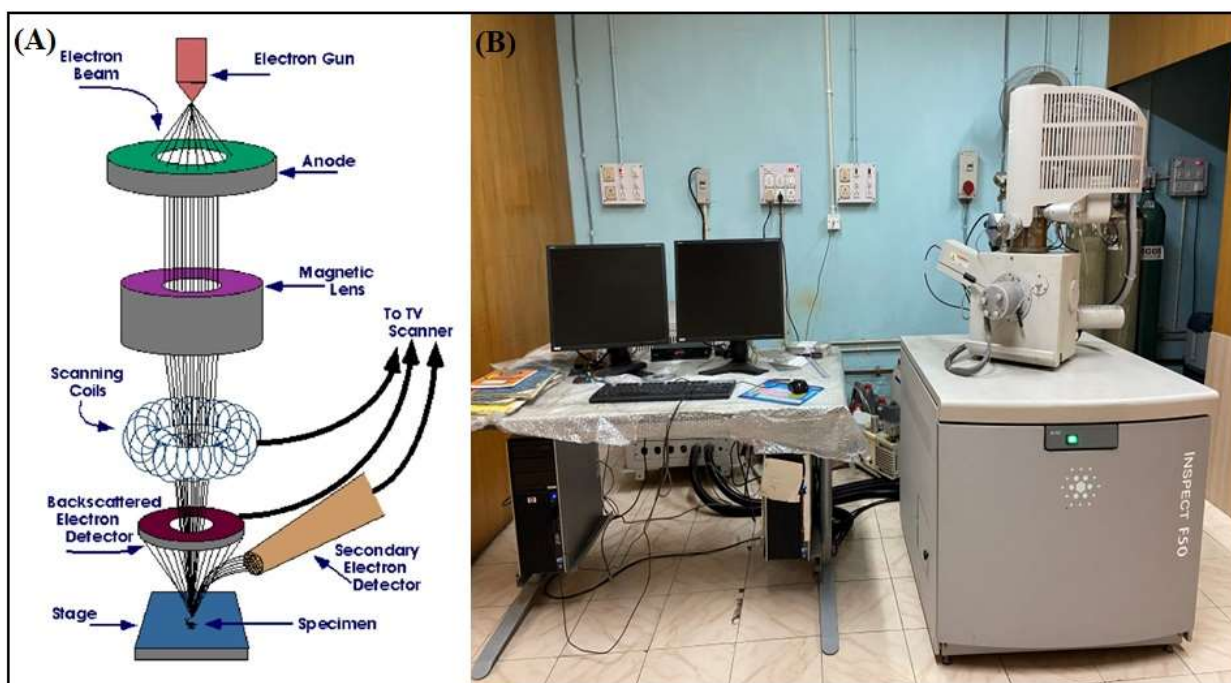


Figure 3.8. (A) Schematic diagram of a field emission scanning electron microscope (FESEM) [115] (B) FESEM Set up (FEI, INSPECT F50) at Jadavpur University.

There are several ways in which the electron beam might interact with the specimen, including: If the incoming electrons approach the atom enough, they will transfer part of their energy to the specimen electrons, mostly in the K-shell. These electrons will then alter their course and ionize the electrons in the test atoms. Secondary electrons are the liberated ionized electrons from the atoms. Once near the specimen's surface, these electrons will go there and collide in elastic and inelastic ways. However, because to their low energy, only electrons that are close to the surface (i.e., 10 nm or less) will exit the surface and be able to be detected and utilized to image the specimen's topography. The incident electrons will be reflected or backscattered when they come into direct contact with an atom. As the atomic number of the specimen changes, various atomic types will produce varied rates of backscattered electrons, which will affect the contrast of the

picture. Typically, atoms with higher atomic numbers will look brighter than those with lower atomic numbers. These electrons are referred to be transmitted electrons if the incident electrons travel through the specimen without contacting the atoms that make up their nuclei. To capture a picture of a thin specimen, these electrons are utilized. Elastic scattering is a different type of scattering that does not cause energy loss in the electrons. The orientation and arrangement of the atoms may be determined using the information provided by these dispersed electrons. When atoms are attacked by incoming electrons, electrons from those atoms will be liberated, leaving the atom in an excited state. The extra energy must be let go of for the atom to return to its ground state. Three methods of releasing extra energy include auger electrons, X-rays, and cathode luminescence. Energy-dispersive X-ray analysis (EDX) is a method that uses the x-ray to determine the elements and their concentrations in the material. Auger electrons can be used for chemical analysis.

3.4.6. Electrical Characterization

The electrical conductivity, thermoelectric power, thermal conductivity, and Hall effect will be investigated at different steady temperatures (room temperature and above). The power factor, carrier concentration, and mobility of the charge carriers will be evaluated and studied.

3.4.6.1. Electrical conductivity:

The temperature variation of the electrical conductivity (σ) of the prepared samples will be measured by four probe methods. The most common technique used for measuring sheet resistance is the four-probe method. This technique involves using four equally spaced, co-linear probes (known as a four-point probe) to make electrical contact with the

material. If the thickness of the measured material is known, then the sample resistance can be used to calculate its resistivity.

$$\rho = \frac{\rho_0}{f\left(\frac{w}{s}\right)} \quad (3.2)$$

The function, $f(w/S)$ is a divisor for computing resistivity which depends on the value of w and S

$$\rho_0 = \frac{V}{I} \times 2\pi S \quad (3.3)$$

V- The potential difference between inner probes in volts.

I- Current through the outer pair of probes in ampere.

S – Spacing between the probes in meter.

3.4.5.2. Thermoelectric power:

An indigenous setup is introduced for the measurement of the thermoelectric power of a sample as shown in figure 3.9.



Figure 3.9. Thermoelectric measurement setup

In this setup, an auxiliary heater was placed at one end of the sample holder to heat one side of the sample, and the other side of the sample was kept at room temperature to establish a temperature difference ΔT while the corresponding potential drop ΔV was measured by a data acquisition system. Also, this method will be used to calculate the power factor of the sample.

3.4.6.3. Thermal conductivity:

Room-temperature thermal conductivity measurements can be carried out for the prepared samples using a Hot Disk thermal constant analyzer. Finally, it can help to calculate the figure of merit ZT of the samples for further needs.

3.5. Accuracy Measurement

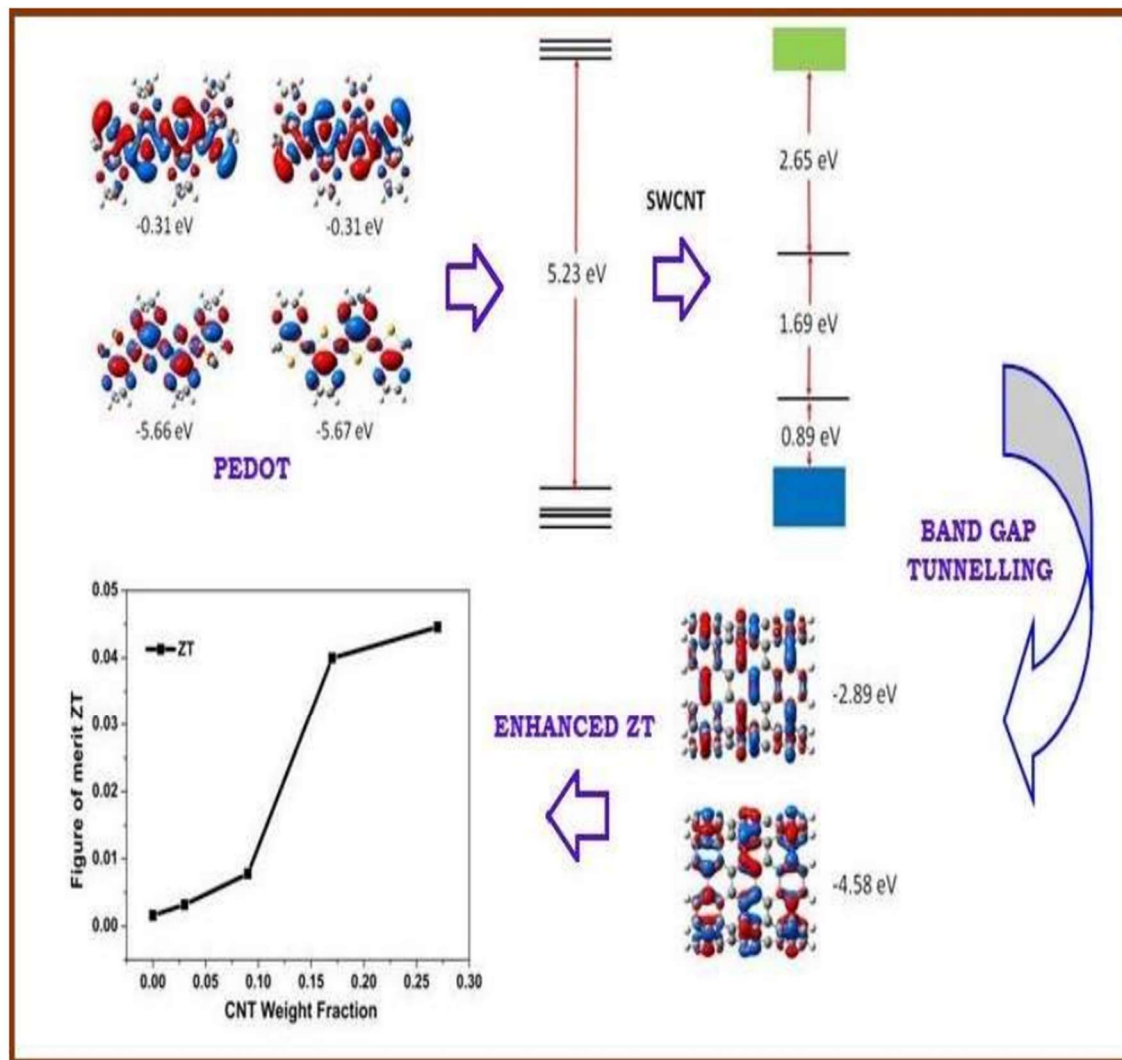
The maximum errors associated with the various results are as follows, considering the constraints of the various measuring instruments:

Electrical Conductivity (σ) = 4 %

Thermoelectric Power (S) = 1.5%

Thermal Conductivity (κ) = 2 %

CHAPTER 4: PEDOT BASED CNT COMPOSITE SYSTEM



4.1. Introduction

In comparison to inorganic materials, thermoelectric (TE) materials from organic semiconductors have lower thermoelectric figures of merit (ZT) values.[116] Organic semiconductors have a wide range of applications due to their benefits such as inexpensive production costs, non-toxicity, and simple access to raw ingredients.[117] The most promising candidate that has previously undergone research as a possible suitable material for TE applications is now conducting polymers. Polyacetylene (PA), [118] polypyrrole (PPY),[119] polyaniline (PANI), [85] polycarbazoles (PC), [120] and poly(3,4-ethylenedioxythiophene): poly(styrenesulfonate) [121] all have TE characteristics. (PEDOT: PSS) and its derivatives exhibit significant potential and merit further research. The study of PEDOT and its derivatives' TE performance is now under progress.[122] Different secondary dopants can significantly improve PEDOT-PSS's somewhat subpar TE efficiency. These secondary dopants often enhance the polymer's morphology while also dramatically increasing electrical conductivity and, as a result, ZT.[87] Electrochemical doping allows for fine control of PEDOT-PSS oxidation, leading in a ten-fold increase in ZT. [123, 124] Because PEDOT-Tos is partly crystalline and has better electrical conduction than PEDOT-PSS, it performs better in terms of TE even without secondary doping. Tosylate doped PEDOT (PEDOT-Tos) is an additional significant doped version of the polymer due to the growing interest in replacing inorganic anode materials with organic materials with ultrahigh conductivity. Positively doped PEDOT-Tos is partly reduced with the help of a powerful electron donor, achieving the ideal oxidation state where its TE efficiency is only four times lower than that of Bi_2Te_3 . [36]

Carbon nanotubes (CNTs) are employed in nanoscale electronics, biosensing, and field-emission displays because of certain special electrical and mechanical characteristics.[125, 126] Carbon nanotubes (CNTs) have recently been employed as an active supplement to improve conjugated polymers' TE performance.[127-133] It is feasible to apply CNT/conducting polymer composites without compromising the chemical structure of the nanotubes by physically modifying the CNT/conducting polymer composites created by stacking the conducting polymer molecules on the CNT sidewalls.[134-136] Single-walled CNT/PEDOT:PSS nanocomposite films with 85 wt% CNTs showed power factors up to $140 \mu\text{Wm}^{-1}\text{K}^{-2}$, [127] whereas, single-walled CNT/PANI nanocomposite films with 64 wt% CNTs exhibits power factors of $176 \mu\text{Wm}^{-1}\text{K}^{-2}$. [129] A PEDOT/SWCNT composite film with 35% SWCNT displayed the maximum power factor $37.8 \mu\text{W m}^{-1}\text{K}^{-2}$ which is 1.7 times higher than the films without containing SWCNTs.[133] The density of the electrical pathway can be increased by incorporating CNTs to the conjugated polymer matrix, thus enhancing the electrical conductivity as well as the TE performances. Though PEDOT-Tos shows a great promise in TE application yet the material has not been explored. Further reports on nanocomposites of PEDOT-Tos with inorganic counter parts are very scanty. In the present study, EDOT is polymerized in situ, to synthesize PEDOT-Tos using *p*-Toluenesulfonic acid (pTSA) as a source of tosylate group. The power factor ($S^2\sigma$) and hence the figure of merit (ZT) of the conducting polymer nanocomposite containing PEDOT-Tos have been enhanced by incorporation of Single-walled carbon nanotubes (SWCNTs) during the polymerization.

4.2. Enhancement of Thermoelectric Performance in Oligomeric PEDOT-SWCNT Nanocomposite via Band Gap Tuning

4.2.1. Experimental

4.2.1.1. Materials Used

3,4ethylenedioxythiophene (EDOT) monomer and pyridine were purchased from Sigma Aldrich. Iron trichloride (FeCl_3), acetonitrile, n-hexane, ethanol, and butanol were purchased from merck chemicals. pTSA was purchased from alfaesar. Deionised water was purchased from hydrolab, India. SWCNT was purchased from US Research Nanomaterials, Inc.

4.2.1.2. Synthesis of PEDOT-Tos

For the synthesis of pTSA doped PEDOT (PEDOT-Tos) conducting polymer, a solution was prepared by using 0.02 mol of FeCl_3 which was dissolved into 25 ml of acetonitrile under magnetic stirring. This solution is named as solution A. 0.01 mol of EDOT was dissolved in 15 ml of n- hexane and named as solution B. A third solution was prepared by 0.02 mol of pTSA in 20 ml butanol and named as solution C. Pyridine was used as an inhibitor of the whole synthesis process. In a typical process, solution A was added to solution B drop by drop. After 15 min stirring, to regulate the polymerization kinetics, Pyridine was added (0.5 mol per 1 mol pTSA) into the mixture of solution A and solution B and was kept stirring at room temperature for 21 hrs. Solution C was then added to the resultant mixture and was kept stirring for 3 hrs at room temperature. The product was collected by centrifugation for 5 min at 7000 rpm and rinsed with deionized water and ethanol in sequence and finally dried in vacuum at $70\text{ }^\circ\text{C}$. We name the pristine sample as sample I.

4.2.1.3. Synthesis of PEDOT-Tos-SWCNT nanocomposite

For the synthesis of PEDOT-Tos-SWCNT nanocomposite, solution A was prepared as discussed above. Solution B was prepared using SWCNT and 0.01 mol of EDOT in 15 ml of n- hexane and ultrasonicated for 1 hr. Solution A was dropped into the SWCNT dispersed solution drop by drop and after 15 min Pyridine was added as described above and the mixture was kept stirring at room temperature for 21 hrs. Solution C as described above was then added into the mixture and was kept stirring at room temperature for 3 hrs. The product was collected by centrifugation for 5 min at 7000 rpm and rinsed with deionized water and ethanol in sequence and finally dried in vacuum at 70C⁰. The SWCNT content was calculated and comes out to be 3 % (Sample II). The above procedure was again repeated for different weight of SWCNT and the weight percentages calculated comes out to be 9 % (Sample III), 17 % (Sample IV), and 27 % (Sample V) respectively.

4.3. Characterization

The samples were structurally characterized by powder x-ray diffraction (XRD) patterns, UV-vis and field emission scanning electron microscopy (FESEM). X-ray powder diffraction measurements were performed using a diffractometer (BRUKER D8 Advance) with Cu K α radiation ($\lambda = 1.54182$ °A). FESEM images were obtained using a Hitachi (S3400N) to get an idea of the surface morphology of the samples. The UV-vis spectra of the prepared samples were recorded by a spectrophotometer (Perkin-Elmer-USA, Lambda-45) using samples dissolved in ethanol in quartz tube with data being recorded in the wavelength range 300– 1050 nm. The variations of the electrical conductivity (σ) as well as the thermoelectric power (S) with the SWCNT concentration

were carried out at room temperature for all the samples. The electrical conductivity of the samples was measured by four probe method. For the measurement of thermoelectric power, temperature difference has been established along the ends of the samples, while the corresponding potential drop was measured by a Hewlett Packard data acquisition system (Model No. 34970A). Room-temperature thermal conductivity measurements were carried out for the prepared samples using a Hot Disk thermal constants analyzer (TPS 2500 S, Sweden).

4.4. Results and Discussion

4.4.1. Electrical Characterization

4.4.1.1. Electrical Conductivity

Figure 4.1a shows the variation of electrical conductivity σ with the SWCNT concentration. The σ value increases gradually with the increase in SWCNT concentration (Sample II) and the value increases significantly for Sample III followed by its drastic rise in case of Sample IV and Sample V reaching a maximum value of 2770.6 Sm^{-1} . The values of electrical conductivity in each case are much higher than that of PEDOT-MWCNT nanocomposites.[137] The enhancement in the σ value suggests a change in the band gap and molecular energy levels of PEDOT-Tos-SWCNT nanocomposite. The σ value follows a power law with the SWCNT concentration [138]

$$\sigma = \sigma_0(P-P_c)^t \quad (4.1)$$

where σ_0 is a proportionality constant related to intrinsic conductivity of SWCNT, P is the weight fractions of SWCNT in the nanocomposites, P_c is the critical weight fraction related to percolation threshold.

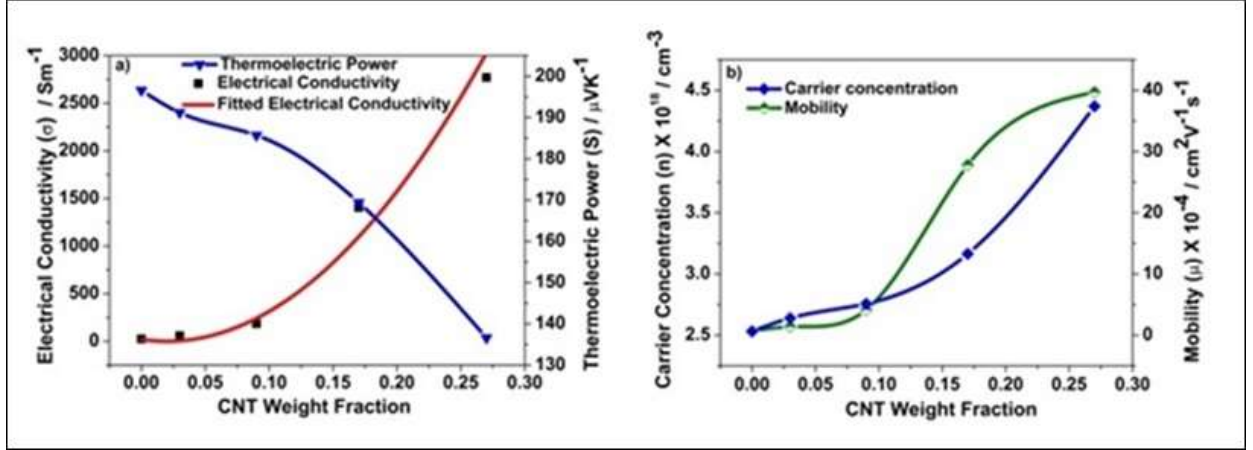


Figure 4.1. Variation of a) Electrical Conductivity and Thermoelectric Power. b) Carrier concentration and mobility with SWCNT weight fraction

Equation (4.1) fits well with the experimental result with $\sigma_0 = 4.7 \times 10^4 \text{ Sm}^{-1}$, $P_c = 0.02$. The threshold value comes out to be 0.02 weight fraction of SWCNT. Moreover, it is revealed that the electrical transport is dominated by the tunnelling phenomenon above the percolation threshold as it reflects from Figure 4.1a.[127]

4.4.1.2. Thermoelectric Power

The variation of thermoelectric power (S) with the SWCNT concentration was depicted in Figure 1a. The S value is reduced to $136.6 \mu\text{VK}^{-1}$ for the Sample V from $196.6 \mu\text{VK}^{-1}$ in case of the Sample I. The decreased value is attributed to the relatively low value of S of SWCNT.[139] Since the electronic environment of the charge carriers influences the value of S, the S values of the nanocomposite lies in between S_{pristine} and S_{SWCNT} . This is since above the value of P_c , the probability of tunnelling is more predominant for the compact SWCNT bundles creating a pathway for the charge carriers. The carrier concentration (n) is evaluated from Mott relation [140] given by

$$S = \pi^2 k^2 m^* T / ((3\pi^2)^{2/3} \hbar^2 |e| n^{2/3}) \quad (4.2)$$

where m^* is the effective mass of the majority carriers having a value of $0.121m_e$ for PEDOT.[141] The n value increases with the increase in the SWCNT content as is seen from Figure 4.1b. This low value of n is supposed to suppress σ . Probably mobility of the charge carriers plays a key role for the high values of σ . The variation of mobility of the charge carriers with SWCNT concentration is depicted in Figure 4.1b.

4.4.1.3. Power Factor

The power factor ($S^2\sigma$) has been evaluated and shown in Figure 4.2a. At the low concentration of SWCNT there is a little increase in $S^2\sigma$. With further increase in SWCNT concentration power factor increases drastically and finally tends to saturate at higher concentration of SWCNT.

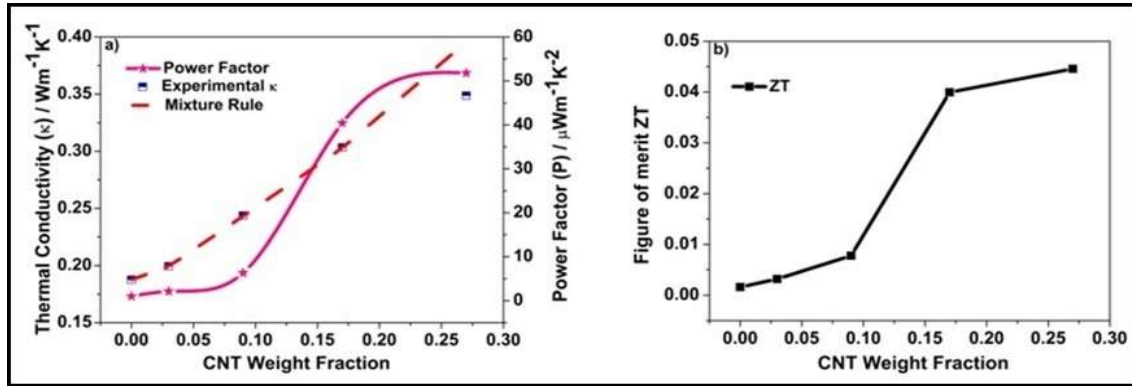


Figure 4.2. Variation of a) Thermal conductivity and Power factor b) Figure of merit with SWCNT weight fraction

A maximum value of $51.8 \mu\text{Wm}^{-1}\text{K}^{-2}$ have been achieved for Sample V which is higher than the reported values at this concentration level of CNT. [128, 133] The addition of SWCNT increases the degree of delocalization of the charge carriers within the π conjugated structure of PEDOT-Tos-SWCNT nanocomposites with a low value of carrier

concentration. However, presence of SWCNT enhances the carrier mobility which is primarily responsible for the enhancement of power factor.

4.4.1.4. Thermal Conductivity and Figure of merit

The increase in the value of thermal conductivity (κ) with the increasing concentration of SWCNT is very small even at higher concentration which is noteworthy as individual κ for SWCNT is rather extremely high (Figure 4.2a).[139] A mixture rule according to Maxwell [142] fitted well with the graph at lower concentration but fails at higher concentrations of SWCNT (Sample V). The Wiedemann-Franz's law ($\kappa/\sigma T \approx L_0$) is followed by an electron system with elastic scattering where $L_0 = 2.45 \times 10^{-8} \text{ (V/K)}^2$. The estimated Lorentz number ($\kappa/\sigma T$) of the samples in comparison to L_0 , is a signature of the portion of heat carried out by electrons. The sample Lorentz numbers are large enough, ranging from 2.5×10^{-5} to $4.1 \times 10^{-7} \text{ (V/K)}^2$, which indicates that the lattice contribution dominates the total κ value rather than the electronic contribution. Reports show that the selective scattering of phonons by the inclusion of nano interfaces minimizes the lattice contribution depending on their respective scattering length.[143] Here the SWCNTs are connected to the polymer matrix by weak van der Waal forces [94] introducing the interfaces which obstruct of phonon transport but facilitate the electrical transport.

The figure of merit (ZT), as calculated from the above data, increases with the increase in SWCNT content reaching a maximum value of 0.045 for sample V (Figure 4.2b) which is twice than that of PEDOT/SWCNT composite films prepared by vapor phase polymerization [133] at this SWCNT percentage. Further this value though less than PEDOT-Tos thin film but is still higher than the reported values for bulk PEDOT based nanocomposite materials. [87, 94, 101 123,143, 144] This signifies that the increasing

concentration of SWCNT expand the pathway for the electric transport without notably raising the thermal transport which is a favorable condition for the improvement of the transport properties thereby enhancing the figure of merit.

4.4.1.5. Relation between all electrical parameters

A correlation between the S , $S^2\sigma$ and σ for all the samples has been shown in Figure 4.3a. It is observed that though the thermoelectric power decreases, the power factor increases with the increase in electrical conductivity thereby showing that the decrement in the thermoelectric power does not suppress the increment in the power factor.

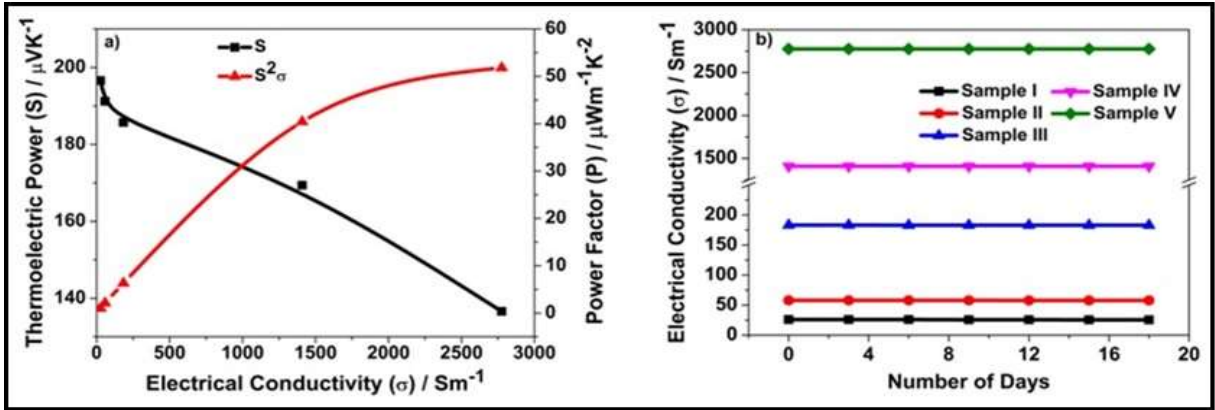


Figure 4.3. Variation of a) Thermoelectric power and Power factor with electrical conductivity b) Electrical conductivity with number of days.

Moreover, the increase in the ordered structure decreases the thermoelectric power due to the band gap tuning which in turn increases the carrier concentration pushing the Fermi level (E_F) into the conduction band increasing the electrical conductivity. As a result, there is an overall increase in thermoelectric power factor which help in the increment of ZT. To observe the air stability of the samples for device applications, the samples were kept at normal atmosphere and measurement of σ was taken after a gap of 3 days till 18

days (Figure 4.3b). No anomaly has been detected during this period and the samples are very much stable in air at room temperature.

4.4.2. Structural Characterization

4.4.2.1. X-ray Diffraction (XRD) Analysis

The ordering of the molecular structure highly influences the electrical transport properties of polymer-based composite. [145-147] The van der Waal and the strong π - π interaction are assumed to be the route for the charge carrier transport. Thus, in order to determine the influence of the structural change of PEDOT-Tos, induced by the addition of different percentage of SWCNT on the transport properties, XRD of the synthesized samples was performed and shown in Figure 4.4a.

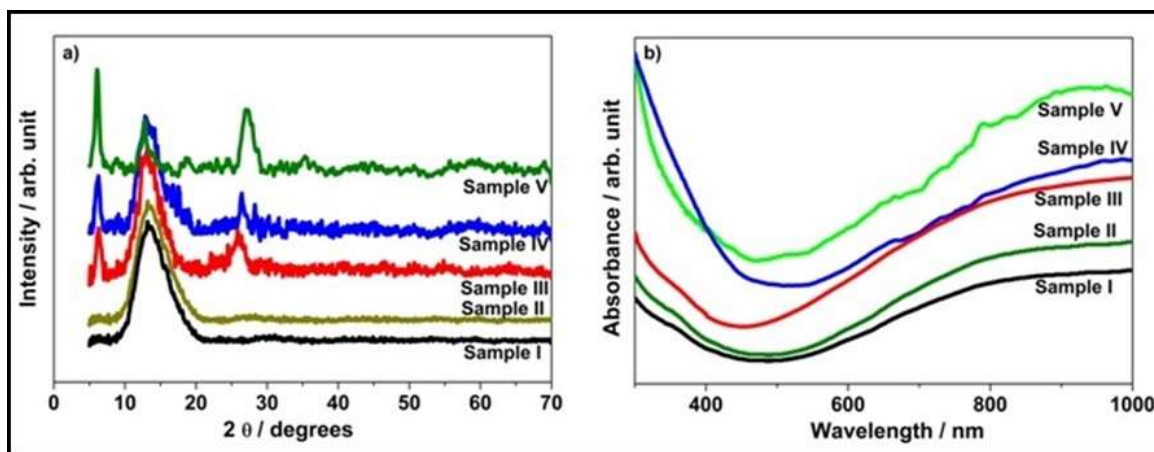


Figure 4.4. Spectral analysis of the synthesized samples a) XRD b) Uv-vis spectra.

In case of pristine PEDOT, X-ray diffraction peaks centered at 6.5° , 13.7° and 28.4° attribute to the (100) (200) and (020) reflection of the polymer backbone with the lattice spacing 13.6 \AA , 6.5 \AA and 3.2 \AA , respectively, which is in tune of other reports. [51, 148] The reflection of these three peaks ensures the presence of crystalline phase. Comparing

the peak positions of the synthesized samples it is observed that there is a change in the peak position in the X-ray diffraction pattern for the composites. For the peak position at $2\theta \sim 6.5^\circ$, a shift towards a lower angle is observed for all three composites, which points out a change in the lattice parameters [149] and with the increase in the SWCNT content the shift increases. It is proposed that the peak at 6.5° is related to the interchain distance within the stack. Thus, the shift points towards an increase in the stacking distance. Further an increase in the intensity is also observed at this peak position with the increase in SWCNT content. This increase in the stacking distance along with the increase in intensity signifies that the crystallinity is upgraded.[148] This improved packing may increase the tunneling of the charge carriers between the chain stacks as well as within the stack. Moreover, significant changes in the XRD pattern were observed for the samples containing 17% and 27% of SWCNT. Peaks appeared at $2\theta \sim 44.2^\circ$ which indicate the presence of SWCNT and the intensity increases with the increase in the SWCNT content. Further, the peak at $2\theta \sim 28.4^\circ$ which is attributed to the π - π stacking distance shifted to a higher angle and get shaped with the increase in the SWCNT content. This indicates a decrease in the interlayer stacking distance. It enhances the π - π coupling providing a pathway for the charge carriers enhancing the TE properties.

4.4.2.2. Uv-vis spectroscopy

The shift as well as increase in intensity at peak positions $2\theta \sim 6.5^\circ$ and 28.4° with the increase in the SWCNT content is a signature of formation of ordered structure.[148] Here SWCNT is assumed to take part in the bottom-up stacking leading to a well-ordered structure which in turn influences the transport properties of the samples. The UV-Vis spectroscopy confirms the change in the electronic states and shown in Figure 4.4b. The

absorption band around 600 nm attributes to the π - π^* transition.[51] Moreover, the delocalization of the charge carriers on the polymer chains is indicated by the free carrier tail at the longer wavelength. [150, 151] The free carrier tail is much prominent with the increase in SWCNT content thereby indicating an increase in the delocalized charge carriers.

4.4.2.3. Field emission scanning electron microscopy (FESEM)

Study of field emission scanning electron microscopy (FESEM) was carried out to further investigate the morphology along with the reorganization process and structural development of PEDOT-Tos in the presence of SWCNT as shown in the Figure 4.5. The pure sample (without SWCNT) displays a granular like structure. The morphology of the samples (3% and 9% SWCNT) is governed by a decrease in grain size and much more packed together as is observed from the FESEM images.

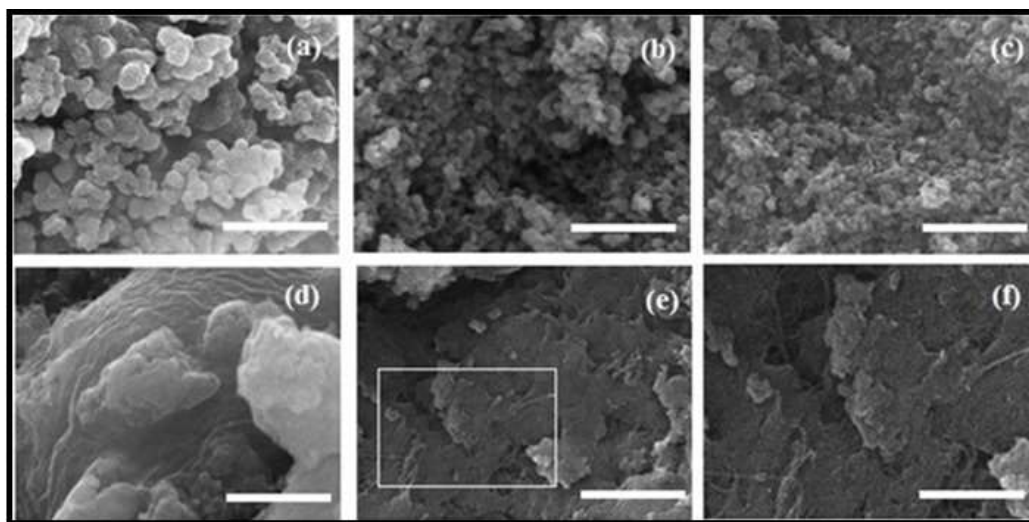


Figure 4.5. FESEM images a-e) Sample I-V, scale bar 1 μ m f) Magnified portion of sample V, scale bar 500 nm.

This spatial compact nature increases with an increase in the SWCNT content in the polymer matrix. Further a morphological transformation is also observed for the samples above 0.17 weight fraction of SWCNT content. Finally Sample V shows a more ordered structure with much more compactness. Thus, the result clearly shows that induction of SWCNTs restructures the PEDOT-Tos matrix to a more crystallize form through the formation of improved compact structure. It is known that a more ordered structure is always favorable for the charge transport [152] and hence influence the transport properties.

4.4.3. Theoretical analysis via DFT

In this bulk material, PEDOT can exist in different stereoisomers which may affect the ZT value of the material. To understand the actual situation we chose an oligomer, instead of polymer for simplicity in calculations, having four monomers joined together. This oligomer can form four stereoisomers (i) all cis, (ii) all trans, (iii) trans with cis and (iv) cis-trans-cis as shown in the top of the figure 4.6a. It is interesting to note from DFT study that cis configuration between two rings introduce a curve in the molecule which produce a cavity with small radius of curvature, unsuitable to accommodate nanotubes. These molecules are less contributing to ZT value of the material. However, the molecules with trans configurations (ii and iii) are planer and fully conjugated (from HOMO and LUMO; Figure 4.6a) produce enough surface for π -staking interactions with SWCNT. The HOMO and LUMO values of these configurations construct a wide valence and conduction band, respectively.

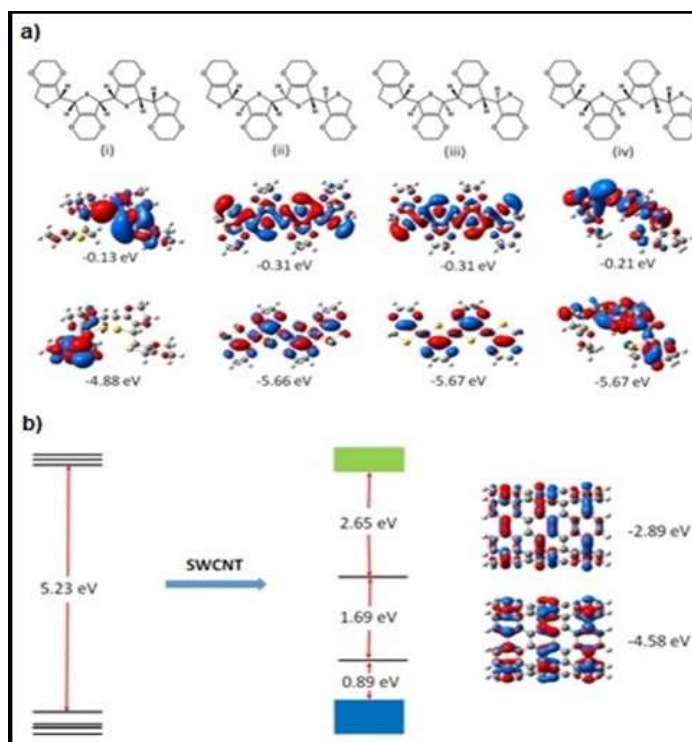


Figure 4.6. a) Probable stereochemistry of the oligomeric bulk material and their HOMO and LUMO b) Energy profile diagram of the PEDOT before and after SWCNT doping.

The band gap is of 5.23eV, quite higher value for semiconductor properties of the pure material (Figure 4.6b). Doping of SWCNT in the PEDOT-Tos, the HOMO and LUMO of it lie in between the bands and fit such a way that the electron from valence band can go to conduction band easily for maximum 2.63 eV energy (Figure 4.6b). In this way PEDOT-Tos-SWCNT nanocomposites become as organic TE material with high ZT value.

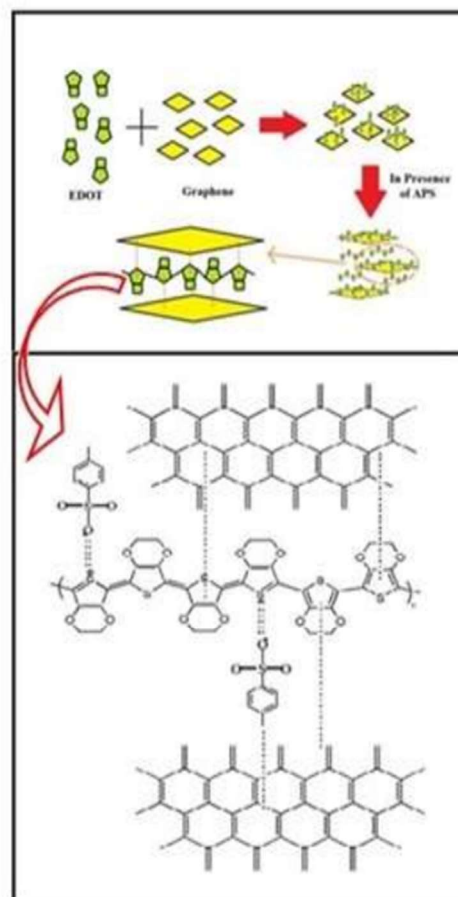
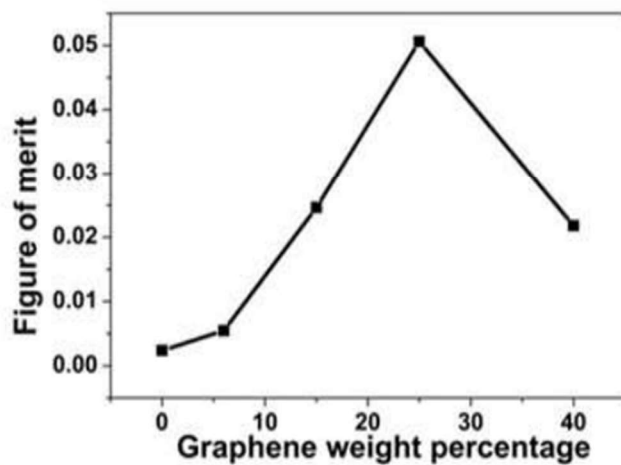
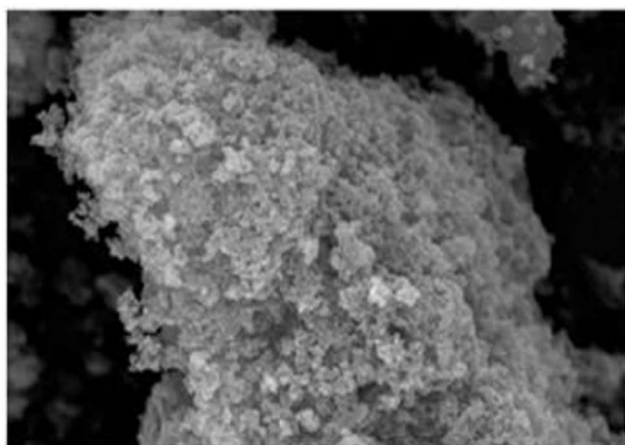
4.5. Conclusions

In summary, PEDOT-Tos-SWCNT nanocomposites have been synthesized by in-situ polymerization with the variation of SWCNT content. For electrical characterization the measurement of σ and S as a function of SWCNT content has been carried out. It is observed that σ increases but S decreases. Though the S values are much higher than

reported ones. Improved degree of crystallinity via the band gap tuning as depicted from DFT calculations, boost up the electrical conductivity which in turn enhance the TE power factor. We ascribe that this effort of improving the degree of crystallinity to pick up the electrical conductivity via band gap tuning is a way to enhance the thermoelectric power factor and hence the figure of merit of conjugated polymer-based nanomaterials. Furthermore, the very low κ values along with high power factor leads to a high value of ZT (0.045). To the best of author's knowledge this value is more than the reported polymer based bulk nanostructured materials.

Thus, the study validates the increase in the TE performance by incorporating SWCNT in PEDOT-Tos and may be constructive in the domain of design and synthesis of polymer nanocomposites for TE applications. The cost-effective procedure, nontoxic properties, and scalability, is the key for the polymer nanocomposites to be used as TE materials. Furthermore, through variation of different parameters and optimization of the constituent composition, there is scope to improve the TE performance of PEDOT-To nanocomposites.

CHAPTER 5: PEDOT BASED GRAPHENE COMPOSITE SYSTEM



5.1. Introduction

One of the major threats facing the 21st century is the crisis of energy. To improve the current efficiency of energy, the conventional fossil fuels are replaced by alternative energy sources viz solar energy, hydrogen energy, biomass energy etc. Now a day, a substantial amount of heat energy is irresistibly generated and wasted in daily life and industrial production. Thermoelectric (TE) materials have potential to convert heat energy directly to electrical energy utilizing the waste heat source [1-3]. This creates an interest in the application of TE materials starting from cochlear implant to thermal charging of photo-detectors and LED. TE devices have some individual advantages other than new energy technologies, such as no noise and long operating lifetime. Performance of a TE material is expressed by its dimensionless figure of merit $ZT = S^2\sigma T/\kappa$, where S is the thermoelectric power or Seebeck coefficient, σ is the electrical conductivity, T is the absolute temperature and κ is the thermal conductivity respectively. But the parameters are so interconnected that achieving a high ZT value is a challenge. During the last three decades research on TE materials progressed a lot since the work of Dresselhaus [153].

Graphene in recent years attracted a lot of attention as a potential TE material due to some of its unique features viz. high carrier mobility and hence high electrical conductivity, two-dimensional (2D) structure etc. Through density functional theory (DFT) calculations a high ZT value of 5.8 of graphene has been reported [154]. But at the same time its high thermal conductivity ($2500\text{-}5300\text{ Wm}^{-1}\text{K}^{-1}$) [155, 156] makes it a weak challenger for TE applications. Since a combination of high electrical conductivity and low thermal conductivity makes an efficient TE material, latest research focuses on

organic polymer TE and their graphene nanocomposites, due to low cost, ease of synthesis and their intrinsic low thermal conductivity. Further the flexibility of the polymers assists them to be incorporated in different topologies.

Consequently, the research on combination of polypyrrole and polyaniline with graphene exhibits a good choice for improving the thermoelectric properties [157-159]. Nevertheless, the ZT values ($\sim 10^{-3}$ to 10^{-4}) are much lower than that of inorganic semiconductors due to low Seebeck coefficient (or thermoelectric power) S. This is followed by the synthesis of PEDOT-PSS graphene nanocomposites for TE applications and attracted much attention [108] but still have low S values. Contrary to PEDOT-PSS, PEDOT-Tos exhibits superior TE performance as has been demonstrated by Bubnova *et al* [20], yet the polymer graphene nanocomposites have been unexplored. It has been reported that the thermoelectric power depends on the density of states (DoS) slope at the Fermi level E_F [21] and through the modification of crystallinity of PEDOT, changes in the DoS can be achieved [20]. For PEDOT, with the increase in the structural order there is an improvement in the carrier delocalization and π orbital overlapping [47] influencing the electronic band structure which influences the charge transport properties. Consequently, it has been suggested that for PEDOT-Tos increase in the structural order, modify the DoS affecting both the electrical conductivity and thermoelectric power positively [20].

In the present study, we focus on the increase in the crystallinity of PEDOT-Tos with the incorporation of graphene. Since the structural order affects the charge carrier transport, a mapping between the structural order and the charge carrier transport has been done. The source of the interconnection between the structural order and the charge carrier transport

are discussed and supported by the spectral analysis and temperature dependent electrical conductivity.

5.2. Dependence of thermoelectric power and electrical conductivity on structural order of PEDOT-Tos-graphene nanocomposite via charge carrier mobility

5.2.1. Experimental

5.2.1.1. Material used

3,4ethylenedioxythiophene (EDOT) monomer was purchased from Sigma Aldrich. Para toluene sulfonic acid (pTSA) and ammonium peroxydisulfate (APS) were purchased from alfa-aesar. Graphene was purchased from Platonic Nanotech Pvt. Ltd. Ethanol was purchased from merck chemicals. Deionised water was purchased from hydrolab, India.

5.2.1.2. Synthesis of PEDOT-Tos by in situ polymerization

PEDOT is synthesized by using in situ polymerization of EDOT monomer in an aqueous solution of PTSA, using APS as oxidant. The solution of EDOT (0.02 mol) which was dissolved in an aqueous solution containing PTSA (0.04 mol) was stirred with a magnetic stirrer, for 30 min at room temperature. APS was used as oxidant and was prepared by dissolving APS (0.02 mol) in 100 ml of water. In the following steps the APS solution was added drop-wise to the aqueous solution of EDOT monomer and the reaction mixture was stirred for 24 h at room temperature. A dark blue precipitate was formed, indicating PEDOT (doped with PTSA). After 24 h the product was collected by centrifugation for 5 min at 7000 rpm and rinsed with deionized water and ethanol in sequence then finally dried in vacuum at 70 °C. We named the sample as S-I.

5.2.1.3. Preparation of PEDOT-Tos/Graphene nanocomposites

For the preparation of nanostructured PEDOT-Tos/Graphene nanocomposite doped with PTSA, graphene was added in a pre-prepared aqueous solution containing PTSA (0.04 mol) and was constantly stirred for 30 min and then ultrasonicated again for 30 min to obtain a well dispersed solution. EDOT (0.02 mol) was mixed to the solution and was constantly stirred for 30 min. This is followed by the addition of APS (0.02 mol) as oxidant to the solution and the reaction mixture was stirred for 24 h at room temperature for direct synthesis of PEDOT-Tos/Graphene nanocomposites. The final product obtained after polymerization was centrifuged for 5 min at 7000 rpm and vacuum dried in an oven at 70 °C. The graphene content was calculated and comes out to be 6 % (S-II). The above procedure was again repeated for different weight of graphene and the weight percentages calculated comes out to be 15 % (S-III), 25 % (S-IV), and 40 % (S-V) respectively.

5.3. Characterization

All the prepared samples were structurally characterized by powder x-ray diffraction (XRD) patterns, UV-vis, Fourier transform infrared (FTIR) spectroscopy and field emission scanning electron microscopy (FESEM). X-ray powder diffraction measurements were performed using a diffractometer (BRUKER D8 Advance) with Cu K α radiation ($\lambda = 1.54182$ Å). The UV-vis spectra of the prepared samples were recorded by a spectrophotometer (Perkin-Elmer-USA, Lambda-45) using samples dissolved in ethanol in quartz tube with data being recorded in the wavelength range 350–1000 nm. FESEM images were obtained using a Hitachi (S3400N) to get an idea of the surface morphology of the samples.

For the measurement of electrical transport properties rectangular shaped pellets (10mm x 5mm x 5mm) of all samples were prepared by cold pressing at 1 ton pressure. The electrical conductivity of the samples was measured by four probe method. For the measurement of thermoelectric power, temperature difference has been established along the ends of the samples, while the corresponding potential drop was measured by a Hewlett Packard data acquisition system (Model No. 34970A). Room-temperature thermal conductivity measurements were carried out for the prepared samples using a Hot Disk thermal constants analyzer (TPS 2500 S, Sweden).

5.4. Results and discussions

5.4.1 Spectral Studies

In polymer-based composite, the degree of the structural order stimulates the electrical transport properties [147]. In the present work the strong π - π interaction and increases in structural order are presumed to be the grounds for the enhancement in the charge carrier transport. Thus, the interactions between PEDOT-Tos and graphene for its different weight percentage into the polymer matrix are identified by X-ray diffraction and shown in figure 5.1. The pristine sample shows peaks at an angle 13.6° and 26.1° which are attributed to the reflection plane (200) and (010) [148, 160]. These peaks signify the presence of crystalline phase in the polymer matrix. The XRD spectra of the composites shows a lower angle shift for the scattering angle 13.6° which suggest a change in the lattice parameter till 25 % graphene concentration in the polymer matrix.

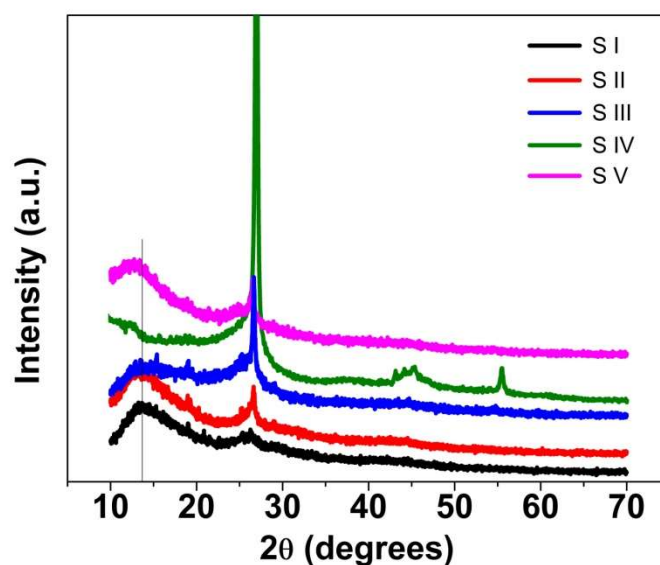


Figure 5.1. XRD spectra of the synthesized samples.

But for 40 % graphene concentration it again shifted to higher angle. All the samples feature a distinct peak at around 26° . This peak is a signature of crystalline nature of PEDOT with increases and ordered π - π interaction of the conjugated units [161]. It is observed that with the increases in graphene content the intensity of the peak increases with a shift to a higher angle till 25 %. Following Bragg's law, the stacking distances were estimated which comes out to be 3.4 Å for the pristine sample. The stacking distance decreases with the graphene content till 25 % (Table 5.1) beyond which the stacking distance increases. This decrease in the interlayer stacking distance and the increase in the intensity of the peak around 26° signify that with the increase in graphene content a closer packing structure is favored with improved π - π coupling, providing a pathway for the charge carriers, stepping up the TE properties. Moreover, it is also observed that 25 wt % of graphene in PEDOT-Tos matrix behaves as the threshold amount beyond which there is a hindrance in the growth of crystallization of the PEDOT-

To creating a barrier to transport the carriers in the composite as observed for graphene-polyaniline nanocomposites [162, 163] and is in tune with the electrical transport properties.

Further we elucidate through UV-Vis and FTIR characteristics of the samples shown in figure 5.2 and figure 5.3 respectively. The UV-Vis spectrum of the pristine sample shows a strong absorption band around 800-900 nm which is assigned to π^* -polaron transition [164]. The spectra of the composite samples, in addition to π^* -polaron transition, also shows a band around 362 nm which is attributed to π - π^* transition.

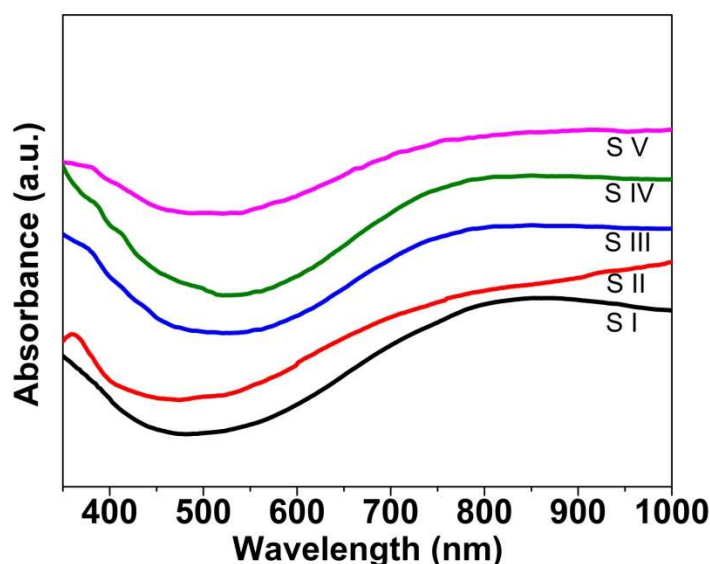


Figure 5.2. UV-vis spectra of the synthesized samples.

This band is red shifted to 378 nm and 387 nm for S-III and S-IV respectively which signify an increase in the interaction between the quinoid ring of the polymer and graphene [143, 157]. Consequently, there is an increase in the delocalization of the charge carriers which in turn increases the electrical transport properties. For S-V the band is blue shifted to 381 nm with respect to S-IV indicating the weakening of π - π^*

transition [163]. It was also observed that the UV-Vis spectra display a trend of a free carrier tail at the longer wavelength for all the samples which indicates the delocalization of the charge carriers [150, 151]. The results reveal the formation of adequate number of charge carriers and PEDOT is in a bipolaronic state.

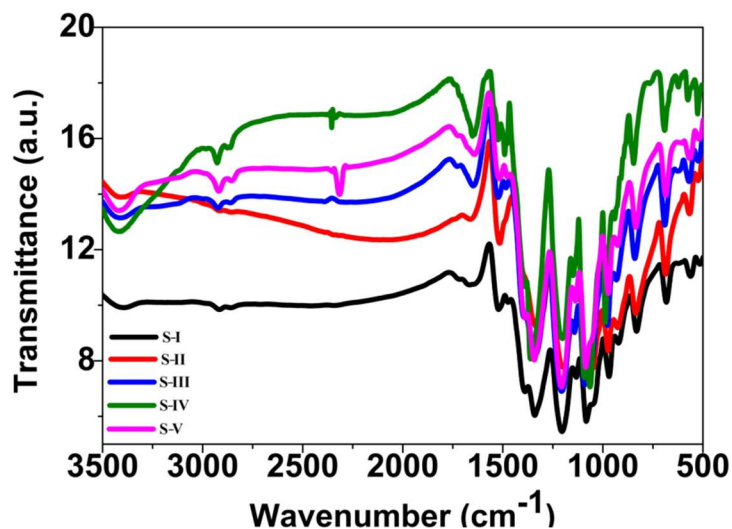


Figure 5.3. FTIR spectra of the synthesized samples.

For the pristine sample the bands observed in FTIR spectra are at 681, 831, 922 and 969 cm^{-1} are assigned to the deformation modes of C-S-C in the thiophene ring [165, 166]. The bands around 1083, 1133 and 1202 cm^{-1} are the signature of C-O-C bending vibration of the ethylenedioxy group [164]. The bands around 1338 and 1519 cm^{-1} are attributed to the C-C stretching and C=C stretching of the quinoidal structure of the thiophene rings [97, 167]. Further the band around 1657 cm^{-1} is assigned to the polarons present in PEDOT. The FTIR spectrum of composite samples show all the bands but with a shift to a higher wave number till 25 %. In addition, a new band around 1481 cm^{-1} is also observed which signifies C=C stretching of the quinoidal structure of the thiophene rings which is also shifted with the increase in graphene concentration till 25 %.

The shift is likely to be the π - π interactions between graphene and the thiophene rings of PEDOT [86]. Consequently, this points out to be a change in the resonant structure of PEDOT with the addition of graphene from a benzenoid structure which supports a coiled conformation to a quinoid one favoring a linear coil conformation resulting in the delocalization of the charge carriers all through the polymer chain [78].

Figure 5.4 shows the Raman spectra of PEDOT-Tos and its nanocomposites containing various percentage of graphene. Pure PEDOT-Tos (fig 5.4) shows peaks at 1254 cm^{-1} corresponding to C-C inter-ring stretching, 1350 cm^{-1} corresponding to single C-C bond stretching, strong peaks at 1425 cm^{-1} of C=C symmetric stretching, while at 1490 and 1550 cm^{-1} correspond to C=C antisymmetric stretching [168, 169, 170].

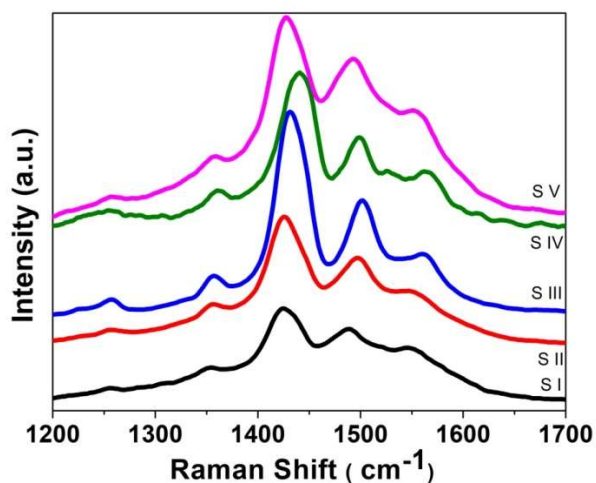


Figure 5.4. Raman spectra of all the synthesized samples.

Changes in the spectra of the nanocomposites are observed which is attributed to the interactions between graphene and PEDOT-Tos. For the nanocomposites samples a shift in the D band towards a higher wave number is observed, compared to graphene. Further it is observed that there is a shift of the G band to a higher wavenumber till sample IV then onwards it again shifts to a lower wavenumber. In addition, comparing the peak

position of PEDOT-Tos at 1425 cm^{-1} , the corresponding peaks for the nanocomposites are shifted to a higher wavenumber of 1440 cm^{-1} till sample IV thereby again it shifted to lower wavenumber for sample V. A similar shift of the band around 1550 cm^{-1} is observed for all samples. These observations follow the same trend of switching of properties beyond 25% graphene content, like the transport properties. This is an indication of π - π interaction between aromatic structures of PEDOT-Tos and graphene [171]. The enhanced transport property of the nanocomposite is probably due to this interaction, which assists the charge transfer processes between PEDOT-Tos and graphene.

5.4.2. Structural Characterization

To further investigate the development of restructuring of PEDOT-Tos with the addition of graphene morphological study has been carried out through scanning electron microscopy (figure 5.5). The SEM image of pristine PEDOT-Tos displays a self-assembled granular structure less compact in nature. With the addition of graphene, the morphology of the sample for S-I show an increase in compactness.

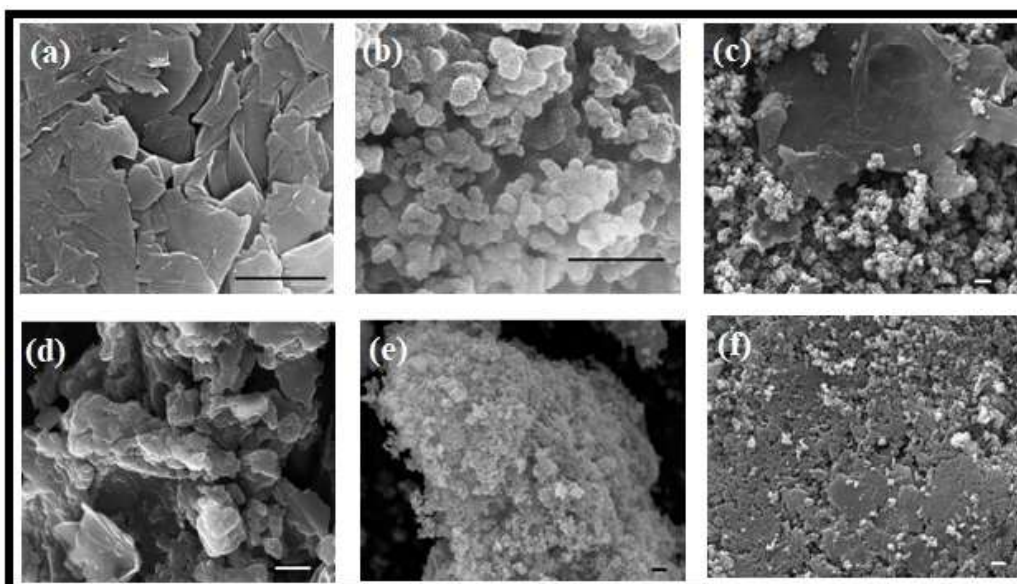


Figure 5.5. FESEM images of (a) graphene and the synthesized samples (b-f) Sample S-I to S-V. Scale bar $1\mu\text{m}$.

With further increase in the graphene concentration in the polymer matrix, this spatial compact nature increases. Further, the SEM images clearly exhibit that the graphene serves as the growth template of PEDOT and the interaction increases with the addition of graphene till S-IV. For S-V we observe that there is again a decrease in the interaction between PEDOT-Tos and graphene which is in tune with XRD, UV-Vis and electrical transport properties.

Thus, addition of graphene in PEDOT-Tos matrix increases the interaction between the constituents resulting in more ordered structure till a threshold value which consequently increases the electrical transport properties. Report shows that a more ordered structure favors charge transport [152].

5.4.3. Electrical characterization

In order to determine the electrical transport properties of the prepared samples, the variation of the electrical conductivity (σ) at room temperature with graphene concentration was measured and plotted in figure 5.6a. The value of σ shows a hike with the increase in graphene concentration reaching a maximum value of 875.2 Sm^{-1} for S-IV, which is more than five times higher than the pristine one, and then it decreases for S-V. The values of electrical conductivity in each case are higher than that of PEDOT-PSS-graphene nanocomposites [172, 173] and PEDOT-rGO nanocomposites. [86] This enhancement in the value of σ indicates a change in structural order of the samples.

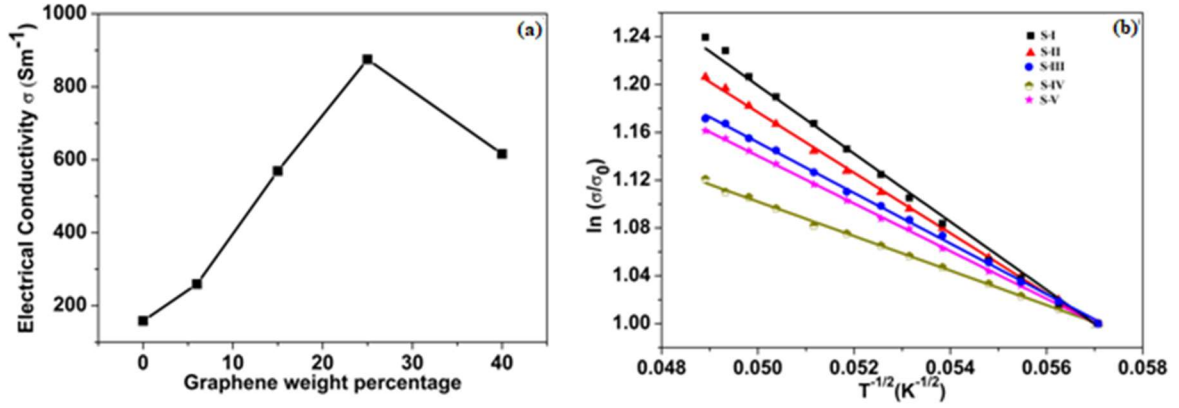


Figure 5.6. (a) Variation of electrical conductivity with percentage graphene weight and (b) temperature dependence of electrical conductivity of all samples

To further investigate the variation of the electrical conductivity with temperature of the prepared samples has been studied and shown in figure 5.6b. For all the prepared samples a rise in σ value has been detected with the rise in temperature representing semiconducting nature. It is well known that for polymers a quasi-one-dimensional variable range hopping (VRH) model explains the electrical conduction mechanism [157, 164]. Along these lines, temperature dependent σ values have been explained according to Mott's VRH model [174]

$$\sigma = \sigma_0 \exp \left[- (T_0/T)^{1/2} \right] \quad (5.1)$$

where σ_0 is the high temperature limit of conductivity and T_0 is the characteristics Mott temperature associated with the carrier hopping barrier.

It is observed that with the increase in graphene loading within PEDOT-Tos matrix T_0 decreases thereby showing that the carrier hopping barrier decreases resulting in an enhancement of σ . Further, the average hopping distance (R_{hop}) and the activation energy (E_{hop}) according to the VRH model is given by [164]

$$R_{hop} = (3/8)(T_0/T)^{1/4} L \quad (5.2)$$

$$E_{hop} = (1/4)k_B T (T_0/T)^{1/4} \quad (5.3)$$

where L is the localization length. Taking the value of the localization length of EDOT monomer units to be 2.29 Å [175] the hopping distance and the activation energy has been estimated at room temperature (Table 5.1).

	d	T₀	R_{hop}	E_{hop}	n	μ
Samples	(Å)	(K)	(Å)	(MeV)	(10¹⁸ x cm⁻³)	(cm²V⁻¹s⁻¹)
S-I	3.4	827.43	1.11	8.32	1.3	7.596
S-II	3.38	651.015	1.04	7.85	1.7	9.522
S-III	3.35	434.055	0.94	7.09	2.4	14.818
S-IV	3.31	346.406	0.89	6.7	3.2	17.089
S-V	3.37	486.846	0.96	7.30	3.9	9.872

Table 5.1. Room temperature values of the characteristic Mott temperature (T_0), hopping distance (R_{hop}), activation energy (E_{hop}), carrier concentration (n) and carrier mobility (μ) of the synthesized samples.

A decrease in the average hopping distance and an increase in the activation energy are reflected. This is a signature of the observed enhancement in the value of the electrical conductivity. In addition, to illuminate the scientific knowledge for the enhanced σ values, the carrier concentration (n) of the samples has been studied from Hall measurement and hence the carrier mobility (μ) has been estimated and the values are tabulated (Table 5.1).

The positive values of R_H (not shown) denote that the majority charge carriers are holes (p-type). A substantial increase in the carrier mobility is observed while the increase in carrier concentration is small. Thus, the enhancement of the electrical conductivity is mainly attributed to the increase in the charge carrier mobility. Generally, for polymeric system, the structure of ordering of polymers greatly influences the electrical transport properties. The ring twisting introduces more π - π conjugate defects resulting in a decrease in the carrier mobility. Here the graphene template most likely helps PEDOT-Tos to switch from a coil-like conformation to an extended conformation thereby increasing the structural order which enhances the hopping rate (including hopping distance and activation energy) within the polymer matrix increasing the value of σ . Further the π - π interaction between the PEDOT-Tos and graphene surface helps to reduce the π - π defects which may be responsible to channel the carrier transport enhancing the charge carrier mobility and hence the electrical conductivity. The decrease in the electrical conductivity is probably due to the following reasons. The excess graphene beyond 25 % probably obstructs the crystallize growth forming barriers to carrier transport. Moreover, the increases in the graphene content beyond this percentage also results in polymer twisting inducing longer hopping distance for the charge carriers resulting in a decrease in the carrier mobility.

The variation of thermoelectric power and power factor with graphene concentration has been shown in Figure 5.7 (a and b). An increase in S is observed reaching a maximum value of $167.2 \mu\text{VK}^{-1}$ for sample S-IV but decrease thereafter.

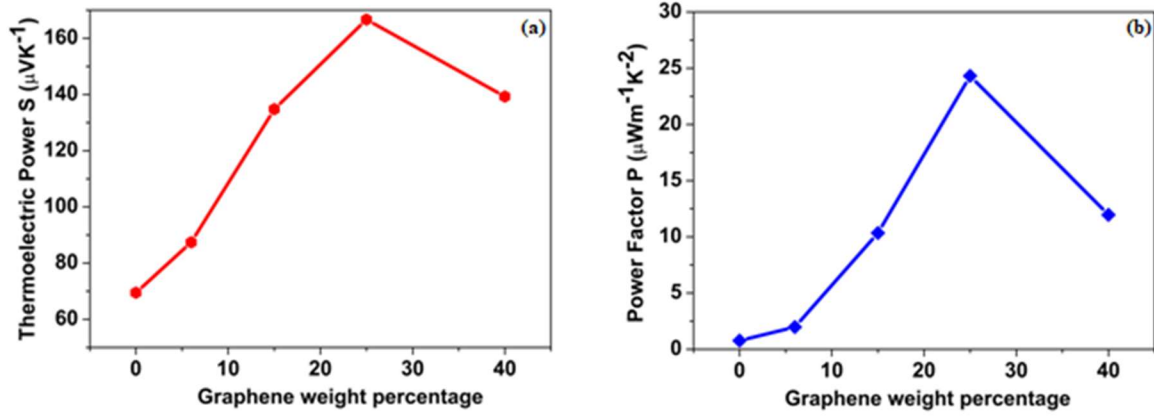


Figure 5.7. Variation of (a) thermoelectric power and (b) power factor with percentage graphene weight.

Since σ and S follow an inverse relation to the gap between narrow transport level and Fermi level, both the parameters cannot increase at the same time [176]. Surprisingly, in the present case both these parameters increase with the increase in the graphene concentration thereby showing that band theory or the electron-phonon scattering based conventional model [177] could not explain the conduction mechanism. To investigate this characteristic of the thermoelectric power, we consider the Mott's formalism consisting of energy dependent mobility $[\mu(E)]$ and carrier concentration (n) terms and is written as

$$S = \frac{C_e}{n} + \frac{\pi^2 k_B^2 T}{3e} \left[\frac{\partial \ln \mu(E)}{\partial E} \right]_{E=E_F} \quad (5.4)$$

where, k_B and C_e are the Boltzmann constant and the specific heat respectively. It is assumed from equation (4) that both n and $\mu(E)$ should influence the thermoelectric power. It is observed that the carrier mobility plays a crucial role till 25 % of graphene content in the polymer since the increase in carrier mobility is much higher than the increase in carrier concentration. Increase in the structural order increases the charge

carrier mobility which in turn increases the electrical conductivity as well as thermoelectric power. Thus, this method proves to be an effective way to improve thermoelectric properties of polymers since enhancement of mobility of inorganic semiconductors now a days are a new route. The decrease of the thermoelectric power after 25 % graphene content is probably due to the increase in the twisted chains producing more defects with the increase in graphene content [178]. This in turn decreases the carrier mobility and the carrier concentration comes into play decreasing the thermoelectric power. Further it has been proposed by Bubnova *et.al.* [20] that with the increase in the structural order the asymmetry of the density of states increases thereby resulting a higher thermoelectric power for PEDOT-Tos. With the increases in crystallinity a broadening of DoS is noticed [21] and it is reported that this broadening is transmitted to all the π bands together with those close to Fermi level [179, 180] which enhances the carrier mobility as well as the thermoelectric power [20]. Here in this case with the increases in the graphene content till 25 % there is an increase in the structural order as well as crystallinity which results in an increase carrier mobility as well as the thermoelectric power. As graphene content is increased beyond 25 % this structural order diminishes resulting in a decrease of the electrical conductivity as well as the thermoelectric power. Since both σ and S values increase with the graphene content, the power factor also increases reaching a maximum value of $24.3 \mu\text{Wm}^{-1}\text{K}^{-2}$ for the sample S-IV, thereby it decreases for the sample S-V.

5.4.4. Thermal Conductivity and figure of merit

The variation of thermal conductivity (κ) with graphene content is measured and studied (figure 5.8).

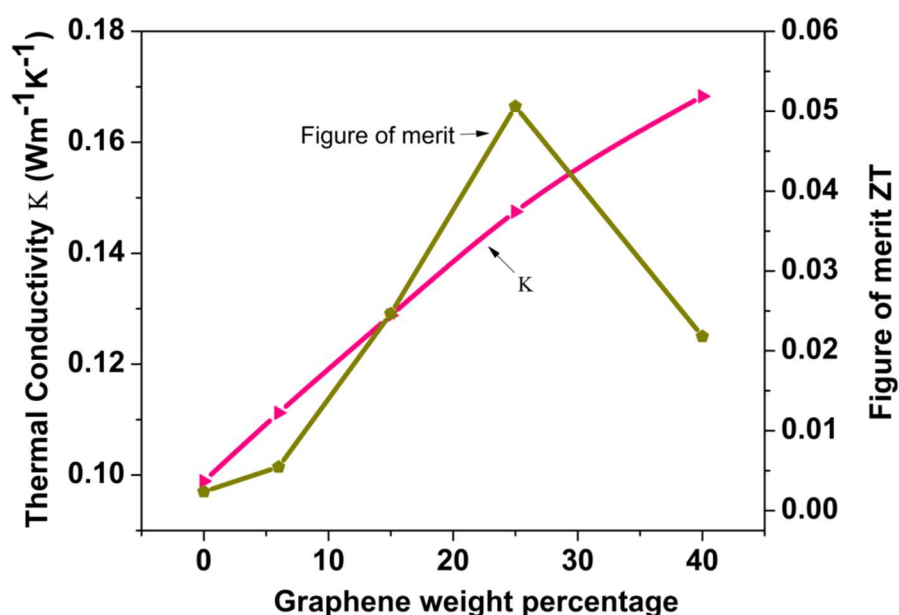


Figure 5.8. Variation of thermal conductivity and figure of merit with percentage graphene weight.

Though the thermal conductivity of graphene is much higher and phonon dominated yet the rise in the κ value with increasing concentration of graphene is insignificant.

The κ values are much lower than the reported graphene based PEDOT nanocomposite [108, 181]. K value comprises of the electron transporting heat κ_e and the phonons travelling through the lattices κ_l . In the present case the κ values are phonon dominated as the electronic contribution is very small. It was observed that the surface porosity and insertion of nano interfaces enhances the scattering of phonons reducing the lattice contribution [143,181]. The graphene multi layers within the PEDOT- Tos matrix probably introduce surface porosity and nano interface which acts as scattering center of phonons reducing the κ_l but the electron mobility can be maintained.

Lastly the figures of merit (ZT) of the prepared samples at room temperature has been evaluated and compared in figure 5.8. The maximum ZT value obtained for S-IV comes out to be 0.0506 which is more than 21 times higher than the pristine sample. Further is it noteworthy that this value is higher than graphene-based polymer nanocomposites [86, 157, 162, 163, 181, 182]. Thus, the increase in graphene concentration within PEDOT-Tos matrix is a signature of enlarging the pathway for the electrical transport till a threshold value without remarkably increase in thermal transport which favor the improvement of the transport properties and as a result the figure of merit increases. There is a scope to further increase the ZT value through variation in the nanostructure of PEDOT-Tos –graphene nanocomposites.

5.5. Proposed mechanism of formation of nanocomposites

The mechanism of the formation of the nanocomposites is schematically shown in figure 5.9. Some of the EDOT monomer adheres to the surface of graphene as soon as it is mixed with the solution containing EDOT and pTSA. The EDOT, absorbed on the surface of graphene acting as template, starts growing in the presence of APS as seen by comparing the SEM micrographs of the nanocomposites. The bonding between the graphene layers and the PEDOT:Tos polymers can be ascribed to π -stacking interactions, the main contribution to which comes from van der Waals forces between the π -systems of graphene and the aromatic thiophene units of the PEDOT chain resulting in an energetically more preferred merging of band structure.

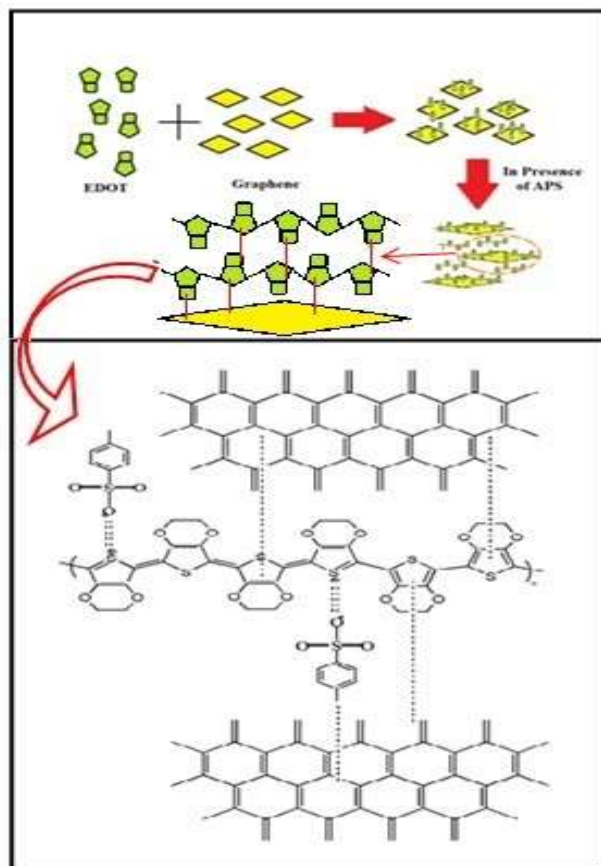


Figure 5.9. Schematic representation of polymerization of EDOT and mechanism of formation of nanocomposites.

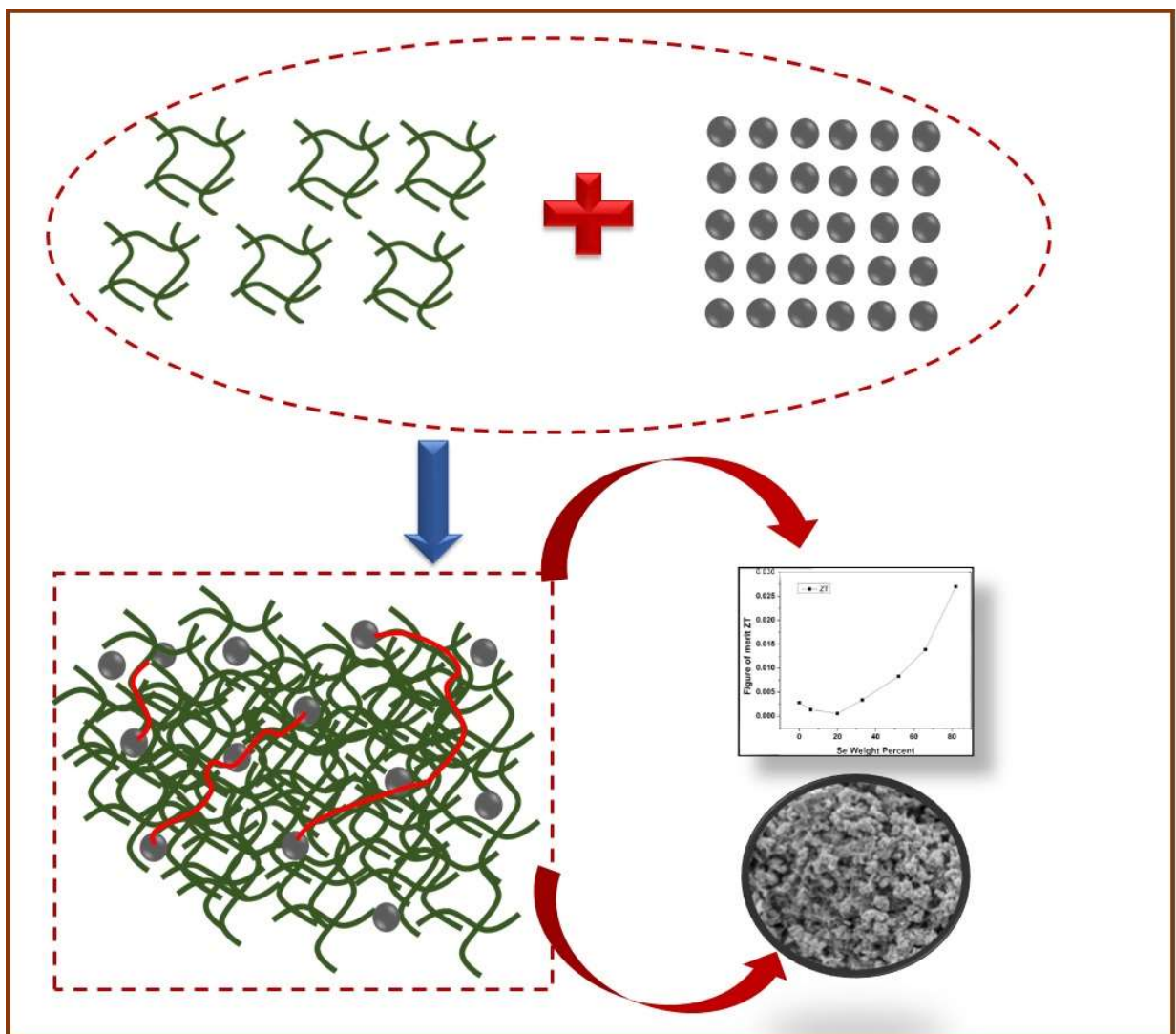
Since the sulphonate, anions neutralize the charges of the EDOT molecules the contributions of electrostatic forces and hydrogen-bonding to the stacking interactions are expected to be minimum. The possible reasons behind the graphene-induced increase in hopping rate and charge carrier mobility have already been discussed before, in the text. This is concordant with an initial decrease in stacking distance with increase in graphene content (upto 25%). The increase of stacking distance with an increase in graphene content beyond 25% can probably arise from increased π -stacking interaction between the graphene layers, with reducing interaction between the graphene and PEDOT layers

(it is to be noted here that thiophene is less aromatic than benzene). This leads to lower π -stacking interaction between the graphene and PEDOT layers and henceforth reduces the stability coming therein.

5.6. Conclusion

PEDOT-Tos-graphene nanocomposite has been synthesized at room temperature via in-situ polymerization. It has been observed from the structural characterization that addition of graphene to the polymer matrix results in more ordered structure. The increase in the degree of ordered structure increases the hopping rate (including hopping distance and activation energy) within the polymer matrix. Moreover, the ordered structure results in π - π interactions leading to a reduction in the π - π conjugation defects in the backbone of the polymer chain. Therefore, the charge carrier mobility of the synthesized samples increases which in turn increases the electrical conductivity. Also, the carrier mobility plays a crucial role till 25 % of graphene content in the polymer to increase the thermoelectric power as well. The change in the thermal conductivity with the graphene content is small and can be attributed to the phonon scattering by the nanointerfaces. The maximum ZT value reaches 0.0506 which is higher than that of PEDOT based bulk nanostructure. This study proves to be helpful in designing and synthesis of polymer nanocomposites for TE applications. Further this method shows an effective way to improve the thermoelectric properties of polymers via the enhancement of mobility of the charge carriers and can be extended to other polymer systems.

CHAPTER 6: PEDOT FUNCTIONALIZED WITH SE COMPOSITE SYSTEM



6.1. Introduction

Global interest in the development of renewable energy has increased as a result of the recent expansion of environmental contamination brought on by excessive consumption of fossil fuels. Because they have the potential to increase the use of the waste heat from the use of fossil fuels, thermoelectric energy conversion devices, among the many pathways, have attracted ongoing interest in the field of renewable energy. The figure of merit (ZT), a dimensionless quantity, $ZT = S^2 \sigma T / \kappa$, where S is thermoelectric power, σ is electrical conductivity, κ is thermal conductivity, and T is absolute temperature, determines how well thermoelectric (TE) materials convert heat energy to electrical energy. [3, 182, 183] Materials should have a high-power factor and low thermal conductivity when used in the thermoelectric area. [184] However, the S , σ , and κ of thermoelectric materials for a particular material are extremely interconnected and in conflict with each other, which makes it challenging to achieve high ZT . [185]

Conductive polymers, provide very advantageous alternatives to the inorganic thermoelectric materials that have received most of the attention. For example, they are environmentally friendly, utilize inexpensive raw ingredients, and are simple to manufacture.[186-189]The most promising of them is poly(3,4-ethylenedioxythiophene, or PEDOT), which has received the greatest attention from several research teams due to its high value when the amounts of doping are altered.[184, 190] An ethylene glycol (EG)-mixed PEDOT:poly(styrenesulfonate) (PEDOT:PSS) film with an exceptional of 639 S/cm was reported by Kim et al.[191]. An EG-treated PEDOT:PSS film with a high value of up to 735 S/cm was created by a different Kim et al. research team.[192] A tosylate-doped PEDOT film with an ideal amount of oxidation was created by Bubnova

et al. and displayed a of 300 S/cm.[36] Although PEDOT materials have high values, their performance is limited compared to inorganic thermoelectric materials because their power factor (S^2) is comparatively low. This is because a high value generated by doping organic polymers often comes with a low S . [193] Numerous research teams have investigated composite ways to increase the S value of PEDOT by using inorganic fillers with high S values in order to get around these inherent problems. Organic-inorganic hybrid thermoelectric materials are the promising candidates for the renewable energy because of the combination of low thermal conductivity of organic thermoelectric materials and high seebeck coefficient of inorganic thermoelectric materials, there is a high possibility to improve the thermoelectric performance.[194] Tunable electrical stability, low cost, and ease in material processing, conducting polymers are widely used as organic thermoelectric material.[195]

Selenium is a viable candidate for hybridization with conducting polymers among the numerous inorganic thermoelectric materials. Thermoelectric materials such as lead selenide (PbSe) and silver selenide (Ag₂Se) can be made from selenium (Se), which is easily synthesized in nanocrystal form and has a high Seebeck coefficient at room temperature of over 1000 V/K [196,197]. However, Se crystal's electrical conductivity is extremely low about 10^{-5} – 10^{-6} S/cm [198]; as a result, Se's own thermoelectric performance is insufficient for any practical usage. So, the incorporation of Se based nanocrystals can be improve the electrical properties of the conducting polymer [113. 199].

In this work PEDOT has been functionalized with selenium (Se) and its structural and electrical transport properties have been investigated. An enhancement of the

thermoelectric properties was observed due to the inclusion of Se in the PEDOT matrix. We propose the formation of interconnected chains of PEDOT with Se which facilitates the electrical transport but hinders the thermal transport thereby enhancing the figure of merit.

6.2. PEDOT Functionalized with Se-Optimization for TE application

6.2.1. Experimental

6.2.1.1. Material used

3,4-Ethylenedioxythiophene (EDOT) was obtained from Sigma-Aldrich (98%) and kept at a low temperature before use. Sodium dodecyl sulfate (SDS) was purchased from SRL. Ferric chloride (FeCl_3) and Ethanol were obtained from Merck. Selenium powder was purchased from RFCL Limited. Deionized water was purchased from Hydro Lab, India.

6.2.1.2. Preparation of hybrid composite

In order to create hybrid composite materials, two substances polymer PEDOT and ingot Selenium nanoparticle are employed. The compounds were developed to get weight percentage variations of Se (6%, 20%, 33%, 52%, 66%, 82%) into the PEDOT polymer using in-situ polymerization.

6.2.1.2.1. Synthesis of Poly(3,4-Ethylenedioxythiophene)

The modified synthesis procedure of the polymer PEDOT was motivated by the previously reported work by Dan Ni et al. [200] PEDOT polymer was synthesized by the self-accumulated micellar prototype method. In this typical procedure, first SDS (30 mmol) was dissolved in 100 ml of deionized (DI) water, and then FeCl_3 (15 mmol) was mixed with that transparent solution and kept for 1 hour stirring at 50° C. After 1 hour of

stirring, the color of the solution turned deep yellow. EDOT monomer (7 mmol) was gradually added to the following solution, and at 50° C, the polymerization process was carried out. After 1 hour, the solution was kept at room temperature for 24 hours. Finally, the products were washed by vacuum filtration with DI water and ethanol several times and dried at 60° C in vacuum for 24 h.

6.2.1.2.2. Synthesis of hybrid composite of Se-PEDOT

For the synthesis of hybrid composites of Se_PEDOT, a similar polymerization process was used as discussed above. Moreover, During the progression of the polymerization process, different weight percentages of ingot selenium nanoparticles are added and stirred for 1 hour, maintaining 50°C. The samples were centrifuged at 5000 rpm for 5 min. several times. The collected samples were dissolved in ethanol, washed by vacuum filtration, and kept dry at 60°C in vacuum for 24 h.

6.3. Characterization

By using Raman spectroscopy, field emission scanning electron microscopy, and powder x-ray diffraction (XRD) patterns, all the produced samples were structurally analyzed. A diffractometer (BRUKER D8 Advance) with Cu K radiation ($\lambda = 1.54182\text{\AA}$) was used to measure the X-ray powder diffraction at an angle range of 10°–70°. Using the materials in powder form, the Raman spectra of the produced samples were recorded by a spectrophotometer (Lab-RAM HR), with data being acquired in the 500–4000 cm^{-1} range. To get an overview of the surface morphology of the materials, FESEM images were taken using an FEI, INSPECT F50.

All samples were cold-pressed into rectangular pellets (10 mm x 5 mm x 5 mm) for the purpose of measuring the electrical transport capabilities. The samples' electrical

conductivity was evaluated using the four-probe technique. A temperature difference along the ends of the samples has been established for the measurement of thermoelectric power, and a Hewlett Packard data acquisition system (Model No. 34970A) was used to measure the linked potential drop. A Hot Disk thermal constants analyzer (TPS 2500 S, Sweden) was used to determine the prepared materials' thermal conductivity at room temperature.

6.4. Result and discussion

6.4.1. Structural Characterization

X-ray diffraction is used to identify the interactions between PEDOT-Tos and graphene for their various weight percentages in the polymer matrix. Figure 6.1a displays the XRD peaks; the peak at $2\theta = 25.9$ corresponds to the structure of the PEDOT chain. [201, 202]

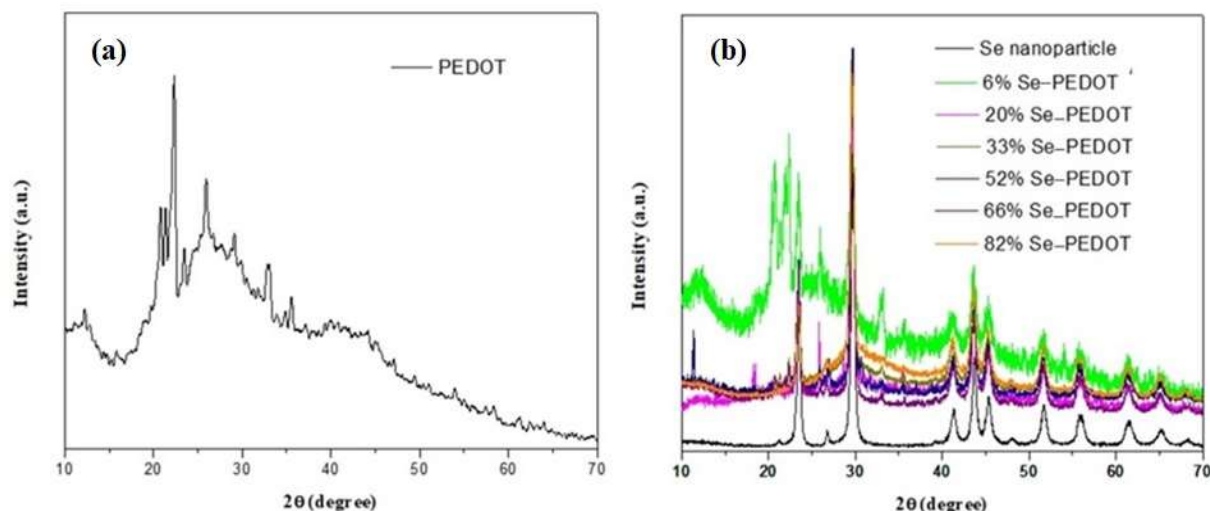


Figure 6.1. XRD analysis of (a) PEDOT (b) various percentage of Se-PEDOT composites

All of the Se nanoparticle's diffraction peaks agree with the crystal structure of pure trigonal phase, and they can all be correlated to the Se phase of trigonal structure with lattice parameters of $a = 0.437$ nm and $b = 0.496$ nm that have been previously published

in the literature. When the amount of Se nanoparticles in the composite is low, as seen in fig. 6.1b, the diffraction peaks are difficult to see. The diffraction peaks become increasingly noticeable as the Se nanoparticle concentration rises, and they are particularly strong for the nanocomposite with 82 wt% Se nanoparticles.

Moreover, this study proposed detailed evidence of the interactions between PEDOT and Se. The distinct peak intensity of PEDOT is upgraded in the composites by incorporating Selenium nanoparticles. This phenomenon suggests that there is an improvement in the ordered structure of the polymer chain due to the incorporation of different concentrations of Se nanoparticles, which in turn influence the charge transport in the composites.

In order to comprehend the interaction between PEDOT and Se nanoparticles better, the Raman spectra of the PEDOT and Se-PEDOT composites were investigated (figure 6.2).

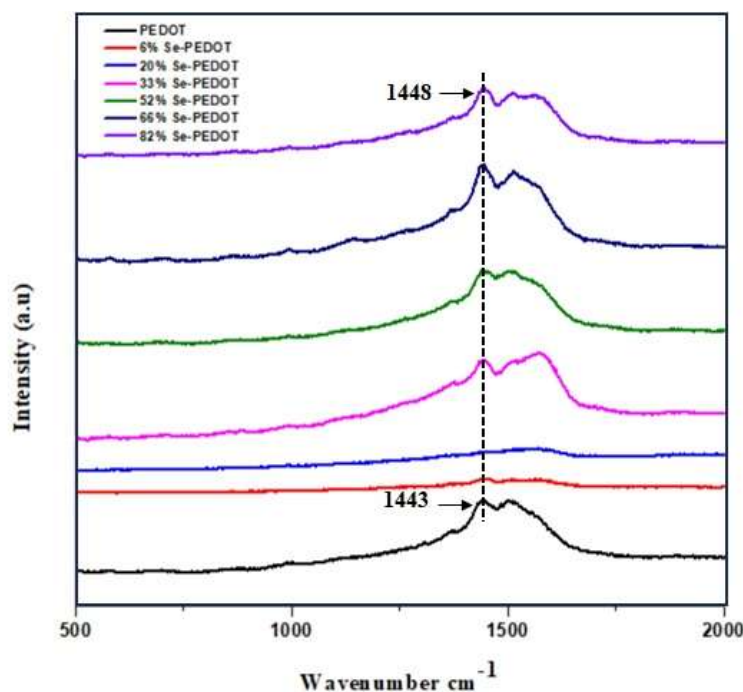


Figure 6.2. Raman spectra analysis of PEDOT and all the Se-PEDOT composites.

It has been established that the interactions between Se nanoparticles and PEDOT change the composites' spectra. The peak at 1443 cm^{-1} indicates the C=C stretching vibration of PEDOT. Furthermore, compared to the PEDOT peak placement at 1443 cm^{-1} , the comparable peaks for the composites are displaced to a higher wavenumber of 1448 cm^{-1} , up to 82% of the Se present in the PEDOT. Due to the Se loading pattern, the polymer chain lengthens in all samples, as seen by the shift change [203]. But no noticeable peak is shown for the 33% concentration of selenium in the composite material, indicating that selenium and PEDOT did not interact.

Figure 6.3 shows FESEM images of pure PEDOT and composites with different Se nanoparticle contents. Randomly distributed Se nanoparticle can be observed, indicating that Se nanoparticles are well dispersed in PEDOT matrix.

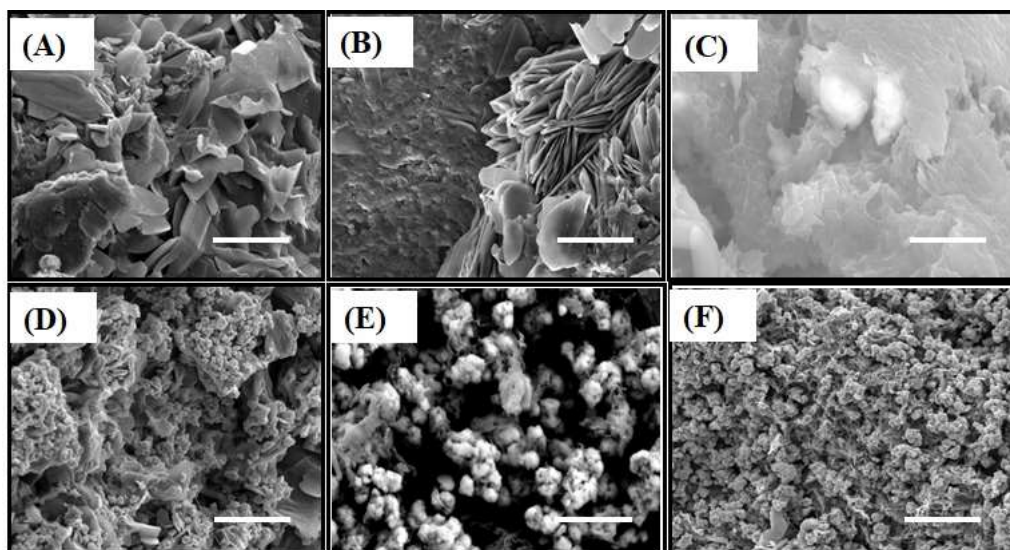


Figure 6.3. FESEM images of (A) PEDOT (B) 6% Se-PEDOT composite (C) 20% Se-PEDOT composite (D) 33% Se-PEDOT composite (E) 66% Se-PEDOT composite and (F) 82% Se-PEDOT composite with $10\text{ }\mu\text{m}$ scale bar.

It is obvious that a percolation network between the PEDOT polymer and the stacked Se nanoparticles in the composite material is formed as a result of the inorganic Se nanoparticle's more electron density than the PEDOT polymer. This network can affect the direction of charge carrier movement.

6.4.2. Electrical Characterization

Figure 6.4 displays the value of the synthesized samples. It has been noted that when the weight percentage of selenium in the polymer matrix increases, the value first drops up to 20% of selenium-PEDOT composite before starting to significantly rise to a maximum of 82% of selenium-PEDOT polymer.

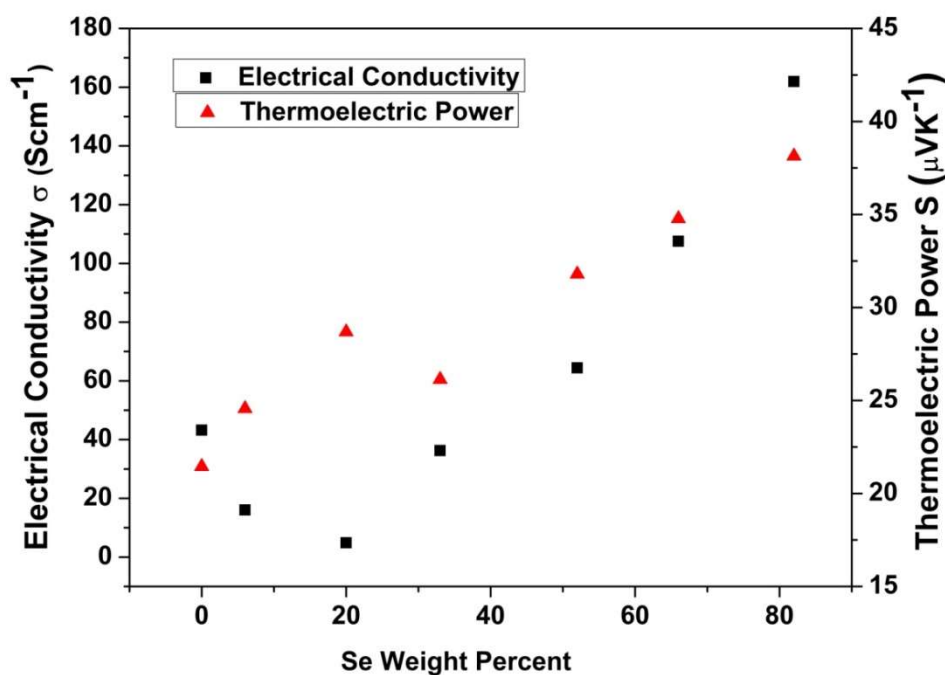


Figure 6.4. Variation of electrical conductivity and thermoelectric power with Se content

The values of Se functionalized PEDOT are significantly greater than those of several PEDOT-based composites. [86, 173]. Within the crystallites in semicrystalline conjugate

polymers, which display appreciable degree of crystallinity along with extensive π - π stacking, para crystalline disorder restricts the transport of charges through the presence of traps [204]. Due to the addition of Se in the PEDOT matrix till 20% Se-PEDOT composite there is a probable change in the micro structure escalating electronic traps within the lamellar stacks of PEDOT. This results in the decrease of the σ value with the addition of Se till 20%. Introduction of Se reduces the π - π stacking distance of PEDOT as confirmed from Raman spectroscopy till 20 % thereby causing the aggregates to be less susceptible to severe disorder on an electronic level. This probably increases the edge after which para crystallinity-induced states have a negative impact on charge transfer.

With increase of Se content above 20% there is an increase in σ value. This increase is due to the elongation of the π - stacking distance, which lessens the effect of positional disorder on charge transfer. From Raman spectroscopy and SEM images it has been observed that the molecular design has been tuned with the addition of Se which in turn improves the orientation. Therefore, the charge transfer is less susceptible to stacking disorder, boosting electrical conductivity. Furthermore, the charge transport percolation mechanism is compatible with the present structural studies. With the increase of Se above 20% the ordered regions increase through interconnection of polymer chains by bridging. Thus, a network is created which facilitates the charge transport within the matrix.

Figure 6.4 shows the relationship between S and Se concentration. It has been noted that S value improves with an increase in Se content up to 20% before decreasing for the remaining 33%. On further increase of Se content, the value of S increases further. As has

been observed that till 20%the variation of σ and S is just opposite which can be correlated with the following equation [139]

$$S = \frac{\pi^2 k^2 m^* T}{(3\pi^2)^{2/3} \hbar^2 |e| n^{2/3}} \quad (6.1)$$

Here, m^* stands for the majority carriers' effective mass, which for PEDOT is $0.121m_e$, and n for the concentration of charge carriers.

Further σ can also be expressed as

$$\sigma = ne\mu \quad (6.2)$$

Where, μ is the mobility of the charge carriers. Interestingly, above 20 % of Se content both the σ and S value increases simultaneously.[140] This may be attributed to the carrier energy filtering effect between PEDOT and Se. It is well known that carrier energy filtering effect restricts the flow of carriers by eliminating the cold carriers having low carrier energy and allowing the hot carriers having high carrier energy due to the dissimilar work function of the organic and inorganic framework. Therefore, even if there is a rise in σ , S value cannot drop.

Sample Name	PEDOT	6%Se-PEDOT	20%Se-PEDOT	33%Se-PEDOT	52%Se-PEDOT	66%Se-PEDOT	82%Se-PEDOT
Carrier Concentration (m^{-3}) ($\times 10^{25}$)	7.38	6.02	4.77	5.48	4.09	3.57	3.11
Mobility ($m^2V^{-1}s^{-1}$) ($\times 10^{-4}$)	3.65	1.66	0.63	4.12	9.84	18.79	32.50

Table 6.1. Carrier concentration and mobility of all the samples

Using equation 6.1 and 6.2 has been calculated the electrical transport parameters which is tabulated in the table 6.1. From the evaluated value of n and μ , it is observed that up to 20% se content composite carrier concentration as well as charge carrier mobility both are reduced. Furthermore, above 20% an opposite behavior is observed in between these electrical parameters i.e., increase in mobility and decrease in carrier concentration.

In the present case numerous interfaces of Se and PEDOT are formed with the increase percentage of Se. As confirmed by the FESEM images well dispersed interconnecting network is formed above 20wt% of Se creating a highly favored interface effect between PEDOT and Se. The work function of Se is 5.9 eV [113] and that of PEDOT is 5.2 eV [205] Thus PEDOT/Se interface creates a barrier of 0.8 eV. Consequently, carriers having lower energy are encumbered. But carriers having higher energy can cross the barrier easily and efficiently thereby enhancing the S value.

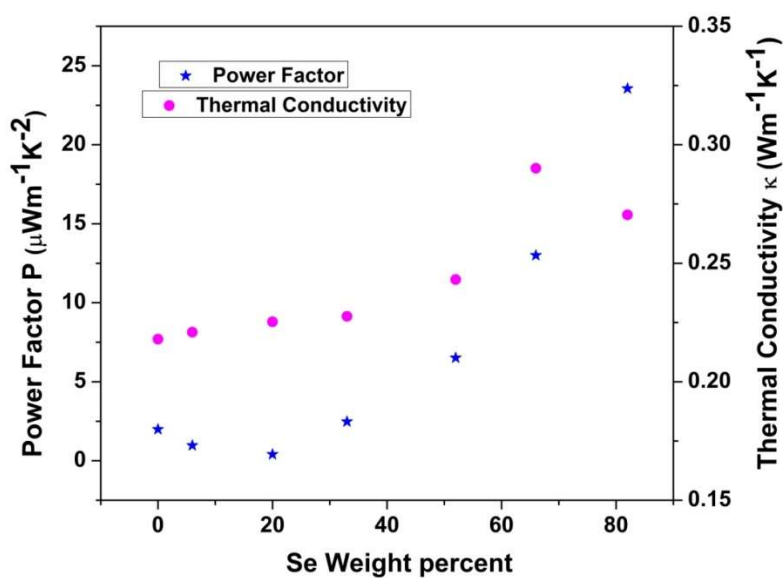


Figure 6.5. Variation of power factor and thermal conductivity with Se content

Figure 6.5 illustrates the power factor (P) of the synthesized samples after evaluation. It is observed that for low concentration of Se the P value decreases till 20 %. Henceforth it starts increasing reaching a maximum of $23.6 \mu\text{Wm}^{-1}\text{K}^{-2}$ for 82% Se-PEDOT composite. This value is even higher than that of reported values of PEDOT:PSS/Se with higher percentage of Se [113]. Addition of Se increases the π - stacking distance thereby decreasing the positional disorder which enhances the electrical conductivity. Further the energy filtering effect also enhances the S value at higher percentage of Se. These combined factors are mostly responsible for increasing the power factor.

The variation of thermal conductivity(κ) with the increase in Se concentration is shown in figure 6.5. An increase in κ value has been observed with the increase in Se content yet the increment is small at higher concentration of Se then Se nanoparticle. Further we observe that for 82% Se-PEDOT composite the value decreases. Following the Wiedemann-Franz's law ($\kappa/\sigma T \approx L_0$ where $L_0=2.45 \times 10^{-8} \text{ V}^2/\text{K}^2$) for an electron system characterized by elastic scattering the Lorentz number of the synthesized sample were estimated and compared to L_0 . The estimated Lorentz numbers, which signify the amount of heat carried out by electrons, are sufficiently large and ranges from $0.538 \times 10^{-7} \text{ V}^2/\text{K}^2$ to $14.98 \times 10^{-7} \text{ V}^2/\text{K}^2$. This is a signature that the total κ value is dominated by the lattice contribution rather the electronic one. The introduction of Se into PEDOT matrix generates nano-interfaces which diminish the lattice contribution depending on the length of scattering [142] but makes electrical transport easier. It is proposed that the interconnected network for 82% Se contain PEDOT creates much more nano-interfaces between PEDOT and Se which facilitates selective scattering of phonons thereby

reducing the total thermal conductivity of the maximum percentage contain sample (82%).

The figure of merit as evaluated (Figure 6.6) decreases initially and then increases beyond 20% of Se content and reaches a maximum of 0.027 for 82% composite material which is quite more than some polymer composites [156, 161, 162].

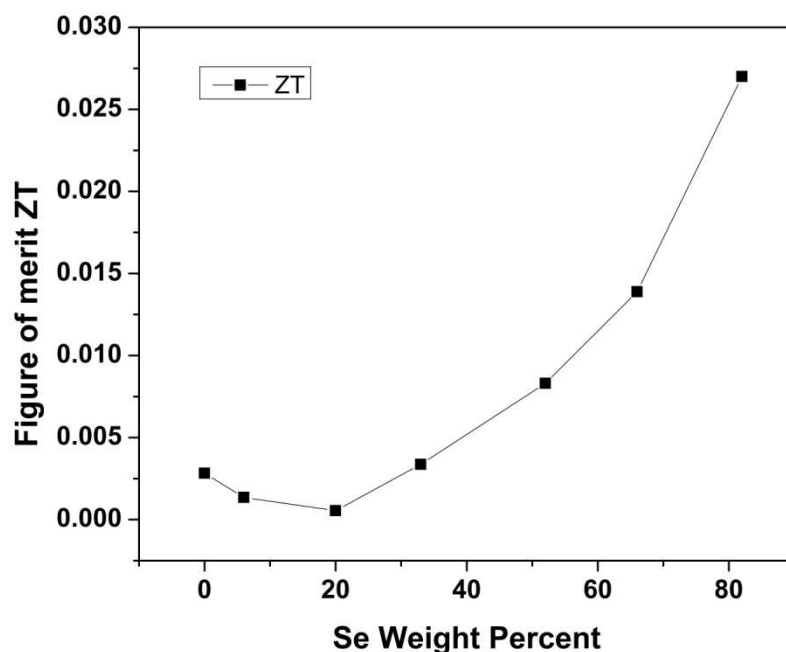


Figure 6.6. Variation of figure of merit with Se content

This indicates that the reorganization of PEDOT chains creating interconnected network with Se nanoparticles broaden the domains of higher conductivity without noticeable increase in the thermal conductivity which is advantageous to improve the transport properties of the samples.

6.5. Conclusion

The self-accumulated micellar prototype approach has been used to synthesis Se-PEDOT composite at room temperature. The structural characterization has shown that the addition of selenium to the polymer matrix improves the ordered structure of the polymer chain because of the incorporation of different selenium nanoparticle concentrations, which in turn affects the charge transport in the composites due to a percolating network created between selenium and PEDOT polymer. It has been shown that the variation of σ and S exhibits opposing behavior up to 20% but interestingly a rise in both σ and S values simultaneously over 20% Se content has been observed. The carrier energy filtering action between PEDOT and Se may be responsible for this. The highest ZT value, which is more than that of organic-inorganic hybrid composite materials, is 0.027. This work demonstrates an efficient technique for enhancing the thermoelectric properties of polymers that have been functionalized with inorganic substances. There is a scope to further enhance the TE performance of Se functionalized PEDOT with inclusion suitable materials like of SWCNT or graphene.

CHAPTER 7: GENERAL CONCLUSION AND FUTURE SCOPE



7.1. General Conclusion

The current thesis focuses on the production of functionalized PEDOT utilizing tosylate and selenium nanoparticles, as well as on their nanocomposites with carbon nanotubes and graphene nanosheets using in situ polymerization. It also examines their electrical characterization with the purpose of improving their thermoelectric properties.

- Enhancing crystallinity enhances electrical conductivity and thermoelectric power factor in conjugated polymer-based nanomaterials.

The work takes advantage of in-situ polymerization to create PEDOT-Tos-SWCNT nanocomposites with various SWCNT concentrations. Greater values and lower S values can be seen in the electrical characterization. Even though the S values are considerably higher than those that are reported. Increased crystallinity by band gap modification enhances electrical conductivity while also enhancing the thermoelectric power factor. Due to the low values and high in power factor, the high ZT (0.045) value surpasses bulk nanostructured materials based on polymers that have been previously described. According to this research, adding SWCNT to PEDOT-Tos enhances TE performance. This information may be helpful when designing and manufacturing polymer nanocomposites for TE applications.

- Enhancing charge carrier mobility enhances thermoelectric properties in polymers and other systems.

A room-temperature in-situ polymerization process was used to synthesis the PEDOT-Tos-graphene nanocomposite. The inclusion of graphene improves the ordered structure, leading to an increase in hopping rate and a decrease in π - π conjugation defects. Thermoelectric power and electrical conductivity both rise as a result of the increased charge carrier mobility. The highest ZT value, which is more

than that of bulk PEDOT-based nanostructures, is 0.0506. The results of the study indicate that carrier mobility, which also influences other polymer systems and enhances thermoelectric characteristics, is an essential aspect in the development and production of polymer nanocomposites for TE applications.

- Due to the addition of Se to the PEDOT matrix, an improvement in the thermoelectric characteristics was seen.

The self-accumulated micellar prototype approach was used to synthesize Se-PEDOT composites at room temperature. The addition of selenium improves the ordered structure of the polymer chain, affecting charge transport. The highest ZT value is 0.027, surpassing organic-inorganic hybrid composite materials. This technique enhances thermoelectric properties of functionalized polymers with inorganic substances.

7.2. Future Scope

Organic TE materials have demonstrated interesting uses in TE devices, with materials based on PEDOT particularly garnering a lot of attention. Through a variety of methods, including refining the structure of the crystal and doping level, creating structures of a nanocomposite, and making use of the ionic TE effects, Over the past ten years, PEDOT's TE performance has greatly improved (ZT value increased from 10^{-3} to 10^{-1}).

It is possible to significantly enhance PEDOT's TE performance, but this requires the establishment of new technologies and methods. A few examples include producing low-dimensional PEDOT crystals to increase carrier mobility, creating new dopants and doping methods to precisely change the oxidation level to achieve at the same time enhanced S, and modifying the composite interface with more logical nanocomposite materials and technologies. Power production takes up the majority of

PEDOT's present work. The integration of TE applications with other technologies, such as sensors, transparent heaters, capacitors, and solar cell, among others, might lead to a future possibility for the widespread usage of PEDOT-based TE materials and devices. It may be crucial for biological applications that this work be expanded to include biocompatible conducting polymers.

CHAPTER 8 – REFERENCES



8.1. References

1. Chen G, Dresselhaus M S, Dresselhaus G, Fluor J P, Caillat T. *Int. Mater. Rev.* **2003**; 48: 45
2. Tritt T M, Böttner H, Chen L. *MRS Bull.* **2008**; 33: 366
3. Synder G J, Toberer E S. *Nat. Mater.* **2008**; 7: 105
4. Chen T, Zheng Z, Liang G, Fan P. *Nanomaterials.* **2020**; 10: 990
5. Rowe D M. Boca Raton (FL): CRC Press, Taylor & Francis Group; 2006.
6. Liu W, Kim H S, Jie Q, et al. *Scr Mater.* **2016**; 111: 3
7. Mori T. *Small.* **2017**; 17:1702013.
8. Russ B, Glaudell A, Urban J J, et al. *Nat Rev Mater.* **2016**; 1: 1
9. Guo C, Chu F, Chen P, Zhu J, Wang H, Wang L, Fan Y and Jiang W J. *Mater. Sci.* **2018**; 53: 6752
10. Yan H et al. *Nat. Mater.* **2016**; 16: 349
11. Sun Y, Li Y, Jin Y, Li Z, Xu W. *Compos. Commun.* **2021**; 27: 100901
12. Wang L, Yao Q, Shi W, Qu S, Chen L. *Mater. Chem. Front.* **2017**;1: 741
13. Park D, Kim M, Kim J. *Polymers.* **2020**;12: 2932
14. Lu Y, Qiu Y, Jiang Q, Cai K, Du Y, Song H, Gao M, Huang C, He J and Hu D. *ACS Appl. Mater. Interfaces.* **2018**; 49: 42310
15. Bharti M et al. *J. Power Sources.* **2019**; 435: 226758
16. Bredas J L, Street G B. *Acc Chem Res.* **1985**; 18: 309
17. Chance R R, Brédas J L, Silbey R. *Phys Rev B.* **1984**; 29: 4491
18. Bubnova O, Crispin X. *Energy Environ Sci.* **2012**; 5: 9345
19. Kaiser A B, Skakalova V. *Chem Soc Rev.* **2011**; 40: 3786
20. Bubnova O, Khan Z U, Wang H, et al. *Nat Mater.* **2014**; 13:190
21. Petsagkourakis I, Pavlopoulou E, Cloutet E, et al. *Org Electron.* **2018**; 52: 335
22. Liu Z, Mao J, Liu T, et al. *MRS Bull.* **2018**; 43:181
23. Gooth J, Schierner G, Felser C, et al. *MRS Bull.* **2018**;43 :187
24. Tian R, Wan C, Hayashi N, et al. *MRS Bull.* **2018**; 43:193
25. Kroon R, Mengistie D A, Kiefer D, et al. *Chem Soc Rev.* **2016**; 45: 6147
26. Buhro L W, Colvin L V. *Nat. Mater.* **2003**; 2 138
27. Yang R. PhD. Thesis, Massachusetts Institute of Technology, (2005)
28. Yang R, Chen G, Dresselhaus M S. *Phys. Rev. B.* **2005**; 72 :125418
29. Toshima N. *Synthetic Metals.* **2017**; 225: 3

30. zyyKoga T, Cronin S B, Dresselhaus M S, Liu J L, Wang K L. *Appl. Phys. Lett.* **2000**; 77: 1490
31. Ravich Y I, Efimova B A, Tamarchenko V I. *Phys. Stat. Sol. B.* **1971**; 43: 453
32. Shirakawa H, Louis E J, MacDiarmid A G, et al. *J Chem Soc Chem Comm.* **1977**;16: 578
33. de Leeuw D M, Kraakman P A, Bongaerts P F G, Mutsaers C M J, Klaassen D B M. *Synthetic Metals.* **1994**; 66: 263
34. Chen X, Xing K-Z, Ingana's O. *Chem. Mater.* **1996**; 8: 2439
35. Yu S H, Lee J H, Choi M S, Park J H, Yoo P J, Lee J Y. *Molecular Crystals and Liquid Crystals.* **2013**; 580: 76
36. Bubnova O, Khan Z U, Malti A, Braun S, Fahlman M, Berggren M, Crispin X. *Nature Materials.* **2011**; 10: 429
37. Xu Y, Jia Y, Liu P, Jiang Q, Hu D, Ma Y. *Chemical Engineering Journal.* **2021**; 404: 126552
38. Petsagkourakis I, Kim N, Tybrandt K, Zozoulenko I, Crispin X. *Adv. Electron. Mater.* **2019**; 5: 1800918.
39. Heywang G, Jonas F. *Adv.mater.* **1992**; 4, 2.
40. Im S G, Gleason K K. *Macromolecules.* **2007**; 40: 6552
41. Edberg J, Iandolo D, Brooke R, Liu X, Musumeci C, Andreasen J W, Simon D T, Evans D, Engquist I, Berggren M. *Advanced Functional Materials.* **2016**; 26: 6950
42. Lee Y H, Oh J, Lee S- S, Kim H, Son J G. *ACS Macro Lett.* **2017**; 6: 386
43. Franco-Gonzalez J F, Zozoulenko I V. *J. Phys. Chem. B.* **2017**; 121: 4299
44. Hwang J, Tanner D B. *Physical Review B.* **2003**; 67: 115205
45. Massonnet N, Carella A, de Geyer A, Faure-Vincent J, Simonato J-P. *Chem. Sci.* **2015**; 6: 412
46. Petsagkourakis I, Pavlopoulou E, Portale G, Kuropatwa B A, Dilhaire S, Fleury G, Hadziioannou G. *Scientific Reports.* **2016**; 6: 30501.
47. Kim N, Lee B H, Choi D, Kim G, Kim H, Kim J-R, Lee J, Kahng Y H, Lee K. *PRL.* **2012**; 109: 106405
48. Winther-Jensen B, Forsyth M, West K, Andreasen JW, Bayley P, Pas S, MacFarlane D R. *Polymer.* **2008**; 49: 481
49. Chacko A P, Jin Y, Shi Y, Bunha A, Chen J, Lessner P M. *ECS Transactions.* **2018**; 85: 115

50. Štul'ík J, Polansk'y R, Ham' a'ček A, Ne'sp'urek S, Slep'čka P, Kolsk'a Z, Švor' c'ík V. *Sensors and Actuators B*. **2018**; 275: 359
51. Kim T Y, Kim J E, Suh K S. *Polym Int*. **2006**; 55: 80
52. Park T, Park C, Kim B, Shin H, Kim E. *Energy Environ. Sci*. **2013**; 6: 788
53. Kai H, Suda W, Ogawa Y, Nagamine K, Nishizawa M. *ACS Appl. Mater. Interfaces*. **2017**; 9: 19513
54. Rosati G, Sappia L, Madrid R, Rozlòsnik, N. *International Scholarly and Scientific Research & Innovation*. **2017**; 11: 586
55. Kim J-S, Jang W, Wang D H. *Polymers*. **2019**; 11:21
56. Khan E H, Thota S, Wang Y, Li L, Wilusz E, Osgood R, Kumar J. *Journal of Electronic Materials*. **2018**; 47: 3963
57. Galliani D, Battiston S, Narducci D. *Journal of Nano science and Nanotechnology*. **2017**; 17: 1579
58. Galliani D, Battiston S, Ruffo R, Trabattoni S, Narducci D. *Journal of Physics D: Applied Physics*. **2017**; 51: 13pp
59. Choi K, Kim S L, Yi S, Hsu J-H, Yu C. *ACS Appl. Mater. Interfaces*. **2018**; 10: 23891
60. Winther-Jensen B, West K. *Macromolecules*. **2004**; 37: 4538
61. Lindell L, Burquel A, Jakobsson F L E, Lemaure V, Berggren M, Lazzaroni R, Cornil J, Salaneck W R, Crispin X. *Chem. Mater*. **2006**; 18: 4246
62. Karagkiozaki V, Karagiannidis PG, Gioti M, Kavatzikidou P, Georgiou D, Georgarakis E, Logothetidis S. *BBA*. **2013**; 1830: 4294
63. Fabretto M, Muller M, Zuber K, Murphy P. *Macromol. Rapid Commun*. **2009**; 30: 1846
64. Fabretto M, Zuber K, Jariego-Moncunill C, Murphy P. *Macromol. Chem. Phys*. **2011**; 212: 2173
65. Zuber K, Fabretto M, Hall C, Murphy P. *Macromol. Rapid Commun*. **2008**; 29: 1503
66. Rehmen J, Zuber K, Modarresi M, Kim D, Charraut E, Jannasch P, Zozoulenko I, Evans D, Karlsson C. *ACS Omega*. **2019**; 4: 2181
67. Hojati-Talemi P, Delaigue M, Murphy P J, Fabretto M V. *ACS Appl. Mater. Interfaces*. **2015**; 7: 8465
68. Khan Z U, Bubnova O, Jafari M J, Brooke R, Liu X, Gabrielsson R, Ederth T, Evans D R, Andreasen J W, Fahlman M, Crispin X. *J. Mater. Chem. C*. **2015**; 3: 10616

69. Fabretto M V, Evans D R, Mueller M, Zuber K, Hojati-Talemi P, Short R D, Wallace G G, Murphy P J. *Chem. Mater.* **2012**; 24: 3998
70. Rudd S, Murphy P J, Evans D R. *Synthetic Metals.* **2018**; 242: 61
71. Rudd S, Dalton M, Buss P, Treijs A, Portmann M, Ktoris N, Evans D. *Scientific Reports.* **2017**; 7: 16581
72. Shahnian S, Rehmen J, Lancaster D G, Monro T M, Ebendorff-Heidepriem H, Evans D, Afshar V S. *Optical Materials Express.* **2019**; 9: 4517
73. Koch L, Polek A, Rudd S, Evans D R. *ACS Appl. Mater. Interfaces.* **2017**; 9: 65
74. Chen S, Kuřhne P, Stanishev V, Knight S, Brooke R, Petsagkourakis I, Crispin X, Schubert M, Darakchieva V, Jonsson M P. *J. Mater. Chem. C.* **2019**; 7: 4350
75. Zhang K, Qiu J, Wang S. *Nanoscale.* **2016**; 8:8033
76. Hojati-Talemi P, Bächler C, Fabretto M, Murphy P, Evans D. *ACS Appl. Mater. Interfaces.* **2013**; 5: 11654
77. Bansal M, Sharma M, Bullen C, Svirskis D. *Materials Science & Engineering C.* **2018**; 84: 248
78. Wang J, Cai K, Shen S. *Organic Electronics.* **2014**; 15: 3087
79. Wang J, Cai K, Song H, Shen S. *Synthetic Metals.* **2016**; 220: 585
80. Losaria P L, Yim J-H. *Journal of Industrial and Engineering Chemistry.* **2019**; 74: 108
81. Chen J, Liu Y, Minet A I, Lynam C, Wang J, Wallace G G. *Chem. Mater.* **2007**; 19: 3595
82. Yang Y, Zhang L, Li S, Wang Z, Xu J, Yang W, Jiang Y. *Nano-Micro Lett.* **2013**; 5: 40
83. Xu L, Xu J, Yang Y, Mao X, He X, Yang W, Zhao Y, Zhou Y. *J Mater Sci: Mater Electron.* **2017**; 29: 2322
84. Mirmohseni A, Price W E, Wallace G G. *Polymer Gels and Networks.* **1993**; 1: 61
85. Yan H, Sada N, Toshima N. *Therm. Anal. Cal.* **2002**; 69: 881
86. Yoo D, Kim J, Lee S H, Cho W, Choi H H, Kim F S, Kim J H. *J. Mater. Chem. A.* **2015**; 3: 6526
87. Wei Q, Mukaida M, Kirihaara K, Naitoh Y, Ishida T. *Materials.* **2015**; 8: 732
88. Stepien L, Roch A, Tkachov R, & Gedrange T. Progress in polymer thermoelectrics. thermoelectrics for power generation - a look at trends in the technology. 2016
89. Fan Z, Ouyang J. *Adv. Electron. Mater.* **2019**, 1800769

90. See K C, Feser J P, Chen C E, Majumdar A, Urban J J, Segalman R A. *Nano Lett.* **2010**; 10: 4664
91. Jiang F, Xiong J, Zhou W, Liu C, Wang L, Zhao F, Liu H, Xu J. *J. Mater. Chem. A.* **2016**; 4: 1
92. Jiang Q, Lan X, Liu C, Shi H, Zhu Z, Zhao F, Xu J, Jiang F. *Mater. Chem. Front.* **2018**; 2: 679
93. Wang X, Meng F, Jiang Q, Zhou W, Jiang F, Wang T, Li X, Li S, Lin Y, Xu J. *ACS Appl. Energy Mater.* **2018**; 1: 3123
94. Yu C, Kim Y S, Kim D, Grunlan J C. *Nano Lett.* **2008**; 8:4428
95. He M, Ge J, Lin Z, Feng X, Wang X, Lu H, Yanga Y, Qiu F. *Energy Environ. Sci.* **2012**; 5: 8351
96. Bae E J, Kang Y H, Jang K-S, Cho S Y. *Scientific Reports.* **2016**; 6:18805
97. Wang Y, Cai K, Yao X. *ACS Appl. Mater. Interfaces.* **2011**; 3: 1163
98. Song H, liu C, Zhu H, Kong F, Lu B, Xu J, Wang J, Zhao F. *Journal of ELECTRONIC MATERIALS.* **2013**; 42: 6
99. Du Y, Cai K F, Chen S, Cizek P, Lin T. *ACS Appl. Mater. Interfaces.* **2014**; 6: 5735
100. Wang Y, Honga M, Liu W-D, Shia X-L, Xu S-D, Sun Q, Gao H, Lu S, Zou J, Chena Z-G. *Chemical Engineering Journal.* **2020**; 397: 125360
101. Zhang B, Sun J, Katz H E, Fang F, Opila R L. *ACS Appl. Mater. Interfaces.* **2010**; 2: 3170
102. Finefrock S W, Zhu X, Sun Y, Wu Y. *Nanoscale.* **2015**; 7: 5598
103. Ju H, Kim J. *Chemical Engineering Journal.* **2016**; 297: 66
104. Cheng X, Wang L, Wang X, Chen G. *Composites Science and Technology.* **2018**; 155: 247
105. Toshima N, Jiravanichanun N, Marutani H. *Journal of ELECTRONIC MATERIALS.* **2012**; 41: 1735
106. Toshima N, Jiravanichanun N. *Journal of ELECTRONIC MATERIALS.* **2013**; 42: 1882
107. Xu K, Chen G, Qiu D. *J. Mater. Chem. A.* **2013**; 1: 12395
108. Xiong J, Jiang F, Shi H, Xu J, Liu C, Zhou W, Jiang Q, Zhu Z, Hu Y. *ACS Appl. Mater. Interfaces.* **2015**; 7: 14917
109. Song H, Liu C, Xu J, Jiang Q, Shi H. *RSC Adv.* **2013**; 3: 22065
110. Shi H, Liu C, Xu J, Song H, Lu B, Jiang F, Zhou W, Zhang G, Jiang Q. *ACS Appl. Mater. Interfaces.* **2013**; 5: 12811

111. Lee H J, Anoop G, Lee H J, Kim C, Park J-W, Choi J, Kim H, Kim Y-J, Lee E, Lee S-G, Kim Y-M, Lee J-H, Jo J Y. *Energy Environ. Sci.* **2016**; 9: 2806
112. He M, Qiu F, Lin Z. *Energy Environ. Sci.* **2013**; 6: 1352
113. Kim C, Hong J, Park J-W. *Polymers.* **2019**; 11: 1052
114. Nasir S, Hussein M Z, Zainal Z, Yusof N A, Mohd Zobir S A, Alibe, I M. *BioRes.* **2019**; 14: 2352
115. Areef Billah A H M. MSc. Full Thesis, 2016
116. Zhang Q, Sun Y M, Xu W, Zhu D B. *Adv. Mater.* **2014**; 26: 6829
117. Hwang S, Potscavage W J, Nakamichi R, Adachi C. *Organic Electronics.* **2016**; 31: 31.
118. Park Y W, Han W K, Choi C H, Shirakawa H. *Phys. Rev. B.* **1984**; 30: 5847.
119. Kemp N T, Kaiser A B, Liu C J, Chapman B, Mercier O, Carr A M, Trodahl H J, Buckley R G, Partridge A C, Lee J Y, Kim C Y, Bartl A, Dunsch L, Smith W T, Shapiro J S. *J. PolymSci B: Polym Phys.* **1999**; 37: 953.
120. Lévesque I, Bertrand P O, Blouin N, Leclerc M, Zecchin S, Zotti G, Ratcliffe C I, Klug D D, Gao X, Gao F, Tse J S. *Chem. Mater.* **2007**; 19: 2128.
121. Jiang F X, Jing-Kun X U, Bao-Yang L U, Yu X I E, Rong-Jin HUANG, Lai-Feng L I. *Chin. Phys. Lett.* **2008**; 25: 2202.
122. Groenendaal L, Jonas F, Freitag D, Pielartzik H, Reynolds J R. *Adv. Mater.* **2000**; 12: 481.
123. Bubnova O, Berggren M, Crispin X J. *Am. Chem. Soc.* **2012**; 134: 16456
124. Massonnet N, Carella A, Jaudouin O, Rannou P, Laval G, Celle C, Simonato J P. *J. Mater. Chem. C.* **2014**; 2: 1278.
125. Iijima S. *Nature (London).* **1991**; 354: 56
126. Dai L M, Mau A W H. *Adv. Mater.* **2001**; 13: 899.
127. Moriarty G P, De S, King P J, Khan U, Via M, King J A, Coleman J N, Grunlan J C. *J. Polym. Sci. Part B: Polym. Phys.* **2013**; 51: 119
128. Bounioux C, Chao P D'iaz, Campoy-Quiles M, Mart'in-Gonz'alez M S, Goñi A R, Yerushalmi-Rozen R, M'uller C. *Energy Environ. Sci.* **2013**; 6: 918
129. Yao Q, Wang Q, Wang L, Chen L. *Energy Environ. Sci.* **2014**; 7: 3801
Hong C T, Kang Y H, Ryu J, Cho S Y, Jang K S. *J. Mater. Chem. A.* **2015**; 3: 21428
130. Du Y, Shen S Z, Yang W D, Cai K F, Casey P. S. *Synth. Met.* **2012**; 162: 375
131. Du Y, Cai K F, Shen S Z, Casey P S. *Synth. Met.* **2012**; 162: 2102

132. Wang J, Cai K, Yin J, Shen S. *Synth. Met.* **2017**; 224: 27
133. Artyukhin A B, Bakajin O, Stroeve P, Noy A. *Langmuir.* **2004**; 20: 1442
134. O'Connell M. J, Boul P, Ericson L. M, Huffman C, Wang Y. H, Haroz E, Kuper C, Tour J, Ausman K. D, Smalley R E. *Chem. Phys. Lett.* **2001**; 342: 265
135. Wu T M, Lin Y W. *Polymer.* **2006**; 47: 3576
136. Reddy K R, Jeong H M, Lee Y, Raghu A V J. *Polym. Sci.* **2010**; 48: 1477.
137. Imani A, Farzi G, Ltaief A. *Int. Nano Lett.* **2013**; 3: 52
138. Yu C, Shi L, Yao Z, Li D, Majumdar A. *Nano lett.* **2005**; 5:1842
139. Cutler M, leavy J, Fitzpatrick R. *Phys. Rev.* **1964**; 133: A1143
140. Pai C, Liu C, Chen W, Jenekhe S. *Polymer.* **2006**; 47: 699
141. Kidalov S V, Shakhov F M. *Materials.* **2009**; 2: 2467
142. Chatterjee K, Mitra M, Ganguly S, Kargupta K, Banerjee D. *Nanotech.* **2013**; 24: 215703
143. Kim D, Kim Y, Choi K, Grunlan J C, Yu C. *ACS. Nano.* **2010**; 4: 513
144. Hiroshige Y, Ookawa M, Toshima N. *Synth. Met.* **2006**; 156: 1341
145. Yan H, Ohta T, Toshima N. *Macromol. Mater. Eng.* **2001**; 286: 139
146. Yao Q, Chen L, Xu X, Wang C. *Chem. Lett.* **2005**; 34: 522.
147. Kim N, Kee S, Lee S H, Lee B H, Kahng Y H, Jo Y R, Kim B J, Lee K. *Adv. Mater.* **2014**; 26: 2268
148. Kawai T, Nakazono M, Yoshino K, *J. Mater. Chem.* **1992**; 2: 903.
149. Lapkowski M, Pron A. *Synth. Met.* **2000**; 110: 79.
150. Garreau S, Duvail J L, Louarn G. *Synth. Met.* **2001**; 125: 325.
151. Heeger A J. *Rev. Mod. Phys.* **2001**; 73: 681.
152. Hicks L D, Dresselhaus M S. *Phys. Rev. B: Condens. Matter Mater. Phys.* **1993**; 4: 12727
153. Ni X, Liang G, Wang J S, Li B. *Appl. Phys. Lett.* **2009**; 95: 1921141
154. Ghosh S, Calizo I, Teweldebrhan D, Pokatilov E P, Nika D L, Baladin A A, Bao W, Miao F, Lau C N. *Appl. Phys. Lett.* **2008**; 92: 1519111
155. Lin J, Teweldebrhan D, Ashraf K, Liu G, Jing X, Yan Z, Li R, Ozkan M, Lake R K, Baladin A A, Ozkan C S. *Small.* **2010**; 6: 1150
156. Mitra M, Kulsi C, Chatterjee K, Kargupta K, Ganguly S, Banerjee D, Goswami S P. *RSC Adv.* **2015**; 5: 31039
157. Wang L, Liu F, Jin C, Zhang T, Yin Q. *RSC Adv.* **2014**; 4: 46187

158. Wang Y, Yang J, Wang L, Du K, Yin Q and Yin Q. *ACS. Appl. Mater. Inter.* **2017**; 9: 20124
159. Zhou J, Li E Q, Li R, Xu X, Ventura I A, Moussawi A, Anjum D H, Hedhili M N, Smilgies D-M, Lubineau G, Thoroddsen S T. *J. Mater. Chem. C* **2015**; 3: 2528
160. Kim T Y, Park C M, Kim J E, Suh K S. *Synth. Met.* **2005**; 149: 169
161. Zhao Y, Tang G S, Yu Z Z, Qi J S. *Carbon*. **2012**; **50**: 3064
162. Lu Y, Song Y, Wang F. *Mater. Chem. Phys.* **2013**; 138: 238
163. Ramakrishnan R, Devaki S J, Aashish A, Thomas S, Varma M R, KPP N. J. *Phys. Chem. C*. 2016; **120**: 4199
164. Selvaganesh S V, Mathiyarasy J, Phani K L N, Yegnaraman V. *Nanoscale Res. Lett.* **2007**; 2: 546
165. Wang Y, Cai K, Chen S, Shen S, Yao X. *J. Nanopart. Res.* **2014**; 16: 2531.
166. Chen L, Liu W, Su X, Xiao S, Xie H, Uher C, Tang X. *Synth. Met.* **2017**; 229: 65
167. Jiang X Y, Wang Z, Han W, Liu Q, Lu S, Wen Y, Hou J, Huang F, Peng S, He D, Cao G. *Appl. Surf. Sci.* **2017**; 407: 398
168. Ouyang J, Xu Q, Chu C W, Yang Y, Li G, Shinar J. *Polymer (Guildf)*. **2004**; 45: 8443
169. Pathak C S, Singh J P, Singh R. *Curr. Appl. Phys.* **2015**; 15: 528
170. Zhang J, Zhao X S. *J. Phys. Chem. C* **2012**; 116: 5420
171. Deetuum C, Samthong C, Thongyai S, Praserttham P, Somwangthanaroj A. *Compos. Sci. Technol.* **2014**; 93: 1.
172. Pathak C S, Singh J P, Singh R. *Chem. Phys. Lett.* **2018**; 694: 75
173. Long Y, Chen Z, Zhang X, Zhang J, Liu Z. *Appl. Phys. Lett.* **2004**; 85: 1796
174. Yang C, Liu P, Wang T. *ACS Appl. Mater. Interfaces*. **2011**; 3: 1109
175. Tsai T C, Chang H C, Chen C H, Whang W T. *Org. Electron.* **2011**; 12: 2159
176. Meng C Z, Liu C H, Fan S A. *Adv. Mater.* **2010**; 22: 535
177. Wang Q, Yao Q, Chang J, Chen L D. *J. Mater. Chem.* **2012**; 22: 17612
178. Koller G, Berkebile S, Oehzelt M, Puschnig P, Draxl C A, Netzer F P, Ramsey M G. *Science*. **2007**; 317: 351
179. Crispin X, Cornil J, Friedlein R, Okudaira K K, Lemaire V, Crispin A, Kestemont G, Lehmann M, Fahlman M, Lazzaroni R, Geerts Y, Wendin G, Ueno N, Bredas J. L, Salaneck W R. *J. Am. Chem. Soc.* **2004**; 126: 11889
180. Kim G H, Hwang D H, Woo S I. *Phys. Chem. Chem. Phys.* **2012**; 14: 3530
181. Xiang J, Drazl L T. *Chem. Phys. Lett.* **2014**; 593: 109

182. Chen Y, Zhao Y, Liang Z. *Energy Environ. Sci.* **2015**; **8**: 401
183. Bell L E. *Science*. **2008**; 321: 1457
184. Yue R, Xu R, *Synth. Met.* **2012**; 162: 912
185. Zebarjadi M, Esfarjani K, Dresselhaus M S, Ren Z F, Chen G. *Energy Environ. Sci.* **2012**; **5**: 5147
186. Bharti M, Singh A, Samanta S, Aswal D. *Prog. Mater. Sci.* **2018**; **93**: 270
187. McGrail B T, Sehirlioglu A, Pentzer E. *Angew. Chem. Int. Ed.* **2015**; **54**: 1710
188. Ju H, Park D, Kim J. *J. Mater. Chem. A*, **2018**; **6**: 5627
189. Kim C S, Yang H M, Lee J, Lee G S, Choi H, Kim Y J, Lim S H, Cho S H, Cho B J. *ACS Energy Lett.* **2018**; **3**: 501
190. Li Y, Du Y, Dou Y, Cai K, Xu J. *Synth. Met.* **2017**; 226: 119
191. Kim G-H, Shao L, Zhang K, Pipe K. P. *Nat. Mater.* **2013**; **12**: 719
192. Kim Y H, Sachse C, Machala M L, May C, Müller-Meskamp L, Leo K. *Adv. Funct. Mater.* **2011**; **21**: 1076
193. He M, Qiu F, Lin Z. *Energy Environ. Sci.* **2013**; **6**: 1352
194. Kim J, Lim J-H. *Journal of the Korean Ceramic Society.* **2017**; **54**: 272
195. McGrail B T, Sehirlioglu A, Pentzer E. *Angew. Chem. Int. Ed.* **2014**; **53**:2-16.
196. Henkels H W. *Phys. Rev.* **1950**, **77**, 734
197. Qin, J, Qiu G, Jian J, Zhou H, Yang L, Charnas A, Zemlyanov D Y, Xu C-Y, Xu X, Wu W. et al. *ACS Nano.* **2017**; **11**: 10222
198. Sinha S, Chatterjee S K, Ghosh J, Meikap A K. *J. Appl. Phys.* **2013**; **113**: 123704.
199. Kim I Y, Chun D W, Kim Sang-Il, Lim J-H. *Frontiers in Chemistry.* **2022**; **9**: 791155
200. Ni D, Song H, Chen Y, Cai K. *Energy.* **2019**; **170**: 53
201. Choi J W, Han M G, Kim S Y, Oh S G, Im S. S. *Synth. Met.* **2004**; **141**: 293
202. Kim T Y, Chang M P, Kim J E, Suh K S. *Synth. Met.* **2005**; **149**: 169
203. Feng L, Yu P, Liu C, Lan J, Lin Y-H, Yang X. *ACS Appl. Mater. Interfaces.* **2022**; **14**: 23765
204. Noriega R, Rivnay J, Vandewal K, Koch F P V, Stingelin N, Smith P, Toney M F, Salleo A. *Nature Materials.* **2013**; **12**: 1038
205. Dzugan T, Blecha T, Hamacek A, Kroupa M, Rcboun J. *32nd International Spring Seminar on Electronics Technology.* **2009**; DOI: 10.1109/ISSE.2009.5207058

PUBLICATIONS

Materials Science inc. Nanomaterials & Polymers

Enhancement of Thermoelectric Performance in Oligomeric PEDOT-SWCNT Nanocomposite via Band Gap Tuning

Shilpa Maity,^[a] Nayim Sepay,^[b] Chiranjit Kulsi,^[c] Arpan Kool,^[d] Sukhen Das,^[a] Dipali Banerjee,^[c] and Krishanu Chatterjee^{*[d]}

Organic thermoelectric (TE) materials, inspite of their low cost, non-toxicity, easy availability, show a low thermoelectric figure of merit (ZT). Herein we report $ZT > 0.04$ for tosylate doped poly(3,4 ethylenedioxythiophene) (PEDOT-Tos) with single walled carbon nanotubes (SWCNT) which is higher than the reported values for bulk nanostructured polymer based composites. The underlying reason for the enhancement of the transport properties is the morphological transformation of the nanocomposites exhibiting an increase degree of ordered

structure of the samples with the increase of SWCNT content as is observed from XRD, UVVIS and FESEM studies. This increase in the ordered structure is due to the decrease in band gap that was found in DFT calculations which in turn increases the electrical conductivity which is responsible for the enhanced power factor. Further the SWCNTs introduce the interfaces that reduce the thermal conductivity due to scattering of phonons which further contributes to the enhancement in the figure of merit.

Introduction

Thermoelectric (TE) materials from organic semiconductors exhibit a lower thermoelectric figures of merit (ZT) values compare to that of inorganic materials.^[1] The advantages of organic semiconductors like the low production cost, non-toxicity, easy availability of raw materials lead to its wide range of applications.^[2] Currently, conducting polymers are the most promising candidate which have already been tested as potentially appropriate materials for TE applications. TE properties of polyacetylene^[3] (PA), polypyrrole^[4] (PPY), polyaniline^[5] (PANI), polycarbazoles^[6] (PC), poly(3,4-ethylenedioxythiophene) : poly(styrenesulfonate)^[7] (PEDOT : PSS) and their derivatives show a lots of promise and certainly worth further investigation. The research on the TE performance of PEDOT and its derivatives is currently underway.^[8] A rather substandard TE efficiency of PEDOT-PSS can be markedly improved by various secondary dopants which usually improve polymer's morphology accompanied by a drastic increase in electrical conductivity and, consequently, in ZT.^[9] The oxidation level of PEDOT-PSS can be precisely controlled by electrochemical doping resulting in a ten-fold increase of ZT.^[10] In contrast to PEDOT-PSS, PEDOT-Tos exhibits superior TE performance even without

secondary doping owing to its partially crystalline nature that allows for an improved electronic conduction. Increased interest in replacing inorganic anode materials with ultrahigh conductivity organic materials, together with recent advances in polymerisation technique, has made tosylic acid doped PEDOT (PEDOT-Tos) another important doped form of the polymer. With the aid of a strong electron donor, positively doped PEDOT-Tos gets partially reduced reaching the optimum oxidation state at which its TE efficiency is just four times smaller than that of Bi_2Te_3 .^[11]

Due to some unique electronic and mechanical properties, carbon nanotubes (CNTs) are used in nanoscale devices, bio sensing and field-emission displays.^[12] Recently, carbon nanotubes (CNTs) have been used as an active supplement for enhancing the TE performance of conjugated polymers.^[13] Physical modification of CNT/conducting polymer composites established through π - π stacking of the conducting polymer molecules on the CNT sidewalls in such a way that implementation of the CNT/conducting polymer composites is possible without compromising the chemical structure of the nanotubes.^[14] Single-walled CNT/PEDOT:PSS nanocomposite films with 85 wt% CNTs showed power factors up to $140 \text{ mWm}^{-1}\text{K}^{-2}$,^[13a] whereas, single-walled CNT/PANI nanocomposite films with 64 wt% CNTs exhibits power factors of $176 \text{ mWm}^{-1}\text{K}^{-2}$.^[13c] A PEDOT/SWCNT composite film with 35% SWCNT displayed the maximum power factor $37.8 \text{ } \mu\text{W mK}^{-2}$ which is 1.7 times higher than the films without containing SWCNTs.^[13g] The density of the electrical pathway can be increased by incorporating CNTs to the conjugated polymer matrix, thus enhancing the electrical conductivity as well as the TE performances.

Though PEDOT-Tos shows a great promise in TE application yet the material has not been explored. Further reports on nanocomposites of PEDOT-Tos with inorganic counter parts are very scanty. In the present study, EDOT is polymerised in situ,

[a] S. Maity, S. Das
Department of Physics, Jadavpur University, Kolkata 700032, India

[b] N. Sepay
Department of Chemistry, Jadavpur University, Kolkata 700032, India

[c] C. Kulsi, D. Banerjee
Department of Physics, IEST, Shibpur, Howrah, West Bengal 711103, India

[d] A. Kool, K. Chatterjee
Department of Physics, Techno India University, Sector-V, Salt Lake, Kolkata-700091, India
Tel.: +919051227187
E-mail: itskrishanu@gmail.com

Supporting information for this article is available on the WWW under <https://doi.org/10.1002/slct.201801384>

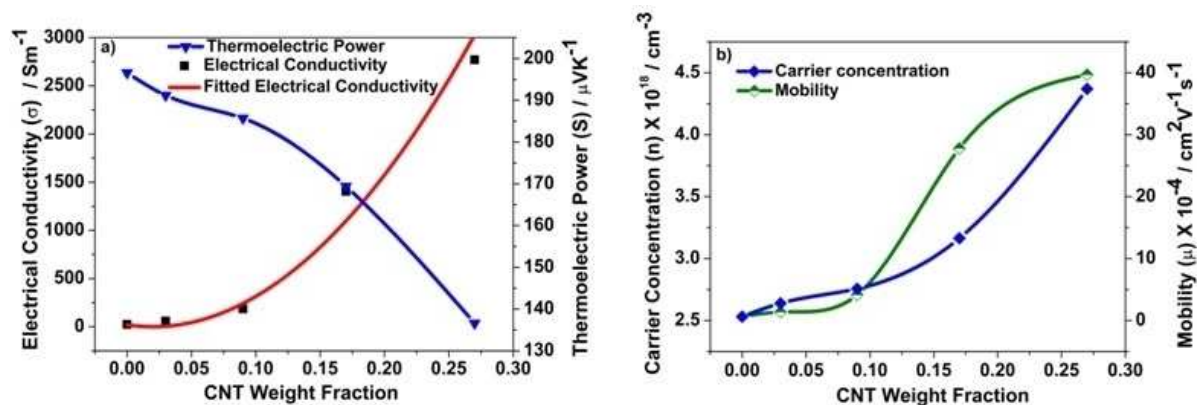


Figure 1. Variation of a) electrical conductivity and the thermoelectric power, b) carrier concentration and mobility with SWCNT weight fraction.

to synthesise PEDOT-Tos using *p*-Toluenesulfonic acid (pTSA) as a source of tosylate group. The power factor ($S^2\sigma$) and hence the figure of merit (ZT) of the conducting polymer nanocomposite containing PEDOT-Tos have been enhanced by incorporation of Single-walled carbon nanotubes (SWCNTs) during the polymerisation.

Results and Discussion

Figure 1a shows the variation of electrical conductivity σ with the SWCNT concentration. The σ value increases gradually with the increase in SWCNT concentration (Sample II) and the value increases significantly for Sample III followed by its drastic rise in case of Sample IV and Sample V reaching a maximum value of 2770.6 Sm^{-1} . The values of electrical conductivity in each case are much higher than that of PEDOT-MWCNT nanocomposites.^[15] The enhancement in the σ value suggests a change in the band gap and molecular energy levels of PEDOT-Tos-SWCNT nanocomposite. The σ value follows a power law with the SWCNT concentration^[16]

$$\sigma = \sigma_0(P - P_c)^t \quad (1)$$

where σ_0 is a proportionality constant related to intrinsic conductivity of SWCNT, P is the weight fractions of SWCNT in the nanocomposites, P_c is the critical weight fraction related to percolation threshold. Equation (1) fits well with the experimental result with $\sigma_0 = 4.7 \times 10^4 \text{ Sm}^{-1}$, $P_c = 0.02$. The threshold value comes out to be 0.02 weight fraction of SWCNT. Moreover it is revealed that the electrical transport is dominated by the tunnelling phenomenon above the percolation threshold as it reflects from Figure 1a.^[13a]

The variation of thermoelectric power (S) with the SWCNT concentration was depicted in Figure 1a. The S value is reduced to 136.6 μVK^{-1} for the Sample V from 196.6 μVK^{-1} in case of the Sample I. The decreased value is attributed to the relatively low value of S of SWCNT.^[17] Since the electronic environment of the charge carriers influences the value of S , the S values of the nanocomposite lies in between S_{pristine} and S_{SWCNT} . This is due to

the fact that above the value of P_c , the probability of tunnelling is more predominant for the compact SWCNT bundles creating a pathway for the charge carriers. The carrier concentration (n) is evaluated from Mott relation^[18] given by

$$S = \pi^2 k^2 m^* T / ((3\pi^2)^{2/3} \hbar^2 |e| n^{2/3}) \quad (2)$$

where m^* is the effective mass of the majority carriers having a value of $0.121m_e$ for PEDOT.^[19] The n value increases with the increase in the SWCNT content as is seen from Figure 1b. This low value of n is supposed to suppress σ . Probably mobility of the charge carriers plays a key role for the high values of σ . The variation of mobility of the charge carriers with SWCNT concentration is depicted in Figure 1b.

The power factor ($S^2\sigma$) has been evaluated and shown in Figure 2a. At the low concentration of SWCNT there is a little increase in $S^2\sigma$. With further increase in SWCNT concentration power factor increases drastically and finally tends to saturate at higher concentration of SWCNT. A maximum value of 51.8 $\mu\text{Wm}^{-1}\text{K}^{-2}$ have been achieved for Sample V which is higher than the reported values at this concentration level of CNT.^[13b,g] The addition of SWCNT increases the degree of delocalization of the charge carriers within the π conjugated structure of PEDOT-Tos-SWCNT nanocomposites with a low value of carrier concentration. However, presence of SWCNT enhances the carrier mobility which is primarily responsible for the enhancement of power factor.

The increase in the value of thermal conductivity (κ) with the increasing concentration of SWCNT is very small even at higher concentration which is noteworthy as individual κ for SWCNT is rather extremely high (Figure 2a).^[17] A mixture rule according to Maxwell^[20] fitted well with the graph at lower concentration but fails at higher concentrations of SWCNT (Sample V). The Wiedemann-Franz's law ($\kappa/\sigma T \approx L_0$) is followed by an electron system with elastic scattering where $L_0 = 2.45 \times 10^{-8} (\text{V/K})^2$. The estimated Lorentz number ($\kappa/\sigma T$) of the samples in comparison to L_0 , is a signature of the portion of heat carried out by electrons. The sample Lorentz numbers are large enough, ranging from 2.5×10^{-5} to $4.1 \times 10^{-7} (\text{V/K})^2$,

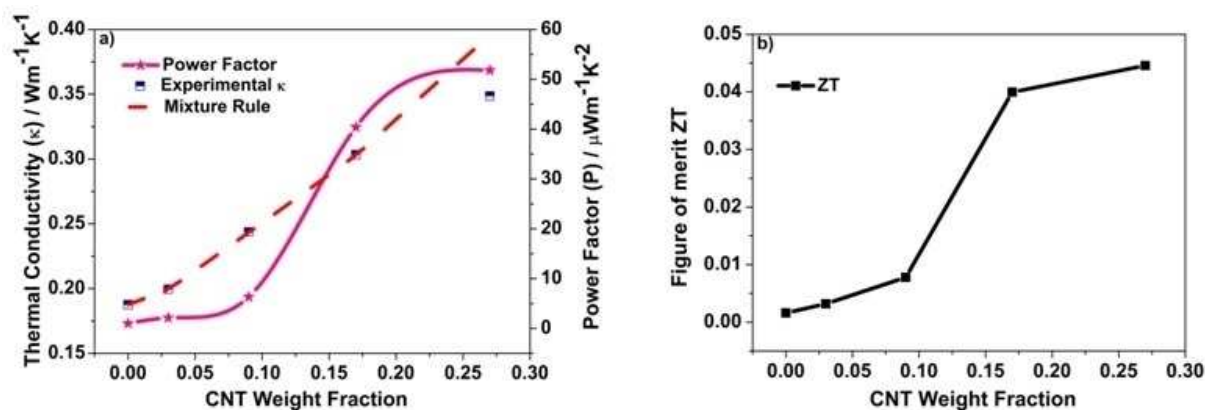


Figure 2. Variation of a) thermal conductivity and power factor and b) figure of merit with SWCNT weight fraction.

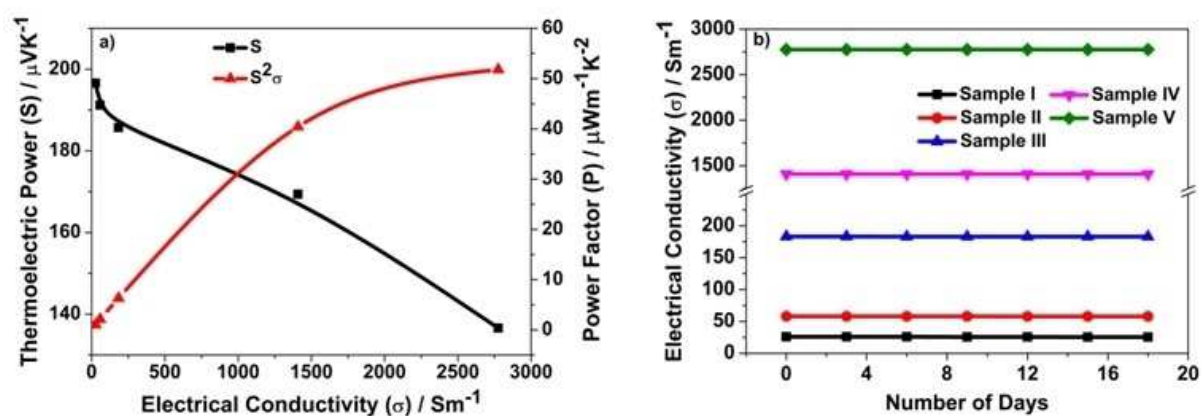


Figure 3. Variation of a) thermoelectric power and power factor with electrical conductivity, b) electrical conductivity with number of days

which indicates that the lattice contribution dominates the total κ value rather than the electronic contribution. Reports show that the selective scattering of phonons by the inclusion of nano interfaces minimizes the lattice contribution depending on their respective scattering length.^[21] Here the SWCNTs are connected to the polymer matrix by weak Van der Waals forces^[22] introducing the interfaces which obstruct the phonon transport but facilitate the electrical transport.

The figure of merit (ZT), as calculated from the above data, increases with the increase in SWCNT content reaching a maximum value of 0.045 for sample V (Figure 2b) which is twice than that of PEDOT/SWCNT composite films prepared by vapour phase polymerisation^[13g] at this SWCNT percentage. Further this value though less than PEDOT-Tos thin film but is still higher than the reported values for bulk PEDOT based nanocomposite materials.^[9,10a,21–23] This signifies that the increasing concentration of SWCNT expand the pathway for the electric transport without notably raising the thermal transport which is a favourable condition for the improvement of the transport properties thereby enhancing the figure of merit.

A correlation between the S , $S^2\sigma$ and σ for all the samples has been shown in Figure 3a. It is observed that though the thermoelectric power decreases, the power factor increases

with the increase in electrical conductivity thereby showing that the decrement in the thermoelectric power does not suppress the increment in the power factor. Moreover the increase in the ordered structure decreases the thermoelectric power due to the band gap tuning which in turn increases the carrier concentration pushing the Fermi level (E_F) into the conduction band increasing the electrical conductivity. As a result there is an overall increase in thermoelectric power factor which help in the increment of ZT. To observe the air stability of the samples for device applications, the samples were kept at normal atmosphere and measurement of σ was taken after a gap of 3 days till 18 days (Figure 3b). No anomaly has been detected during this period of time and the samples are very much stable in air at room temperature.

The ordering of the molecular structure highly influences the electrical transport properties of polymer based composite.^[24] The Van der Waals and the strong π – π interaction are assumed to be the route for the charge carrier transport. Thus, in order to determine the influence of the structural change of PEDOT-Tos, induced by the addition of different percentage of SWCNT on the transport properties, XRD of the synthesised samples was performed and shown in Figure 4a. In case of pristine PEDOT, X-ray diffraction peaks centered at 6.5° , 13.7°

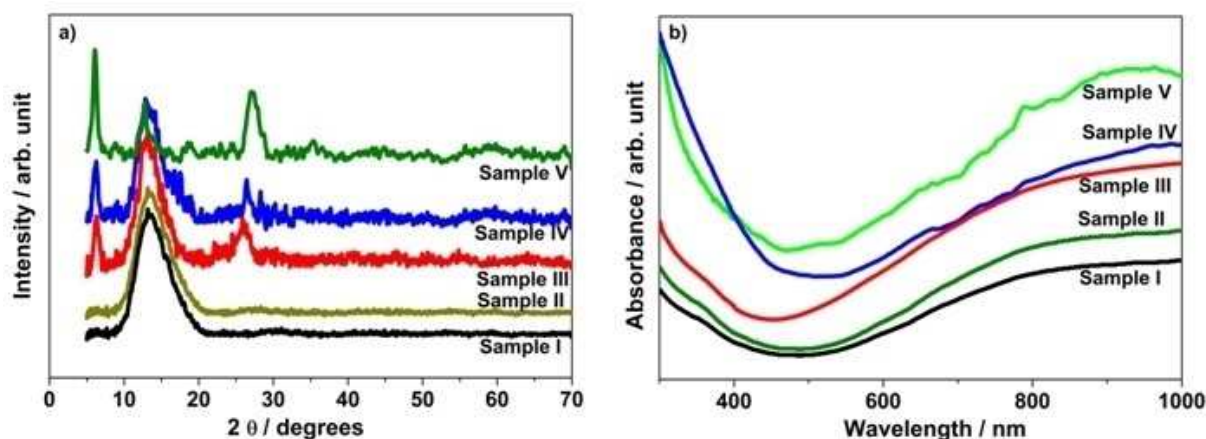


Figure 4. Spectral analysis of the synthesised samples. a) XRD and b) UV-Vis spectra.

and 28.4° attribute to the (100) (200) and (020) reflection of the polymer backbone with the lattice spacing 13.6 Å, 6.5 Å and 3.2 Å, respectively, which is in tune of other reports.^[25] The reflection of these three peaks ensures the presence of crystalline phase. Comparing the peak positions of the synthesised samples it is observed that there is a change in the peak position in the X-ray diffraction pattern for the composites. For the peak position at $2\theta \sim 6.5^\circ$, a shift towards a lower angle is observed for all three composites, which points out a change in the lattice parameters^[26] and with the increase in the SWCNT content the shift increases. It is proposed that the peak at 6.5° is related to the interchain distance within the stack. Thus the shift points towards an increase in the stacking distance. Further an increase in the intensity is also observed at this peak position with the increase in SWCNT. This increase in the stacking distance along with the increase in intensity signifies that the crystallinity is upgraded.^[25a] This improved packing may increase the tunneling of the charge carriers between the chain stacks as well as within the stack. Moreover, significant changes in the XRD pattern were observed for the samples containing 17% and 27% of SWCNT. Peaks appeared at $2\theta \sim 44.2^\circ$ which indicate the presence of SWCNT and the intensity increases with the increase in the SWCNT content. Further, the peak at $2\theta \sim 28.4^\circ$ which is attributed to the π - π stacking distance shifted to a higher angle and also get shaped with the increase in the SWCNT content. This indicates a decrease in the interlayer stacking distance. It enhances the π - π coupling providing a pathway for the charge carriers enhancing the TE properties.

The shift as well as increase in intensity at peak positions $2\theta \sim 6.5^\circ$ and 28.4° with the increase in the SWCNT content is a signature of formation of ordered structure.^[25a] Here SWCNT is assumed to take part in the bottom-up stacking leading to a well ordered structure which in turn influences the transport properties of the samples. The UV-Vis spectroscopy confirms the change in the electronic states and shown in Figure 4b. The absorption band around 600 nm attributes to the π - π^* transition.^[25b] Moreover, the delocalization of the charge

carriers on the polymer chains is indicated by the free carrier tail at the longer wavelength.^[27,28] The free carrier tail is much prominent with the increase in SWCNT content thereby indicating an increase in the delocalized charge carriers.

Study of field emission scanning electron microscopy (FESEM) was carried out to further investigate the morphology along with the reorganization process and structural development of PEDOT-Tos in the presence of SWCNT as shown in the Figure 5. The pure sample (without SWCNT) displays a granular like structure. The morphology of the samples (3% and 9% SWCNT) are governed by a decrease in grain size and much more packed together as is observed from the FESEM images.

This spatial compact nature increases with an increase in the SWCNT content in the polymer matrix. Further a morphological transformation is also observed for the samples above 0.17 weight fraction of SWCNT content. Finally Sample V shows a more ordered structure with much more compactness. Thus the result clearly shows that induction of SWCNTs restructures the PEDOT-Tos matrix to a more crystalline form through the formation of improved compact structure. It is known that a more ordered structure is always favourable for the charge transport^[29] and hence influence the transport properties.

In this bulk material, PEDOT can exist in different stereoisomers which may affect the ZT value of the material. To understand the actual situation we chose an oligomer, instead of polymer for simplicity in calculations, having four monomers joined together. This oligomer can form four stereoisomers (i) all cis, (ii) all trans, (iii) trans with cis and (iv) cis-trans-cis as shown in the top of the Figure 6a. It is interesting to note from DFT study that cis configuration between two rings introduce a curve in the molecule which produce a cavity with small radius of curvature, unsuitable to accommodate nanotubes. These molecules are less contributing to ZT value of the material. However, the molecules with trans configurations (ii and iii) are planer and fully conjugated (from HOMO and LUMO; Figure 6a) produce enough surface for π -stacking interactions with SWCNT. The HOMO and LUMO values of these configurations construct a wide valence and conduction band, respectively.

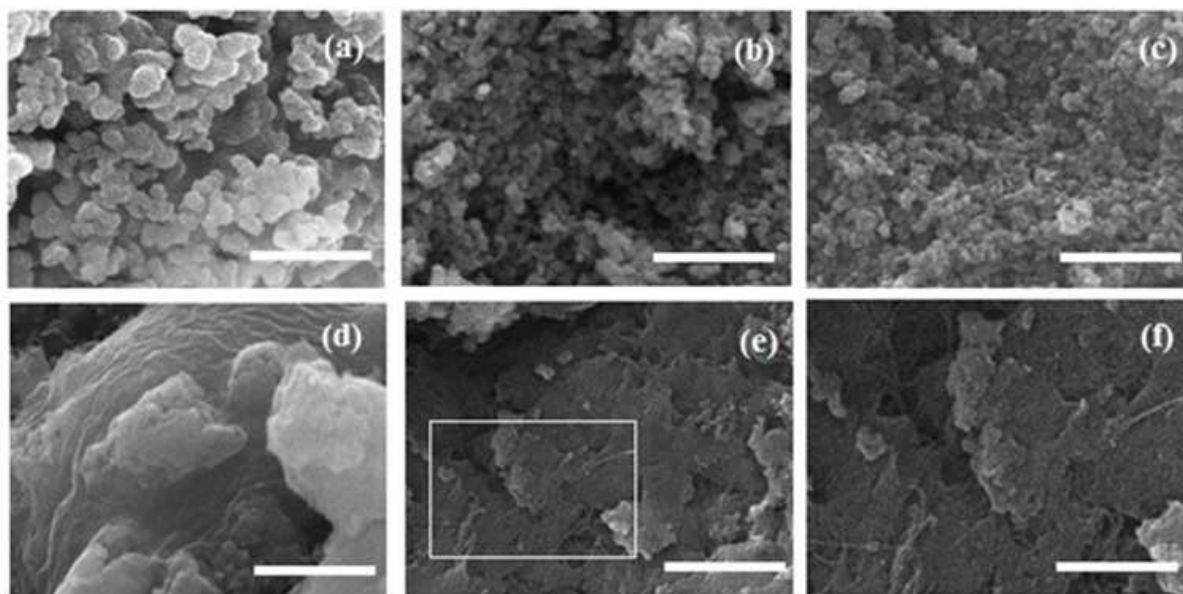


Figure 5. FESEM images a-e) Sample I–V. Scale bars μm , f) Magnified portion of Sample V. Scale bar 500 nm.

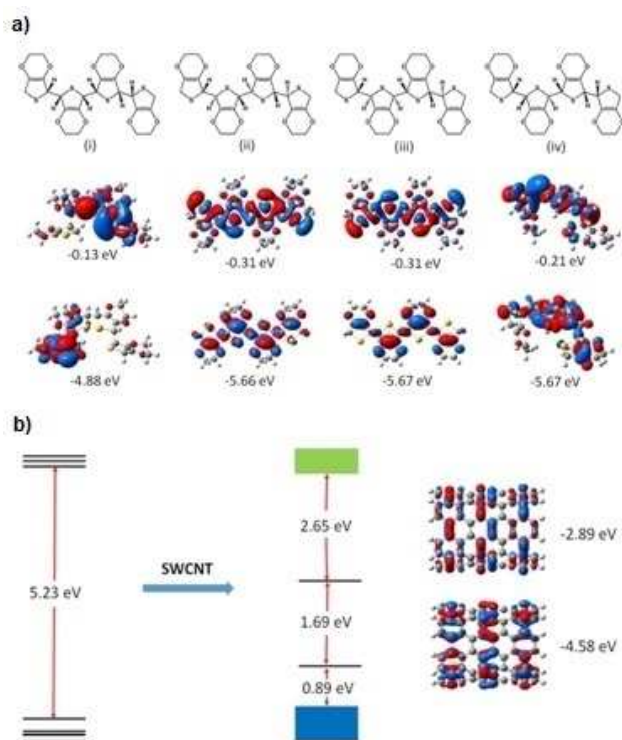


Figure 6. a) Probable stereochemistry of the oligomeric bulk material and their HOMO and LUMO, b) energy profile diagram of the PEDOT before and after SWCNT doping.

The band gap is of 5.23 eV, quite higher value for semiconductor properties of the pure material (Figure 6b). Doping of SWCNT in the PEDOT-Tos, the HOMO and LUMO of it lie in between the bands and fit such a way that the electron from valence band can go to conduction band easily for maximum

2.63 eV energy (Figure 6b). In this way PEDOT-Tos-SWCNT nanocomposites become as organic TE material with high ZT value.

Conclusions

In summary, PEDOT-Tos-SWCNT nanocomposites have been synthesised by in-situ polymerisation with the variation of SWCNT content. For electrical characterisation the measurement of σ and S as a function of SWCNT content has been carried out. It is observed that σ increases but S decreases. Though the S values are much higher than reported ones. Improved degree of crystallinity via the band gap tuning as depicted from DFT calculations, boost up the electrical conductivity which in turn enhance the TE power factor. We ascribe that this effort of improving the degree of crystallinity to pick up the electrical conductivity via band gap tuning is a way to enhance the thermoelectric power factor and hence the figure of merit of conjugated polymer based nanomaterials. Furthermore the very low κ values along with high power factor leads to a high value of ZT (0.045). To the best of author's knowledge this value is more than the reported polymer based bulk nanostructured materials.

Thus the study validates the increase in the TE performance by incorporating SWCNT in PEDOT-Tos and may be considered to be constructive in the domain of design and synthesis of polymer nanocomposites for TE applications. The cost effective procedure, nontoxic properties and scalability, is the key for the polymer nanocomposites to be used as TE materials. Furthermore, through variation of different parameters and optimization of the constituent composition, there is scope to improve the TE performance of PEDOT-Tos nanocomposites.

Supporting Information Summary

The supporting information contains the details of materials and synthesis procedure along with the characterisation

Conflict of Interest

The authors declare no conflict of interest.

Keywords: Band gap tuning · Electrical conductivity · Figure of merit · Polymer nanocomposites · Thermoelectric power

- [1] a) Q. Zhang, Y. M. Sun, W. Xu, D. B. Zhu, *Adv. Mater.* **2014**, *26*, 6829; b) C. Wan, X. K. Gu, F. Dang, T. Itoh, Y. Wang, H. Sasaki, M. Kondo, K. Koga, K. Yabuki, G. J. Snyder, R. Yang, K. Koumoto, *Nature Mater.* **2015**, *14*, 622.
- [2] S. Hwang, W. J. Potscavage, R. Nakamichi, C. Adachi, *Organic Electronics*. **2016**, *31*, 31.
- [3] Y. W. Park, W. K. Han, C. H. Choi, H. Shirakawa, *Phys. Rev. B*. **1984**, *30*, 5847.
- [4] N. T. Kemp, A. B. Kaiser, C. J. Liu, B. Chapman, O. Mercier, A. M. Carr, H. J. Trodahl, R. G. Buckley, A. C. Partridge, J. Y. Lee, C. Y. Kim, A. Bartl, L. Dunsch, W. T. Smith, J. S. Shapiro, *J. Polym Sci B: Polym Phys*. **1999**, *37*, 953.
- [5] H. Yan, N. Sada, N. J. Toshima, *Therm. Anal. Cal.* **2002**, *69*, 881.
- [6] I. Lévesque, P. O. Bertrand, N. Blouin, M. Leclerc, S. Zecchin, G. Zotti, C. I. Ratcliffe, D. D. Klug, X. Gao, F. Gao, J. S. Tse, *Chem. Mater.* **2007**, *19*, 2128.
- [7] F. X. Jiang, X. U. Jing-Kun, L. U. Bao-Yang, XIE. Yu, HUANG. Rong-Jin, L. I. Lai-Feng, *Chin. Phys. Lett.* **2008**, *25*, 2202.
- [8] L. Groenendaal, F. Jonas, D. Freitag, H. Pielartzik, J. R. Reynolds, *Adv. Mater.* **2000**, *12*, 481.
- [9] Q. Wei, M. Mukaida, K. Kiriha, Y. Naitoh, T. Ishida, *Mater.* **2015**, *8*, 732.
- [10] a) O. Bubnova, M. Berggren, X. J. Crispin, *Am. Chem. Soc.* **2012**, *134*, 16456; b) N. Massonnet, A. Carella, O. Jaudouin, P. Rannou, G. Laval, C. Celle, J. P. Simonato, *J. Mater. Chem. C*. **2014**, *2*, 1278.
- [11] O. Bubnova, Z. Ullah Khan, A. Malti, S. Braun, M. Fahlman, M. Berggren, X. Crispin, *Nat. Mater.* **2011**, *10*, 429.
- [12] a) S. Iijima, *Nature (London)*. **1991**, *354*, 56; b) L. M. Dai, A. W. H. Mau, *Adv. Mater.* **2001**, *13*, 899.
- [13] a) G. P. Moriarty, S. De, P. J. King, U. Khan, M. Via, J. A. King, J. N. Coleman, J. C. Grunlan, *J. Polym. Sci. Part B: Polym. Phys.* **2013**, *51*, 119; b) C. Bounioux, P. D'iaz-Chao, M. Campoy-Quiles, M. S. Mart'in-Gonz'alez, A. R. Göni, R. Yerushalmi-Rozen, C. Müller, *Energy Environ. Sci.* **2013**, *6*, 918; c) Q. Yao, Q. Wang, L. Wang, L. Chen, *Energy Environ. Sci.* **2014**, *7*, 3801; d) C. T. Hong, Y. H. Kang, J. Ryu, S. Y. Cho, K. S. Jang, *J. Mater. Chem. A*. **2015**, *3*, 21428; e) Y. Du, S. Z. Shen, W. D. Yang, K. F. Cai, P. S. Casey, *Synth. Met.* **2012**, *162*, 375; f) Y. Du, K. F. Cai, S. Z. Shen, P. S. Casey, *Synth. Met.* **2012**, *162*, 2102; g) J. Wang, K. Cai, J. Yin, S. Shen, *Synth. Met.* **2017**, *224*, 27.
- [14] a) A. B. Artyukhin, O. Bakajin, P. Stroeve, A. Noy, *Langmuir* **2004**, *20*, 1442; b) M. J. O'Connell, P. Boul, L. M. Ericson, C. Huffman, Y. H. Wang, E. Haroz, C. Kuper, J. Tour, K. D. Ausman, R. E. Smalley, *Chem. Phys. Lett.* **2001**, *342*, 265; c) T. M. Wu, Y. W. Lin, *Polymer*. **2006**, *47*, 3576.
- [15] K. R. Reddy, H. M. Jeong, Y. Lee, A. V. Raghu, *J. Polym. Sci.* **2010**, *48*, 1477.
- [16] A. Imani, G. Farzi, A. Ltaief, *Int. Nano Lett.* **2013**, *3*, 52.
- [17] C. Yu, L. Shi, Z. Yao, D. Li, A. Majumdar, *Nano Lett.* **2005**, *5*, 1842.
- [18] M. Cutler, J. Leavy, R. Fitzpatrick, *Phys. Rev.* **1964**, *133*, A1143.
- [19] C. Pai, C. Liu, W. Chen, S. Jenekhe, *Polymer*. **2006**, *47*, 699.
- [20] S. V. Kidalov, F. M. Shakhov, *Materials*. **2009**, *2*, 2467.
- [21] K. Chatterjee, M. Mitra, S. Ganguly, K. Kargupta, D. Banerjee, *Nanotech.* **2013**, *24*, 215703.
- [22] C. Yu, Y. S. Kim, D. Kim, J. C. Grunlan, *Nano Lett.* **2008**, *8*, 4428.
- [23] a) D. Kim, Y. Kim, K. Choi, J. C. Grunlan, C. Yu, *ACS. Nano*. **2010**, *4*, 513; b) B. Zhang, J. Sun, H. E. Katz, F. Fang, R. L. Opila, *Appl. Mater. Interfaces*. **2010**, *2*, 3170.
- [24] a) Y. Hiroshige, M. Ookawa, N. Toshima, *Synth. Met.* **2006**, *156*, 1341; b) H. Yan, T. Ohta, N. Toshima, *Macromol. Mater. Eng.* **2001**, *286*, 139; c) Q. Yao, L. Chen, X. Xu, C. Wang, *Chem. Lett.* **2005**, *34*, 522.
- [25] a) N. Kim, S. Kee, S. H. Lee, B. H. Lee, Y. H. Kahng, Y. R. Jo, B. J. Kim, K. Lee, *Adv. Mater.* **2014**, *26*, 2268; b) T. Y. Kim, J. E. Kim, K. S. Suh, *Polym. Inter.* **2006**, *55*, 80.
- [26] T. Kawai, M. Nakazono, K. Yoshino, *J. Mater. Chem.* **1992**, *2*, 903.
- [27] M. Lapkowski, A. Pron, *Synth. Met.* **2000**, *110*, 79.
- [28] S. Garreau, J. L. Duvail, G. Louarn, *Synth. Met.* **2001**, *125*, 325.
- [29] A. J. Heeger, *Rev. Mod. Phys.* **2001**, *73*, 681.

Submitted: May 8, 2018

Accepted: August 2, 2018

PAPER

Dependence of thermoelectric power and electrical conductivity on structural order of PEDOT-Tos-graphene nanocomposite via charge carrier mobility

To cite this article: Shilpa Maity *et al* 2019 *Mater. Res. Express* **6** 105095

View the [article online](#) for updates and enhancements.



IOP | ebooks™

Bringing you innovative digital publishing with leading voices to create your essential collection of books in STEM research.

Start exploring the collection - download the first chapter of every title for free.

Materials Research Express



PAPER



Dependence of thermoelectric power and electrical conductivity on structural order of PEDOT-Tos-graphene nanocomposite via charge carrier mobility

RECEIVED
17 May 2019

REVISED
7 August 2019

ACCEPTED FOR PUBLICATION
27 August 2019

PUBLISHED
18 September 2019

Shilpa Maity¹, Chiranjit Kulsi², Shiladitya Banerjee³, Sukhen Das^{1,5}  and Krishanu Chatterjee^{4,5} 

¹ Department of Physics, Jadavpur University, Kolkata 700032, India

² Department of Physics, IEST, Shibpur, Howrah, West Bengal 711103, India

³ Department of Chemistry, Techno India University, Salt Lake, Kolkata-700091, India

⁴ Department of Physics, Techno India University, Salt Lake, Kolkata-700091, India

⁵ Authors to whom any correspondence should be addressed.

E-mail: sdasphysics@gmail.com and itskrishanu@gmail.com

Keywords: polymer nanocomposites, electrical conductivity, thermoelectric power, charge carrier mobility, figure of merit

Supplementary material for this article is available [online](#)

Abstract

Nanocomposites of tosylate doped poly (3, 4 ethylenedioxythiophene) (PEDOT-Tos) and graphene with improved structural order were synthesized and investigated as organic thermoelectric (TE) materials. A TE figure of merit $ZT > 0.05$ is reported. Gradual incorporation of graphene results in an increase in the degree of structural order of the samples. A consequent increase in the figure of merit is observed, the maximum value crossing 0.05 (higher than that reported for bulk nanostructured polymer based composites) for a graphene content of 25%. The tuning of the ordered structure boosts up the charge carrier mobility, which in turn improves the thermoelectric power (S) simultaneously with the electrical conductivity (σ). Consequently there is an increase in the TE power factor. Moreover, the thermal conductivity of the nanocomposites is very low due to selective phonon scattering by the introduction of the nanointerfaces designed in the PEDOT-Tos-graphene nanocomposites, which further contributes to the enhancement in ZT . An opposite trend is observed in structure and ZT , for a graphene content of 40%; arising probably from reduced π -stacking interactions between graphene and the PEDOT units. This study proves to be an effective way and can escort the future design and synthesis of high-performance thermoelectric conjugated polymers.

1. Introduction

One of the major threats facing the 21st century is the crisis of energy. To improve the current efficiency of energy, the conventional fossil fuels are replaced by alternative energy sources viz solar energy, hydrogen energy, biomass energy etc. Now a day, a substantial amount of heat energy is irresistibly generated and wasted in daily life and industrial production. Thermoelectric (TE) materials have potential to convert heat energy directly to electrical energy utilizing the waste heat source [1–3]. This creates an interest in the application of TE materials starting from cochlear implant to thermal charging of photo-detectors and LED. TE devices have some individual advantages other than new energy technologies, such as no noise and long operating lifetime. Performance of a TE material is expressed by its dimensionless figure of merit $ZT = S^2\sigma T/\kappa$, where S is the thermoelectric power or Seebeck coefficient, σ is the electrical conductivity, T is the absolute temperature and κ is the thermal conductivity respectively. But the parameters are so interconnected that achieving a high ZT value is a challenge. During the last three decades research on TE materials progressed a lot since the work of Dresselhaus [4].

Graphene in recent years attracted a lot of attention as a potential TE material due to some of its unique features viz high carrier mobility and hence high electrical conductivity, two dimensional (2D) structure etc.

Through density functional theory (DFT) calculations a high ZT value of 5.8 of graphene has been reported [5]. But at the same time its high thermal conductivity ($2500\text{--}5300\text{ W m}^{-1}\text{ K}^{-1}$) [6, 7] makes it a weak challenger for TE applications. Since a combination of high electrical conductivity and low thermal conductivity makes an efficient TE material, latest research focuses on organic polymer TE and their graphene nanocomposites, due to low cost, ease of synthesis and their intrinsic low thermal conductivity. Further the flexibility of the polymers assists them to be incorporated in different topologies.

Consequently the research on combination of polypyrrole and polyaniline with graphene exhibits a good choice for improving the thermoelectric properties [8–10]. Nevertheless the ZT values ($\sim 10^{-3}$ to 10^{-4}) are much lower than that of inorganic semiconductors due to low Seebeck coefficient (or thermoelectric power) S . This is followed by the synthesis of PEDOT-PSS graphene nanocomposites for TE applications and attracted much attention [11] but still have low S values. Contrary to PEDOT-PSS, PEDOT-Tos exhibits superior TE performance as has been demonstrated by Bubnova *et al* [12], yet the polymer graphene nanocomposites have been unexplored. It has been reported that the thermoelectric power depends on the density of states (DoS) slope at the Fermi level E_F [13] and through the modification of crystallinity of PEDOT, changes in the DoS can be achieved [12]. For PEDOT, with the increase in the structural order there is an improvement in the carrier delocalization and π orbital overlapping [14] influencing the electronic band structure which has an effect on the charge transport properties. Consequently it has been suggested that for PEDOT-Tos increase in the structural order, modify the DoS affecting both the electrical conductivity and thermoelectric power positively [12].

In the present study, we focus on the increase in the crystallinity of PEDOT-Tos with the incorporation of graphene. Since the structural order affects the charge carrier transport, a mapping between the structural order and the charge carrier transport has been done. The source of the interconnection between the structural order and the charge carrier transport are discussed and supported by the spectral analysis and temperature dependant electrical conductivity.

2. Experimental

2.1. Material used

3, 4 ethylenedioxythiophene (EDOT) monomer was purchased from Sigma Aldrich. Para toluene sulfonic acid (pTSA) and ammonium peroxydisulfate (APS) were purchased from alfa-aesar. Graphene was purchased from Platonic Nanotech Pvt. Ltd Ethanol was purchased from merck chemicals. Deionised water was purchased from hydrolab, India.

2.2. Synthesis of PEDOT-Tos by *in situ* polymerization

PEDOT is synthesized by using *in situ* polymerization of EDOT monomer in an aqueous solution of PTSA, using APS as oxidant. The solution of EDOT (0.02 mol) which was dissolved in an aqueous solution containing PTSA (0.04 mol) was stirred with a magnetic stirrer, for 30 min at room temperature. APS was used as oxidant and was prepared by dissolving APS (0.02 mol) in 100 ml of water. In the following steps the APS solution was added drop-wise to the aqueous solution of EDOT monomer and the reaction mixture was stirred for 24 h at room temperature. A dark blue precipitate was formed, indicating PEDOT (doped with PTSA). After 24 h the product was collected by centrifugation for 5 min at 7000 rpm and rinsed with deionized water and ethanol in sequence then finally dried in vacuum at 70°C . We named the sample as S-I.

2.3. Preparation of PEDOT-Tos/Graphene nanocomposites

For the preparation of nanostructured PEDOT-Tos/Graphene nanocomposite doped with PTSA, graphene was added in a pre-prepared aqueous solution containing PTSA (0.04 mol) and was constantly stirred for 30 min and then ultrasonicated again for 30 min to obtain a well dispersed solution. EDOT (0.02 mol) was mixed to the solution and was constantly stirred for 30 min. This is followed by the addition of APS (0.02 mol) as oxidant to the solution and the reaction mixture was stirred for 24 h at room temperature for direct synthesis of PEDOT-Tos/Graphene nanocomposites. The final product obtained after polymerization was centrifuged for 5 min at 7000 rpm and vacuum dried in an oven at 70°C . The graphene content was calculated and comes out to be 6% (S-II). The above procedure was again repeated for different weight of graphene and the weight percentages calculated comes out to be 15% (S-III), 25% (S-IV), and 40% (S-V) respectively.

2.4. Characterization

All the prepared samples were structurally characterized by powder x-ray diffraction (XRD) patterns, UV-vis, fourier transform infrared (FTIR) spectroscopy and field emission scanning electron microscopy (FESEM). X-ray powder diffraction measurements were performed using a diffractometer (BRUKER D8 Advance) with $\text{Cu K}\alpha$ radiation ($\lambda = 1.54182\text{ \AA}$). The UV-vis spectra of the prepared samples were recorded by a

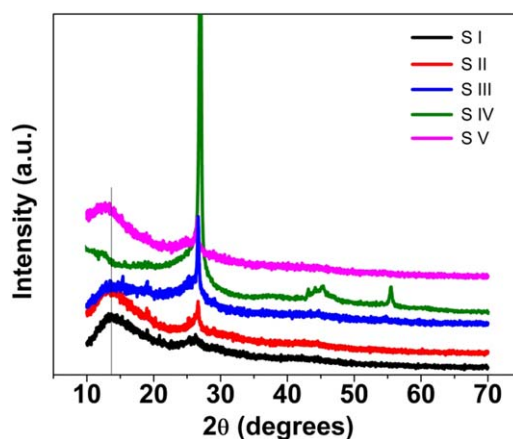


Figure 1. XRD spectra of the synthesized samples.

spectrophotometer (Perkin-Elmer-USA, Lambda-45) using samples dissolved in ethanol in quartz tube with data being recorded in the wavelength range 350–1000 nm. FESEM images were obtained using a Hitachi (S3400N) to get an idea of the surface morphology of the samples.

For the measurement of electrical transport properties rectangular shaped pellets (10 mm × 5 mm × 5 mm) of all samples were prepared by cold pressing at 1 ton pressure. The electrical conductivity of the samples was measured by four probe method. For the measurement of thermoelectric power, temperature difference has been established along the ends of the samples, while the corresponding potential drop was measured by a Hewlett Packard data acquisition system (Model No. 34970 A). Room-temperature thermal conductivity measurements were carried out for the prepared samples using a Hot Disk thermal constants analyser (TPS 2500 S, Sweden).

3. Results and discussions

3.1. Spectral studies

In polymer based composite, the degree of the structural order stimulates the electrical transport properties [15]. In the present work the strong π – π interaction and increases in structural order are presumed to be the grounds for the enhancement in the charge carrier transport. Thus, the interactions between PEDOT-Tos and graphene for its different weight percentage into the polymer matrix are identified by x-ray diffraction and shown in figure 1.

The pristine sample shows peaks at an angle 13.6° and 26.1° which are attributed to the reflection plane (200) and (010) [16, 17]. These peaks signify the presence of crystalline phase in the polymer matrix. The XRD spectra of the composites shows a lower angle shift for the scattering angle 13.6° which suggest a change in the lattice parameter till 25% graphene concentration in the polymer matrix. But for 40% graphene concentration it again shifted to higher angle. All the samples feature a distinct peak at around 26° . This peak is a signature of crystalline nature of PEDOT with increases and ordered π – π interaction of the conjugated units [18]. It is observed that with the increases in graphene content the intensity of the peak increases with a shift to a higher angle till 25%. Following Bragg's law, the stacking distances were estimated which comes out to be 3.4 Å for the pristine sample. The stacking distance decreases with the graphene content till 25% (table 1) beyond which the stacking distance increases. This decrease in the interlayer stacking distance and the increase in the intensity of the peak around 26° signify that with the increase in graphene content a closer packing structure is favoured with improved π – π coupling, providing a pathway for the charge carriers, stepping up the TE properties. Moreover, it is also observed that 25 wt% of graphene in PEDOT-Tos matrix behaves as the threshold amount beyond which there is a hindrance in the growth of crystallization of the PEDOT-Tos creating a barrier to transport the carriers in the composite as observed for graphene-polyaniline nanocomposites [19, 20] and is in tune with the electrical transport properties.

Further we elucidate through UV–vis and FTIR characteristics of the samples shown in figures 2 and 3 respectively.

The UV–vis spectrum of the pristine sample shows a strong absorption band around 800–900 nm which is assigned to π^* -polaron transition [21]. The spectra of the composite samples, in addition to π^* -polaron transition, also shows a band around 362 nm which is attributed to π – π^* transition. This band is red shifted to 378 nm and 387 nm for S-III and S-IV respectively which signify an increase in the interaction between the

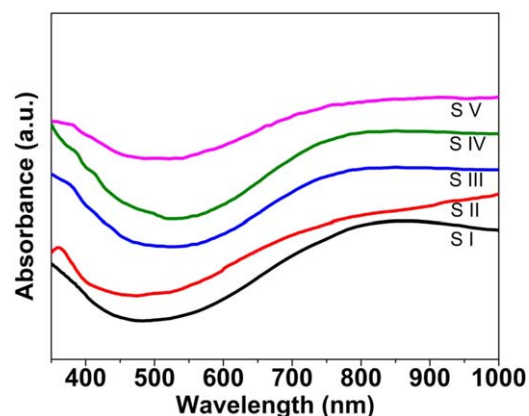


Figure 2. UV-vis spectra of the synthesized samples.

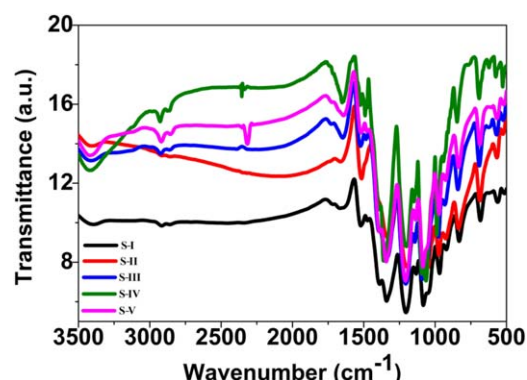


Figure 3. FTIR spectra of the synthesized samples.

Table 1. Room temperature values of the characteristic Mott temperature (T_0), hopping distance (R_{hop}), activation energy (E_{hop}), carrier concentration (n) and carrier mobility (μ) of the synthesized samples.

Sample name	d (Å)	T_0 (K)	R_{hop} (Å)	E_{hop} (meV)	n ($10^{18} \times \text{cm}^{-3}$)	M ($\text{cm}^2 \text{V}^{-1} \text{s}^{-1}$)
S-I	3.4	827.43	1.11	8.32	1.3	7.596
S-II	3.38	651.015	1.04	7.85	1.7	9.522
S-III	3.35	434.055	0.94	7.09	2.4	14.818
S-IV	3.31	346.406	0.89	6.7	3.2	17.089
S-V	3.37	486.846	0.96	7.30	3.9	9.872

quinoid ring of the polymer and graphene [8–22]. Consequently there is an increase in the delocalization of the charge carriers which in turn increases the electrical transport properties. For S-V the band is blue shifted to 381 nm with respect to S-IV indicating the weakening of $\pi-\pi^*$ transition [20]. It was also observed that the UV-vis spectra display a trend of a free carrier tail at the longer wavelength for all the samples which indicates the delocalization of the charge carriers [23, 24]. The results reveal the formation of adequate number of charge carriers and PEDOT is in a bipolaronic state.

For the pristine sample the bands observed in FTIR spectra are at 681, 831, 922 and 969 cm^{-1} are the assigned to the deformation modes of C–S–C in the thiophene ring [25, 26]. The bands around 1083, 1133 and 1202 cm^{-1} are the signature of C–O–C bending vibration of the ethylenedioxy group [21]. The bands around 1338 and 1519 cm^{-1} are attributed to the C–C stretching and C=C stretching of the quinoidal structure of the thiophene rings [27, 28]. Further the band around 1657 cm^{-1} is assigned to the polarons present in PEDOT. The FTIR spectrum of composite samples show all the bands but with a shift to a higher wave number till 25%. In

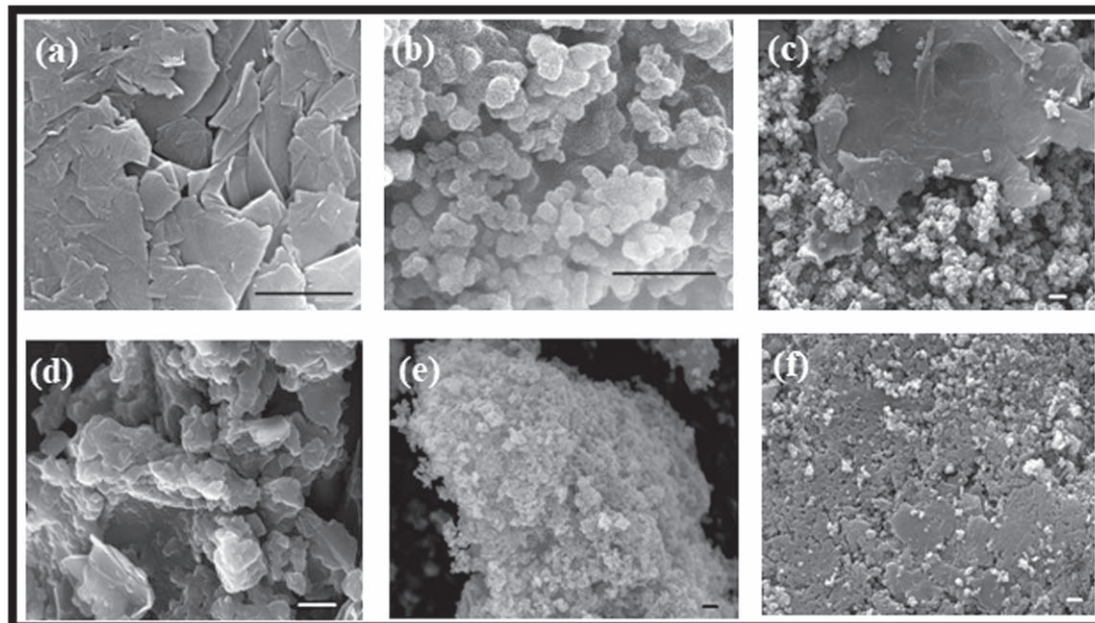


Figure 4. FESEM images of (a) graphene and the synthesized samples (b)–(f) Sample S-I to S-V. Scale bar 1 μm .

addition a new band around 1481 cm^{-1} is also observed which signifies C=C stretching of the quinoidal structure of the thiophene rings which is also shifted with the increase in graphene concentration till 25%.

The shift is likely to be the π – π interactions between graphene and the thiophene rings of PEDOT [29]. Consequently this points out to be a change in the resonant structure of PEDOT with the addition of graphene from a benzenoid structure which supports a coiled conformation to a quinoid one favouring a linear coil conformation resulting in the delocalization of the charge carriers all through the polymer chain [30].

3.2. Structural characterization

To further look into the development of restructuring of PEDOT-Tos with the addition of graphene morphological study has been carried out through scanning electron microscopy (figure 4). The SEM image of pristine PEDOT-Tos displays a self-assembled granular structures less compact in nature.

With the addition of graphene, the morphology of the sample for S-I shows an increase in compactness. With further increase in the graphene concentration in the polymer matrix, this spatial compact nature increases. Further, the SEM images clearly exhibit that the graphene serves as the growth template of PEDOT and the interaction increases with the addition of graphene till S-IV. For S-V we observe that there is again a decrease in the interaction between PEDOT-Tos and graphene which is in tune with XRD, UV–vis and electrical transport properties. Thus addition of graphene in PEDOT-Tos matrix increase the interaction between the constituents resulting in more ordered structure till a threshold value which consequently increases the electrical transport properties. Report shows that a more ordered structure favours charge transport [31].

3.3. Electrical characterization

In order to determine the electrical transport properties of the prepared samples, the variation of the electrical conductivity (σ) at room temperature with graphene concentration was measured and plotted in figure 5(a). The value of σ shows a hike with the increase in graphene concentration reaching a maximum value of 875.2 Sm^{-1} for S-IV, which is more than five times higher than the pristine one, and then it decreases for S-V.

The values of electrical conductivity in each case are higher than that of PEDOT-PSS-graphene nanocomposites [32, 33] and PEDOT-rGO nanocomposites [29]. This enhancement in the value of σ indicates a change in structural order of the samples.

To further investigate the variation of the electrical conductivity with temperature of the prepared samples has been studied and shown in figure 5(b). For all the prepared samples a rise in σ value has been detected with the rise in temperature representing semiconducting nature. It is well known that for polymers a quasi one dimensional variable range hopping (VRH) model explains the electrical conduction mechanism [8, 21]. Along these lines, temperature dependent σ values have been explained according to Mott's VRH model [34]

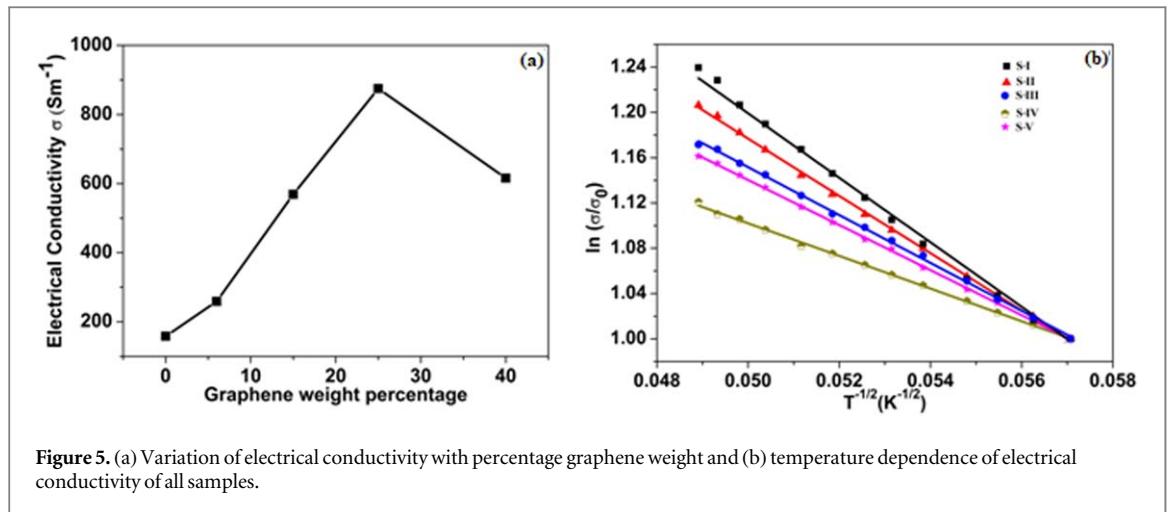


Figure 5. (a) Variation of electrical conductivity with percentage graphene weight and (b) temperature dependence of electrical conductivity of all samples.

$$\sigma = \sigma_0 \exp [-(T_0/T)^{1/2}] \quad (1)$$

where σ_0 is the high temperature limit of conductivity and T_0 is the characteristics Mott temperature associated with the carrier hopping barrier. T_0 values have been evaluated by fitting equation (1) and tabulated (table 1). It is observed that with the increase in graphene loading within PEDOT-Tos matrix T_0 decreases thereby showing that the carrier hopping barrier decreases resulting in an enhancement of σ . Further, the average hopping distance (R_{hop}) and the activation energy (E_{hop}) according to the VRH model is given by [21]

$$R_{\text{hop}} = (3/8)(T_0/T)^{1/4}L \quad (2)$$

$$E_{\text{hop}} = (1/4)k_B T (T_0/T)^{1/4} \quad (3)$$

where L is the localization length. Taking the value of the localization length of EDOT monomer units to be 2.29 \AA [35] the hopping distance and the activation energy has been estimated at room temperature (table 1). A decrease in the average hopping distance and an increase in the activation energy are reflected. This is a signature of the observed enhancement in the value of the electrical conductivity.

In addition, to illuminate the scientific knowledge for the enhanced σ values, the carrier concentration (n) of the samples has been studied from Hall measurement and hence the carrier mobility (μ) has been estimated and the values are tabulated (table 1).

The positive values of R_H (not shown) denote that the majority charge carriers are holes (p-type). A substantial increase in the carrier mobility is observed while the increase in carrier concentration is small. Thus the enhancement of the electrical conductivity is mainly attributed to the increase in the charge carrier mobility. Generally for polymeric system, the structure of ordering of polymers greatly influences the electrical transport properties. The ring twisting introduces more π - π conjugate defects resulting in a decrease in the carrier mobility. Here the graphene template most likely helps PEDOT-Tos to switch from a coil-like conformation to an extended conformation thereby increasing the structural order which enhances the hopping rate (including hopping distance and activation energy) within the polymer matrix increasing the value of σ . Further the π - π interaction between the PEDOT-Tos and graphene surface helps to reduce the π - π defects which may be responsible to channel the carrier transport enhancing the charge carrier mobility and hence the electrical conductivity. The decrease in the electrical conductivity is probably due to the following reasons. The excess graphene beyond 25% probably obstructs the crystallize growth forming barriers to carrier transport. Moreover the increases in the graphene content beyond this percentage also results in polymer twisting inducing longer hopping distance for the charge carriers resulting in a decrease in the carrier mobility.

The variation of thermoelectric power and power factor with graphene concentration has been shown in figures 6(a) and (b). An increase in S is observed reaching a maximum value of $167.2 \mu\text{VK}^{-1}$ for sample S-IV but decrease thereafter.

Since σ and S follow an inverse relation to the gap between narrow transport level and Fermi level, both the parameters cannot increase at the same time [36]. Surprisingly, in the present case both these parameters increases with the increase in the graphene concentration thereby showing that band theory or the electron-phonon scattering based conventional model [37] could not explain the conduction mechanism. To investigate this characteristic of the thermoelectric power, we consider the Mott's formalism consisting of energy dependent mobility [$\mu(E)$] and carrier concentration (n) terms and is written as

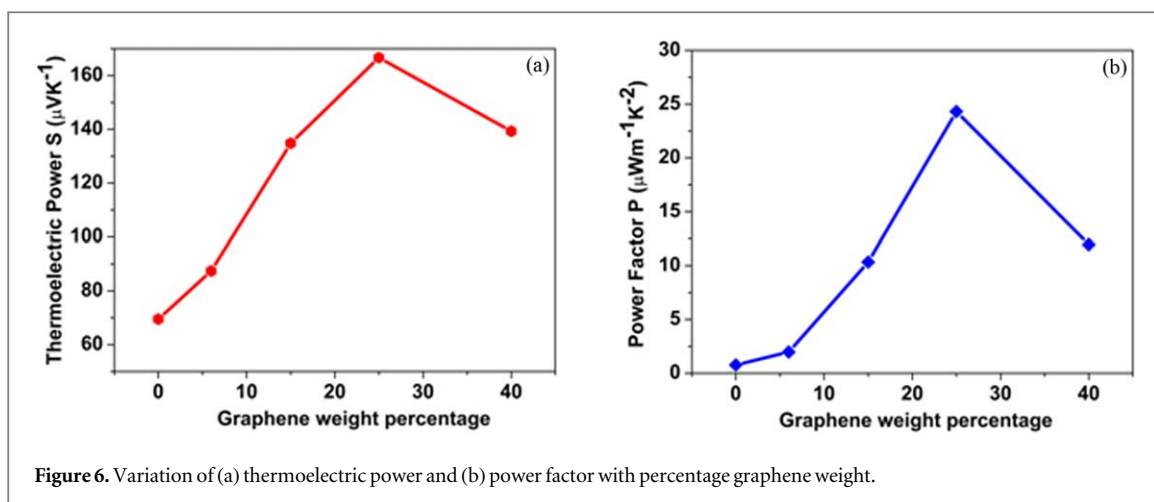


Figure 6. Variation of (a) thermoelectric power and (b) power factor with percentage graphene weight.

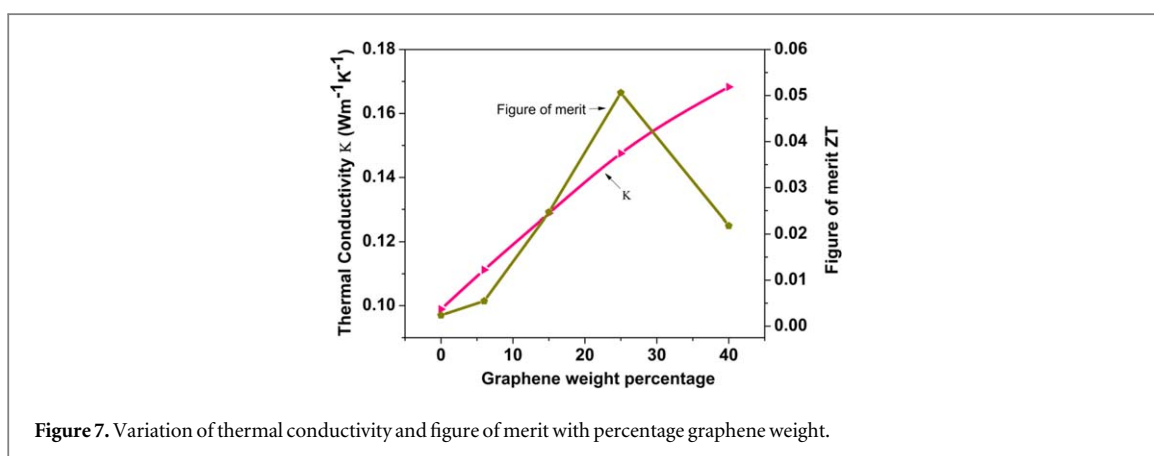


Figure 7. Variation of thermal conductivity and figure of merit with percentage graphene weight.

$$S = \frac{C_e}{n} + \frac{\pi^2 k_B^2 T}{3e} \left[\frac{\partial \ln \mu(E)}{\partial E} \right]_{E=E_F} \quad (4)$$

where, k_B and C_e are the Boltzmann constant and the specific heat respectively. It is assumed from equation (4) that both n and $\mu(E)$ should influence the thermoelectric power. It is observed that the carrier mobility plays a crucial role till 25% of graphene content in the polymer since the increase in carrier mobility is much higher than the increase in carrier concentration. Increase in the structural order increases the charge carrier mobility which in turn increases the electrical conductivity as well as thermoelectric power. Thus this method proves to be an effective way to improve thermoelectric properties of polymers since enhancement of mobility of inorganic semiconductors now a days are a new route. The decrease of the thermoelectric power after 25% graphene content is probably due to the increase in the twisted chains producing more defects with the increase in graphene content [38]. This in turn decreases the carrier mobility and the carrier concentration comes into play decreasing the thermoelectric power. Further it has been proposed by Bubnova *et al* [12] that with the increase in the structural order the asymmetry of the density of states increases thereby resulting a higher thermoelectric power for PEDOT-Tos. With the increases in crystallinity a broadening of DoS is noticed [13] and it is reported that this broadening is transmitted to all the π bands together with those close to Fermi level [39, 40] which enhances the carrier mobility as well as the thermoelectric power [12]. Here in this case with the increases in the graphene content till 25% there is an increase in the structural order as well as crystallinity which results in an increase in carrier mobility as well as the thermoelectric power. As graphene content increases beyond 25% this structural order diminishes resulting in a decrease of the electrical conductivity as well as the thermoelectric power. Since both σ and S values increase with the graphene content, the power factor also increases reaching a maximum value of $24.3 \mu\text{Wm}^{-1}\text{K}^{-2}$ for the sample S-IV, thereby it decreases for the sample S-V.

3.4. Thermal conductivity and figure of merit

The variation of thermal conductivity (κ) with graphene content is measured and studied (figure 7). Though the thermal conductivity of graphene is much higher and phonon dominated yet the rise in the κ value with increasing concentration of graphene is insignificant.

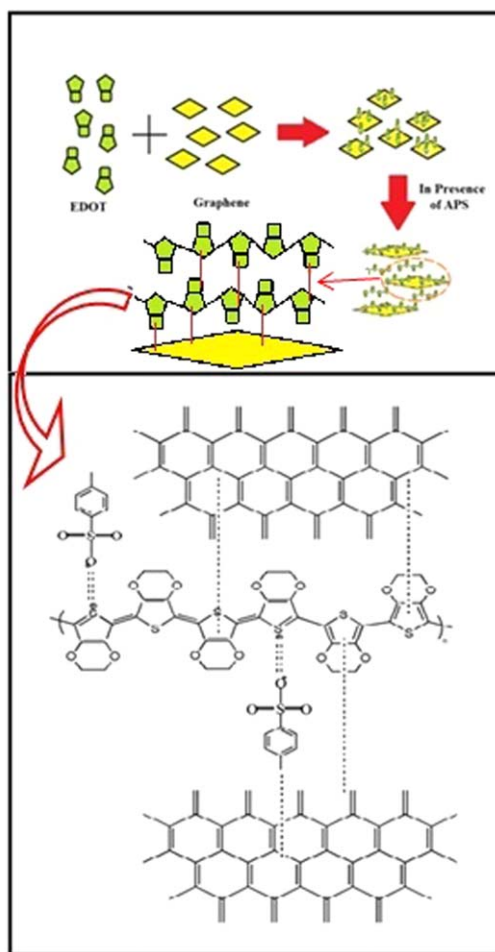


Figure 8. Schematic representation of polymerization of EDOT and mechanism of formation of nanocomposites.

The κ values are much lower than the reported graphene based PEDOT nanocomposite [11, 41]. κ value comprises of the electron transporting heat κ_e and the phonons travelling through the lattices κ_l . In the present case the κ values are phonon dominated as the electronic contribution is very small.

It was observed that the surface porosity and insertion of nano interfaces enhances the scattering of phonons reducing the lattice contribution [22, 41]. The graphene multi layers within the PEDOT-Tos matrix probably introduce surface porosity and nano interface which acts as scattering center of phonons reducing the κ_l but the electron mobility can be maintained.

Lastly the figures of merit (ZT) of the prepared samples at room temperature has been evaluated and compared in figure 7. The maximum ZT value obtained for S-IV comes to be 0.0506 which is more than 21 times higher than the pristine sample. Further it is noteworthy that this value is higher than graphene based polymer nanocomposites [8, 19, 20, 29, 41, 42]. Thus the increase in graphene concentration within PEDOT-Tos matrix is a signature of enlarging the pathway for the electrical transport till a threshold value without remarkably increase in thermal transport which favour the improvement of the transport properties and as a result the figure of merit increases. There is a scope to further increase the ZT value through variation in the nanostructure of PEDOT-Tos-graphene nanocomposites.

3.5. Proposed mechanism of formation of nanocomposites

The mechanism of the formation of the nanocomposites is schematically shown in figure 8. Some of the EDOT monomer adheres to the surface of graphene as soon as it is mixed with the solution containing EDOT and pTSA. The EDOT, absorbed on the surface of graphene acting as template, starts growing in the presence of APS as seen by comparing the SEM micrographs of the nanocomposites. The bonding between the graphene layers and the PEDOT:Tos polymers can be ascribed to π -stacking interactions, the main contribution to which comes from van der Waals forces between the π -systems of graphene and the aromatic thiophene units of the PEDOT chain resulting in an energetically more preferred merging of band structure.

Since the sulphonate anions neutralize the charges of the EDOT molecules the contributions of electrostatic forces and hydrogen-bonding to the stacking interactions are expected to be minimum. The possible reasons behind the graphene-induced increase in hopping rate and charge carrier mobility have already been discussed before, in the text. This is concordant with an initial decrease in stacking distance with increase in graphene content (upto 25%). The increase of stacking distance with an increase in graphene content beyond 25% can probably arise from increased π -stacking interaction between the graphene layers, with reducing interaction between the graphene and PEDOT layers (it is to be noted here that thiophene is less aromatic than benzene). This leads to lower π -stacking interaction between the graphene and PEDOT layers and henceforth reduces the stability coming therein.

4. Conclusion


PEDOT-Tos-graphene nanocomposite has been synthesized at room temperature via *in situ* polymerization. It has been observed from the structural characterization that addition of graphene to the polymer matrix results in more ordered structure. The increase in the degree of ordered structure increases the hopping rate (including hopping distance and activation energy) within the polymer matrix. Moreover the ordered structure results in π - π interactions leading to a reduction in the π - π conjugation defects in the backbone of the polymer chain. As a consequence the charge carrier mobility of the synthesized samples increases which in turn increases the electrical conductivity. Also the carrier mobility plays a crucial role till 25% of graphene content in the polymer to increase the thermoelectric power as well. The change in the thermal conductivity with the graphene content is small and can be attributed to the phonon scattering by the nanointerfaces. The maximum ZT value reaches 0.0506 which is higher than that of PEDOT based bulk nanostructure. This study proves to be helpful in designing and synthesis of polymer nanocomposites for TE applications. Further this method shows an effective way to improve the thermoelectric properties of polymers via the enhancement of mobility of the charge carriers and can be extended to other polymer systems.

Acknowledgments

The authors acknowledge the Department of Chemistry, Techno India University, West Bengal for various help.

ORCID iDs

Sukhen Das  <https://orcid.org/0000-0001-8372-3076>

Krishanu Chatterjee  <https://orcid.org/0000-0001-6400-3110>

References

- [1] Chen G, Dresselhaus M S, Dresselhaus G, Fluor J P and Caillat T 2003 Recent developments in thermoelectric materials *Int. Mater. Rev.* **48** 45–66
- [2] Tritt T M, Böttner H and Chen L 2008 Thermoelectrics: direct solar thermal energy conversion *MRS Bull.* **33** 366–8
- [3] Synder G J and Toberer E S 2008 Complex thermoelectric materials *Nat. Mater.* **7** 105–14
- [4] Hicks L D and Dresselhaus M S 1993 Effect of quantum-well structures on the thermoelectric figure of merit *Phys. Rev. B: Condens. Matter Mater. Phys.* **4** 12727–31
- [5] Ni X, Liang G, Wang J S and Li B 2009 Disorder enhances thermoelectric figure of merit in armchair graphene nanoribbons *Appl. Phys. Lett.* **95** 192114
- [6] Ghosh S, Calizo I, Teweldebrhan D, Pokatilov E P, Nika D L, Baladin A A, Bao W, Miao F and Lau C N 2008 Extremely high thermal conductivity of graphene: prospects for thermal management applications in nanoelectronic circuits *Appl. Phys. Lett.* **92** 151911
- [7] Lin J et al 2010 Gating of single-layer graphene with single-stranded deoxyribonucleic acids *Small.* **6** 1150–5
- [8] Mitra M, Kulsi C, Chatterjee K, Kargupta K, Ganguly S, Banerjee D and Goswami S P 2015 Reduced graphene oxide-polyaniline composites-synthesis, characterization and optimization for thermoelectric applications *RSC Adv.* **5** 31039–48
- [9] Wang L, Liu F, Jin C, Zhang T and Yin Q 2014 Preparation of polypyrrole/graphene nanosheets composites with enhanced thermoelectric properties *RSC Adv.* **4** 46187–93
- [10] Wang Y, Yang J, Wang L, Du K, Yin Q and Yin Q 2017 Polypyrrole/graphene/polyaniline ternary nanocomposite with high thermoelectric power factor *ACS Appl. Mater. Inter.* **9** 20124–31
- [11] Xiong J, Jiang F, Shi H, Liu C, Zhou W, Jiang Q, Zhu Z and Hu Y 2015 Liquid exfoliated graphene as dopant for improving the thermoelectric power factor of conductive PEDOT:PSS nanofilm with hydrazine treatment *ACS Appl. Mater. Inter.* **7** 14917–25
- [12] Bubnova O et al 2014 Semi-Metallic polymers *Nat. Mater.* **13** 190–4
- [13] Petsagkourakis I et al 2018 Correlating the seebeck coefficient of thermoelectric polymer thin films to their charge transport mechanism *Org. Electron.* **52** 335–41
- [14] Kim N, Lee B H, Choi D, Kim G, Kim H, Kim J R, Lee J, Kahng Y H and Lee K 2012 Role of interchain coupling in the metallic state of conducting polymers *Phys. Rev. Lett.* **109** 106405

- [15] Yao Q, Chen L D, Xu X C and Wang C F 2005 The High thermoelectric properties of conducting polyaniline with special submicron-fibre structure *Chem. Lett.* **34** 522–3
- [16] Kim N, Kee S, Lee S H, Lee B H, Kahng Y H, Jo Y R, Kim B J and Lee K 2014 Highly conductive PEDOT:PSS nanofibrils induced by solution-processed crystallization *Adv. Mater.* **26** 2268–72
- [17] Zhou J et al 2015 Semi-metallic, strong and stretchable wet-spun conjugated polymer microfibers *J. Mater. Chem. C* **3** 2528–38
- [18] Kim T Y, Park C M, Kim J E and Suh K S 2005 Electronic, chemical and structural change induced by organic solvents in tosylate-doped poly(3, 4-Ethylenedioxythiophene) (Pedot-Ots) *Synth. Met.* **149** 169–74
- [19] Zhao Y, Tang G S, Yu Z Z and Qi J S 2012 The effect of graphite oxide on the thermoelectric properties of polyaniline *Carbon* **50** 3064–73
- [20] Lu Y, Song Y and Wang F 2013 Thermoelectric properties of graphene nanosheets-modified polyaniline hybrid nanocomposites by an *in situ* chemical polymerization *Mater. Chem. Phys.* **138** 238–44
- [21] Ramakrishnan R, Devaki S J, Aashish A, Thomas S, Varma M R and Kpp N 2016 Nanostructured semiconducting PEDOT-TiO₂/ZnO hybrid composites for nanodevice applications *J. Phys. Chem. C* **120** 4199–210
- [22] Chatterjee K, Mitra M, Kargupta K, Ganguly S and Banerjee D 2013 Synthesis, characterization and enhanced thermoelectric performance of structurally ordered cable-like novel polyaniline–bismuth telluride nanocomposite *Nanotechnol.* **24** 215703 (10pp)
- [23] Lapkowski M and Pron A 2000 Electrochemical oxidation of poly(3, 4 ethylenedioxythiophene)—‘*in situ*’ conductivity and spectroscopic investigations *Synth. Met.* **110** 79–83
- [24] Garreau S, Duvail J L and Louarn G 2002 Spectroelectrochemical studies of Poly(3,4-Ethylenedioxythiophene) in aqueous medium *Synth. Met.* **125** 325–9
- [25] Selvaganesh S V, Mathiyarasy J, Phani K L N and Yegnaraman V 2007 Chemical synthesis of PEDOT–Au nanocomposite *Nanoscale Res. Lett.* **2** 546–9
- [26] Wang Y, Cai K, Chen S, Shen S and Yao X 2014 One-Step interfacial synthesis and thermoelectric properties of Ag/Cu-Poly(3,4-ethylenedioxythiophene) nanostructured composites *J. Nanopart. Res.* **16** 2531
- [27] Wang Y, Cai K and Yao X 2011 Facile fabrication and thermoelectric properties of PbTe-modified Poly(3,4-ethylenedioxythiophene) nanotubes *ACS Appl. Mater. Interfaces* **3** 1163–6
- [28] Chen L, Liu W, Su X, Xiao S, Xie H, Uher C and Tang X 2017 Chemical synthesis and enhanced electrical properties of bulk Poly(3, 4-ethylenedioxythiophene)/reduced graphene oxide nanocomposites *Synth. Met.* **229** 65–71
- [29] Yoo D, Kim J, Lee S H, Cho W, Choi H H, Kim F S and Kim J H 2015 Effects of one- and two- dimensional carbon hybridization of PEDOT:PSS on the power factor of polymer thermoelectric energy conversion devices *J. Mater. Chem. A* **3** 6526–33
- [30] Wang J, Cai K and Shen S 2014 Enhanced thermoelectric properties of Poly(3, 4 ethylenedioxythiophene) thin films treated with H₂SO₄ *Org. Electron.* **15** 3087–95
- [31] Heeger A 2001 Nobel lecture: semiconducting and metallic polymers: the fourth generation of polymeric materials *J. Rev. Mod. Phys.* **73** 681–700
- [32] Deetum C, Samthong C, Thongyai S, Praserttham P and Somwangthanaroj A 2014 Synthesis of well dispersed graphene in conjugated Poly(3, 4 ethylenedioxythiophene): polystyrene sulfonate via click *Chemistry. Compos. Sci. Technol.* **93** 1–8
- [33] Pathak C S, Singh J P and Singh R 2018 Preparation of novel graphene-PEDOT:PSS nanocomposite films and fabrication of heterojunction diodes With N–Si *Chem. Phys. Lett.* **694** 75–81
- [34] Long Y, Chen Z, Zhang X, Zhang J and Liu Z 2004 Synthesis and electrical properties of carbon nanotube polyaniline composites *Appl. Phys. Lett.* **85** 1796–8
- [35] Yang C, Liu P and Wang T 2011 Well-Defined core-shell carbon black/polypyrrole nanocomposites for electrochemical energy storage *ACS Appl. Mater. Interfaces* **3** 1109–14
- [36] Tsai T C, Chang H C, Chen C H and Whang W T 2011 Widely variable seebeck coefficient and enhanced thermoelectric power of PEDOT:PSS films by blending thermal decomposable ammonium formate *Org. Electron.* **12** 2159–64
- [37] Meng C Z, Liu C H and Fan S A 2010 Promising approach to enhanced thermoelectric properties using carbon nanotube networks *Adv. Mater.* **22** 535–9
- [38] Wang Q, Yao Q, Chang J and Chen L D 2012 Enhanced thermoelectric properties of CNT/PANI composite nanofibers by highly orienting the arrangement of polymer chains *J. Mater. Chem.* **22** 17612–8
- [39] Koller G, Berkebile S, Oehzelt M, Puschnig P, Draxl C A, Netzer F P and Ramsey M G 2007 Intra- and intermolecular band dispersion in an organic crystal *Science* **317** 351–5
- [40] Crispin X et al 2004 Electronic delocalization in discotic liquid crystals: a joint experimental and theoretical study *J. Am. Chem. Soc.* **126** 11889–99
- [41] Kim G H, Hwang D H and Woo S I 2012 Thermoelectric properties of nanocomposite thin films prepared with Poly(3, 4-ethylenedioxythiophene) poly(styrenesulfonate) and graphene *Phys. Chem. Chem. Phys.* **14** 3530–6
- [42] Xiang J and Drazl L T 2014 Improving thermoelectric properties of graphene/polyaniline paper by folding *Chem. Phys. Lett.* **593** 109–14

REVIEW

Poly(3,4 ethylenedioxythiophene)-tosylate—Its synthesis, properties and various applications

Shilpa Maity¹ | Salini Datta² | Megha Mishra² | Shiladitya Banerjee³ |
Sukhen Das¹ | Krishanu Chatterjee² 

¹Department of Physics, Jadavpur University, Kolkata, India

²Department of Physics, Techno India University, Kolkata, India

³Department of Chemistry, Techno India University, Kolkata, India

Correspondence

Sukhen Das, Department of Physics, Jadavpur University, Kolkata 700032, India.
Email: sdasphysics@gmail.com

Krishanu Chatterjee, Department of Physics, Techno India University, Salt Lake, Kolkata 700091, India.
Email: itskrishanu@gmail.com

Abstract

The discovery of conducting polymers (CPs) opens up a new path for the researchers to design them accordingly to some specific applications. Poly(3,4-ethylenedioxythiophene)-tosylate (PEDOT-Tos) being one of the bicyclic polythiophene derivatives has been drawing much attention in the recent years. PEDOT is a well-known CP with high electrical conductivity and balanced with small counter ion Tos seems to be a material capable in various applications. The improved structural order with the semi-metallic character as supported by the electronic band structure activates the scientific community to employ PEDOT-Tos in various applications. Reports show that for the last decade categorically PEDOT-Tos has been synthesized, which finds applications not only in thermoelectrics, different type of sensors including mechanical and optical, as electrodes in organic electronics but also in biomedical applications specifically in tissue culture. The present work aims at implementing a comprehensive update on the synthesis of PEDOT-Tos with the structure and properties and also a state-of-art review as a promising material in various applications with anticipation that the present work motivate the researchers to bring out PEDOT-Tos as a multifunctional material.

KEYWORDS

applications, poly(3,4-ethylenedioxythiophene)-tosylate, properties, structure, synthesis

1 | INTRODUCTION

The last two decades have witnessed a substantial increase in research in the field of conducting polymers (CPs), mostly π -conjugated polymers owing to their unique optical and electrical properties and ease of synthesis.^{1–3} The external stimuli have a hold over the electronic conjugation of the CPs and modulated the latter which influences the exclusive properties that can be optimized. Consequently, the synthesis techniques can modify the conductivity, pH, color or refractive index of the CPs. As an effective part of organic electronics the CPs thus find applications in various electronic devices starting from organic field effect transistors (OFETs),⁴ organic light emitting diodes (OLEDs),⁵ photovoltaic cells,⁶ sensors,⁷ memories⁸ to thermoelectric generators.^{9–13} CPs like polypyrrole (PPy), polyaniline

(PANI), polythiophene and their derivatives are probably the most potential candidates for various applications. Poly(3,4-ethylenedioxythiophene) (PEDOT) is apparently considered the suitable one among the available CPs with respect to the conductivity, processability and stability.^{14,15}

Although PEDOT is an insoluble polymer, but in the presence of poly(4 styrenesulfonate) (PSS),^{16,17} it becomes aqueous and processable. Positively charged PEDOT is stabilized by charge balancing counter polyanion dopant PSS¹⁸ and thus as a charge transporting species PEDOT-PSS becomes hole conductive.¹⁷ Although PEDOT-PSS is advantageous in various applications,¹⁹ it finds limitations due to the high hydrophilicity of PSS. Because of the water soluble PSS chain, PEDOT-PSS is strongly sensitive to humidity and shows a tendency of swelling in aqueous media thereby limiting its potential

application as thermistor or in other electronic devices.^{18,20-24} To overcome the hydrophilicity of the PEDOT-PSS, tosylate doped PEDOT (PEDOT-Tos) comes into play as the hydrophilic nature decreases due to the removal of the sulfonic acid from polymer structure and balanced ionicity. PEDOT-Tos has attracted noticeable attention in recent days due to its processibility in solution, large variation in conductivities,²⁵ high electrochemical and thermal stability.²⁶ PEDOT-Tos has also a very low band gap of around 1.5 eV and doping of the PEDOT with tosylate ion can change the absorption level in NIR region making the polymer transparent.²⁶ Further, PEDOT-Tos is one of the desirable candidates to replace the ITO in flexible electronics and displays²⁷ and by controlling the oxidation level, the thermoelectric (TE) efficiency can also be increased.¹¹ Owing to these properties, PEDOT-Tos has been found wide applications starting from energy conversion to storage field. In this review, we present the different synthesis procedure of PEDOT-Tos, its structure and properties and report on the progress on various applications with a detailed description.

2 | STRUCTURE AND PROPERTIES

Commercialization of the first generation of CP such as polyacetylene falls short of success because of their stability issues in air. The invention of PEDOT, on the other hand, has led the way to obtain better air stability and thermal stability in the doped state as well as good electrical conductivity as the free radicals and positive electronic charges are even out by electron donating oxygen substituent within the conjugated backbone chain.²⁸ PEDOT-Tos is one of the bicyclic polythiophene derivatives balanced with small counter ion Tos as shown in Figure 1. The small Tos counter ion provides a more ordered and crystalline molecular structure as confirmed from Grazing incidence wide-angle X-ray scattering (GIWAXS) as shown in Figure 2A which is observed for the first time by Bubnova et al^{33a} and interprets well-ordered crystallites within less ordered amorphous matrix. It shows various sharp peaks along off axis and considerable in plane scattering. The small angle diffraction peaks at $Q = 0.45 \text{ \AA}^{-1}$ and $Q = 0.89 \text{ \AA}^{-1}$ is attributed to the lamellar stacking of (100) and (200)

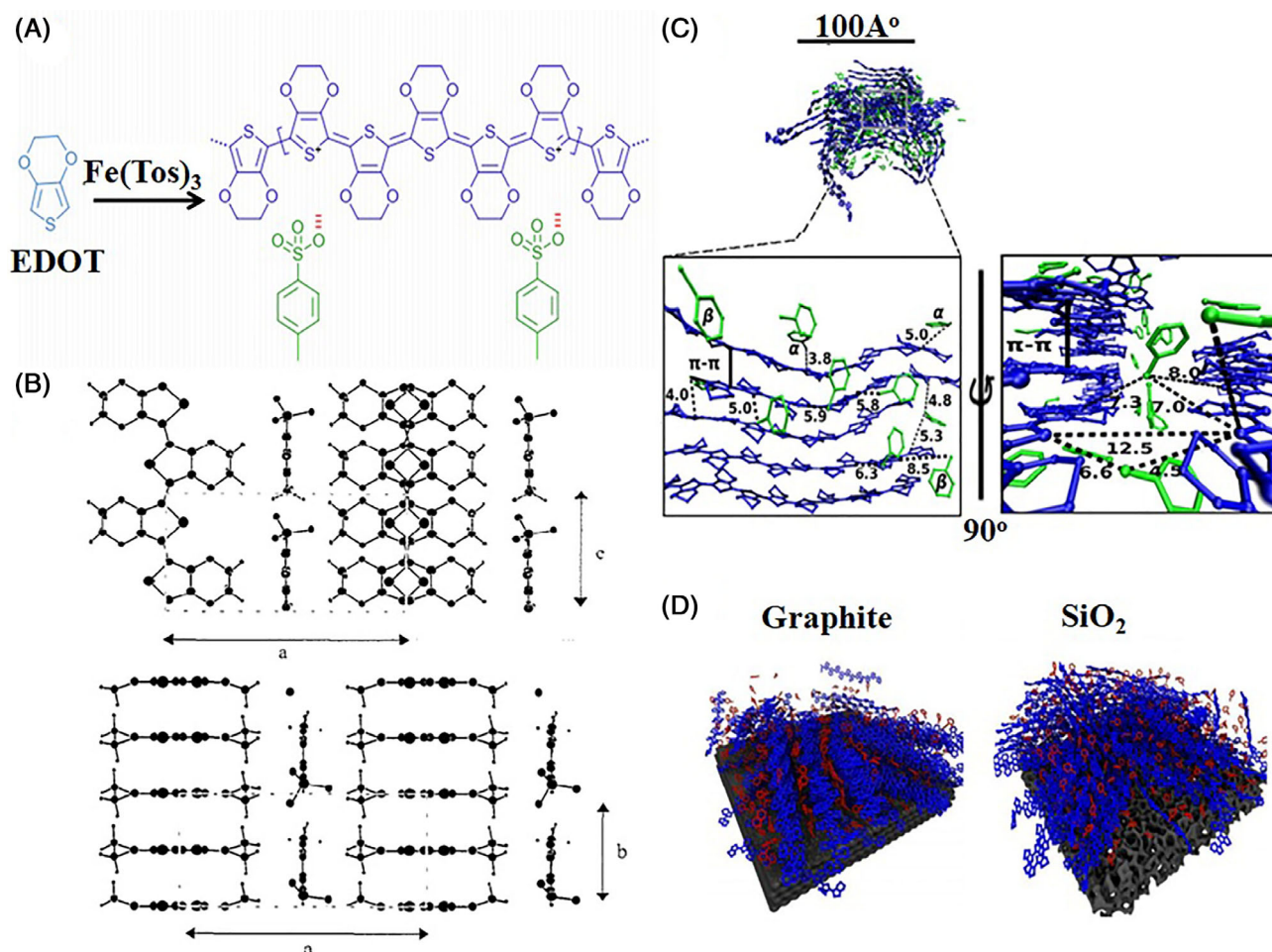
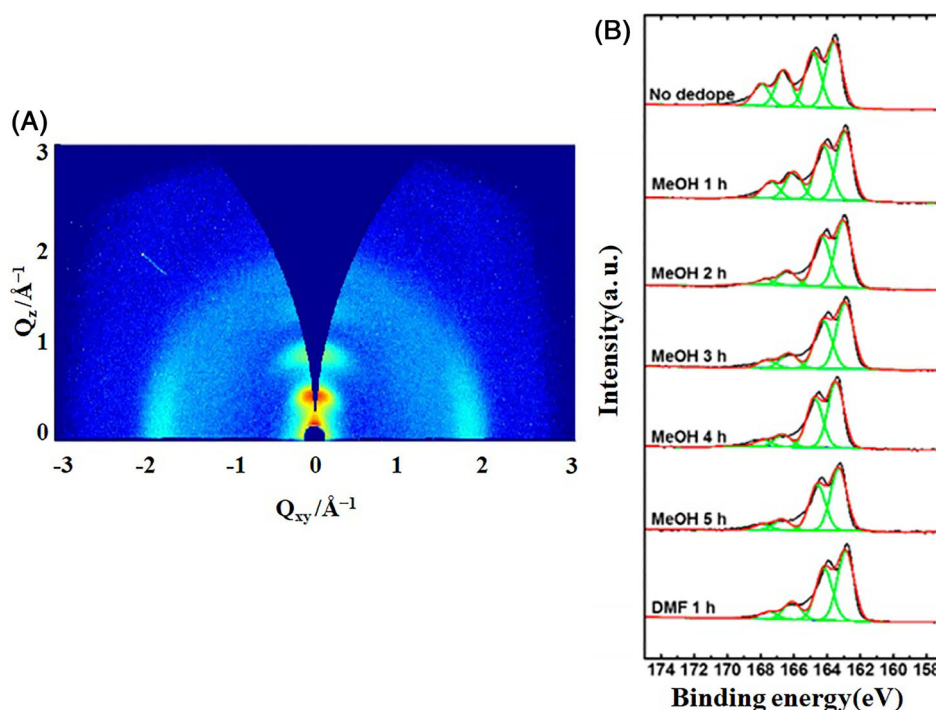


FIGURE 1 (A) Structure of PEDOT-Tos. (B) Structural model of PEDOT-Tos, in projection along B (upper) and along C (lower). Reproduced with permission.²⁹ Copyright 1999, Elsevier. (C) Molecular structure of the PEDOT:Tos, where PEDOT is shown in blue, Tos in green. Adapted with permission.³⁰ Copyright 2017, American Chemical Society. (D) PEDOT-Tos deposited on graphite and amorphous SiO₂ substrates after water evaporation. Adapted with permission.³¹ Copyright 2018, American Chemical Society

FIGURE 2 (A) GIWAXS of PEDOT-Tos. Reproduced with permission.^{32a} Copyright 2020, John Wiley and Sons. (B) S(2p) XPS spectra of PEDOT-Tos films after the immersion dedoping process with methanol from initial washing to 5 hours of immersion and with DMF for 1 hour. Reproduced with permission.^{32b} Copyright 2017, American Chemical Society



planes of PEDOT-Tos whereas the peak at $Q = 1.82 \text{ \AA}^{-1}$ is due to the $\pi - \pi$ inter-ring (010) stacking of PEDOT.^{33a-35} Thus the proposed unit cell structure of PEDOT-Tos is orthorhombic with lattice parameters $a = 14.0 \text{ \AA}$, $b = 6.8 \text{ \AA}$ and $c = 7.8 \text{ \AA}$ ²⁹ with the polymer chains along the c axis and a axis normal to the substrate as shown in Figure 1B. This representation points toward a lamellar structure of PEDOT-Tos with π -stacked lamellae chains of the polymer separated by an inter-lamella space occupied by the tosylate anion.^{36,37} A highly favored interaction is introduced due to the small stacking distance of the lamellar structure of PEDOT-Tos which is responsible for the increase in crystallinity.³⁴

The oxidation level of PEDOT-Tos can be tracked by using X-ray photoelectron spectroscopy (XPS) technique. Figure 2B shows the XPS spectra of PEDOT-Tos. Interestingly PEDOT-Tos contains two different sulfur atoms; one in the sulfonate group of Tos having a binding energy of 166–170 eV which is higher than the binding energy (163–166 eV) of the other in the thiophene units in PEDOT.^{32b,35} This difference is attributed to the different environment of the sulfur atoms. The sulfur atoms in the sulfonate group of Tos are attached with three electronegative oxygen atoms which results in higher binding energies. The areal ratio of $S(2p)_{\text{tosylate}}/S(2p)_{\text{thiophene}}$ gives a measure of the oxidation level of PEDOT-Tos.^{11,32b,35} Further, the spectral shape of C(1s), O(1s) and S(2p) was modified by the oxidation level of PEDOT-Tos when exposed into the different pH solution,³⁸ concentration of oxidant,³⁹ reducing agent,¹¹ washing solvents^{32b} and different solution treatment^{35,40} which in turn enhances various properties of the polymer.

The development of computational microscopy in recent days seems to be a potential technique to figure out the morphology of CPs and has been reported for PEDOT-Tos.^{30-31,41} Such computational structure of PEDOT-Tos is shown in Figure 1C where it is

proposed that the PEDOT chains are aggregated in crystallites consisting of 3–6 π - π stacked chains. These crystallites are within an amorphous matrix of PEDOT chains and are connected by inter-penetrating π - π stacked chains such that percolative paths in the structure are formed.³⁰ Substrate-dependent morphology was also reported through computational microscopy as shown in Figure 1D. It has been suggested that existence of substrate influences the growth of lamellar structure. It was observed that face on orientation is preferred for ordered substrate as a result of the interaction of substrate atoms and the p-orbitals in PEDOT chains. On the other hand edge on orientation is preferred on amorphous SiO_2 .³¹

The properties of the CPs are greatly influenced by their oxidation level, inter-chain interactions, chain alignment, conjugation length, degree of disorder, and so on. In a single polymer chain, charge defects namely polarons and bipolarons are formed due to the removal of topmost electrons of the valance band which are stabilized by atomic or molecular counterions^{33a} as shown in Figure 3. PEDOT-Tos being semi-metallic in nature, it has been proposed that the electronic structure follows a bipolaronic network with an empty delocalized bipolaron band which merges into the delocalized valence band. Two new states (i, i^*) are induced due to the local structural distortion out of which one of the levels is destabilized from the top of the valance band. The random orientation of the tosylate counter ions is the reason of the creation of the states in the gap.⁴² For the case of bipolaron, the level i^* is empty. The density of valence electronic states (DOVS) for PEDOT-Tos has been depicted by ultraviolet photoelectron spectroscopy (UPS) shows a large DOVS at the Fermi level E_F without a disorder-induced tail. Moreover, PEDOT-Tos has a lower work function of 4.3 eV and the valence band is closer to E_F . The electronic structure, as calculated with molecular dynamics^{41,43} simulations through a semi-empirical approach, indicates a change in density

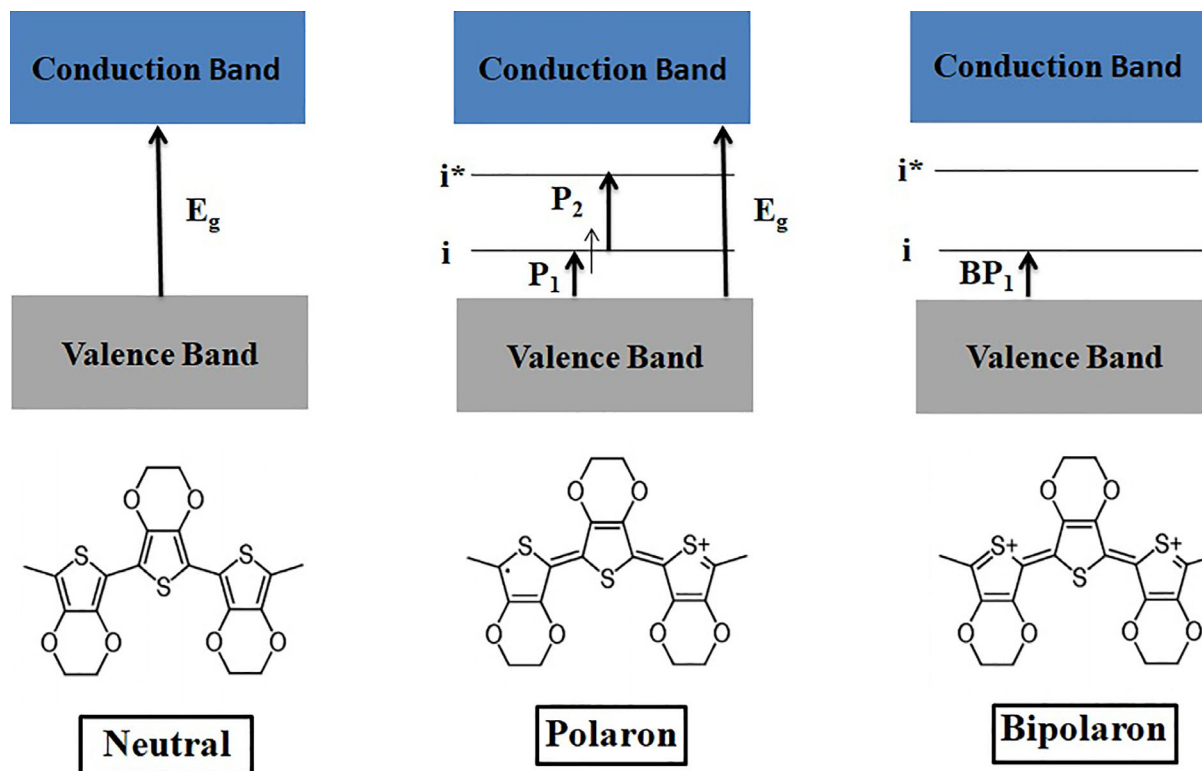


FIGURE 3 Electronic structure of polarons and bipolarons in nondegenerate ground-state polymers. Vertical lines show the electronic transitions. The allowed transitions are $P_1 = i$, $P_2 = i^* - i$, $BP_1 = i$ (here BP means bipolaron.) The small arrow stands for an electron with a spin (either up or down). Adapted with permission.^{33b} Copyright 2003, The American Physical Society

of state (DoS) from insulating to semi-metallic with the increase in carrier concentration with a fall of the gap between the bipolaron and valence bands.⁴² Thus, random distribution of the counter ions enhances the path from insulating to a semi-metallic state.

3 | SYNTHESIS

PEDOT-Tos, with outstanding properties, has already become famous in the field of CPs. It is already known that variation in the synthesis process affects the structures (micro or nano) which in turn influence the application based properties of the CPs. To date, several attempts have been made to fabricate PEDOT-Tos with controlled architectures. Figure 4 shows an exhaustive overview of the typical synthesis procedures, namely, chemical polymerization, vapor phase polymerization and electrochemical polymerization. Moreover, the synthesis process of PEDOT-Tos based nanocomposite materials will also be discussed in this section.

3.1 | Chemical polymerization

For the large-scale production of PEDOT nanomaterials, chemical polymerization is one of the effective methods. This method is relatively simple to perform. The oxidizing rate of EDOT as well as the

formation of higher molecular weight of polymer can be controlled easily by the chemical polymerization process. Although the study of PEDOT-Tos is currently underway, the polymer had been chemically synthesized long ago in 1994 by Leeuw et al.²⁵ For the typical synthesis procedure, the monomer ethylenedioxythiophene (EDOT), the oxidizing agent iron(III) tris-*p*-toluenesulfonate and imidazole were first dissolved in *n*-butanol. The whole oxidant solution was then filtered through a 0.5 cm filter. Pre washed substrates (typically 5 × 5 cm) of glass or plastic was taken on which the solution was spin coated at 1000 rpm and baked on a hotplate (or in a convection furnace) at 110°C for 5 minutes. The process of heating initiated the polymerization of the monomer EDOT to PEDOT doped with tosylate.^{44,45} Then onward different modifications of the above process have been done to synthesize the polymer. For example, PEDOT-Tos powders as well as thin films have also been synthesized by the above said process in different organic solvents,^{35,46} namely, methanol, ethanol, *n*-butanol, hexanol and dodecylbenzenesulfonic acid (DBSA), which influence the electrical parameters of the samples. A strong interaction exists between alcoholic solvents and PEDOT-Tos through hydrogen bonding which changes the molecular ordering of the samples.⁴⁶ PEDOT-Tos thin films were also polymerized by using various high boiling point additives like acetonitrile (ACN), toluene (Tol), chlorobenzene (CB), dimethylformamide (DMF), dimethylsulfoxide (DMSO), ethylene glycol (EG), propylene carbonate (PC) in order to tune the structure of the polymer. In situ polymerization of EDOT and ferric para toluene

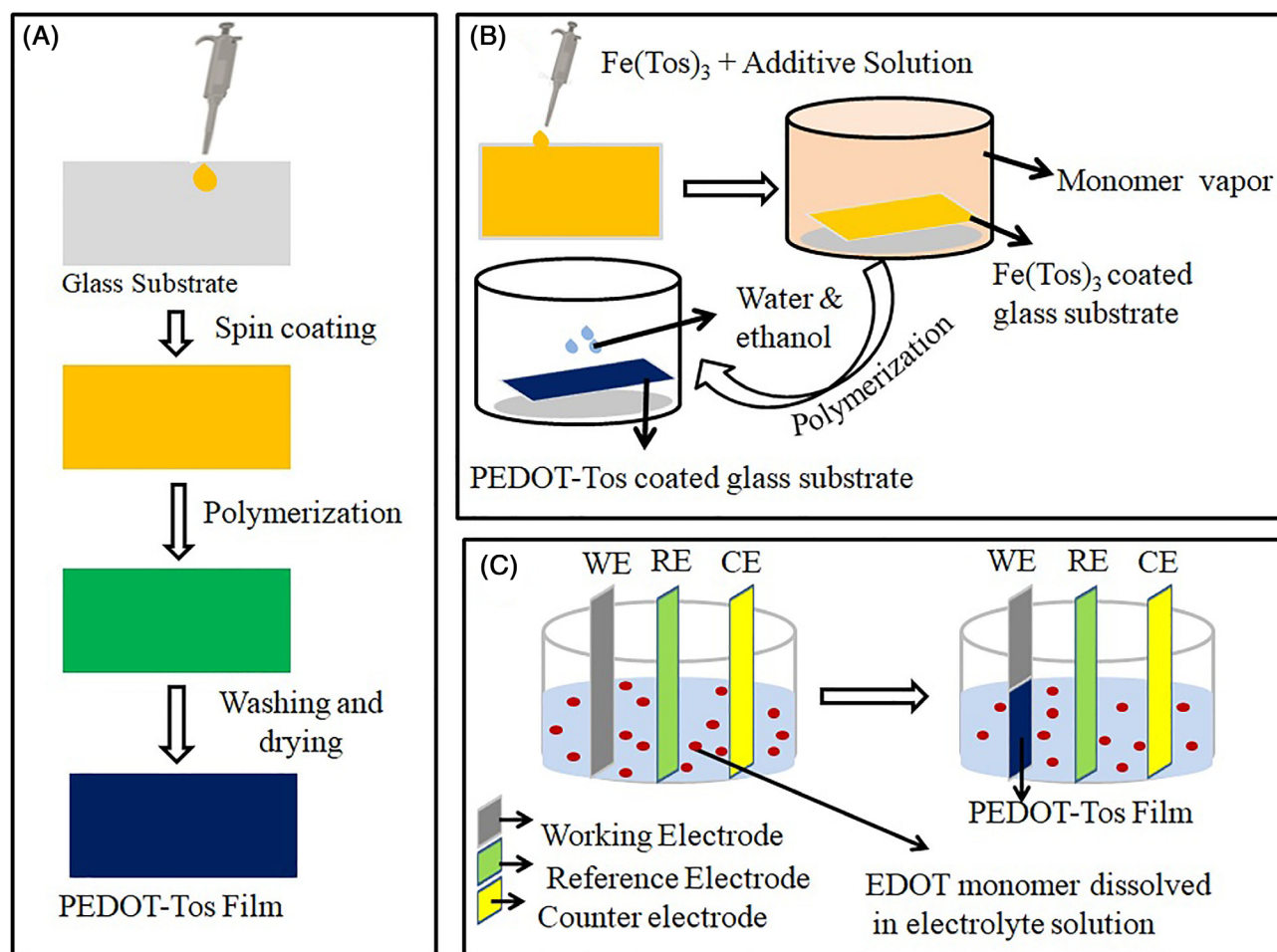


FIGURE 4 Schematics diagram of various polymerization methods of forming PEDOT-Tos films: (A) The chemical polymerization process. (B) The vapor phase polymerization process. (C) The electrochemical polymerization process. Reproduced with permission.²⁸ Copyright 2019, John Wiley and Sons

sulfonate as dopant in poly(vinyl pyrrolidone) matrix have also been reported with incorporation of co-dopants (Methanesulfonic acid [MSA], 2-naphthalenesulfonic acid [NSA] and p-toluenesulfonic acid monohydrate [PSA]) in the backbone of PEDOT, which were dissolved in the oxidant solution before mixing it with the monomer solution. Moreover, Pyridine as well as tri-block copolymer was used in the process of synthesis to control the kinetics of the polymerization.^{27,47} Again addition of copolymer like PEO-b-PPO-b-PEO BCP, polyurethane (PU) and polyethylene glycol (PEG) to the oxidation polymerization reaction is another modification which was reported recently.^{32b,48,49} Even to control the oxidation level in PEDOT-Tos so as to enhance its structural and electrical properties, two different approaches were adopted, for example, the variation of the concentrations of iron(III) p-toluenesulfonate solution³⁹ and the use of reducing agents like tetrakis(dimethylamino) ethylene(TDAE)¹¹ and L-ascorbic acid (vitamin C).⁴⁰

To extend the beneficial effects for the practical applications, organic-inorganic hybrid materials were the best candidate for the same. So synthesis of nanocomposites of PEDOT-Tos with inorganic

counterparts is currently underway. Nanocomposite thin films of PEDOT-Tos with Mn_3O_4 ⁵⁰ and CuO ⁵¹ has been synthesized by chemical polymerization using different concentrations of the inorganic counter parts. For PEDOT-Tos Mn_3O_4 nanocomposite films, a modification has been done through esterification between EDOT-methanol and glutaric anhydride for attaining a monomer adorned with a glutaryl. PEDOT-Tos layers over the TiO_2 nanotubes were also synthesized by chemical polymerization process. In a typical synthesis process, PEDOT-Tos was also synthesized using solution-casting chemical polymerization, which was then spin-coated on different substrates, namely, TiO_2 nanotube⁵² or CNT-sprayed glass substrates.⁵³ Variation in the concentration of CNT was carried out to change the amount of PEDOT interfering with CNTs. Again CNT was also added in the polymerization solution of PEDOT where iron (III) chloride was used as oxidant and p-toluenesulfonic acid (pTSA) was used as the source of tosylate group.⁵⁴ Modification of the process in terms of oxidant was also observed in PEDOT-Tos Graphene⁵⁵ nanocomposites powder. Ammonium peroxy disulfate (APS) was used as oxidant in this case.

3.2 | Vapor phase polymerization

A new synthesis route to obtain PEDOT-Tos is vapor phase polymerization (VPP), in which the film of the oxidizing component with pyridine was exposed to EDOT vapors to initiate the polymerization.⁵⁶⁻⁵⁸ The advantage of VPP over chemical synthesis is that it is a bottom-up approach where the monomers are stacked up leading to a well-ordered crystalline structure of the polymer.²⁸

Different approaches are made to modify the oxidant film for well-ordered structure of PEDOT-Tos. An oxidant solution, containing iron(III) p-toluenesulfonate with butanol added with different copolymers such as polyethylene glycol,⁵⁸ poly(ethylene glycol-*ran*-(propylene glycol) (PEG-*ran*-PPG)⁵⁹⁻⁶¹ or PEG/PDMS/PEG,⁶² was spin coated onto a prewashed/ITO coated glass and kept on a hot plate to evaporate the solvent, and finally oxidant coated substrate was exposed to EDOT vapor for polymerization. In another approach, the plasma treated PVDF films were coated with the oxidant solution of iron(III) p-toluenesulfonate on both sides, through dip coating method, and the oxidant coated PVDF film was placed into the VPP chamber and exposed to EDOT monomer vapor to achieve the PEDOT-Tos coated PVDF flexible film for further practical application.⁶³ Addition of triblock polymer PEG-PPG-PEG to the mixture of oxidant solution with alcohols^{38,62,64-69} along with different additives such as deionized water, DMF⁷⁰ DMSO or EDTA⁷¹ was also attempted for the synthesis of PEDOT-Tos films through VPP. Such procedure was repeated for multiple layer synthesis of PEDOT-Tos by sequential polymerization, until the free standing PEDOT-Tos film was obtained.⁷² The tripolymer PEG-PPG-PEG with the additives were used to control the crystallization of PEDOT-Tos.

Further modification of the VPP technique had been done for the synthesis of the PEDOT-Tos-PPP where the films were prepared at air rather than under vacuum.^{73,74} Modification of the substrate in the VPP technique has also been done for the synthesis of a stretchable and flexible PEDOT-Tos film under nitrogen flow.⁷⁵ VPP was also employed to develop a composite film of aligned carbon nanotubes with PEDOT-Tos on PVDF film.⁷⁶ Another composite film PEDOT-Tos/Graphene was developed on a Ta₂O₅ covered porous pellet. A FeTos/graphene layer was formed on the porous Ta₂O₅ pellet and was exposed to the EDOT monomer vapor to form PEDOT-Tos/Graphene composite film.⁷⁷ Further, a rGO/CNTs/PEDOT-Tos composite film was also fabricated by simple VPP deposition, an oxidant Iron(III) p-toluene sulfonate hexahydrate (Fe(OTs)₃) solution was uniformly applied on to a CNT and rGo solution sprayed substrate which was transferred in to the EDOT vapor chamber for the deposition and polymerization with required condition.⁷⁸

3.3 | Electrochemical polymerization

The chemical synthesis or the vapor phase polymerization EDOT is oxidized using an oxidant but for electrochemical polymerization (ECP) a potential is applied to an electrode to oxidize the EDOT. The setup for the ECP is typically is a one-compartment three-electrode

cell with a working electrode, Ag/AgCl as a reference electrode and platinum foil as a counter electrode. Since low polymerization potential made polymer film adhesive,⁷⁹ the applied potential was preferred to be in between 1.0 and 1.2 V. The electrolyte in the cell is a solution of 3,4-ethylenedioxythiophene and iron(III) tris-p-toluenesulfonate in n-butanol. PEDOT-Tos was electro polymerized on a gold layer on polyethylene substrate which is the working electrode.²⁶

In conclusion, though the chemical polymerization process is a simple method to synthesize PEDOT-Tos with higher molecular weight, the vapor phase polymerization (VPP) technique is a new route of synthesis with a bottom-up approach which is advantageous over chemical polymerization process as it gives well-ordered crystalline polymer structures which is a basic necessity for the improvement of different parameters of PEDOT-Tos. On the other hand, the advantage of electrochemical polymerization technique is that unlike the chemical polymerization or the VPP method use of reagent as an oxidant is not required. The potential applied in this process oxidize the EDOT monomer. But the setup of the electrochemical polymerization technique is more complicated, then the chemical polymerization as well as vapor phase polymerization.

4 | APPLICATIONS

PEDOT-Tos being a polymer of high interest in the research field, it has been synthesized for various applications starting from thermoelectrics to biomedical. The details of those applications are discussed in the following section.

4.1 | Thermoelectric application

With the advancement of civilization, there is an increase in the demand of electricity which in turn mainly depends on burning of fossil fuels. Consequently, the rising of CO₂ gas production day by day has an adverse effect in the context of the global warming. So the search of alternative technologies comes into play to overcome such problems. One such alternative technology is the use of thermoelectric generators (TEGs), which can produce electricity from waste heat and natural heat sources too. The efficiency of a thermoelectric material is characterized by the dimensionless thermoelectric figure of merit $ZT = \sigma S^2 T / \kappa$, where σ , S and κ are the electrical conductivity, the Seebeck coefficient and thermal conductivity of the material, respectively, and T is the operating temperature. Recently polymers based thermoelectric devices shows the capability in the application of near-room temperature energy harvesters. PEDOT-Tos is one of such polymer thermoelectric materials whose thermoelectric application is currently underway. Different strategies have been adopted by the researchers to increase the figure of merit of PEDOT-Tos, for example, controlling the oxidation level, treating with acids and bases, using additives adding inorganic counterparts, and so on.

It has been observed that the control of the oxidation level of PEDOT-Tos using tetrakis(dimethylamino) ethylene (TDAE),¹¹

aqueous vitamin C solution⁴⁰ or variation in concentrations of iron(III) p-toluenesulfonate hexahydrate with respect to n-butanol³⁹ greatly influence the electrical conductivity and thermoelectric power which in turn affect the ZT.

The vice versa effect of the electrical conductivity and thermoelectric power with increase in oxidation level for polymers indicates that the power factor can be optimized at a specific oxidation state. Thus PEDOT-Tos has been reduced by TDAE and it was observed that the power factor reaches its maximum value at 22% of oxidation level. As for CPs, the oxidation state does not influence the thermal conductivity,⁸⁰ consequently at this lower oxidization level the figure of merit (ZT) of the polymer reaches its maximum value of 0.25¹¹ at a room temperature with a low intrinsic thermal conductivity about 0.37 Wm⁻¹ K⁻¹. Similarly, with different percentages of aqueous solutions of vitamin C, the oxidation level of PEDOT-Tos film has also been tuned. It was observed that the ZT value reaches its maximum at around 23% of oxidation level.⁴⁰ The variation in concentrations of iron(III) p-toluenesulfonate hexahydrate (1, 10, 20, 40, 60, and 80 wt % with respect to n-butanol) can also modify the oxidization level of the conjugated polymer PEDOT. The loading of the oxidant also influence the size of the particle. It was observed that the power factor has a high value at around 20% of oxidation level which again decreases with the increase in the oxidation level. But it again increases and reaches to the maximum value at 80% of oxidation level which is probably due to the increase in the electrical conductivity with oxidation level.^{11,39} Treating the PEDOT-Tos thin films synthesized by both VPP and chemical process by acids and bases is another way to influence the thermoelectric properties. It was observed that PEDOT-Tos films go through a same type of transformation in thermoelectric properties when the films are treated with acids and bases. With the variation of pH, a maximum value of the power factor was obtained for pH < 7.³⁸ A change in structure of PEDOT-Tos thin films were observed when treated with co-solvents during the polymerization. There is an enhancement in the power factor due to the increase in the electrical conductivity which is due to the influence of structural change in the PEDOT-Tos thin films.³⁵

The thermoelectric properties of PEDOT-Tos polymer is also tuned by the inclusion of nanoparticles in the polymer matrix such as Mn₃O₄ nanoparticle,⁵⁰ CuO nanoparticle,⁵¹ carbon nanotubes^{53,54} or graphene.⁵⁵ The inclusion of nanoparticles can influence the crystallinity of PEDOT which modify the DoS slope which in turn affect the thermoelectric power. Since for PEDOT, the increase in the order of the structure improves the carrier delocalization and π orbital overlapping,³⁶ which modify the electronic band structure affecting the charge transport properties, and all the strategies discussed are focused on the enhancement of the molecular ordered structure. Consequently this has an effect on the charge carrier mobility and an increase in the electrical as well as thermoelectric power of PEDOT-Tos has been observed, resulting in a higher value in ZT. This indicates great potential of PEDOT-Tos in the fabrication and performance of organic thermoelectric devices.^{15,70} Reports show that the power output of a TEG fabricated using PEDOT-Tos for p type legs and TTF-TCNQ/PVC blend or n doped graphene for n types legs^{11,70} gives a

maximum power output of 0.128 μ W at $\Delta T = 10^\circ\text{C}$ and 26.0 nW cm⁻² at ΔT 9.5 K respectively. Taking advantage of high electrical conductivity of PEDOT-Tos at oxidation level, 24.1% thin films on various substrates were synthesized using Poly(ethylene glycol)-block-poly(propylene glycol)-blockpoly(ethylene glycol) triblock copolymer (PEPG) as inhibitor. An attempt was made to fabricate a flexible thermoelectric device which generates electricity by touch of fingertips as shown in Figure 5. At a room temperature of 27°C, the fabricated device generates a voltage of 8-10 mV by the touch of fingertips. Moreover, composites of PEDOT-Tos are also viable candidate for production of cost-effective thermoelectric generator (TEG) at industrial scale.⁸¹ A maximum thermoelectric power of 70 μWm^{-1} K⁻² was also obtained from PEO-b-PPO-b-PEO BCP and Fe(Tos)₃ oxidant blended PEDOT-Tos films from disordered nanostructures rather than ordered nanostructures. This is attributed to the easier mass transport of oxidant and monomers in the disordered nanostructures.^{32b} The thermoelectric properties are summarized in Table 1.

4.2 | Electrode application

Among all other applications, displays and solar cells are very known applications in our daily life. For the above applications, nowadays, the authors are focused on the area of flexible electronic system with transparent, fully flexible, stable, low-work-function electrodes. PEDOT-Tos is one of the promising candidates because of its excellent electrical conductivity upon doping, electro optical properties and π -conjugated structure. Tuning the work function of the PEDOT-Tos electrodes can be achieved by controlling the submonolayer surface redox reaction with a strong electron donor such as tetrakis(dimethylamino)ethylene (TDAE). The surface modification by TDAE allows decreasing the work function and creating a transparent film of PEDOT-Tos electrode. The work function value reaches as low as 3.8 eV, which is lower than that of a reasonable electron-injecting electrode, that is, aluminum-(oxide) electrode (4.1 eV). The TDAE-PEDOT-Tos interface formation has been investigated both experimentally and theoretically. Both the theoretical and experimental studies, via density functional theory and wavefunction based quantum chemical calculations and photoelectron spectroscopy respectively,⁵⁷ have explained that the work function decreases by 0.5 eV because the electrons are transferred from TDAE to PEDOT-Tos surface. In 2013, Yang et al reported a capacitor cathode film of poly(3,4-ethylenedioxythiophene) (PEDOT)/graphene nanocomposites on a solid porous tantalum pentoxide surface using chemical vapor phase polymerization process.^{77,82} The outer layer of (PEDOT)/graphene improved the mechanical strength of the tantalum electrolyte based capacitor cathode. High conducting nature of the (PEDOT)/graphene composite can reduce the cathode films resistance and the contact resistance between (PEDOT)/graphene and the latter formed carbon paste. Due to the entire porous surface of the dielectric Ta₂O₅ being fully covered with inner layer of PEDOT films, the whole system achieved the full capacitance. The capacitance of the system increases with the polymerization time (around 1 hour) until a homogeneous PEDOT coating is formed inside the tantalum oxide pores. The

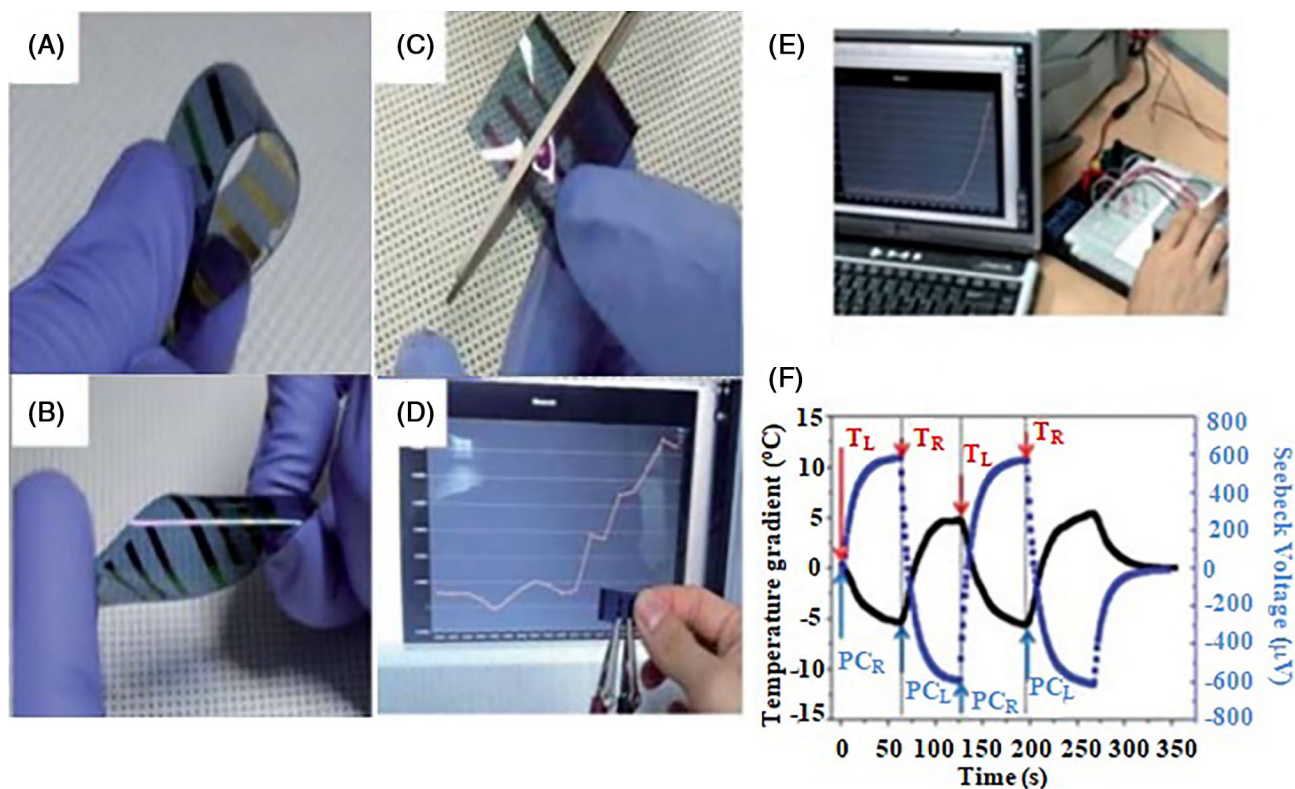


FIGURE 5 Photographic images and electricity generation by the touch of fingertips of the flexible PP-PEDOT thermoelectric film. (A) Bending, (B) twisting, and (C) cutting with scissors images of PP-PEDOT films. (D) Electricity generation by fingertip touch at one side with air and (E) a Peltier module reference. (F) Electricity generation (blue square) and the corresponding temperature gradient (black square) measured from (E) (TL: touch left side, TR: touch right side with fingertips, PCR: a right side Peltier device cooling, and PCL: a left side Peltier device cooling to generate the temperature difference). Reproduced with permission.⁴⁷ Copyright 2008, Royal Society of Chemistry

observed maximum capacitance of the PEDOT/graphene film is 67.3 μF and loss percentage around 1.7.⁷⁷ The tantalum capacitor based on VPP PEDOT/PEDOT-graphene results ultralow ESR, ca. 12 m Ω , and displays excellent capacitance versus frequency characteristics. In conclusion, the tosylate doped PEDOT/PEDOT-graphene film, with high conductive and mechanical strength, shows promising future for high performance electrode materials such as capacitors, organic solar cells and energy storage device applications. To produce robust ultrathin films with increased optical transmission, the effect of adding aprotic polar solvents or chelating ligands to the oxidant mixture of Fe (Tos) was investigated in the PEDOT CP. The change in redox behavior of the oxidant solution can influence the number of accessible polymerization nucleation sites. A smaller number of polymerization nucleation sites can hamper the PEDOT film growth and simultaneously expect to yield larger polymer grains which influence the enhancement in mechanical properties.⁷¹ Nowadays, hydrogel-based microelectrodes that have molecular permeability are considered for bioelectronics device applications, due to the possibility of stimulating living tissues or recording a wide range of biological signals. Thus tosylate doped PEDOT coated hydrogel substrate for the implantation of flexible, biocompatible and wearable microelectrodes as shown in Figure 6A. Moreover, the possibility of using PEDOT-Tos patterns on hydrogel substrates for bioelectronic devices as to microelectrodes is

shown in Figure 6B. It is observed that the microelectrodes arrays of PEDOT-Tos on flexible agarose hydrogel substrate was designed effectively and fabricated. Transfer of various shapes and sizes of PEDOT-Tos pattern from glass to agarose hydrogel substrates was also initiated through a direct transfer process. The linear I-V characteristics indicates that as the film thickness decreased from 203 to 26 nm, the sheet resistance of PEDOT films decreased from 1010 to 610 Ω , as shown in Figure 7. The sheet resistance and electrical conductivity of PEDOT on glass substrate are 625 Ω and 300 S cm^{-1} , respectively, whereas 810 Ω and 235 S cm^{-1} are the sheet resistance and conductivity of those PEDOT on PEG hydrogel, which explains that due to the wet environment of hydrogel, the conductivity of the PEDOT on PEG hydrogel decreases slightly.⁸³ PEDOT-Tos deposited insulator electrodes were also used in 0.4 M $\text{K}_4\text{Fe}(\text{CN})_6/\text{K}_3\text{Fe}(\text{CN})_6$ redox electrolyte based thermogalvanic devices as shown in Figure 6C, which are as efficient as platinum and porous carbon material electrodes.⁸⁴ The authors have evaluated the voltammetry response by coating PEDOT-Tos layer by layer from 1 layer up to 12 layers, which results in the increase in the thickness of the film from 223 to 2600 nm. From the response of voltammetry, increase in thickness of PEDOT-Tos coated electrodes admitted an increment of both the capacitive (I_c) and redox peak (I_R) current, respectively, which represent the capacitive charging and the redox process. The capacitive current (I_c) showed a linear dependence

TABLE 1 Overview of thermoelectric properties of PEDOT-Tos and its composites

Materials used	Polymerization Method	σ (S/cm ⁻¹)	S (μ V/K)	P (μ Wm ⁻¹ K ⁻²)	κ (Wm ⁻¹ K ⁻¹)	(ZT)	References
PEDOT-Tos treated with TDAE	Chemical polymerization	300	780	324	0.37 \pm 0.07	0.25	11
PEDOT-Tos with PEO-b-PPO-b-PEO BCP and Fe(Tos)3 oxidant blend	Vapor phase polymerization	850	24	70	—	—	32b
PEDOT-Tos treated with DMF	Chemical polymerization	640	34 \pm 5	78.5	—	—	35
pH \leq 7 treated PEDOT-Tos	Vapor phase polymerization	970	15	26	—	—	38
PEDOT-Tos	Chemical polymerization	2.7 \times 10 ⁻⁵	64.1	1.07 \times 10 ⁻³	—	—	39
Untreated PEDOT-Tos Film	Chemical Polymerization	364	58	122.4	0.37	0.103	40
PEDOT-Tos treated with 0.1% of Vitamin C	Chemical polymerization	176	89	139.4	0.37	0.117	40
PEDOT-Tos treated with 5% of Vitamin C	Chemical polymerization	144	110	174.2	0.37	0.146	40
PEDOT-Tos/ Mn ₃ O ₄ nanoparticle	Chemical polymerization	240 \pm 9	14.8 \pm 0.5	5.5 \pm 0.7	—	—	50
PEDOT-Tos/SWCNT with TDAE	Chemical polymerization	0.027	1.4 \times 10 ⁴	1200	0.52	0.7	53
PEDOT-Tos/SWCNT	Chemical polymerization	27.7	196.6	51.8	0.37	0.045	54
PEDOT-Tos/Graphene	Chemical polymerization	8.75	167.2	24.3	0.16	0.0506	55
0.2 wt% PEDOT NW/PEDOT-Tos	Vapor phase polymerization	1270	59.3	446.6	0.260	0.44	70

on the thickness of the PEDOT-Tos layer; being 11 times higher for the 12-times thicker electrode. However, the I_R value for 12 times thicker electrodes is only 1.2 times higher than that of the thinner electrode, suggesting that large redox couples do not penetrate the PEDOT-Tos electrode to a significant extent. But, the redox peak current shows a moderate increase, reaching values comparable with the platinum electrodes. Recently, Abdelnasser et al design a mixed organic-inorganic system containing visible-light absorption properties of the CP, poly(3,4-ethylenedioxythiophene) (PEDOT) doped with tosylate and excellent charge transport properties of TiO₂ nanotubes creating an efficient photoelectrode. These photoelectrodes can be used in solar-light chemical energy conversion applications. The optical characteristics of the UV-vis diffuse reflectance spectra reveals that, in the visible range, the hybrid electrodes show better absorption properties than pure TiO₂ nanotubes.⁵² An absorption band and energy gap for the pure nanotubes are 382.62 nm and 3.24 eV, respectively, which moved to a higher wavelength region after the incorporation of PEDOT-Tos, proving the greater ability of PEDOT-TiO₂ hybrid electrode, to capture a large number of photons in comparison to the pure TiO₂ nanotubes. The photocurrent responses of the fabricated electrodes using 1 M KOH electrolyte using a three-electrode PEC cell revealed that the highest photocurrent density obtained with the highest absorption electrodes was approximately six times greater than the pure TiO₂ as shown in Figure 8. The electrode based on conductive composite PEDOT-Tos/PU, a fully organic hydrogel-hybrid, has achieved high electrical conductivity, excellent stability, good biocompatibility and larger mechanical searchability.⁸⁵ The summarized electrode applications are shown in Table 2.

4.3 | Sensors application

As a consequence of electrochemical oxidation or reduction, the electrical and optical properties of PEDOT-Tos change significantly due to the doping or de-doping process (anion uptake or release). Thus the anion uptake of PEDOT-Tos can be employed in advanced sensors applications. The temperature sensing behavior of the PEDOT-Tos was first investigated by Yu et al.⁸⁶ A monotonous decrease in the resistance of the synthesized PEDOT-Tos thin films was observed with the increase in temperature from -20°C to 60°C. The thin films were sealed with epoxy resin and then thermally treated to improve the stability. The decrease in resistance with temperature is correlated through Steinhart-Hart equation recommending the PEDOT-Tos films as a flexible thin film thermistor. Although the humidity influences the resistance of the film, its effect on the properties of the films was not taken into account in this study. But a recent study shows that the hydrophilicity is diminished due to the lack of sulfonic acid in the PEDOT-Tos structure and as a consequence the effect of humidity on resistance declines.⁴⁵ The resistance of the synthesized samples shows a remarkable change with the increase in temperature. Further the thin films are also very responsive to a very small change in temperature suggesting that the PEDOT-Tos films are promising candidate for the flexible organic thermistors.

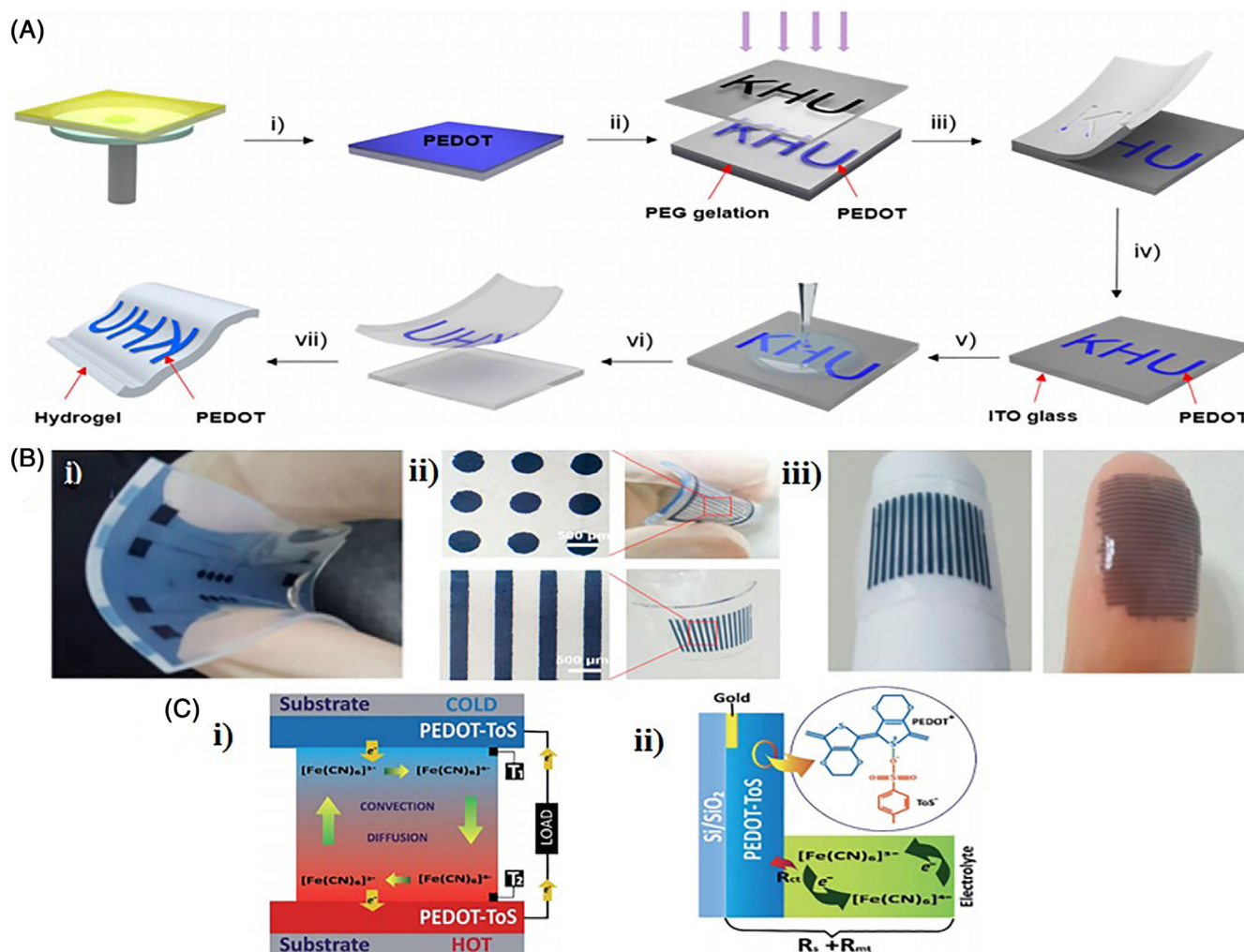


FIGURE 6 (A) Schematic illustration of the fabrication of conducting polymer patterns on either hydrogel substrate: (i) solution phase monomer casting and oxidative polymerization of conducting polymer (PEDOT); (ii) PEG photolithography process using UV light via a photomask; (iii) peeling off of the PEG hydrogel layer; (iv) conductive polymer pattern on conductive indium tin oxide (ITO)-coated glass; (v, vi) second gel precursor solution (agarose or PEG) was poured onto the PEDOT-patterned ITO glass and a second gelation was conducted; (vii) peeling off of the second gel layer and transfer of the PEDOT pattern from the glass to the hydrogel substrate; (vii) conductive polymer pattern on a flexible hydrogel layer. Adapted with permission.⁸³ Copyright 2016, American Chemical Society. (B) (i) Photographs of a PEDOT electrode array pattern on (i) on a flexible agarose hydrogel layer. (ii) Optical microscopic images of PEDOT patterns of various sizes and shapes (500 μm in diameter and 300 μm in width) on flexible agarose hydrogel layers. (iii) PEDOT-patterned agarose layers showed good adhesion properties both on paper and natural human skin. Adapted with permission.⁸³ Copyright 2016, American Chemical Society. (C) (i) Sketch of thermogalvanic cell materials/redox electrolytes used (T1 and T2 thermo-couples for temperature measurement of the electrode). (ii) Sketch of ohmic loss contributions of PEDOT-Tos electrode and electrolyte. Reproduced with permission.⁸⁴ Copyright 2012, Royal Society of Chemistry

The optical and laser-induced damage (LID) behavior of a PEDOT-Tos layer below thickness of 500 nm can implement a new optical fiber sensing application.⁶⁷ The PEDOT-Tos deposited on the tip of a single mode optical fiber with a desired thickness through VPP. The LID is observed in the PEDOT-Tos using both CW and pulsed laser to determine the degradation time validated through a mathematical model which was developed based on the experimental results. Avoiding the degradation of the PEDOT-Tos layer can play an important role for the practical applications. It was proposed that irradiance should not exceed 31.8 W/mm² (average power lower limit 2.70 mW with a modified diameter of 10.4 \pm 0.5 μm) in

low peak power around 67.53 mW to avoid LID at a wavelength of 1550 nm.⁶⁷

PEDOT-Tos based materials are also used in the selection of NO₃⁻ not only from an aqueous environment containing NO₃⁻ but also from the mixture of other ions present in concentrations (ppm) in real agricultural soil.⁶⁶ Although nitrate (NO₃⁻) is a vital commodity for the growth of a plant, usage of nitrate-based fertilizer and chemical materials can affect the environment as well as increase the health issues in human. So for detecting and monitoring the anion contamination is an important issue. The PEDOT-Tos thin films when exposed to the mixture ion solution containing NO₃⁻ were redoped without

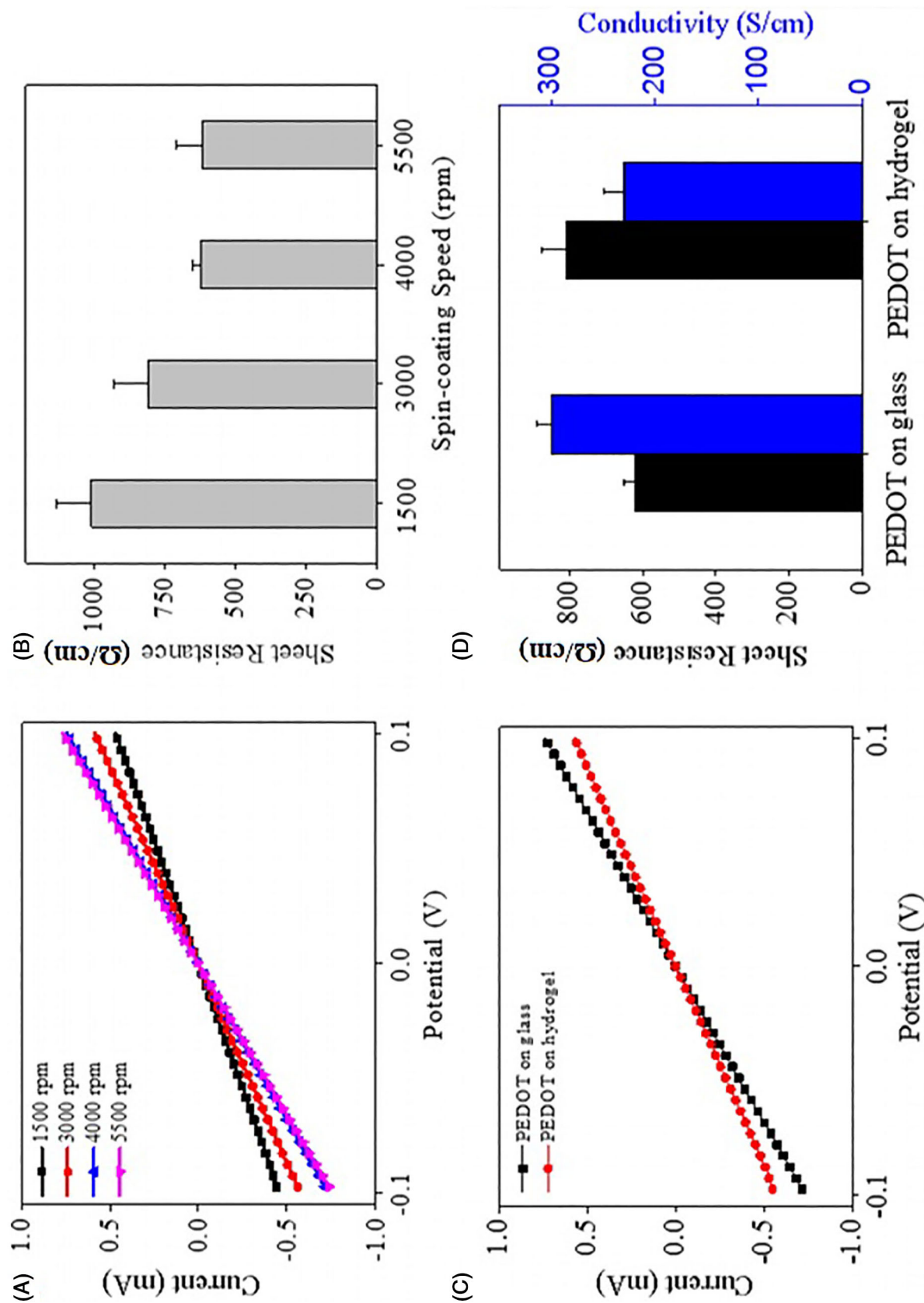


FIGURE 7 (A) Current-voltage (I-V) characteristics of PEDOT films of various thickness on glass substrates. Spin-coating speeds from 1500 to 5500 rpm were used to control the thickness of the film. (B) Sheet resistance of PEDOT film on glass substrate as a function of spin-coating speed. (C) Current-voltage (I-V) characteristics of PEDOT film on glass before direct transfer and hydrogel substrate after direct transfer process. (D) Sheet resistance and conductivity of PEDOT films on glass and hydrogel substrates. PEDOT film on a glass substrate was transferred to PEG hydrogel substrate by a direct transfer process. Adapted with permission.⁸³ Copyright 2016, American Chemical Society

any electrical stimulation. Thus any change in the electrical properties of the thin films could be utilized to identify the nitrate concentration from solution. Therefore PEDOT-Tos thin film is efficient for selecting and sensing the nitrate (NO_3^-) from real-life agriculture soil. PEDOT-Tos film with thermoplastic polyurethane (TPU) exhibits an excellent mechanical property which is due to the diffusion of the EDOT monomer in the TPU matrix polymerized in oxidant interface as shown in Figure 9A. The resulting PEDOT was formed uniformly in both sides of the TPU matrix. This has been exploited for the synthesis of a strain sensor.⁷⁵ The strain sensor with 7% Fe(Tos) shows a quite enviable stretchability (>300%). From the result, it is obtained that a hydrogen

bond created in between the polar sulfone group of tosylate anions and N-H group of polyurethane behaves like an effective plasticizer. Moreover, the sample in Figure 10 shows good sensitivity, small hysteresis, resistance variation reproducibility under various strain modes and durability. The summarized sensor applications are tabulated in Table 3.

4.4 | Biomedical and other applications

CP has great contribution in nanomedicine research field, neurite outgrowth and differentiation of neuronal synaptic network instead of earlier in-vitro techniques. Nanomedicine aims to remove stent malposition, restenosis and late stent thrombosis. For organic bioelectronics interfaces PEDOT is a potential candidate due to its suppleness,²⁹ improved biocompatibility and the intrinsic transport properties of electrons^{58,87} among the CPs. Further, the presence of dioxyalkylene bridging group in PEDOT-Tos improves its electrical conductivity due to its low band gap and redox potential in comparison to other polymers with regards to environmental, chemical and thermal stability.⁸⁷

PEDOT-Tos has evolved a new perspective in tissue regeneration for cardiovascular implants. PEDOT-Tos thin films were proposed as a suitable candidate in cell adhesion and proliferation effect as compared to controls due to their nanoporosity and hydrophilicity.⁵⁸ Their conductivity and hydrophilicity were increased by PEGylation and results cell viability. The study of the synaptic activity of rat hippocampal neurons by calcium imaging and immunofluorescence using tosylate doped PEDOT has been reported.⁸⁷ Immunofluorescence imaging differentiated the growth of neuron morphology on poly-L-Lysin coated glass from that on PEDOT-Tos. The immunofluorescence investigation executed on mature neuron culture on PEDOT-tosylate

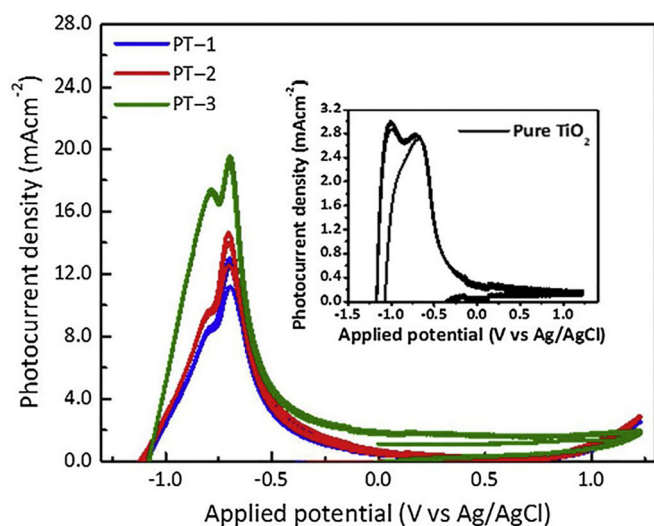


FIGURE 8 Photocurrent density versus applied potential in 1 M KOH electrolyte under AM 1.5 G for pure TiO_2 (inset) and PEDOT- TiO_2 nanotube photoelectrodes. Reproduced with permission.⁵² Copyright 2019, Elsevier

TABLE 2 Summarized electrode applications of PEDOT-Tos and its composites

Materials used	Polymerization method	Proposed application	References
PEDOT-Tos/ TiO_2 nanotube	Simple solution-casting polymerization process	Photoelectrodes can be used in solar-light chemical energy conversion applications	52
PEDOT-Tos modified by surface reaction with TDAE	Vapor phase polymerization	Formation of a transparent, low-work-function, plastic electrode with low work function 3.8 eV	57
PEDOT-Tos	Vapor phase polymerization	Transparent conducting electrode (TCE) applications.	71
PEDOT/PEDOT-Graphene	Vapor phase polymerization	Provide a mechanical strength to Ta_2O_5 dielectric films for use as a solid tantalum electrolyte capacitor.	77
PEDOT-Tos with Polyethylene glycol	Chemical oxidative polymerization	Development of versatile bioelectronics systems like electrical stimuli-responsive drug	83
PEDOT-Tos with the ferro/ferricyanide redox electrolyte	Chemical polymerization	Conducting polymer films as electrode in a thermogalvanic cell.	84
PEDOT/ polyurethane	Electropolymerization	Patterned electrode-hydrogel hybrid device can be used in biosensing and drug delivery.	85

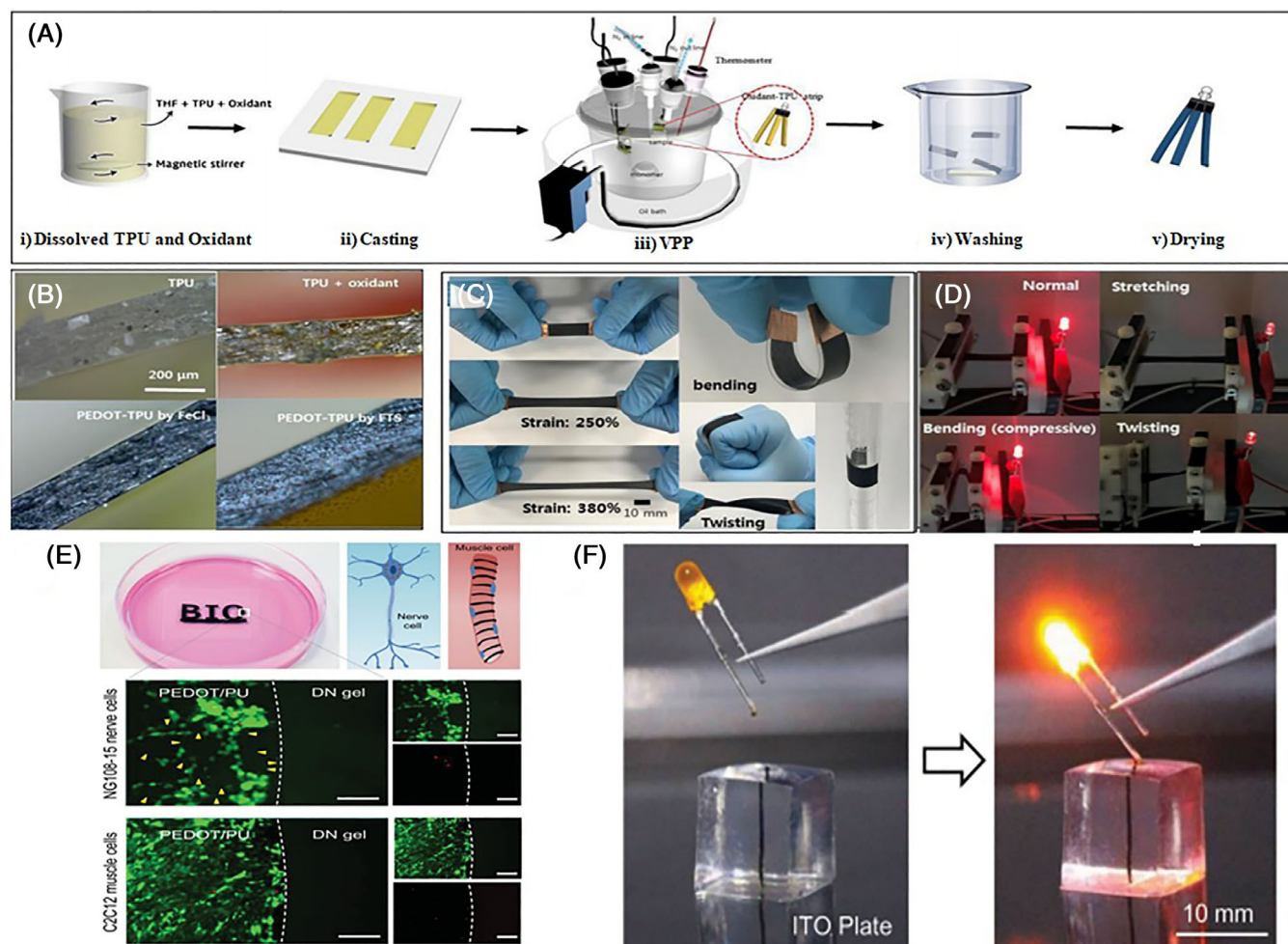


FIGURE 9 (A) Schematic illustration showing the fabrication of a conductive PEDOT-TPU hybrid elastomer via VPP. (B) Optical microscopic images of TPU, oxidant-embedded TPU and PEDOT-TPU hybrids. (C) Photographs of the demonstration of the sensors elastic and flexible properties. (D) LED attached to the PEDOT-Tos hybrid elastomer subjected to stretching, bending and twisting. Reproduced with permission.⁷⁵ Copyright 2019, Elsevier. (E) Nerve and muscle cell culture on PEDOT/PU-DN hydrogel hybrids. Fluorescent microscope images of attachment and proliferation of NG108-15 neuronal cells (middle panel) and C2C12 muscle cells (bottom panel). Dual staining of cells using Calcein-AM and propidium iodide was used to identify live (green) and dead (red) cells. Each panel shows the composite (red + green) image on the left and the individual (red or green) images on the right. Scale bars are 200 μm . Yellow arrows in the middle panel highlight the neurites of the NG108-15 cells. (F) Images showing the electrification using a 3D PEDOT/PU-hydrogel hybrid. The composite wire running through the cube of DN hydrogel electrically connects the ITO plate to an LED. Reproduced with permission.⁸⁵ Copyright 2014, WILEY-VCH Verlag GmbH & Co. KGaA, Weinheim

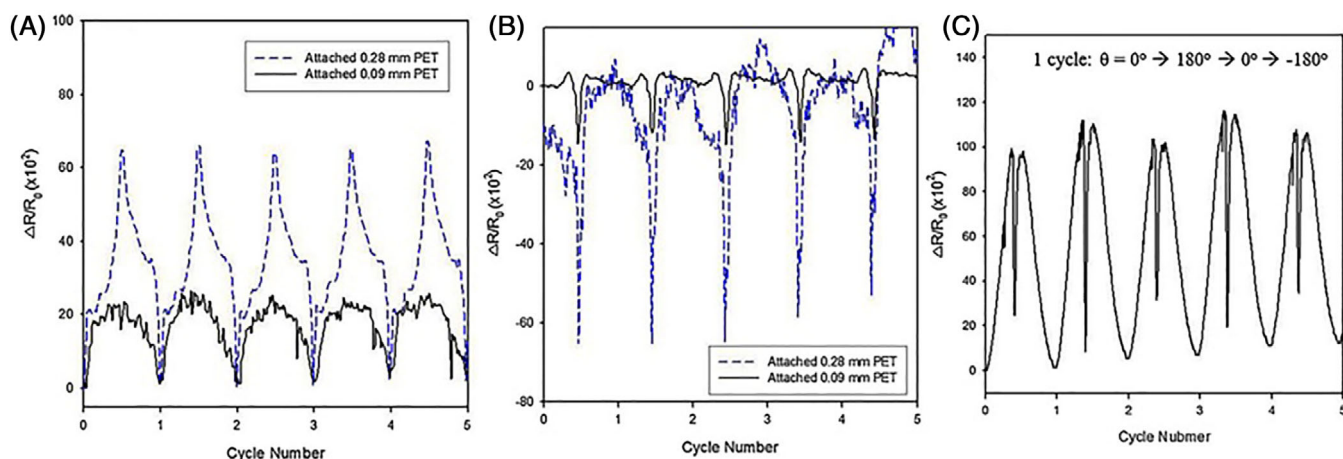


FIGURE 10 Strain sensing behavior of the PEDOT-TPU hybrid strain sensor attached to a PET substrate during (A) (outward) tensile bending and (B) (inward) compressive bending. (C) Sensor response to twisting motion. The sensor response during twisting was measured while twisting 360° over 1 cycle. Reproduced with permission.⁷⁵ Copyright 2019, Elsevier

revealed good biocompatibility, morphological reliability and maturation phases compared to control. The growth and development of hippocampal neurons were also quantified by calcium imaging. Fabrication of electrode on stretchable and flexible substrate has given a new dimension in the advance field of tissue engineering with

integrated electronics. A conductive hybrid consisting of PEDOT-Tos and polyurethane (PU) with elastic double-network hydrogel was fabricated with good biocompatibility. This hydrogel-based device has been applicable for the adhesion, proliferation and differentiation of neural and muscle tissue culture system, thus advancing the field of

TABLE 3 Summarized sensor applications of PEDOT-Tos and its composites

Materials used	Polymerization method	Proposed applications	References
PEDOT-Tos	Chemical Polymerization	Stable humidity based flexible organic thermistor.	45
	Vapor Phase polymerization	Selecting and sensing NO_3^- from environment.	66
	Vapor Phase polymerization	Optical fiber sensing using both CW and pulsed laser.	67
	Chemical Polymerization	Temperature sensing about temperature from -20°C to 60°C .	86
PEDOT-Tos film with thermoplastic polyurethane (TPU)	Vapor phase polymerization	Stretchable strain sensor.	75

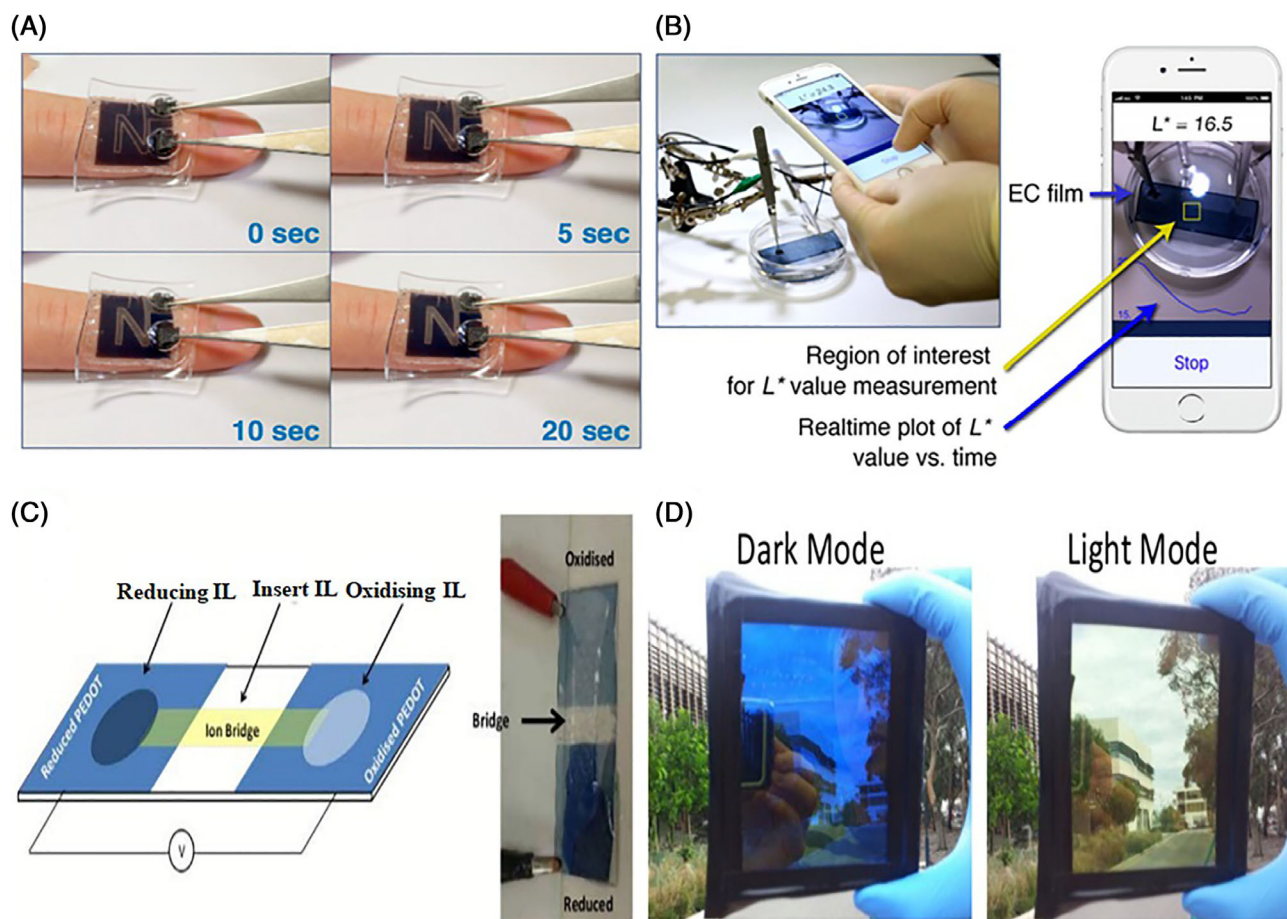


FIGURE 11 (A) Color change of the EC film/hydrogel hybrid device placed on a human finger. (B) Custom mobile phone app that measures the L^* value of the PEDOT/PU film and plots its temporal change in a real-time manner. Measurement of the L^* value of the PEDOT/PU film by the app (left) and a screenshot of the app (right). Adapted with permission.⁴⁸ Copyright 2017, American Chemical Society. (C) The architecture of the prototype metal-free fuel cell. One PEDOT-Tos electrode is reduced, the other is oxidized, and they are bridged with an ion channel using the inert IL. An example of the working ICP-IL fuel cell is presented, showing the reduction and oxidation occurring at each half of the cell. (D) The prototype smart window can be switched between its dark and light modes through application of a 1.5 V potential. Reproduced with permission.⁸⁹ Copyright 2013, Royal Society of Chemistry

tissue engineering with integrated electronics.⁸⁵ Figure 9B shows the nerve and muscle cell culture on PEDOT/PU-DN hydrogel hybrids and the electrification using a 3D PEDOT/PU-hydrogel hybrid. Further the electronic influence of the stem cell adhesion and density was also reported using PEDOT-Tos based surface switch electrodes where it was observed that there are significantly more cells on the oxidized surfaces.⁸⁸

CPs also experience the phenomenon of electrochromism which has been stated in many scientific reports. PEDOT-Tos/PU film combined with hydrogel as a support can work as a free-standing electrochromic film. The observable color change of the film can be detected by eye and can be measured by digital camera image

processing during the redox reactions which can also be integrated into a mobile phone app (CIELAB color scale) as shown in Figure 11. Interaction between the inherently CPs (ICP) and ionic liquids (IL) analyzed as a combination of processes steered by the chemical nature of IL and ICP, and any externally applied electric field. These are classified as hard base anions induce oxidation or reduction of the ICP when paired with cations respectively. PEDOT-Tos as ICP oxidized or reduced by the specific IL in order to fabricate organic electronic devices (OEDs) such as, electrochromic displays, optical memories, smart windows, supercapacitors, fuel cells with excellent performance.⁸⁹ Figure 11 also presents some of the above said applications. With a newly developed patterning technique for conductive

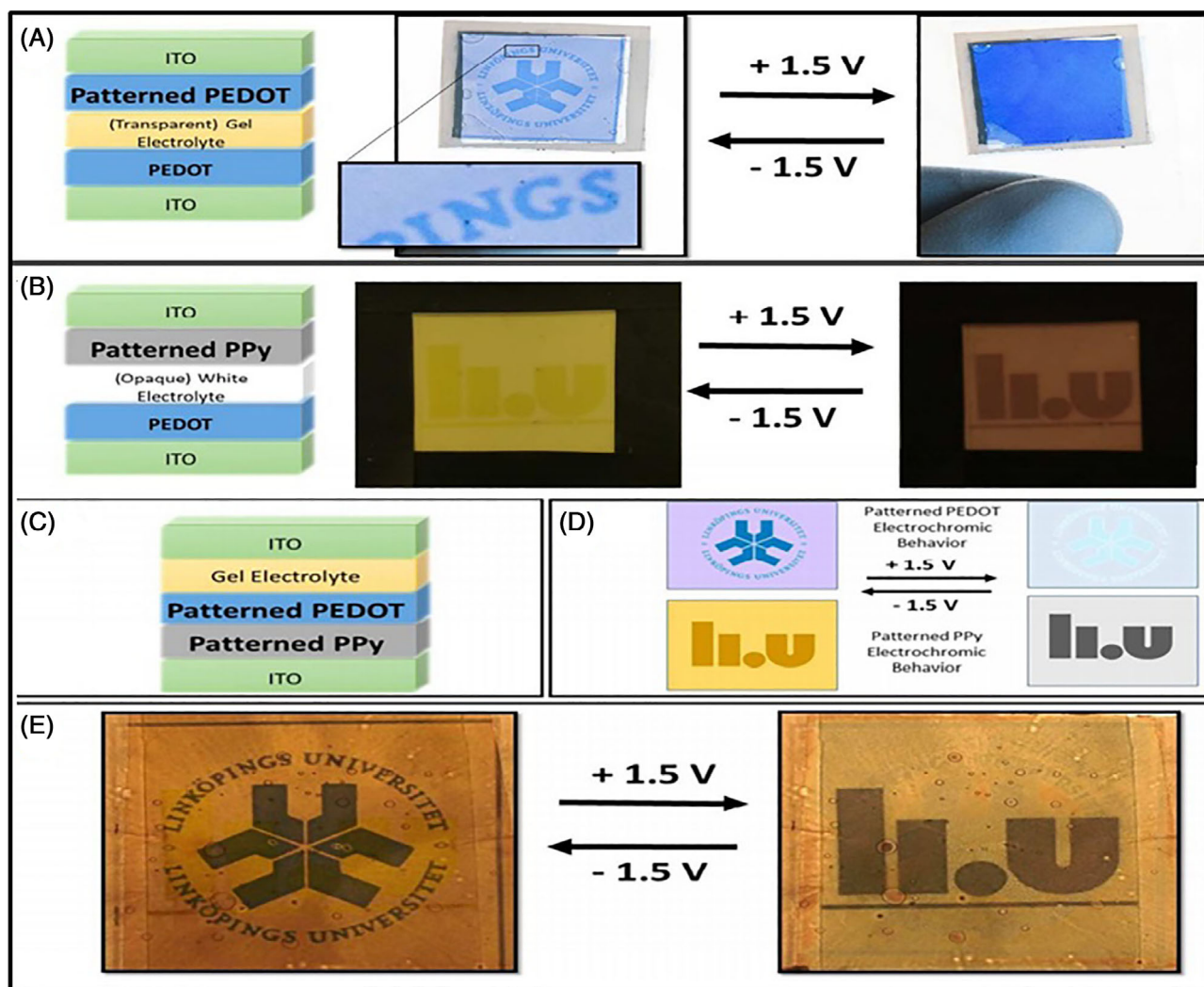


FIGURE 12 Prototype patterned electrochromic devices. (A) PEDOT electrochromic device design incorporating a UV-light patterned PEDOT layer with PEDOT as the counter polymer. The device is shown in both states where the university logo becomes visible during reduction of the patterned PEDOT and disappears during oxidation with the aid of the counter PEDOT's dark reduced state. (B) Electrochromic device design incorporating a UV-light patterned PPy layer with PPy as the counter polymer. The PPy device in both states is presented with the pattern becoming visible when the patterned PPy layer is oxidized and disappears when it is reduced. Voltages stated are applied to the patterned CPs. (C) Dual image electrochromic device architecture showing the change in structure with both CPs deposited onto one ITO substrate. (D) Individual electrochromic behavior of the two patterned CPs when under applied voltages of +1.5 and -1.5 V. The images appear and disappear in opposites allowing a double image device. (E) Dual image electrochromic device in both states showing clearly both individual images. Reproduced with permission.⁹⁰ Copyright 2013, Royal Society of Chemistry

TABLE 4 Summarized biomedical and other applications of PEDOT-Tos and its composites

Materials used	Polymerization method	Proposed application	References
PEDOT-Tos	Chemical oxidative polymerization	Good cathode materials under high temperature high humidity conditions.	44
PEDOT-TOS/PEG hybrid polymer	Chemical polymerization	EIS-based and amperometric affinity/catalytic biosensors.	49
PEDOT-Tos	Vapor phase polymerization	Tissue regeneration activities	58
	Vapor phase polymerization	Charge storage capacity for more efficient energy storage devices.	62
	Chemical polymerization	Capable of harvesting healthy primary neural networks	87
	Vapor phase polymerization	Electronic control of stem cell differentiation.	88
PEDOT-Tos with variety of ILs	Vapor phase polymerization	Electrochemic devices, Optical memory, Smart window, Supercapacitors, Fuel cell.	89
PEDOT-Tos with 30 wt% Fe(PTS) ₃	Chemical polymerization	Thin film transistor electrode	91
PEDOT-Tos with polyvinylpyrrolidone (PVP)	Chemical polymerization	water-free process for organic electronic devices	93

polymers, combining UV-light exposure with vapor phase polymerization, a high-resolution electrochromic device was fabricated from PEDOT-Tos and polypyrrole where the displaying images appear and disappear with the change in applied voltage. Finally a dual-image electrochromic and infra-red camouflaging were devised by incorporation of patterned PEDOT-Tos as well as the patterned polypyrrole on the same electrode under the exposure of UV-light as shown in Figure 12. Since polymer tantalum capacitors are emerging as an excellent choice for circuit designs that require stable capacitance, long life, high reliability and smaller size, PEDOT-Tos based capacitors have been fabricated, which shows high longevity and reliability due to its conductivity, stability under high temperature and high humidity conditions.⁴⁴ PEDOT-Tos films used as electrodes are also employed for the fabrication of organic thin film transistors (OTFTs).⁹¹ The fabricated thin film transistors formed on 30 wt% iron(III) p-toluenesulfonate hexahydrate Fe(PTS)₃ revealed the saturation mobility of 0.16 cm²/Vs and subthreshold slope of 0.5 V/decade.

Piezoelectric nanocomposite based nanogenerators have been employed using PEDOT-Tos and ZnO nanowires but the infiltration is poor and the thickness of the polymer above nanowires is difficult to control.⁹² PEDOT-Tos thin film electrode was also modified by PEG at different molecular weights for biosensor applications. The kinetics of the modified films at the nanoscale was influenced by different bias voltages and changes depending on the PEG molecular weight making the films a potential candidate for biosensing applications.⁴⁹ A water-free process was also employed to synthesize PEDOT-Tos modified with PVP for organic electronics.⁹³ The charge storage capacity of PEDOT-Tos films was also investigated and compared with the addition of PEG/ PPG/PEG and PEG/PDMS/PEG where it shows that though the addition of triblock copolymers increases the electrical conductivity but they adversely impact the charge storage capacity.⁶² All the biomedical and other applications are summarized in Table 4.

5 | CONCLUSION

Till date the applications of polymers as engineered materials are a growing field of organic electronics. The CPs prove to be a new class of materials together with promising results in the direction of polymer based industry. Out of the known CPs, PEDOT-Tos acquires a special position due the diverse applications. The π stacked lamellar structure improves the structural order and at the same time the electronic band structure supports the semi-metallic character of PEDOT-Tos.

Its electrical conductivity and thermal conductivity are comparable with inorganic counterparts. With tunable properties, the thermoelectric power as well as the electrical conductivity of PEDOT-Tos can be increased simultaneously which promotes the material to be a potential thermoelectric candidate. The development of PEDOT-Tos as an electrode opens up new directions of research. The efficiency of PEDOT-Tos as electrode in thermogalvanic cell is found to be quite promising and advantageous. In addition the organic electrodes comprised of PEDOT-Tos can be used in versatile system starting from dye sensitized solar cell to bioelectronics. The electrochemical oxidation and reduction due to doping and de-doping process can be utilized in various sensor applications. Indeed PEDOT-Tos is so unique that it is considered to be a viable candidate due to its low band gap, redox potential as well as improved biocompatibility in biomedical applications also which includes a new perspective in tissue regeneration for cardiovascular implants and in cell adhesion and proliferation.

The ease of synthesis and mechanical flexibility of PEDOT-Tos allows designing nanocomposites which can be used in device applications in diverse fields. We certainly expect that the uniqueness of PEDOT-Tos as a multifunctional material opens up a new era of intelligent materials with promising opportunities in multiparameter space: from thermoelectrics to tissue culture.

ORCID

Krishanu Chatterjee  <https://orcid.org/0000-0001-6400-3110>

REFERENCES

- Kim Y, Kim Y, Kim S, Kim E. Electrochromic diffraction from nano patterned poly(3-hexylthiophene). *ACS Nano*. 2010;4:5277-5284.
- Koh JK, Kim J, Kim B, Kim JH, Kim E. High efficient, iodine-free dye-sensitized solar cells with solid-state synthesis of conducting polymers. *Adv Mater*. 2011;23:1641-1646.
- Kim J, You J, Kim B, Park T, Kim E. Solution processable and patternable poly(3,4-alkylenedioxythiophene)s for large-area electrochromic films. *Adv Mater*. 2011;23:4168-4173.
- Dodabalapur A, Torsi L, Katz HE. Organic transistors: two-dimensional transport and improved electrical characteristics. *Science*. 1995;268:270-271.
- Burroughes JH, Bradley DDC, Brown AR, et al. Light-emitting diodes based on conjugated polymers. *Nature*. 1990;347:270-271.
- Reddy VS, Karak S, Ray SK, Dhar A. Carrier transport mechanism in aluminum nanoparticle embedded AlQ₃ structures for organic bistable memory devices. *Org Electron*. 2009;10:138-144.
- Street RA, Mulato M, Lau R, Ho J. Image capture array with an organic light sensor. *Appl Phys Lett*. 2009;78:4193-4195.
- Cavallini M, Biscarini F, Leon S, Zerbetto F, Bottari G, Leigh DA. Information storage using supramolecular surface patterns. *Science*. 2003;299:531.
- Maddison DS, Unsworth J. Electrical conductivity and thermoelectric power of polypyrrole with different doping levels. *Synth Met*. 1988;26:99-108.
- Aich RB, Blouin N, Bouchard A, Leclerc M. Electrical and thermoelectric properties of poly(2,7-Carbazole) derivatives. *Chem Mater*. 2009;21:751-757.
- Bubnova O, Khan ZU, Malti A, et al. Optimization of the thermoelectric figure of merit in the conducting polymer poly(3,4-ethylenedioxythiophene). *Nat Mater*. 2011;10:429-433.
- Yue R, Xu J. Poly(3,4-ethylenedioxythiophene) as promising organic thermoelectric materials: a mini-review. *Synth Met*. 2012;162:912-917.
- Taggart DK, Yang Y, Kung S-C, McIntire TM, Penner RM. Enhanced thermoelectric metrics in ultra-long electrodeposited PEDOT nanowires. *Nano Lett*. 2011;11:125-131.
- Aranguren P, Roch A, Stepien L, et al. Optimized design for flexible polymer thermoelectric generators. *Appl Therm Eng*. 2016;5:402-411.
- Wei Q, Mukaida M, Kiriha K, Naitoh Y, Ishida T. Recent progress on PEDOT-based thermoelectric materials. *Materials*. 2015;8:732-750.
- Bharti M, Singh A, Samanta S, Aswal DK. Conductive polymers: creating their niche in thermoelectric domain. *Prog Mater Sci*. 2017;93:270-310.
- Kus M, Okur S. Electrical characterization of PEDOT:PSS beyond humidity saturation. *Sens Actuat B*. 2009;143:177-181.
- Zhang H, Xu J, Wen Y, Wang Z, Zhang J. Conducting poly(3,4-ethylenedioxythiophene):poly(styrenesulfonate) film electrode with superior long-term electrode stability in water and synergistically enhanced electrocatalytic ability for application in electrochemical sensors. *Synth Met*. 2015;204:39-47.
- Sun K, Zhang S, Li P, et al. Review on application of PEDOTs and PEDOT:PSS in energy conversion and storage devices. *J Mater Sci Mater Electron*. 2015;26:4438-4462.
- Kim G-H, Kim J, Pipe KP. Humidity-dependent thermoelectric properties of poly(3,4-ethylenedioxythiophene):poly(styrene sulfonate). *Appl Phys Lett*. 2016;108:093301-5.
- Nardes AM, Kemerink M, de Kok MM, Vinken E, Maturova K, Janssen RAJ. Conductivity, work function, and environment stability of PEDOT:PSS thin films treated with sorbitol. *Org Electron*. 2008;9:727-734.
- Benoudjit A, Bader MM, Salim WWAW. Study of electropolymerized PEDOT:PSS transducers for application as electrochemical sensors in aqueous media. *Sens Biosensing Res*. 2018;17:18-24.
- Duc C, Malliaras GG, Senez V, Vlandas A. Long-term ageing of PEDOT:PSS: wettability study. *Synth Met*. 2018;238:14-21.
- Zafar Q, Abdullah SM, Azmer MI, Najeeb MA, Qadir W, Sulaiman K. Influence of relative humidity on the electrical response of PEDOT:PSS based organic field-effect transistor. *Sens Actuat B*. 2018;255:2652-2656.
- de Leeuw DM, Kraakman PA, Bongaerts PFG, Mutsaers CMJ, Klaassen DBM. Electroplating of conductive polymers for the metallization of insulators. *Synth Met*. 1994;66:263-273.
- Chen X, Xing K-Z, Inganäs O. Electrochemically induced volume changes in poly(3,4-ethylenedioxythiophene). *Chem Mater*. 1996;8:2439-2443.
- Yu SH, Lee J, Choi MS, Park JH, Yoo PJ, Lee JY. Improvement of electrical conductivity of poly(3,4-ethylenedioxythiophene) (PEDOT) thin film. *Mol Cryst Liq Cryst*. 2013;580:76-82.
- a) Petsagkourakis I, Kim N, Tybrandt K, Zozoulenko I, Crispin X. Poly(3,4-ethylenedioxythiophene): chemical synthesis, transport properties, and thermoelectric devices. *Adv Electron Mater*. 2019;5:1800918.
- Aasmundtveit KE, Samuelsen EJ, Pettersson LAA, Inganäs O, Johansson T, Feidenhans R. Structure of thin films of poly(3,4-ethylenedioxythiophene). *Synth Met*. 1999;101:561-564.
- Franco-Gonzalez JF, Zozoulenko IV. Molecular dynamics study of morphology of doped PEDOT: from solution to dry phase. *J Phys Chem B*. 2017;121:4299-4307.
- Franco-Gonzalez JF, Rolland N, Zozoulenko IV. Substrate-dependent morphology and its effect on electrical mobility of doped PEDOT thin films. *ACS Appl Mater Interfaces*. 2018;10:29115-29126.
- a) Edberg J, Iandolo D, Brooke R, et al. Patterning and conductivity modulation of conductive polymers by UV light exposure. *Adv Funct Mater*. 2016;26:6950-6960. b) Lee YH, Oh J, Lee S-S, Kim H, Son JG. Highly ordered nanoconfinement effect from evaporation-induced self-assembly of block copolymers on in situ polymerized PEDOT: Tos. *ACS Macro Lett*. 2017;6:386-392.
- a) Bubnova O, Khan ZU, Wang H, et al. Semi-metallic polymers. *Nat Mater*. 2014;13:190-194. b) Hwang J, Tanner DB. Optical properties of nondegenerate ground-state polymers: three dioxothiophene-based conjugated polymers. *Phys Rev B*. 2003;67:115205.
- Massonnet N, Carella A, de Geyer A, Faure-Vincent J, Simonato J-P. Metallic behaviour of acid doped highly conductive polymers. *Chem Sci*. 2015;6:412-417.
- Petsagkourakis I, Pavlopoulou E, Portale G, et al. Structurally-driven enhancement of thermoelectric properties within poly(3,4-ethylenedioxythiophene) thin films. *Sci Rep*. 2016;6:30501.
- Kim N, Lee BH, Choi D, et al. Role of interchain coupling in the metallic state of conducting polymers. *PRL*. 2012;109:106405.
- Winther-Jensen B, Forsyth M, West K, et al. Order-disorder transitions in poly(3,4-ethylenedioxythiophene). *Polymer*. 2008;49:481-487.
- Khan ZU, Bubnova O, Jafari MJ, et al. Acido-basic control of the thermoelectric properties of poly(3,4-ethylenedioxythiophene)tosylate (PEDOT-Tos) thin films. *J Mater Chem C*. 2015;3:10616-10623.
- Kim J-S, Jang W, Wang DH. The investigation of the seebeck effect of the poly(3,4-ethylenedioxythiophene)-tosylate with the various concentrations of an oxidant. *Polymers*. 2019;21:11.
- Khan EH, Thota S, Wang Y, et al. Environment-friendly post-treatment of PEDOT-Tos films by aqueous vitamin C solutions for tuning of thermoelectric properties. *J Electron Mater*. 2018;47:3963-3968.
- Modarresi M, Franco-Gonzalez JF, Zozoulenko I. Morphology and ion diffusion in PEDOT:Tos. A coarse grained molecular dynamics simulation. *Phys Chem Chem Phys*. 2018;20:17188-17198.

42. Muñoz WA, Singh SK, Franco-Gonzalez JF, Linares M, Crispin X, Zozoulenko IV. Insulator to semimetallic transition in conducting polymers. *Phys Rev B*. 2016;94:205202.
43. Rolland N, Franco-Gonzalez JF, Volpi R, Linares M, Zozoulenko IV. Understanding morphology-mobility dependence in PEDOT:Tos. *Phys. Rev Mater*. 2018;2:045605-9.
44. Chacko AP, Jin Y, Shi Y, Bunha A, Chen J, Lessner PM. Advances in reliability of conducting polymers and conducting polymer based capacitors in high humidity environment. *ECS Trans*. 2018;85:115-127.
45. Štulík J, Polanský R, Hamáček A, et al. Comparison of organic thermistors based on PEDOT:PSS and PEDOT:Tos thin films under various thermal and humidity conditions. *Sens Actuat B*. 2018;275:359-366.
46. Kim TY, Kim JE, Suh KS. Effects of alcoholic solvents on the conductivity of tosylate-doped poly(3,4-ethylenedioxythiophene) (PEDOT-OTs). *Polym Int*. 2006;55:80-86.
47. Park T, Park C, Kim B, Shin H, Kim E. Flexible PEDOT electrodes with large thermoelectric power factors to generate electricity by the touch of fingertips. *Energy Environ Sci*. 2013;6:788-792.
48. Kai H, Suda W, Ogawa Y, Nagamine K, Nishizawa M. Intrinsically stretchable electrochromic display by a composite film of poly(3,4-ethylenedioxythiophene) and polyurethane. *ACS Appl Mater Interfaces*. 2017;9:19513-19518.
49. Rosati G, Sappia L, Madrid R, Rozlósnik N. Iron(III)-Tosylate doped PEDOT and PEG: a nanoscale conductivity study of an electrochemical system with biosensing applications. *Int Sch Sci Res Innov*. 2017;11:586-594.
50. Galliani D, Battiston S, Narducci D. Tuning PEDOT:Tos thermoelectric properties through nanoparticle inclusion. *J Nanosci Nanotechnol*. 2017;17:1579-1585.
51. Galliani D, Battiston S, Ruffo R, Trabattoni S, Narducci D. Modulation of charge transport properties in poly(3,4-ethylenedioxythiophene) nanocomposites for thermoelectric applications. *J Phys D Appl Phys*. 2017;51:13.
52. Abdelnasser S, Park G, Han H, Toth R, Yoon H. Enhanced photocatalytic performance of poly(3,4-ethylenedioxythiophene)coated TiO₂ nanotube electrodes. *Synth Met*. 2019;251:120-126.
53. Choi K, Kim SL, Yi S, Hsu J-H, Yu C. Promoting dual electronic and ionic transport in PEDOT by embedding carbon nanotubes for large thermoelectric responses. *ACS Appl Mater Interfaces*. 2018;10:23891-23899.
54. Maity S, Sepay N, Kulsi C, et al. Enhancement of thermoelectric performance in oligomeric PEDOT-SWCNT nanocomposite via band gap tuning. *ChemistrySelect*. 2018;3:8992-8997.
55. Maity S, Kulsi C, Banerjee S, Das S, Chatterjee K. Dependence of thermoelectric power and electrical conductivity on structural order of PEDOT-Tos-graphene nanocomposite via charge carrier mobility. *Mater Res Express*. 2019;6:105095-105105.
56. Winther-Jensen B, West K. Vapor-phase polymerization of 3,4-ethylenedioxythiophene: a route to highly conducting polymer surface layers. *Macromolecules*. 2004;37:4538-4543.
57. Lindell L, Burquel A, Jakobsson FLE, et al. Transparent, plastic, low-work-function poly(3,4-ethylenedioxythiophene) electrodes. *Chem Mater*. 2006;18:4246-4252.
58. Karagkiozaki V, Karagiannidis PG, Gioti M, et al. Bioelectronics meets nanomedicine for cardiovascular implants: PEDOT-based nanocoatings for tissue regeneration. *BBA*. 2013;1830:4294-4304.
59. Fabretto M, Muller M, Zuber K, Murphy P. Influence of PEG-ran-PPG surfactant on vapour phase polymerised PEDOT thin films. *Macromol Rapid Commun*. 2009;30:1846-1851.
60. Fabretto M, Zuber K, Jariego-Moncuill C, Murphy P. Measurement protocols for reporting PEDOT thin film conductivity and optical transmission: a critical survey. *Macromol Chem Phys*. 2011;212:2173-2180.
61. Zuber K, Fabretto M, Hall C, Murphy P. Improved PEDOT conductivity via suppression of crystallite formation in Fe(III) tosylate during vapor phase polymerization. *Macromol Rapid Commun*. 2008;29:1503-1508.
62. Rehmen J, Zuber K, Modarresi M, et al. Structural control of charge storage capacity to achieve 100% doping in vapor phase-polymerized PEDOT/tosylate. *ACS Omega*. 2019;4:21818-21826.
63. Hojati-Talemi P, Delaigue M, Murphy PJ, Fabretto MV. Flexible polymer-on-polymer architecture for piezo/pyroelectric energy harvesting. *ACS Appl Mater Interfaces*. 2015;7:8465-8471.
64. Fabretto MV, Evans DR, Mueller M, et al. Polymeric material with metal-like conductivity for next generation organic electronic devices. *Chem Mater*. 2012;24:3998-4003.
65. Rudd S, Murphy PJ, Evans DR. Diffusion controlled vapour deposition of mixed doped PEDOT. *Synth Met*. 2018;242:61-66.
66. Rudd S, Dalton M, Buss P, et al. Selective uptake and sensing of nitrate in poly(3,4-ethylenedioxythiophene). *Sci Rep*. 2017;7:16581.
67. Shahnian S, Rehmen J, Lancaster DG, et al. Towards new fiber optic sensors based on the vapor deposited conducting polymer PEDOT: Tos. *Opt Mater Express*. 2019;9:4517-4531.
68. Koch L, Polek A, Rudd S, Evans DR. Macroscopic electrical wires from vapour deposited poly(3,4-ethylenedioxythiophene). *ACS Appl Mater Interfaces*. 2017;9:65-70.
69. Chen S, Kühne P, Stanishev V, et al. On the anomalous optical conductivity dispersion of electrically conducting polymers: ultra-wide spectral range ellipsometry combined with a Drude-Lorentz mode. *J Mater Chem C*. 2019;7:4350-4362.
70. Zhang K, Qiu J, Wang S. Thermoelectric properties of PEDOT nanowire/ PEDOT hybrids. *Nanoscale*. 2016;8:8033-8041.
71. Hojati-Talemi P, Bächler C, Fabretto M, Murphy P, Evans D. Ultrathin polymer films for transparent electrode applications prepared by controlled nucleation. *ACS Appl Mater Interfaces*. 2013;5:11654-11660.
72. Bansal M, Sharma M, Bullen C, Svirskis D. Free standing PEDOT films prepared by vapour phase polymerisation as electrically tuneable barriers to drug permeability. *Mater Sci Eng C*. 2018;84:248-253.
73. Wang J, Cai K, Shen S. Enhanced thermoelectric properties of poly(3,4-ethylenedioxythiophene) thin films treated with H₂SO₄. *Org Electron*. 2014;15:3087-3095.
74. Wang J, Cai K, Song H, Shen S. Simultaneously enhanced electrical conductivity and seebeck coefficient in poly (3,4-ethylenedioxythiophene) films treated with hydroiodic acid. *Synth Met*. 2016;220:585-590.
75. Losaria PL, Yim J-H. A highly stretchable large strain sensor based on PEDOT-thermoplastic polyurethane hybrid prepared via in situ vapor phase polymerization. *J Ind Eng Chem*. 2019;74:108-117.
76. Chen J, Liu Y, Minet AI, Lynam C, Wang J, Wallace GG. Flexible, aligned carbon nanotube/conducting polymer electrodes for a lithium-ion battery. *Chem Mater*. 2007;19:3595-3597.
77. Yang Y, Zhang L, Li S, et al. Vapor phase polymerization deposition conducting polymer nanocomposites on porous dielectric surface as high performance electrode materials. *Nano-Micro Lett*. 2013;5:40-46.
78. Xu L, Xu J, Yang Y, et al. A flexible fabric electrode with hierarchical carbon-polymer composite for functional supercapacitors. *J Mater Sci Mater Electron*. 2017;29:2322-2330.
79. Mirmohseni A, Price WE, Wallace GG. Electrochemically controlled transport across conducting polymer composites m basis of smart membrane materials. *Polym Gels Netw*. 1993;1:61-77.
80. Yan H, Sada N, Toshima N. Thermal transporting properties of electrically conductive polyaniline films as organic thermoelectric materials. *J Therm Anal Calorim*. 2002;69:881-887.
81. Stepien L, Roch A, Tkachov R, Gedrange T. Progress in polymer thermoelectrics. *Thermoelectrics for Power Generation - A Look at Trends in the Technology*. London, UK: IntechOpen; 2016. <https://dx.doi.org/10.5772/66196>.

82. Yang Y, Li S, Zhang L, Xu J, Yang W, Jiang Y. Vapor phase polymerization deposition of conducting polymer/graphene nanocomposites as high performance electrode materials. *ACS Appl Mater Interfaces*. 2013;5:4350-4355.
83. Kim D, Kim J, Ko Y, Shim K, Kim JH, You J. A facile approach for constructing conductive polymer patterns for application in electrochromic devices and flexible microelectrodes. *ACS Appl Mater Interfaces*. 2016;8:33175-33182.
84. Wijeratne K, Vagin M, Brooke R, Crispin X. Poly(3,4-ethylenedioxythiophene)-tosylate (PEDOT-Tos) electrodes in thermogalvanic cells. *J Mater Chem A*. 2017;5:19619-19625.
85. Sasaki M, Karikkineth BC, Nagamine K, Kaji H, Torimitsu K, Nishizawa M. Highly conductive stretchable and biocompatible electrode-hydrogel hybrids for advanced tissue engineering. *Adv Healthc Mater*. 2014;3:1919-1927.
86. Yu SH, Choi MS, Yoo PJ, et al. Temperature sensing behavior of poly(3,4-ethylenedioxythiophene) thin film. *Synth Met*. 2013;185-186:52-55.
87. Chatterjee K. In vitro growth and differentiation of neuronal synaptic network on PEDOT: tosylate substrate. *IJTRSET*. 2017;6:12441-12450.
88. Salto C, Saindon E, Bolin M, et al. Control of neural stem cell adhesion and density by an electronic polymer surface switch. *Langmuir*. 2008;24:14133-14138.
89. Brooke R, Fabretto M, Krasowska M, et al. Organic energy devices from ionic liquids and conducting polymers. *J Mater Chem C*. 2016;4:1550-1556.
90. Brooke R, Edberg J, Iandolo D, Berggren M, Crispin X, Engquist I. Controlling the electrochromic properties of conductive polymers using UV-light. *J Mater Chem C*. 2018;6:4663-4670.
91. Ali MA, Kim HH, Jeong KH, et al. Application of tosylate-doped poly(3,4-ethylenedioxythiophene) (PEDOT) films into bottom contact pentacene organic thin film transistors (OTFTs). *Thin Solid Films*. 2010;518:6315-6319.
92. Dahiya AS, Morini F, Boubenia S, Nadaud K, Alquier D, Poulin-Vittrant G. Organic/inorganic hybrid stretchable piezoelectric nanogenerators for self-powered wearable electronics. *Adv Mater Technol*. 2017;3:1700249.
93. He J, Su J, Wang J, Zhang L. Synthesis of water-free PEDOT with polyvinyl pyrrolidone stabilizer in organic dispersant system. *Org Electron*. 2018;53:117-126.

How to cite this article: Maity S, Datta S, Mishra M, Banerjee S, Das S, Chatterjee K. Poly(3,4-ethylenedioxythiophene)-tosylate—Its synthesis, properties and various applications. *Polym Adv Technol*. 2020;1–19. <https://doi.org/10.1002/pat.5193>

TOPICAL REVIEW

Polymer chalcogenides—new smart materials for thermoelectric applications

To cite this article: Shilpa Maity *et al* 2022 *Smart Mater. Struct.* **31** 073001

View the [article online](#) for updates and enhancements.

You may also like

- [Varieties of charge distributions in coat proteins of ssRNA+ viruses](#)
Anže Lošdorfer Boži and Rudolf Podgornik
- [Tetrazole amphiphile inducing growth of conducting polymers hierarchical nanostructures and their electromagnetic absorption properties](#)
Aming Xie, Mengxiao Sun, Kun Zhang et al.
- [Efficient estimation of contact probabilities from inter-bead distance distributions in simulated polymer chains](#)
Dario Meluzzi and Gaurav Arya



ECS Membership = Connection

ECS membership connects you to the electrochemical community:

- Facilitate your research and discovery through ECS meetings which convene scientists from around the world;
- Access professional support through your lifetime career;
- Open up mentorship opportunities across the stages of your career;
- Build relationships that nurture partnership, teamwork—and success!

Join ECS!

Visit electrochem.org/join



Topical Review

Polymer chalcogenides—new smart materials for thermoelectric applications

Shilpa Maity¹, Umme Karnij Salma Parvin², Sukhen Das^{1,*}  and Krishanu Chatterjee^{2,*} ¹ Department of Physics, Jadavpur University, Kolkata 700032, India² Department of Physics, Techno India University, Salt Lake, Kolkata 700091, IndiaE-mail: sdasphysics@gmail.com and itskrishanu@gmail.com

Received 8 February 2022, revised 24 May 2022

Accepted for publication 1 June 2022

Published 16 June 2022



Abstract

The breakthrough invention of conducting polymers (CPs) initiates a new pathway for the researchers to make use of their properties in thermoelectric (TE) applications. They are considered to be potential candidates in TE application when combined with inorganic counterparts. Different strategies were undertaken to enhance structural order and hence the TE performance of the CPs which trigger the scientific community to focus more on this area. Consequently, the use of nano filler in the polymer matrix proved to be a better way to improve the TE properties and chalcogenide materials could be the best candidates to be used as nano filler due to their high TE parameters. Thus, composites of CPs with different chalcogenides have been drawing attention in the field of TEs in recent years. The present work points towards a comprehensive update on different synthesis process of composites of various CPs with a number of chalcogenides along with a state-of-art review of these promising materials in TEs for device applications with the expectation that this work will surely motivate the researchers to optimize the best candidate.

Keywords: polymer chalcogenide composites, synthesis methods, thermoelectric properties, thermoelectric applications

(Some figures may appear in color only in the online journal)

1. Introduction

Chances of possibility of running out of fossil fuels in near future due to its high consumption led researchers to study eco-friendly conversion of renewable energy for power generation and controlling the same. This conversion of energy being one of the most important topics of research for the developing world, conversion of wind energy, sunlight, nuclear power etc into utilizable form and storing it for future comes into play. During conversion, a maximum portion of energy is generated as waste heat into the atmosphere. Thermoelectric (TE)

generators could be the perfect solution which use this waste thermal energy and convert it to electricity. Generally, the TE performance of a material is expressed by the dimensionless figure of merit (ZT) defined as $ZT = S^2 \sigma T / (K_e + K_l)$ where S , σ , K_e , K_l and T are the Seebeck coefficient (or TE power), electrical conductivity, the electronic and lattice contribution to the total thermal conductivity and absolute temperature respectively [1]. So high power factor (PF) ($S^2 \sigma$) and low thermal conductivity (K) are the prerequisite conditions for high ZT to achieve an excellent TE performance.

Conducting polymers (CPs) are now a days thought to be potential TE candidates due to their ease of synthesis and cost effectiveness but are characterized by low electrical and thermal conductivity [1C]. The TE performance of

* Authors to whom any correspondence should be addressed.

several CPs such as polypyrrole [2], polyaniline (PANI) [3], poly(3,4-ethylenedioxythiophene) (PEDOT) [4], poly(styrene sulfonate)—doped PEDOT (PEDOT:PSS) [5] have been studied in the last decade. Efforts have been made in recent days to tune the electronic band structure of these CPs aiming to improve the TE performance yet the ZT values did not meet up the standards to be used commercially. Manipulation of band gaps [6–9], modulation doping [10, 11] and alloying with other TE materials [12–14] are some of the targeted strategies to further enhance the TE performance of the CPs. Inclusion of nano fillers in the polymer matrix is also thought to be a possible way to enhance the TE performance and, in that case, chalcogenide materials could be the best TE candidates due to their high TE parameters.

Thus, to achieve a high ZT value, composites of polymer-based chalcogenide materials are attracted huge attention for the TE applications. Chalcogenides are characterized by high Seebeck coefficient (S) and electrical conductivity (σ) whereas polymers without electrical optimization, possess an intrinsically low thermal conductivity (K). So, the combination can furnish the merits of both the materials suppressing the demerits thereby enhancing the PF and hence the ZT. Moreover, due to energy filtering effect of the polymer/chalcogenide interfaces, there might be a high chance in improvement of TE performance of the polymer/chalcogenide composites.

In this review, we summarize an up-to-date developments and optimization strategies of polymer-based chalcogenide composites. Further, some suggestions are offered to prepare the next generation polymer-based chalcogenide composite material with high TE properties.

2. Synthesis methods

Since different synthesis methods can yield different structures which in turn affects the TE properties, various synthesis methods viz *in-situ* polymerization, solution mixing, electro deposition, mechanical mixing etc have been employed for the synthesis of polymer/chalcogenide composites. Among all these methods, *in-situ* polymerization and solution mixing are commonly used to procure the effective structure of the different types of these composites.

2.1. In-situ polymerization

The main advantage of the *in-situ* polymerization technique is that during *in situ* polymerization the monomeric molecules can graft the inorganic chalcogenide nanoparticles (NPs) more homogeneously which allows preparing high content inorganic chalcogenide NPs composite inside the polymer chain.

Reports shows that nanocomposites of PANI and bismuth/tin chalcogenides have synthesized by means of *in-situ* polymerization technique [3, 15, 18, 19]. In a typical process, either nanorods of Bi_2Te_3 /hexagonal nanoplates (NPs) of Bi_2Se_3 or nanosheets (NSs) of SnSe/SnS or Ag_2Te [9] are mixed with a solution of aniline. Sulfosalicylic acid (SSA) and dodecylbenzenesulfonic acid (DBSA) were the dopants used in the first and second case respectively. The

transmission electron microscopy (TEM) or field emission scanning electron microscopy (FESEM) images indicate that the chalcogenides NPs are coated with PANI. PEDOT-coated $\text{SnSe}_{0.97}\text{Te}_{0.03}$ NSs was synthesized from the polymerization of 3,4-ethylenedioxythiophene in the presence of $\text{SnSe}_{0.97}\text{Te}_{0.03}$ NS powder and dodecyl benzenesulfonic acid in deionized water [20]. Ammonium persulfate (APS) was added as an oxidative agent in all the above cases.

2.2. Solution mixing

Solution mixing method is one of the convenient methods to prepare a polymer/chalcogenide composite. The process involves the mixing of both the polymer and chalcogenide NPs by dissolving into the solvent and then evaporates to form a composite film. Three steps are mainly followed in this protocol. Firstly, the dispersion of NPs in the solvent by sonication or stirring vigorously was done. Then mixing the polymer solution with the NP solution and finally with or without vacuum environment controlling the evaporation of the solvent.

Li intercalated Sn-Se-Te (x) or $\text{SnSe}_{1-x}\text{Te}_x$ powders (where x denotes different loading ratios) was dispersed in PEDOT-PSS solution and was sonicated. The final solution was either drop casted on glass [21] or filtered through nylon membrane filter paper to obtain the composite samples [16]. Further, by alternate stacking of PEDOT-coated $\text{SnSe}_{0.97}\text{Te}_{0.03}$ and PEDOT coated Te-substituted SnSe NSs (Te-s-SnSe NSs) with PEDOT-PSS, multilayered films are fabricated through solution mixing technique respectively [22] as shown in figure 1(B). Composites of PEDOT:PSS and copper chalcogenides (and also its alloy) has been synthesized by solution mixing. PEDOT:PSS coated polycrystal (PC) Cu_7Te_4 ($\text{PC-Cu}_7\text{Te}_4$) nanorods [13] or $\text{PC-Cu}_x\text{Se}_y$ nanowires (NWs) [14] were prepared using the PC-Te nanorods or PC-Se as templates respectively. The composite containing tellurides was drop casted on a pre-cleaned common glass substrates whereas samples containing the selenides was obtained on a porous nylon membrane by vacuum assisted filtration. The composite samples containing selenides are hot pressed instead of the cold one for further modification [23]. Moreover incorporation of Ag in the PC samples containing selenides [4] filtered through nylon membrane has been done and dried under vacuum at 40 °C for 4 h to obtain the composite film. Different amount of Bi_2Te_3 powder were also added to PEDOT/PSS solution doped with dimethyl sulfoxide (DMSO) and vacuum dried to obtained free standing films [24]. Furthermore, Bi_2Te_3 NWs were also added to Poly(3-hexylthiophene) (P3HT) doped with anhydrous FeCl_3 in different weight percentage and drop casted on glass slide and dried in vacuum at room temperature to obtain Bi_2Te_3 -P3HT nanocomposite films [25]. Dun *et al* reported a Cu-doped Bi_2Se_3 NP and polyvinylidene fluoride (PVDF) composite drop casted on glass substrate and baked at 80 °C overnight in air and finally peeled off the thin films from the glass substrate to obtain the flexible TE film [26]. Bi_2Se_3 was also added to a solution of PANI and tetrahydrofuran to synthesize PANI/ Bi_2S_3 nanocomposite via a facile chemisorption method. The synthesis

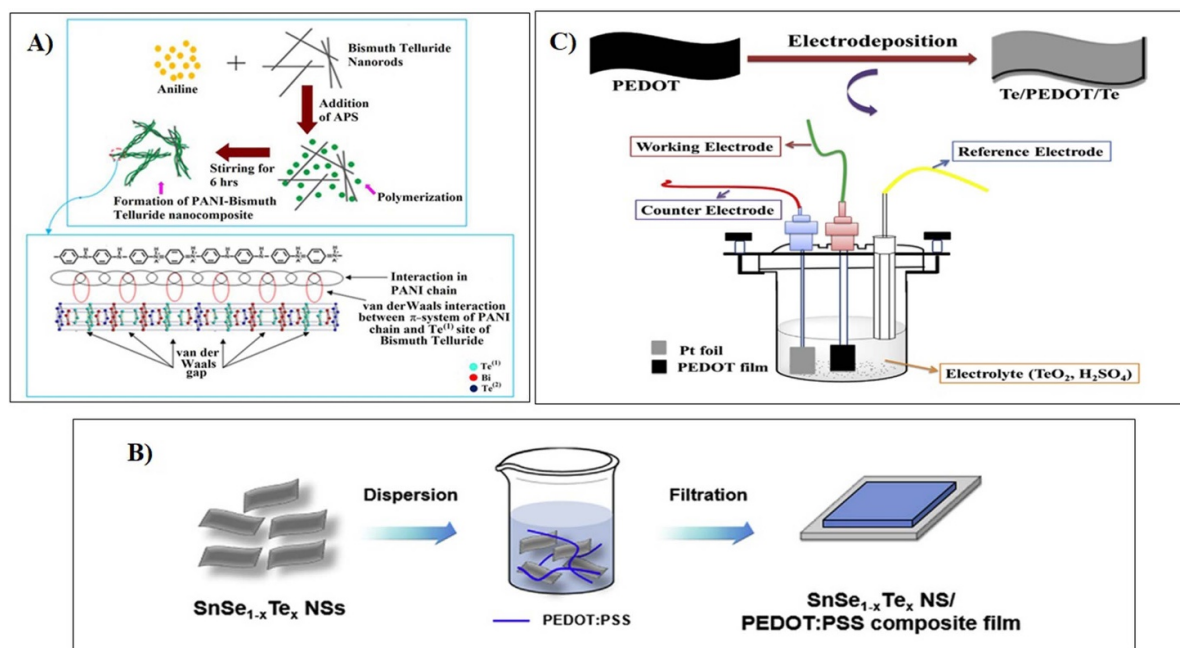


Figure 1. (A) Schematic representation of formation of PANI-Bi₂Te₃ nanocomposite. Reproduced from [15]. © IOP Publishing Ltd. All rights reserved. (B) Schematic images for the preparation SnSe_{1-x}Te_x NS/PEDOT:PSS composites. Reprinted from [16]. Copyright (2019) Elsevier B.V. All rights reserved. (C) Schematic diagram of Te electrodeposition on the free-standing PEDOT film. Reprinted from [17]. Copyright (2019) The Chinese Ceramic Society. Production and hosting by Elsevier B.V.

was followed by filtration and drying to obtain the precipitates [1A]. In an aqueous solution of PEDOT-PSS, the reduction of sodium selenite has been performed to synthesize selenium NPs coated with PEDOT:PSS. Thin films were casted from the above solution for TE characterization [27]. A combination of solution casting and hot compaction approach was also proposed by Kim *et al* to fabricate Te NW/Poly (methyl methacrylate) (PMMA) [28] and Ag₂Te NW/PMMA [29] composites. Polyvinylpyrrolidone (PVP) coated Ag-rich Ag₂Te NWs composite film was also synthesized via wet chemical reaction [30]. Films of the composite sample were prepared by vacuum filtration of the PVP coated Ag₂Te NWs on porous nylon membrane which were dried in vacuum and heat-treated for further characterization and application. Composites of Bi_{0.5}Sb_{1.5}Te₃ (BST) alloy with 10% or 20% ethylene glycol (EG) doped PEDOT-PSS was also synthesized by mixing the two in an ultrasonic bath for 4 h, and subsequently drying at 35 °C for 10 h forming thin and flexible pieces [31].

2.3. Mechanical mixing

Solid mixing has been also used to synthesis the polymer/chalcogenide composites. Typically, in this method the polymers or the inorganic NPs are either bought or synthesized separately. The NPs are then incorporated into the polymer matrix by using mortar pastel or high energy ball milling technique. In some cases, modification or post treatment has also been done.

Bi₂Te₃/PANI composite was synthesized by mechanical mixing method. Bi₂Te₃ was synthesized hydrothermally and PANI was synthesized by chemical oxidation process [32]. The prepared Bi₂Te₃ and PANI powders were added to ethyl

alcohol and using ZrO₂ ball, the mixture was milled for 3 h in the grinding media. The final product was dried in vacuum at 333 K for 24 h. Similarly, mechanical blending process was also used to fabricate BST/PANI composite [6, 33] with different wt% (1–7 wt%) of BST pressed under pressure of about 1 GPa. Composites of BiCuSeO with sulfosalicylic acid-doped PANI was also prepared by ball milling followed by hot pressing [34]. Ao *et al* synthesized polythiophene (PTh)/bismuth telluride (Bi₂Te₃) nanocomposite with different weight percentage of PTh by mixing in an agate mortar and then sintering the composite samples applying spark plasma sintering technique [35]. Nanocomposites of PANI, multiwalled carbon nanotubes (MWCNTs) with binary metal selenide NPs (MSe NPs) have also been synthesized by solid mixing where are mixed with polymerized PANI by using a mortar and pestle [36].

2.4. Electrodeposition

Though electrodeposition technique is one of the convenient methods for the production of TE material in the form of film, it is not so much explored to synthesized polymer chalcogenides composites.

Chatterjee *et al* synthesized PANI-bismuth telluride nanocomposite using electrodeposition method [37]. Two solutions (solution A containing bismuth doped PANI and solution B containing equal volumes of bismuth nitrate solution and tellurium oxide solution) has been prepared. Solution B was added dropwise to solution A to ensure the incorporation of Bi₂Te₃ in PANI matrix. Since the deposition of bismuth telluride was much faster than that of PANI to prevent

the formation of bilayer solution B is added dropwise in solution A in this process. The electrochemical deposition process set up where three electrodes are aluminum foil as the anode, indium tin oxide as the cathode and a saturated calomel electrode as the reference electrode. To prepare a free-standing-coated PEDOT film, Ni *et al* used a free-standing PEDOT NW film as a working electrode rather than an electrolyte containing mixture solution of TeO_2 and H_2SO_4 in an ice bath using an electrochemical workstation. Ag/AgCl electrode as a reference electrode and a Pt foil as a counter electrode [17] as shown in figure 1(C). The obtained films were washed with water and ethanol and dried at 60 °C.

3. Thermoelectric (TE) properties of polymer/chalcogenide composite

The functionality of a TE material is evaluated from the figure of merit (ZT), as discussed in the introduction. In this segment we try to focus on the practical features of measuring the values of all the parameters to characterize the performance of polymer/chalcogenide composite TE materials for the desired application. Table 1 summarizes the TE properties of polymer-based chalcogenides.

As has been discussed earlier, the electrical conductivity, TE power and thermal conductivity contributes to the figure of merit of the TE materials. Talking to these parameters, it has been observed that different chalcogenide materials were used as filler in the polymer matrix so as to modify the σ , S or K values which in turn can affect the ZT. The general strategy is to vary the filler concentration in the polymer matrix.

3.1. Electrical conductivity and thermoelectric (TE) power

The origin of the electrical conductivity in case of CPs is due to doping which generates the charge carriers and the hopping of charge carriers along the polymer chains [38]. Reports are already present regarding the doping and dopant effects on the transport parameters of the polymers. Here we focus on the modification of the electrical conductivity and TE power by the introduction of chalcogenides as fillers.

PANI based chalcogenide composites are studied mostly in the recent past. The temperature variation of σ value for PANI/ Bi_2Te_3 nanocomposite shows a decrement [15] indicating a metallic behavior but is nonlinear and is also 1.5 times higher than that of PANI. This is due to the fact that the charge transport of PANI is connected with metallic conduction within the metal islands with a hopping or tunneling effect because of the insulating barriers. The combined effect of the carrier concentration and the higher degree of ordering of the chain packing of PANI is responsible for the high S value of the composites than its constituents. As a consequence of this ordered structure of PANI/ Bi_2Te_3 composite, the PF ($S^2\sigma$) is found to be more than its constituents above 380 K as shown in figure 2.

The temperature dependence of electrical conductivity of BiCuSeO/PANI (BCSO/PANI) bulk composites with different

amount of BCSO filler [34] also shows a decrement in the value. Moreover, with the increasing amount of filler the σ value also decreases in spite of high electrical conductivity value of BCSO ($\sim 50\,000\text{ S m}^{-1}$). The decrement nature may be due to the inhomogeneous interfacial states between the chalcogenide filler and the polymer matrix which in turn rise in interfacial resistance. The composite having 40 wt% of BiCuSeO has a maximum S value around $87\text{ }\mu\text{V K}^{-1}$ because of higher S value of BiCuSeO phase. The increment of S enhances the PF ($S^2\sigma$) to a highest value of $7\text{ }\mu\text{Wm}^{-1}\text{ K}^{-2}$ for 40 wt% composite. A comparison of the electrical conductivity has been done for PANI/Single walled carbon nanotube (SWCNT)/Te and PANI/Te nanocomposite [9]. The σ value for PANI/SWCNT/Te decreases with the increase in Te content in the PANI/SWCNT matrix whereas for PANI/Te nanocomposite, it increases slightly. A comparison of experimental and theoretical S values of the composites shows that the synergetic energy filtering effect at the interfaces of organic/inorganic nanocomposites, where the carriers having high energy were favorably allowed to cross the energy barrier at the interface which results in an enhancement in the S value [39, 40]. Further for the composites having one dimensional morphological filler, this effect is more pronounced [25]. Since both the single walled nanotubes (SWNTs) and Te nanorods possess a one-dimensional morphology, thus a synergetic energy filtering effect was observed for PANI/SWNT/Te and PANI/Te at the interfaces, which results in an increase in the S value [9]. A maximum PF for 10% Te content in the ternary composite was obtained. The electrical conductivity of PANI coated SnSe NSs [19] and PANI-coated SnS NSs [3A] increases initially till 350 K and then onwards decreases with temperature. The deposited PANI layer formed a highly conductive network in the PANI-SnSe or PANI-SnS composite structure and interestingly an increase in the σ value has been observed with the additional coating cycle of PANI content. This is attributed to the increase in the carrier concentration with the coating cycle of PANI. The S value of both DBSA doped PANI-coated $\text{SnSe}_{0.8}\text{S}_{0.2}$ (PANI-SnSeS)/PVDF composite [19] and DBSA doped PANI-coated porous SnS NSs (PANI-pSnS) composite [3A] shows a similar trend with the increase in temperature within the range 300 K–500 K. The PF of the PANI-SnSeS/PVDF composite reached a maximum value of $\sim 134\text{ }\mu\text{Wm K}^{-2}$ at 400 K. Interestingly with PANI coating the σ increases and S decreases for both the cases.

Figure 3 shows 2D PANI-bismuth selenide (PANI/ Bi_2Se_3) composite exhibiting a change in electrical conductivity which increases with temperature indicating a semiconducting behavior [18]. Though the electrical conductivity is low, due to high S value, the PF reached a maximum value from 1.08 to $29.32\text{ }\mu\text{Wm}^{-1}\text{ K}^{-2}$. Here also the energy filtering effects play a key role for the increase in S value. Probably the reduction of Mott temperature (T_0) reduces the carrier hopping distance and the hopping activation energy which leads to the increment of the electrical conductivity. Same trend has been observed for PANI/ Bi_2S_3 nanocomposite [1A] where conducting interfaces are formed between PANI and Bi_2S_3 nanoflowers thereby reducing the barrier distance at the interface

Table 1. Overview of TE properties of polymer based chalcogenide composites.

Composites	Synthesis method	n (cm ⁻³)	μ (cm ² (V S) ⁻¹)	σ (S cm ⁻¹)	S (μ V K ⁻¹)	$S^2\sigma$ (μ Wm ⁻¹ K ⁻²)	K (Wm ⁻¹ K ⁻¹)	ZT	Reference
PANI-Bi ₂ Te ₃	<i>In situ</i> polymerization	—	—	11.626	59	2.5	0.10	.004	[15]
CSA:PANI/BST NP (15%)	Mechanical mixing	2.93×10^{20}	0.15	6.5	54	1.78	0.45	16×10^{-4}	[6]
PANI-coated SnSeS NS/polyvinylidene difluoride (3:1 ratio)	<i>In situ</i> method	—	—	~10	~395	~134	—	—	[19]
PANI-coated porous SnS NSs at 450 K	<i>In situ</i> polymerization	—	—	—	—	—	—	0.078	[3A]
PANI-Bi ₂ Se ₃ (30 wt%) at 300 K	<i>In situ</i> polymerization	2.66×10^{18}	65.93	28.06	102.22	29.32	0.19	0.046	[18]
PANI-Bi ₂ Se ₃ (30 wt%) at 410 K				30.4	188.2	107.67	0.25	0.18	
PANI/Bi ₂ S ₃ at 353 K	Facile chemisorption route	—	—	21	~219	—	0.62	0.06	[1A]
PbTe-PANI composite at 373 K	<i>In situ</i> polymerization	—	—	0.022	578	0.757	—	—	[41]
Ag ₂ Te-PANI	<i>In situ</i> polymerization	—	—	0.043	251	—	0.387	2.09×10^{-4}	[42]
PANI/SWNT/Te	<i>In situ</i> synthesis	—	—	345	54	101	0.3	—	[9]
Ag ₂ Se	Mechanical mixing	—	—	0.29	65	12.5	0.31	0.012	[36]
NPs/MWCNT/PANI									
Te-PEDOT:PSS films mixed with 0.3 wt% of SSWNT	Solution mixing	—	—	139	118	206	—	—	[45]
PEDOT:PSS/BST composite	<i>In situ</i> polymerization	25×10^{19}	5	~155	~21	~9	0.26	~0.009	[12]
Bi ₂ Te ₃ /PEDOT:PSS composite (4.10 wt% of Bi ₂ Te ₃)	Solution mixing	—	—	1295.21	~20	~32.26	0.2	~0.05	[52]
SnSe _{0.97} Te _{0.03} NS/PEDOT:PSS composite	Solution mixing	2.15×10^{19}	7.9	27.2	90	14.73	—	—	[16]
PEDOT-coated SnSe _{0.97} Te _{0.03} NS/PEDOT:PSS composite (20% filler)	<i>In situ</i> method	1.08×10^{21}	1.9	~250	~76	—	0.38	0.18	[20]

(Continued.)

Table 1. (Continued.)

Composites	Synthesis method	n (cm ⁻³)	μ (cm ² (V S) ⁻¹)	σ (S cm ⁻¹)	S (μ V K ⁻¹)	$S^2\sigma$ (μ Wm ⁻¹ K ⁻²)	K (Wm ⁻¹ K ⁻¹)	ZT	Reference
PEDOT:PSS/PEDOT-SnSeTe NSs/PEDOT:PSS (PSP) multilayer film	Solution mixing	4.13×10^{20}	1.48	80	112	110	—	—	[22A]
Sn-Se-Te NSs/PEDOT:PSS composite (15% filler)	Solution mixing	—	—	~280	~60	~130.3	—	—	[21]
PEDOT-Te-s	Solution-processable method	—	—	~120	~122	222	—	—	[22B]
SnSe/PEDOT:PSS	Solution mixing	—	—	0.71 (± 0.10)	44.5 (± 6.7)	15.0	—	—	[27]
PEDOT:PSS/Se at 120 °C	<i>In situ</i> and vacuum-assisted filtration method	—	—	~1080	~121.8	~1603	~0.8	>0.6	[4]
PEDOT/Ag ₂ Se/CuAgSe	Electrode position	—	—	561.4	65.4	240.0	—	—	[17]
Te-coated PEDOT composite	Solution mixing	—	—	~660	~51.98	178.59	—	—	[11]
PEDOT:PSS/Ag ₂ Se (80% Ag ₂ Se)	Vacuum-assisted filtration method	—	—	122.4	51.6	51.4	0.156	0.076	[5]
PEDOT:PSS/Te	Solution mixing	—	—	0.2	40	5.49	0.2	0.013 ± 0.001	[62]
Te: (PEDOT:PSS)	<i>In situ</i> method	—	—	123.72	24.5	7.45	0.047	0.048	[51]
Bi ₂ Te ₃ -PEDOT:PSS (3% SDS, 10% EG)	Electropolymerization	—	—	900.3 \pm 20.5	43.4 \pm 0.6	169.8 \pm 7.8	—	—	[43]
PEDOT/Te/SWCNT	Solution mixing	—	—	—	220	84	—	—	[54]
PEDOT:PSS/Cu _{1.75} Te (14 mol% of Cu)	Solution mixing	2.026	—	~0.2	377	~2	0.28	2.8×10^{-3}	[28]
Te NWs/PMMA composites	Solution mixing	3.12 $\times 10^{19}$	—	5.12	~93	4.5	~0.3	0.005	[29]
Ag ₂ Te NW/PMMA nanocomposites (50% Ag ₂ Te)	Solution mixing	6.4 $\times 10^{18}$	48.8	0.51	~80	32.6	0.42	0.02	[57]

(Continued.)

Table 1. (Continued.)

Composites	Synthesis method	n (cm^{-3})	μ ($\text{cm}^2(\text{V S})^{-1}$)	σ (S cm^{-1})	S ($\mu\text{V K}^{-1}$)	$S^2\sigma$ ($\mu\text{Wm}^{-1}\text{K}^{-2}$)	K ($\text{Wm}^{-1}\text{K}^{-1}$)	ZT	Reference
Cu doped Bi_2Se_3 nanoplatelet/PVDF composite	Solution mixing	1.13×10^{19}	84.4	1.46×10^2	-84	103	0.32	0.10	[26]
PVP/Ag/Ag ₂ Te	Wet chemical method	—	—	360.9	-77.5	216.5	0.2–0.4	0.15–0.3	[30]
PVDF/Ta ₄ SiTe ₄ at 220 K	Chemical vapor transportation	—	—	~98	-325	1060	—	—	[61]
PTIn/bismuth telluride (Bi_2Te_3) nanocomposite (5 wt% PTh) at 473 K	Mechanical mixing	—	—	0.79	156	175	0.55	0.18	[35]
P3HT- Bi_2Te_3 nanocomposites (20% Bi_2Te_3)	Solution mixing	—	—	0.045	118	6.3	~0.86	—	[25]

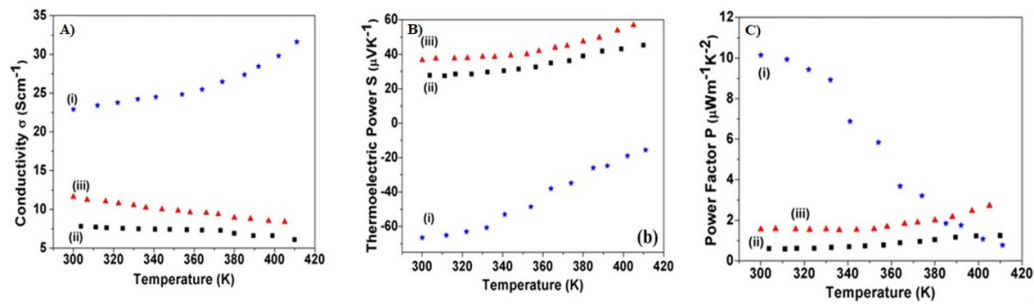


Figure 2. (A) Variation of the electrical conductivity with temperature of (i) Bi₂Te₃, (ii) PANI and (iii) PANI-Bi₂Te₃ nanocomposite. (B) Variation of the TE power with temperature of (i) Bi₂Te₃, (ii) PANI and (iii) PANI-Bi₂Te₃ nanocomposite and (C) variation of the PF with temperature of (i) Bi₂Te₃, (ii) PANI and (iii) PANI-Bi₂Te₃ nanocomposite. Reproduced from [15]. © IOP Publishing Ltd. All rights reserved.

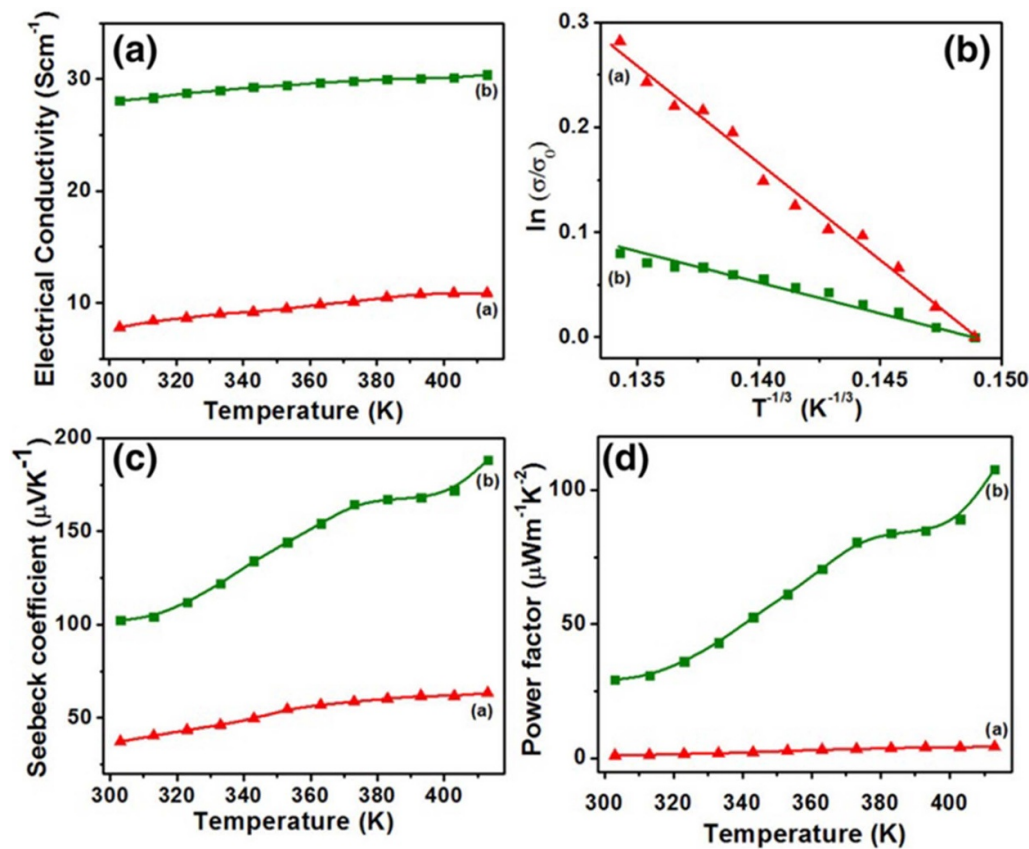


Figure 3. (a) Temperature dependence of electrical conductivity (σ), (b) plot of $\ln(\sigma/\sigma_0)$ versus $T^{-1/3}$, (c) Seebeck coefficient (S), (d) TE PF (P) of (a) PANI and (b) PANI-Bi₂Se₃ composite. [18]. John Wiley & Sons. Copyright (2018) Wiley Periodicals, Inc.

of the composite, resulting in the enhancement of the σ value. In addition to the increase in the σ value, the S value of the composite also increases. The S value though reduced with the inclusion of PANI in the composite system yet increases with temperature. Very slight increase in the σ value with the variation of temperature is also observed in case of PANI-PbTe nanocomposites though the increase is negligible with respect to the other PANI-chalcogenides composites [41]. A visible difference in the electrical conductivity is also shown in Ag₂Te-PANI core-shell composite (4.3 S m⁻¹) [42] with respect to pristine PANI. In PANI-PbTe composite and Ag₂Te-PANI composite due to interaction between PANI and NPs the

S value decreases with increasing temperature. An increase in the electrical conductivity of BST NPs embedded camphor sulfonic acid-doped PANI (CSA:PANI) with temperature has also been observed though at the same time there is a reduction in the σ value with the filler concentration [6].

The combined effect of decrease in carrier concentration and increase in mobility though decreases the σ but increases the S value. The maximum PF value of 1.78 $\mu\text{W m}^{-1} \text{K}^{-2}$ obtained at 400 K temperature for CSA:PANI composite with 15 wt% BST NP. But the PF value decreases with further increase of the BST NP up to 20 wt%, because of reduction in electrical conductivity of the composites. The decrease with

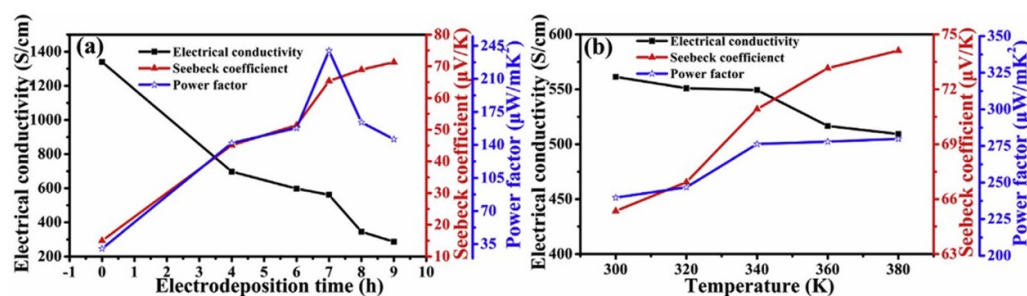


Figure 4. (a) TE performance of the Te-coated PEDOT films as a function of electrodeposition time. (b) Temperature dependence of the TE performance of the Te-coated PEDOT film electrodeposited for 7 h. Reprinted from [17]. Copyright (2019) The Chinese Ceramic Society. Production and hosting by Elsevier B.V.

the filler content is probably due to some unusual behavior between the polymer matrix and the filler agent. A series of ternary composites comprising PANI/MWCNT and metal selenides (viz CuSe, Ag₂Se, In₂Se₃, Sb₂Se₃) has been synthesized and compared [36]. It is observed that at room temperature the electrical conductivities of the samples are much higher. Further the σ value of the composites comprising of CuSe/MWCNT/PANI (CSCP) (4570 $S m^{-1}$) and Sb₂Se₃/MWCNT/PANI (SSCP) (4975 $S m^{-1}$) are more than the other two. This could be attributed to the formation of giant network within the hybrid enhancing the charge carrier mobility thereby increasing the electrical conductivity. It is noticed that the hybrid composites of Ag₂Se NPs/MWCNT/PANI (ASCP) showed p type behavior with positive S value and CuSe NPs/MWCNT/PANI (CSCP), In₂Se₃ NPs/MWCNT/PANI (ISCP), Sb₂Se₃ NPs/MWCNT/PANI (SSCP) composites showed n type character with negative S value. Due to the increase in charge carrier concentration, CSCP, ISCP and SSCP composites shows a lower value of S compare to the ASCP composite. The maximum value of S and further the value of PF for the ASCP composite are 65 $\mu V K^{-1}$ and 12.5 $\mu W m^{-1} K^{-2}$ respectively. In recent days, in the field of TE applications, PEDOT based chalcogenide composites attracts the attention over the PANI based chalcogenide composites due to its noticeable TE properties.

Figure 4 shows the electrical conductivity of Te-coated PEDOT films as a function of electrodeposition time and temperature which indicates that in both the cases the σ value of PEDOT-PSS/Te composites decreasing [17]. The temperature variation σ values indicate a metallic behavior or degenerate semiconductor transport behavior. With the variation of factionalized Te (PF-Te) content, σ of PEDOT-PSS/PF-Te also decreases [5]. Further with the increase of SWCNT content in PEDOT/Te/SWCNT composites a maximum σ value of $900.3 \pm 20.5 S cm^{-1}$ was obtained for 15% of Te and 50 wt% of SWCNT content due to the enhancement in the charge mobility in the composite [43]. On the other hand composite of reduce graphene oxide (rGO)/PEDOT:PSS/Te NWs depicts a huge increase in the σ value when treated with HI vapor [44]. A comparison of nanocarbon inclusion in PEDOT-PSS-Te composites shows that with the increase in nanocarbon the σ value increases much more for single bundled single-walled carbon nanotubes (SSWNTs) than for

graphene NPs (GNPs) which is due to the fact that the carrier concentration increases much more in case of SSWNT incorporated PEDOT-PSS-Te than that of GNP incorporated PEDOT-PSS-Te [45]. Te-coated PEDOT:PSS films shows an increasing tendency of S with respect to the electrodeposition time as well as temperature [17] which influence the maximum value of PF about $\sim 240.0 \mu W m^{-1} K^{-2}$. An enhanced S value is observed for PEDOT-PSS/PF-Te due to the energy filtering effect with the Te variation in the composite [5]. It is also observed that with an increase in nanocarbon content the S value of PEDOT/PSS/Te decreases. The PF of Te-coated PEDOT:PSS films is higher than the previous work on PEDOT:PSS/SWCNT/Te composites [42, 44] as well as PEDOT:PSS/Te composites [46]. The possible explanation of variations of σ and S in Te embedded polymer is due to the trend following the composite model which is a function of the polymer content and also the trend as a function of the length and diameter of the NW and electron-phonon scattering [46]. Though both being the probable explanations, yet the possible outcome from either explanation is that, longer is the NWs, larger will be the S value and lower will be the σ value. From an optimization viewpoint the high value of S is appealing. The σ of PEDOT/Bi₂Te₃ (100) hybrid films decreases greatly with the inclusion of Bi₂Te₃ as filler. Probably the interfacial transport is also responsible for such properties of the hybrid's films along with the simple mixed effect [47]. The energy barriers can be developed due to the energy filtering effect at the interfaces of organic-inorganic composites scattering low energy carriers [48–50], the relaxation time may depend on the energy and thus enhance the asymmetric carrier transport boosting up the S value [47]. For PEDOT-Bi₂Te₃ nano composites, the interfacial surface to volume ratio increases the sites of selective scattering thereby increasing the S . Further inclusion of Bi₂Te₃ NW within PEDOT:PSS dosed with 3% sodium dodecyl sulphate (SDS) and 10% EG increases the electrical conductivity from 0 to 1 wt% which is attributed to the free electron transfer from the n-type Bi₂Te₃ to the p type PEDOT:PSS. The chance of de doping of p-type PEDOT:PSS, due to the excess transfer of electrons, is dominated by the improvement of hole mobility thereby enhancing the electrical conductivity of the samples and also improved the S value (24.5 $\mu V K^{-1}$) which in turn enhance the PF (7.45 $\mu W m^{-1} K^{-2}$) of the composite [51]. The σ value of

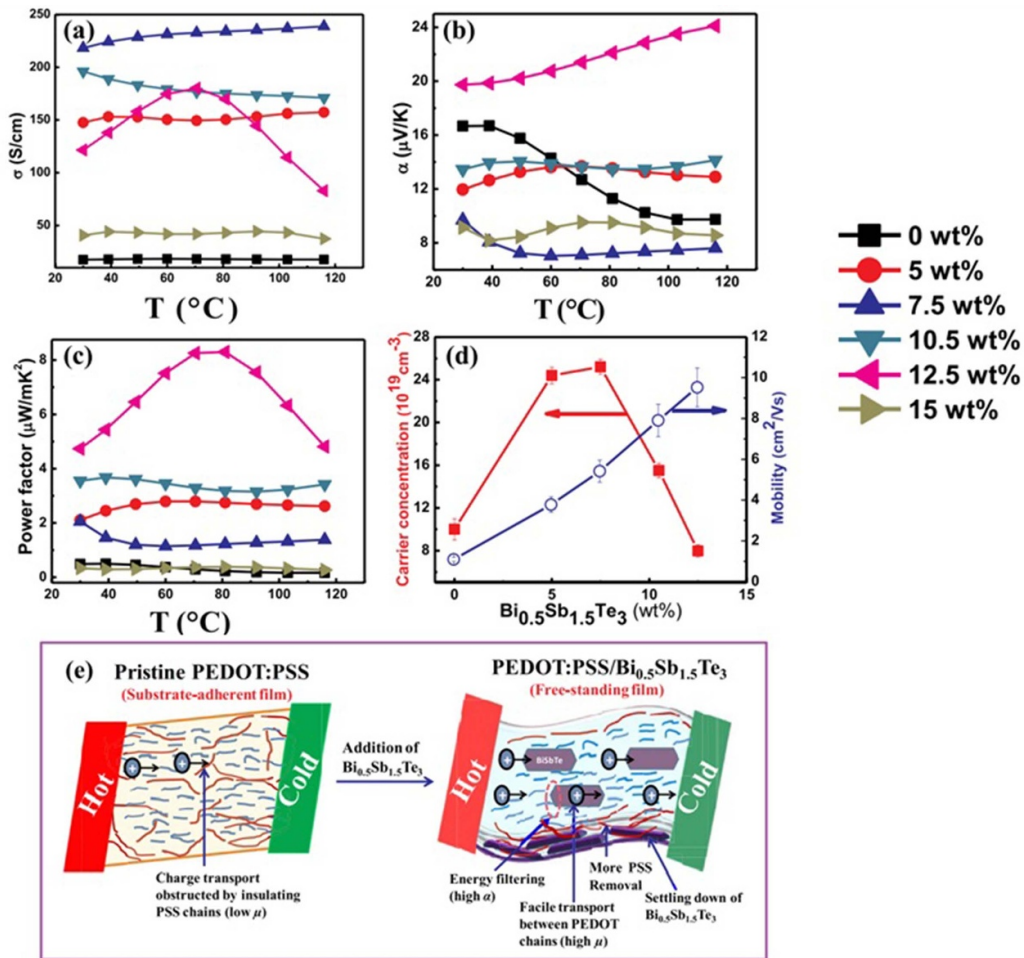


Figure 5. Temperature dependence of TE properties. (a) Electrical conductivity. (b) Seebeck coefficient. (c) Power factor (PF). (d) Hall data of carrier concentration and charge carrier mobility at room temperature. (e) Schematic revealing the proposed mechanism behind improved TE PF and peeling-off in case of the composite films. Reprinted from [12]. Copyright (2019) Elsevier B.V. All rights reserved.

PEDOT-PSS is improved by the inclusion of BST content and increases with the filler content (<10%) [12]. Also, there is a little change with temperature for the samples with filler content less than 10 wt%. But with an increase in BST to 12.5 wt% a huge variation in the σ value is observed compared to the other samples. With further increase in the filler content the nature remains same as the previous samples but with lower σ values as shown in figure 5.

The investigation of S value of PEDOT:PSS/BST NS composite exhibits a low variation with temperature. The highest S value obtained is $\sim 20 \mu\text{V K}^{-1}$ at 30°C having 12.5 wt% of BST in the composite which is due to the energy filtering reducing the carrier concentration as well as facile transport of charge carriers with a highest PF of $\sim 8 \mu\text{W m K}^{-2}$ at 70°C . But with exfoliated BST, a high σ value is obtained for PEDOT-PSS-BST samples than the previous one. This is attributed to the ordered molecular structure and the anisotropy and dispersion in parallel to the in-plane direction of the film [52]. The S value of the spin coated films are higher than that of the drop casted ones perhaps due to the rough surface for strong carrier scattering and quantum confinement effect [53]. Though the spin coated composite had highest S

value of $47.5 \mu\text{V K}^{-1}$ for the 9.65 wt% BST NSs containing composite, yet the PF for the drop casted ones is more than that of the spin coated ones and is attributed to the higher σ values [52]. Selenium NPs coated with PEDOT:PSS shows a greater electrical conductivity than PEDOT:PSS as well as synthesized Se powder which is further enhanced by annealing the samples maintaining the S value. Both the σ and S value decreases when annealed at a temperature of 200°C which is probably due to the degradation of the polymer [27]. Moreover, the σ value increases by the addition of excess PEDOT-PSS to these samples till 10% by weight thereby no further increase was achieved. Low electrical conductivity of Ag₂Se NWs effected the value of electrical conductivity of a Ag₂Se NW/PEDOT:PSS composite [11] by decreasing the conductivity value with increase in the Ag₂Se content. The S value initially decreases and then changes in sign at 50 wt% of the filler and then onwards increases further. The PF of the PEDOT:PSS/Ag₂Se NWs composite with 80 wt% inclusion of Ag₂Se NWs is $178.59 \mu\text{W m K}^{-2}$. The electrical conductivity of Li intercalated SnSe_{1-x}Te_x powders, Sn-Se-Te (x), PEDOT coated Te-s-SnSe NSs or alternate stacking of PEDOT-coated SnSe_{0.97}Te_{0.03} [16, 21, 22] with

Table 2. Carrier concentration and mobility values of $\text{SnSe}_{1-x}\text{Te}_x$ NS/PEDOT:PSS composite films with different Te contents. Reprinted from [16]. Copyright (2019) Elsevier B.V. All rights reserved.

Te content (atom. %)	n (cm^{-3})	μ (cm^2 (V s) $^{-1}$)
0	1.57×10^{19}	5.1
1	1.63×10^{19}	5.4
2	1.68×10^{19}	6.1
3	1.73×10^{19}	6.7
5	1.82×10^{19}	7.1
10	2.15×10^{19}	7.9

PEDOT/PSS were also studied. The fabricated $\text{SnSe}_{0.9}\text{Te}_{0.1}$ via intercalation of Li ions and exfoliation has a σ value of 12.8 S cm^{-1} for SnSe samples which increases for the $\text{SnSe}_{0.9}\text{Te}_{0.1}$ NS/PEDOT:PSS composite [16] up to maximum value of 27.2 S cm^{-1} with the variation of Te content. This modification in the composite is attributed to the carrier transport properties with variable amount of Te content in the composites as shown in the table 2 where it is observed that with the increase in the Te content there is an increase in the carrier concentration as well as in the carrier mobility thereby increasing the σ value.

But for Sn–Se–Te NSs/PEDOT:PSS composite films the σ value decreases with the increasing amount of filler content [21]. Same trend is also followed in PEDOT-coated $\text{SnSe}_{0.97}\text{Te}_{0.03}$ NS/PEDOT:PSS composites [20] where with different wt% of PEDOT-coated $\text{SnSe}_{0.97}\text{Te}_{0.03}$ NS as filler shows a reduction of the electrical conductivity of the composite with increasing filler content. The decrease in the carrier concentration is responsible for the above phenomena. A significant improvement shows in the σ value for a PEDOT:PSS/PEDOT-SnSeTe NSs/PEDOT:PSS (PSP) multilayer film which is higher than SnSeTe/PEDOT:PSS composite with the same amount of SnSeTe [22A]. For PEDOT-coated Te-s-SnSe NSs/PEDOT:PSS multilayer film a noticeable increment in the electrical conductivity is detected which is due to modified interchain interaction and hopping mechanism of charge carriers within the stretched PEDOT chain. The TE properties of a Sn–Se–Te NSs/PEDOT:PSS composite are investigated. From the investigation, it is observed that the S value increases due to the decrease in carrier concentration of Sn–Se–Te NSs/PEDOT:PSS. The maximum PF obtained is $\sim 130.3 \mu\text{Wm}^{-1} \text{ K}^{-2}$ which is higher than $\text{SnSe}_{0.97}\text{Te}_{0.03}$ NS/PEDOT:PSS composite ($14.73 \mu\text{Wm}^{-1} \text{ K}^{-2}$). Also, the S value shows an opposite trend with the previous composite. A PEDOT-coated $\text{SnSe}_{0.97}\text{Te}_{0.03}$ NS/PEDOT:PSS composite is prepared with the variation of PEDOT-coated $\text{SnSe}_{0.97}\text{Te}_{0.03}$ NS from 0 to 50 wt%. Among all the variation of composites, 20 wt% PEDOT-coated $\text{SnSe}_{0.97}\text{Te}_{0.03}$ NS content PEDOT-coated $\text{SnSe}_{0.97}\text{Te}_{0.03}$ NS/PEDOT:PSS composite shows a high value of S and σ value which improves the TE properties [20]. Multilayer strategies containing polymer and chalcogenides interlayers with polymer enhanced the TE properties of the multilayer composites. Ju *et al* reported that the PF of multilayer

film of PEDOT-coated Te-substituted SnSe NSs with three repeated stacking of PEDOT:PSS ($222 \mu\text{Wm}^{-1} \text{ K}^{-2}$) [22B] is high compare with a PSP multilayer film ($110 \mu\text{Wm}^{-1} \text{ K}^{-2}$) [22A]. For Te- $\text{Cu}_{1.75}\text{Te}$ /PEDOT:PSS NWs at room temperature it was observed that the σ decreases with copper loading. The σ values are measured from the NW mesh as a result the carrier transport at the interface between NWs should contribute in the σ values. The S values predicted from the standard medium theory lies generally in between the end point materials, but for Te- $\text{Cu}_{1.75}\text{Te}$ /PEDOT:PSS it has been observed that the S value ($220 \mu\text{V K}^{-1}$) exceeds the S value of the components ($\sim 190 \mu\text{V K}^{-1}$ for PEDOT:PSS-Te and $\sim 10 \mu\text{V K}^{-1}$ for PEDOT:PSS- $\text{Cu}_{1.75}\text{Te}$ at room temperature) [54]. This is attributed to the induction of additional charge carrier scattering during the formation of subphase. The maximum PF obtained for the sample is $84 \mu\text{Wm}^{-1} \text{ K}^{-2}$. A study of the Te/PEDOT:PSS/ Cu_7Te_4 ternary composite films, reveals that due to low electrical conductivity of PEDOT:PSS/Te (PC/Te) composite the σ value of Te/PEDOT:PSS/ Cu_7Te_4 ternary composite decreases whereas the S value increases with the increase in PC/Te percentage at room temperature [13]. The maximum PF obtained ($65.3 \mu\text{Wm}^{-1} \text{ K}^{-2}$) is less than that of Te- $\text{Cu}_{1.75}\text{Te}$ /PEDOT:PSS. The interface generated in a ternary composite fulfills the condition of energy filtering enhancing the TE properties [5]. The band structure of the interfacial band diagram of Te/PEDOT:PSS and Cu_7Te_4 /PEDOT:PSS is shown in figure 6 which in the present case is responsible for the energy filtering. Further temperature dependency of σ and S for $-\text{Cu}_7\text{Te}_4$ 95 wt% PC-Te composite film shows an increase in σ as well as S $25.3\text{--}42 \text{ S cm}^{-1}$. Thus, a maximum PF of $112.3 \mu\text{Wm}^{-1} \text{ K}^{-2}$ at 380 K is obtained. For PEDOT:PSS/ Cu_2Se NW composite with Cu/Se nominal molar ratio 3 manifests that σ value is reduced with increasing temperature till 360 K and then onwards a rapid increase is noticed till 418 K whereas the S value first increases till 340 K then decreases till 380 K thereafter increases slowly again as shown in figure 7.

Difference between cold pressed and hot pressed samples shows that for hot pressed samples the value of σ of PEDOT:PSS/ Cu_2Se decreases with temperature till 380 K and then increases markedly as temperature increases from 380 K to 420 K. Meanwhile the S value increases first till 400 K and then decreases rapidly above 400 K. The result indicates the phase transition from α -phase to the cubic β -phase in the temperature range 360 K–380 K. It was observed that the hot pressed PEDOT:PSS/ Cu_2Se NW composite on a flexible nylon membrane has a higher $S^2\sigma$ value ($820 \mu\text{Wm}^{-1} \text{ K}^{-2}$) [23] than cold pressed composites film ($270.3 \mu\text{Wm}^{-1} \text{ K}^{-2}$) [14]. Analyzing the structural characterization, it was observed that the chief transport channel is the Cu_2Se -based inorganic filler for the carriers in the CP-PC-3C1S film giving rise to a strong energy-filtering effect enhancing S . Since bulk Cu_2Se can exhibits higher S and lower σ than Cu_{2-x}Se [55, 56] thus a change phase from Cu_{2-x}Se to Cu_2Se causes a lower value of σ and higher value of S during hot pressing. In addition to the Cu_{2-x}Se /PEDOT:PSS, the presence of heterointerfaces of Cu_2Se /PEDOT:PSS and Cu/ Cu_2Se after hot pressing, is also responsible to enhance the energy-filtering effect, which

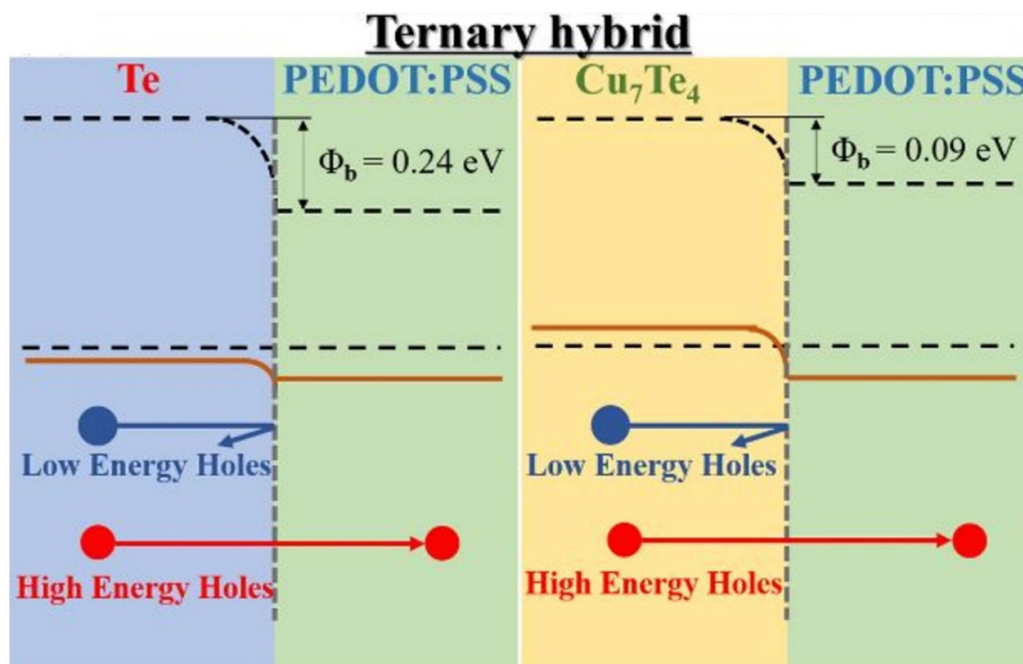


Figure 6. Band structure of the interfacial band diagram of Te/PEDOT:PSS and Cu_7Te_4 /PEDOT:PSS. Reprinted with permission from [13]. Copyright (2018) American Chemical Society.

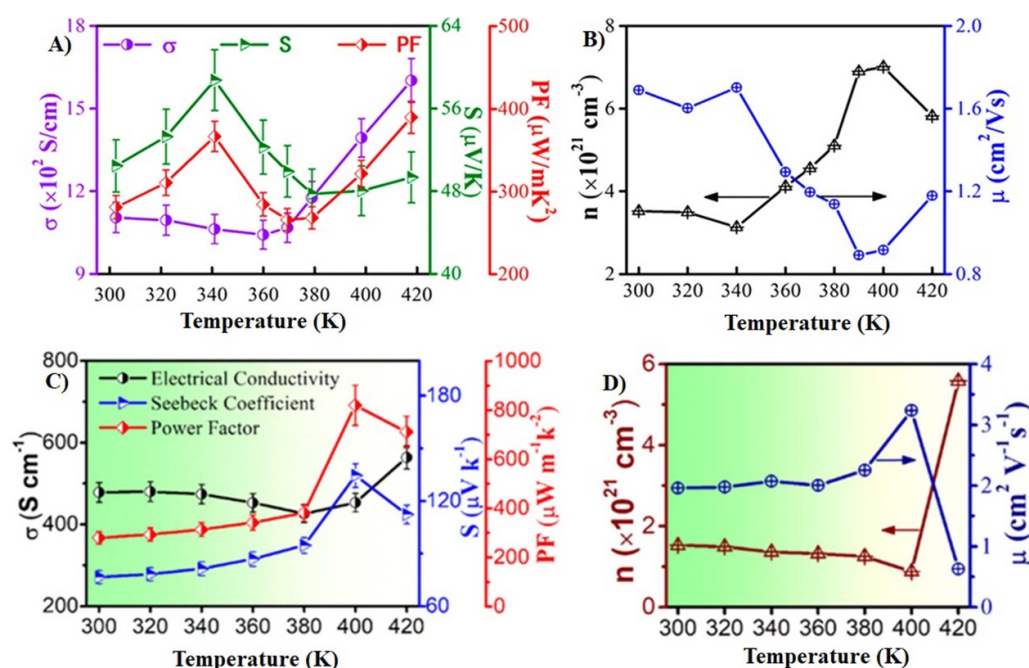


Figure 7. Temperature dependence of (A) electrical conductivity, Seebeck coefficient, and PF (B) carrier concentration and mobility for the PC- Cu_3Se_1 composite film. Reprinted with permission from [14]. Copyright (2019) American Chemical Society. (C) Temperature dependence of TE properties, and (D) n and mobility μ for the HP-PC-3C1S film. Reprinted with permission from [23]. Copyright (2021) American Chemical Society.

results a higher S value. But for PEDOT/ Ag_2Se / CuAgSe composite film with Cu:Ag:Se nominal molar ratio 1:4:3 an opposite trend is observed where σ increases initially up to 1244 S cm^{-1} till 380 K but rapidly decreases in the temperature range 380 K–400 K. For S , a turning point at around 320 K is observed probably due to the incorporation of PEDOT. Then

onwards it starts decreasing till 380 K and then again increases. The change around 380 K is again due to the phase change of α - to β - of Ag_2Se . But for very high value of σ and S the PF obtained is $\sim 1603 \mu\text{W m}^{-1} \text{ K}^{-2}$ [4] film at room temperature which is record value than the reported PEDOT:PSS/ Ag_2Se NWs composite ($178.59 \mu\text{W m}^{-1} \text{ K}^{-2}$) with 80 wt% inclusion

of Ag₂Se NWs [11] PVP/Ag/Ag₂Te (370.1 $\mu\text{Wm}^{-1}\text{K}^{-2}$ at 393 K) [30] and Te/PEDOT:PSS/Cu₇Te₄ nanocomposite (65.3 $\mu\text{Wm}^{-1}\text{K}^{-2}$) with 95 wt% PEDOT:PSS coated Te (PC-Te) nanorods content [13]. Reports show that the 3D oriented Te NWs/PMMA bead composites had greater electrical conductivity than the Te NWs/PMMA resin composites at a given Te content [28]. The greater amount of Te NWs in both the composite supply more charges (e.g. hole) which lead to increase in carrier concentration, and thus increases electrical conductivity of the samples. Similarly, because of high carrier concentration, the electrical conductivity of the Ag₂Te NW/PMMA nanocomposites increased up to 5.12 S cm⁻¹ with increasing Ag₂Te NWs content [29]. An effect of alignment of Te NWs on a PMMA polymer matrix improved the *S* value, PF as well as the figure of merit of the composite which in turn suitable for the application in TE devices. Kim *et al* achieved the high *S* value as well as PF in the PMMA/Te NWs composite with low Te NWs content. This result indicates that with high *S* value of Te NWs are well connected without interruption with the composite and also polymer matrix having no impact on the properties of Te NWs [28]. With the increase in Ag₂Te NW content the σ value increases but the *S* value decreases for Ag₂Te NW PMMA nanocomposites. The maximum PF obtained is for 50% Ag₂Te NW. Bi₂Se₃ NP/PVDF composites shows a low electrical conductivity at room temperature [57] than a single Bi₂Se₃ layer. Scattering of charge carriers by the polymer in between NP–NP junctions causes the reduction of σ . In spite of the scattering, the variation of σ of the composites shows a metallic behavior. But interestingly, when Cu doped Bi₂Se₃ incorporated in the Cu doped Bi₂Se₃/PVDF composite the conductivity is gradually increased from 0.49×10^4 S m⁻¹ to 1.46×10^4 S m⁻¹ with Cu concentration 0–0.1 in Cu_xBi₂Se [26]. Though the *S* value increases with temperature from low to room for Bi₂Se₃ NP/PVDF composites yet with the doping of Cu it decreases. Cu doped Bi₂Se₃ NPs/PVDF composite shows a multiphase n-type nature with large value in PF (103 $\mu\text{Wm}^{-1}\text{K}^{-2}$) [24] which is compared with the reported layered Bi₂Se₃ NP/PVDF composites (30 $\mu\text{Wm}^{-1}\text{K}^{-2}$) [57]. But with higher doping both the σ and the *S* values decreases which is probably due to the impurity phases (p-type Cu_{2-x}Se) during the NP [58–60]. A semiconducting behavior is noticed for PVP/Ag/Ag₂Te composite where the electrical conductivity increased from 360.9 to 540.6 S cm⁻¹ at temperature range from 300 K to 393 K which is due to the increase in carrier concentration. Interestingly both the *S* value and σ value increases with an increase in temperature for PVP/Ag/Ag₂Te composite. The rise in *S* value is attributed to the increase in the average energy of the electrons crossing the junction. Hence a rise in PF is observed [30]. But for 50 wt% Ta₄SiTe content PVDF/Ta₄SiTe₄ composite, the nature of electrical conductivity as a function of temperature shows a typical degenerate semiconducting behavior [61]. The composite exhibits a noticeable *S* and *S*² σ value. Study of PTh/Bi₂Te₃ composite shows that σ decreases with the increase in PTh content as because of decreased carrier concentration and carrier mobility but *S* increases for 5% PTh then onwards it decreases. A change in the nature of σ and *S* with the temperature variation is also observed with the PTh content [35].

To enhance the TE properties of different polymer-chalcogenide composites, the size and the structures of the inorganic chalcogenides component could play a very important role. As has been discussed earlier that the general strategy is to vary the nano filler concentration in the polymer matrix but reports showing the contribution of the size and morphology on TE properties are really scanty for polymer chalcogenides composites.

It has been observed that Te NW coated PEDOT:PSS hybrid composite has a highly conducting interface between Te NW and bulk polymer, which is responsible for the exclusive TE properties of the composite. Further with the increase in the length of the NW the *S* value increases but the σ value decreases. Thus, the production of long NWs could really enhance the PF [46]. Further nanorod like structure of Te also contribute to enhance the PF of the PEDOT:PSS/Te composite material [5, 45, 62] but as observed the optimized PF of the nanorod structured composite is lower than the Te NW coated PEDOT:PSS composite [46].

In case of synthesized Bi₂Te₃ nanorod/PANI composite, it is also observed PANI grown along the surface of Bi₂Te₃ nanorod different synthesis process shows different value of TE power. Longer the nanorods more is the TE power [15, 37]. Further the PF of Bi₂Te₃/PANI with rod like Bi₂Te₃ nanostructure [15] is higher than flakes like Bi₂Te₃ nanostructure [32]. A difference in the TE property was also observed for PEDOT:PSS when Ag₂Te nanocrystal [63] and Ag₂Te NW were used as the filler material [64] synthesized and characterized by Finefrock *et al* [63].

Thus a very few attempt has been made to study the effect of morphology of different fillers to improve the efficiency of polymer-chalcogenide composite materials indicating that there is a plenty of scope to further improve the TE properties of polymer chalcogenides composite.

3.2. Thermal conductivity and figure of merit

The thermal conductivity (κ) is the sum of electronic thermal contribution and the lattice thermal contribution. The general strategy to achieve a high ZT value for the TE materials, along with the increase in PF (*S*² σ), is to lower the value of κ . For two component organic inorganic nanocomposites, the lattice thermal contribution can be reduced by selective scattering of phonons at the grain boundaries thereby reducing the total thermal conductivity.

A low κ value is observed for Te embedded polymer (in the range of 0.2–0.4 Wm⁻¹ K⁻¹ for PANI-Te nanocomposites, from 0.1 to 1.6 Wm⁻¹ K⁻¹ for Te-coated PEDOT films, from 0.197 to 0.218 Wm⁻¹ K⁻¹ for PEDOT:PSS/PF-Te and from 0.24 to 0.29 Wm⁻¹ K⁻¹ for Te/PMMA nanocomposites) [5, 9, 17, 28] due to strong phonon scattering at polymer-Te interface. As a consequence, the ZT values of Te coated or embedded polymer evaluated or estimated is in the range of 0.05–0.8 [5, 9, 17], though the ZT value of Te NW/PMMA composites are much lower [28] than the other owing to the lower electrical conductivity.

Reports show that also with the inclusion of Bi_2Te_3 NPs in the polymer matrix, the κ value decreases. A room temperature κ shows a low value about $0.1096 \text{ W m}^{-1} \text{ K}^{-1}$ of a PANI- Bi_2Te_3 nanocomposite than its constituents [15]. Though an initial increase in κ value has been noticed for BCSO/PANI with increase in BCSO but it decreases with higher content of BCSO which is due to the phonon scattering again [34]. The ZT value is much less than PANI- Bi_2Te_3 nanocomposite. Further with the increase of filler like BST NP, the κ value decreases and around 20% filler composites κ is nearly equal to the pristine PANI [6]. The ZT value increases with the increase in temperature. The highest ZT value obtained is for 15% at room temperature. Though the reported κ value of PANI- Bi_2Se_3 composite is $0.19 \text{ W m}^{-1} \text{ K}^{-1}$ which is comparable to that of PANI- Bi_2Te_3 nanocomposite [18] yet the ZT value (0.0046) is higher than PANI- Bi_2Te_3 nanocomposite as well as its constituents. On the other hand, the κ value of PANI/ Bi_2S_3 nanocomposites was found to be more than PANI/ Bi_2Te_3 or PANI/ Bi_2Se_3 but the ZT value is comparable with PANI/ Bi_2Se_3 nanocomposites [1A]. The κ value of PANI- Ag_2Te core shell structure [42] is found to be more than PANI- Ag_2Se and the ZT value of later comes out to be 0.012 [36]. The temperature dependency of thermal conductivity and figure of merit (ZT) of two PANI coated PANI-pSnS NSs composites reveal that κ decreases and ZT increases with increase in temperature which is a similar trend for chalcogenide-based composites. For the two PANI coated PANI-pSnS NSs composites, the ZT value reached 0.078 at 450 K which is much higher than pristine pSnS NSs [3A].

For a PEDOT-coated $\text{SnSe}_{0.97}\text{Te}_{0.03}$ NS/PEDOT:PSS composites with 20% filler content the κ value is lower than $0.5 \text{ W m}^{-1} \text{ K}^{-1}$ and thus for 20% filler content, the composite achieved the maximum value of ZT about 0.18 [20]. Te/PEDOT:PSS/ Cu_7Te_4 composite shows a low thermal conductivity of $0.198 \text{ W m}^{-1} \text{ K}^{-1}$ with 95% PEDOT:PSS coated Te as a filler which is very close to a PEDOT:PSS/Te composite as reported [5] and finally achieved a maximum ZT value around 0.1 [13]. With Cu_2Se as filler, the κ value of PEDOT:PSS is in the range $0.25\text{--}0.3 \text{ W m}^{-1} \text{ K}^{-1}$ [14] which is lower than PEDOT:PSS- Ag_2Se / CuAgSe composite [4]. This value leads to a high ZT value 0.3 at room temperature compared with the reported Ag_2Te NW/PMMA nanocomposites [29] and PVP/Ag/ Ag_2Te /nylon film [30].

Bi_2Te_3 NW/PEDOT:PSS composite dosed with 3 wt% SDS and 10 vol% EG, influenced the thermal conductivity and finally the ZT value. The composite achieved the K and ZT value of $0.047 \text{ W m}^{-1} \text{ K}^{-1}$ and 0.048 respectively [51]. With almost same S value, it is observed that the 3D aligned Te NWs/PMMA composite shows a higher value in figure of merit (2.8×10^{-3}) than the randomly dispersed composite (6.4×10^{-4}) [28]. Insulating polymer PVDF based Bi_2Se_3 NP/PVDF composite, $\text{Cu}_{0.1}\text{Bi}_2\text{Se}_3$ NP/PVDF composite [26] and layered Bi_2Se_3 NP/PVDF composite [57] shows the K values $0.29 \text{ W m}^{-1} \text{ K}^{-1}$, $0.32 \text{ W m}^{-1} \text{ K}^{-1}$ and $0.42 \text{ W m}^{-1} \text{ K}^{-1}$ respectively. The calculated ZT value of $\text{Cu}_{0.1}\text{Bi}_2\text{Se}_3$ NP/PVDF composite (0.10) is higher than Bi_2Se_3 NP/PVDF composite (0.04).

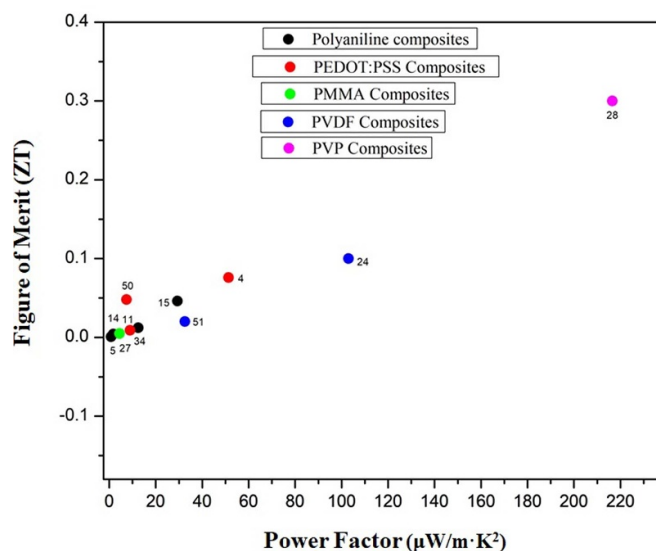


Figure 8. Figure of merit vs PF graph for various polymer chalcogenide composites.

It is well known that the K of the polymeric samples has a low value. The κ values of the polymer chalcogenides discussed here mostly lies in the range $0.1\text{--}0.4 \text{ W m}^{-1} \text{ K}^{-1}$ which is mainly due to scattering of phonons as discussed earlier.

So, the high ZT value is attributed to the high-PF of the samples. Thus, PF with ZT has been plotted for different samples and shown in figure 8. It is observed that the samples having high PF have high ZT values.

4. Device application

The research on TE aims to fabricate TE modules for device applications. Though inorganic TE materials generate higher output power, yet organic TE materials come into play in recent days, due to their advantages as discussed earlier. As a result, prototype thermoelectric generators (TEG) with polymeric-chalcogenides based materials are under process.

PVDF/ Ta_4SiTe_4 composite films were used to construct a TE module having four single legs. The performance of the module at $\Delta T = 9.2 \text{ K}$, 19.9 K , 30.1 K , and 35.5 K was conducted and it was observed that at $\Delta T = 35.5 \text{ K}$ a maximum output power of $1.68 \mu\text{W}$ is obtained [61]. Same was fabricated for PANI/SWNT/Te nanocomposite films with a 10 wt% Te content and the maximum output power attained is $1 \mu\text{W}$ with a power density of $62.4 \mu\text{W cm}^{-2}$ at $\Delta T = 40 \text{ K}$ [9]. The maximum power observed for a TEG fabricated with p-type PEDOT:PSS coated nylon and n-type air plasma treated Ag_2Te nanocrystal coated nylon was found to be 5 nW for a temperature difference of 20 K [63].

Based on PEDOT:PSS/PF-Te (70 wt%) composite material, a prototype TE power generator has been device as shown in the figure 9 using eight unit-legs of the composite having a dimension of $25 \times 5 \text{ mm}^2$ with Ag paste as an electrode on a polyimide substrate. The measured output voltage of the

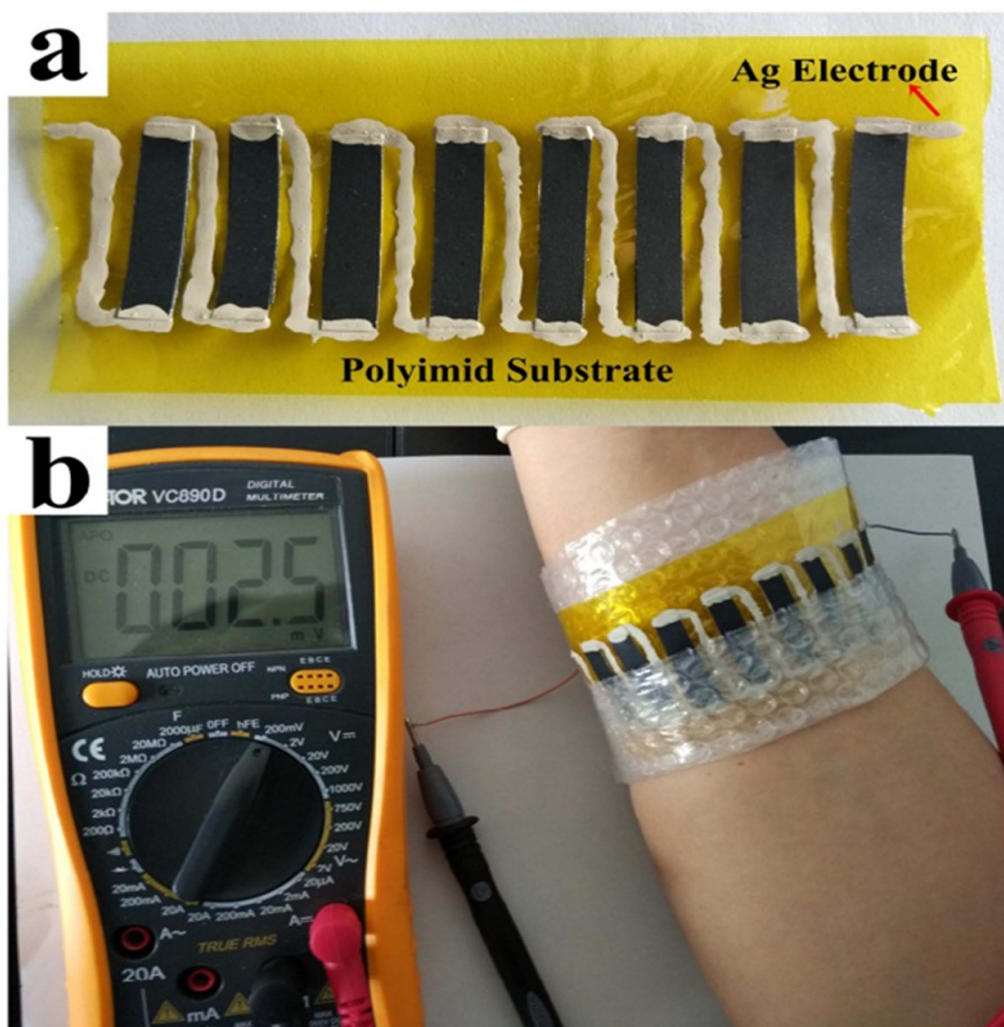


Figure 9. (a) Photograph of a flexible device consisting of eight (PEDOT:PSS/PF-Te)-Ag thermocouples on a polyimide substrate and (b) output performance of the device due to the temperature difference between a forearm (~ 305.4 K) and the ambient (~ 292 K). Reprinted from [5]. Copyright (2017) Published by Elsevier Ltd.

module is 2.5 mV with the temperature difference approximately 13.4 K which is a little lower than the calculated value. This difference is attributed to the resistance of the device. The output voltage of 14 legs TEGs devised on a glass substrates by spray printing of Te-PEDOT:PSS nanocomposites, GNP added Te-PEDOT:PSS, and SSWNT added Te-PEDOT:PSS are 26, 23, and 24 mV, respectively [45]. Though the output voltage of the Te-PEDOT:PSS content TEG is higher than SSWNT added Te-PEDOT:PSS, the output current is higher for SSWNT added Te-PEDOT:PSS content TEG ($20 \mu\text{A}$) than the TEGs comprising of Te-PEDOT:PSS without nanocarbon ($0.7 \mu\text{A}$) and Te-PEDOT:PSS with GNP ($1.2 \mu\text{A}$). Among these three TEGs, the one prepared from SSWNT added Te-PEDOT:PSS shows an improved output power of 126 nW. Further the TEG from SSWNT added Te-PEDOT:PSS is modified with 28 legs on flexible polyacrylate substrate and the generated voltage of 7.8 mV was determined from the thermal energy applied by the human body. With the temperature difference of 53°C , a single thermo-element device consist of PEDOT:PSS/BST film presented an open circuit voltage

$\sim 536 \mu\text{V}$ and current $\sim 134 \mu\text{A}$ [11]. Further a TE converter based on Bi_2Te_3 -PEDOT:PSS nanofilm network material exhibit an output power of $130 \mu\text{W}$ at temperature difference about 80 K with a good stability [51].

An eight single-leg flexible TE device was assembled figure 10 using PC- Cu_7Te_4 /PC-Te composite [13]. The output voltages of the optimized composite are observed to be 14.2, 21.4, 26.3 and 31.2 mV with a temperature difference of 18.2 K, 27.1 K, 31.4 K and 39.1 K respectively. The result shows, for the temperature gradient at 39.1 K, per 1 K temperature difference the output voltage of p-leg is about $103 \mu\text{V}$ which is comparably higher than the value $\sim 80.7 \mu\text{V}$ at 300 K. After twisting 70 times, the output voltage is decreased only 10% at the temperature gradient of 39.1 K, which indicates a good flexible nature of the TE device.

Figure 11 shows that a maximum output power of $\sim 94.7 \text{ nW}$ is generated with $\sim 1200 \Omega$ load resistance at 39.1 K temperature gradient. Whereas for a TE prototype device of nine legs prepared using PEDOT:PSS/ Cu_xSe_y nanocomposite [14], the obtain maximum output voltage and power is

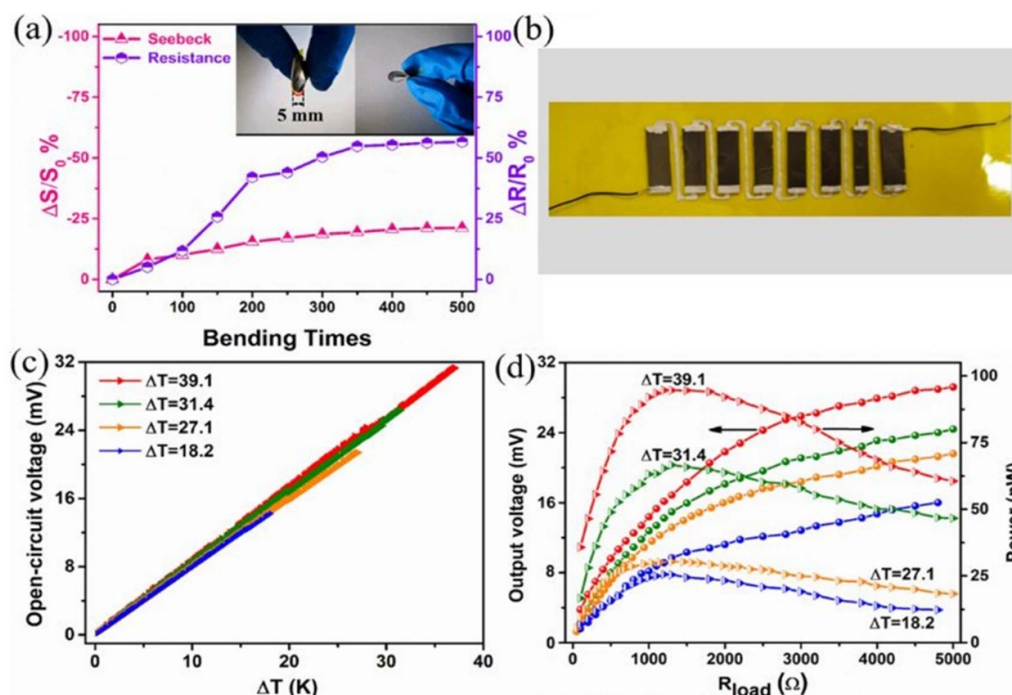


Figure 10. (a) Flexibility of the film. The change of the Seebeck coefficient and electrical resistance of the PC- Cu_7Te_4 /95 wt% PC-Te film drop-cast onto the polyimide substrate over different bending times with the insets exhibiting a bending test, where the bending diameter is 5 mm, (b) a digital photo of the TE device fabricated using the as-prepared film, (c) the relationship between output voltage and temperature difference, (d) output voltage and power as a function of load resistance at various temperature differences. Reprinted with permission from [13]. Copyright (2018) American Chemical Society.

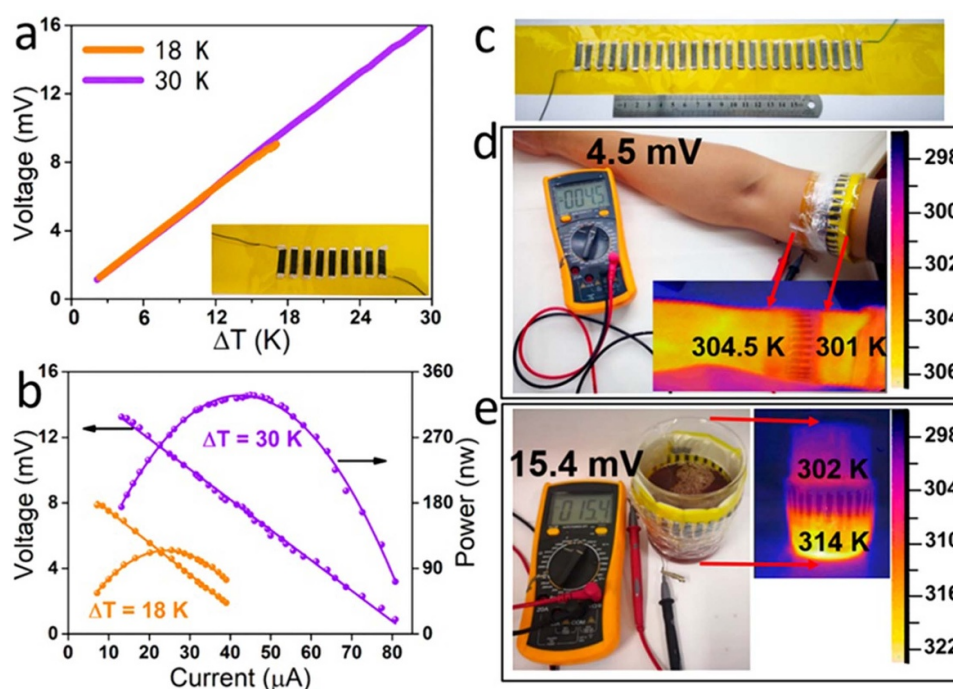


Figure 11. Performance of the TE device fabricated with the PC- Cu_3Se_1 composite film: (a) the relationship between output voltage and temperature gradient (the inset is a digital photo of the nine-leg TE device); (b) the output voltage and power versus current at different temperature differences. Demonstration of power generation by a 25-leg TE device: (c) a digital photo of the device, (d) a photo of 4.5 mV voltage created due to the temperature difference between an arm and the ambient, (e) a photo of 15.4 mV voltage created when the tea water was poured into the 500 ml beaker until the liquid level reached the lower edge of the device. The device is wound around the arm or the beaker; one side of the device was attached to an arm skin or the beaker, and the other side is exposed to the air by using a bubble film as a thermal insulator. The insets in parts (d) and (e) are infrared thermal images showing the temperature differences between the arm and the ambient (~ 3.5 K) and between the outer surface of the beaker and the ambient (~ 12 K), respectively. Reprinted with permission from [14]. Copyright (2019) American Chemical Society.

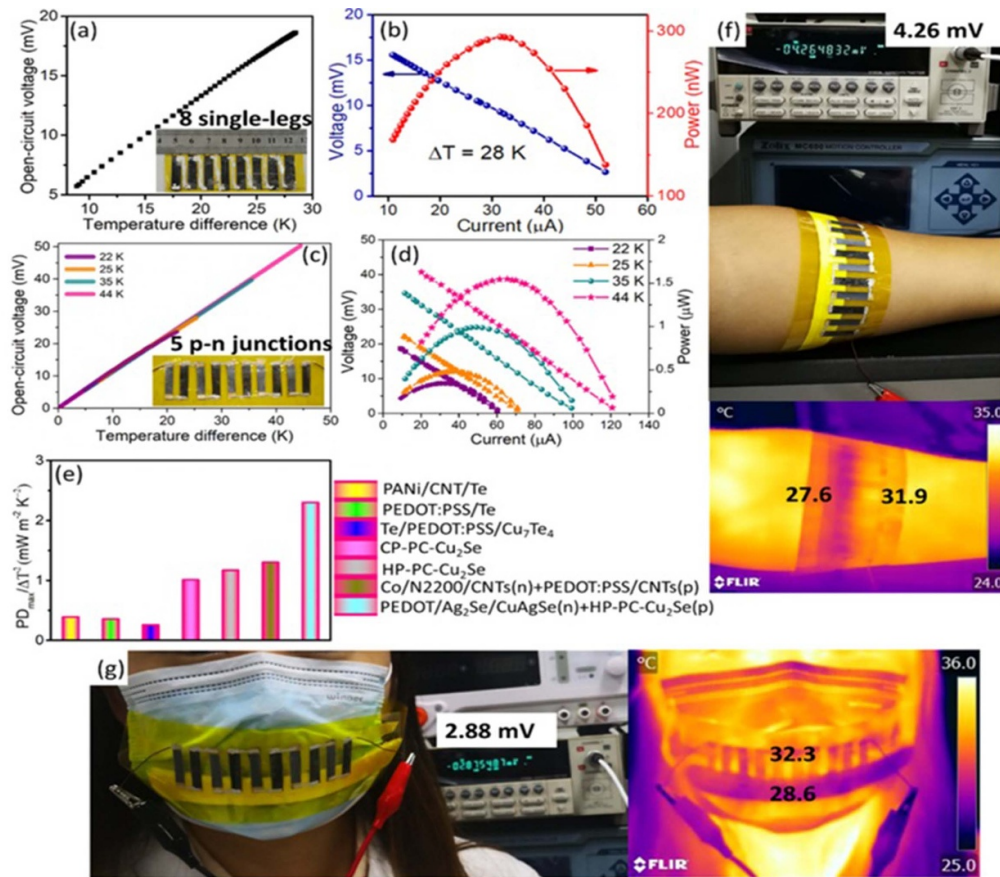


Figure 12. Output performance of the f-TEG assembled with the HP-PC-3C1S film on nylon. (a) Open-circuit voltage at various ΔT values (the inset shows a photograph of the TE prototype generator). (b) Output voltage (U) and output power (P) versus current (I) at ΔT of 28 K. Output performance of the 5 p-n units f-TEG assembled with the HP-PC-3C1S film and the PEDOT/Ag₂Se/CuAgSe composite film. (c) Open-circuit voltage at various ΔT values (the inset shows a photograph of the TE prototype generator). (d) U and P versus I at different ΔT values. (e) Comparison of $PD_{\max}/\Delta T^2$ between our f-TEG and reported ones assembled by inorganic/organic composites. (f) Photo of 4.26 mV voltage produced from the ΔT between an arm and the ambient; the temperature difference is shown in an infrared thermal image (~ 4.3 K). (g) Photo of 2.88 mV voltage created from the ΔT between wearing a mask and the ambient; the temperature difference is shown in an infrared thermal image (the maximum $\Delta T \sim 3.7$ K). Reprinted with permission from [23]. Copyright (2021) American Chemical Society.

16 mV and ~ 328 nW respectively at ΔT of 30 K. Further this is modified by increasing the number of legs to 25 and the voltage developed is measured between human arm or a beaker containing tea and the ambient. An output voltage of 4.5 mV with a temperature difference of 3.5 K is observed for the first case and output voltage of 15.4 mV with a temperature difference of 12 K is observed for the second one. A n-type TE module consists of 11 legs of (PEDOT)/Ag₂Se/CuAgSe ternary composite (PC-Cu₁Ag₄Se₃) [4] was also fabricated. At the temperature difference (DT) of 36 K, TE module produced its maximum output voltage, power and power density of 45.8 mV, 3.212 mW, 8.4 W m^{-2} respectively, which are higher than previously reported n-type nylon membrane supported PVP/Ag/Ag₂Te hybrid films-based TE prototype device [30]. Recently a flexible TEG (f-TEG) has been fabricated by pairing p-type hot pressed PEDOT:PSS/Cu₂Se-based composite (HP-PC-3C1S) with n-type PC-Cu₁Ag₄Se₃ composite [23]. The open circuit voltage (V_{oc}) for a p-n junction f-TEG is expressed by $V_{oc} = n \times (|S_n| + S_p) \times \Delta T$, where

n is the number of p-n units, S_n and S_p is the Seebeck coefficients of n-type and p-type component and ΔT is the temperature difference. Using the above expression, they calculated the V_{oc} value of 22, 25, 35, and 44 mV when ΔT is 22, 25, 35, and 44 K, respectively for the f-TEG. At 44 K temperature difference, the p-n junction f-TEG shows the maximum output power and power density of 1548.1 nW and $\sim 4.43 \text{ W m}^{-2}$ respectively, which indicating an enhanced output performance. One side of the assembled p-n junction f-TEG is attached to an arm and other side is in air using an air-laid paper as a thermal insulator as shown in figure 12.

The output voltage observed is 4.26 mV with the temperature difference ~ 4.3 K between a forearm and air. Similarly, pasting the f-TEG on a surgical mask [23], an output voltage of 2.88 mV is produced with the maximum ΔT of 3.7 K between the hot side and the ambient during exhalation.

All the results demonstrate a promising technique to create a flexible TE film with high TE performance for practical applications in wearable energy harvesting.

5. Conclusion

The development of CPs as functional TE materials finds huge applications in the domain of TEs. This class of materials combined with inorganics counterparts, mainly inorganic chalcogenides, shows promising results in the direction of TE industries. Out of the known methods of synthesis it has been observed that *in-situ* polymerization and solution mixing are the most commonly used procedures employed for the synthesis of these composites. The strategic approach taken for enhancing the TE parameters is to use the chalcogenides materials as nano filler within the polymer matrix. This can introduce a higher ordering of the polymer chains thereby increasing the electrical mobility of the charge carriers which increases the electrical conductivity. Further due to the introduction of the nano-interfaces of organic/inorganic nanocomposites there is a synergetic energy filtering effect where the carriers having high energy were favorably allowed to cross the energy barrier at the interface which results in an enhancement in the S value. At the same time these interfaces for two component organic inorganic nanocomposites, the lattice thermal contribution can be reduced by selective scattering of phonons at the grain boundaries thereby reducing the total thermal conductivity. All these factors really influence the figure of merit thereby increases it. Further, there is plenty of scope to study the effect of different nanostructures of a particular filler on the TE properties of polymer chalcogenides composites for optimization for the best candidate. Moreover, the development of the lab-based models using these composites opens up new directions of research in TE field and is found to be advantageous. Certainly, the polymer chalcogenides are so distinctive that they well thought out to be extremely capable and hopeful TE candidates. Further ease of synthesis and mechanical flexibility of those materials permits various design to be used in device applications. The inimitability of these materials undoubtedly opens up a new era of smart materials with the initiation of opportunities in TE domain.

Data availability statement

No new data were created or analyzed in this study.

Acknowledgments

One of the authors, Shilpa Maity acknowledges the Department of Science and Technology, Government of India for financial support vide Reference No. DST/WOS-A/PM-73/2019 under Women Scientist Scheme to carry out this study.

ORCID iDs

Sukhen Das  <https://orcid.org/0000-0001-8372-3076>
 Krishanu Chatterjee  <https://orcid.org/0000-0001-6400-3110>

References

- [1] (A) Sharma S, Singh H H, Kumar S and Khare N 2021 PANI coupled hierarchical Bi_2S_3 nanoflowers based hybrid nanocomposite for enhanced thermoelectric performance *Nanotechnology* **32** 335705; (B) Zhang Y, Zhang Q and Chen G 2020 Carbon and carbon composites for thermoelectric applications *Carbon Energy* **2** 408–36; (C) Yao C-J, Zhang H-L and Zhang Q 2019 Recent progress in thermoelectric materials based on conjugated polymers *Polymers* **11** 107
- [2] Wu J, Sun Y, Pei W-B, Huang L, Xu W and Zhang Q 2014 Polypyrrole nanotube film for flexible thermoelectric application *Synth. Met.* **196** 173–7
- [3] (A) Ju H, Park D and Kim J 2018 Fabrication of porous SnS nanosheets and their combination with conductive polymer for hybrid thermoelectric application *Chem. Eng. J.* **356** 950–4; (B) Wu J, Sun Y, Xu W and Zhang Q 2014 Investigating thermoelectric properties of doped polyaniline nanowires *Synth. Met.* **189** 177–182
- [4] Lu Y, Qiu Y, Cai K, Li X, Gao M, Jiang C and He J 2014 Ultrahigh performance PEDOT/Ag₂Se/CuAgSe composite film for wearable thermoelectric power generators *Mater. Today Phys.* **14** 100223
- [5] Song H and Cai K 2017 Preparation and properties of PEDOT:PSS/Te nanorod composite films for flexible thermoelectric power generator *Energy* **125** 519–25
- [6] Guo C, Chu F, Chen P, Zhu J, Wang H, Wang L, Fan Y and Jiang W 2018 Effectively enhanced thermopower in polyaniline/ $\text{Bi}_{0.5}\text{Sb}_{1.5}\text{Te}_3$ nanoplate composites via carrier energy scattering *J. Mater. Sci.* **53** 6752–62
- [7] Yan H *et al* 2016 Hybrid metal–organic chalcogenide nanowires with electrically conductive inorganic core through diamonded-directed assembly *Nat. Mater.* **16** 349–55
- [8] Sun Y, Li Y, Jin Y, Li Z and Xu W 2021 MINIREVIEW: crystalline organic metal chalcogenides for thermoelectric conversion *Compos. Commun.* **27** 100901
- [9] Wang L, Yao Q, Shi W, Qu S and Chen L 2017 Engineering carrier scattering at the interfaces in polyaniline-based nanocomposites for high thermoelectric performances *Mater. Chem. Front.* **1** 741–8
- [10] Liu D, Yan Z, Zhao Y, Zhang Z, Zhen Y, Zhang B, Shi P and Xue C 2021 Facile MWCNTs–SnSe/PEDOT:PSS ternary composite flexible thermoelectric films optimized by cold-pressing *J. Mater. Res. Technol.* **15** 4452–60
- [11] Park D, Kim M and Kim J 2020 Fabrication of PEDOT:PSS/Ag₂Se nanowires for polymer-based thermoelectric applications *Polymers* **12** 2932
- [12] Bharti M *et al* 2019 Boosting thermoelectric power factor of free-standing poly(3,4 ethylenedioxythiophene): poly(styrenesulphonate) films by incorporation of bismuth antimony telluride nanostructures *J. Power Sources* **435** 226758
- [13] Lu Y, Qiu Y, Jiang Q, Cai K, Du Y, Song H, Gao M, Huang C, He J and Hu D 2018 Preparation and characterization of Te/PEDOT:PSS/Cu₇Te₄ ternary composite films for flexible thermoelectric power generator *ACS Appl. Mater. Interfaces* **49** 42310–9
- [14] Lu Y, Ding Y, Qiu Y, Cai K, Yao Q, Song H, Tong L, He J and Chen L 2019 Good performance and flexible PEDOT:PSS/Cu₂Se nanowire thermoelectric composite films *ACS Appl. Mater. Interfaces* **11** 12819–29
- [15] Chatterjee K, Mitra M, Kargupta K, Ganguly S and Banerjee D 2013 Synthesis, characterization and enhanced thermoelectric performance of structurally ordered cable-like novel polyaniline–bismuth telluride nanocomposite *Nanotechnology* **24** 215703

- [16] Ju H, Park D, Kim K and Kim J 2019 Chemical exfoliation of $\text{SnSe}_{1-x}\text{Te}_x$ nanosheets with conductive PEDOT:PSS for flexible thermoelectric composite films *J. Alloys Compd.* **792** 638–43
- [17] Ni D, Song H, Chen Y and Cai K 2020 Significantly enhanced thermoelectric performance of flexible PEDOT nanowire film via coating Te nanostructures *J. Mater.* **6** 364–70
- [18] Mitra M, Kulsi C, Kargupta K, Ganguly S and Banerjee D 2018 Composite of polyaniline-bismuth selenide with enhanced thermoelectric performance *J. Appl. Polym. Sci.* **135** 46887
- [19] Ju H, Park D and Kim J 2018 Fabrication of polyaniline-coated SnSeS nanosheet/polyvinylidene difluoride composites by a solution-based process and optimization for flexible thermoelectric *ACS Appl. Mater. Interfaces* **10** 11920–5
- [20] Ju H, Park D and Kim J 2019 Effect of polymer nanolayer in tin-chalcogenide nanosheet/conductive polymer flexible composite films and their enhanced thermoelectric performance *Nanoscale* **11** 8502–9
- [21] Ju H, Park D, Kim K and Kim J 2019 Exfoliated Sn-Se-Te based nanosheets and their flexible thermoelectric composites with poly(3,4-ethylenedioxythiophene): poly(styrenesulfonate) fabricated by solution processing *Org. Electron.* **71** 131–5
- [22] (A) Ju H and Kim J 2019 Transparent and hybrid multilayer films with improved thermoelectric performance by chalcogenide-interlayer-induced transport enhancement *ACS Appl. Mater. Interfaces* **11** 35354–61; (B) Ju H, Park D and Kim J 2019 Thermoelectric enhancement in multilayer thin-films of tin chalcogenide nanosheets/conductive polymer *Nanoscale* **11** 16114–21
- [23] Lu Y, Li X, Cai K, Gao M, Zhao W, He J and Wei P 2021 Enhanced-performance PEDOT:PSS/ Cu_2Se -based composite films for wearable thermoelectric power generators *ACS Appl. Mater. Interfaces* **13** 631–8
- [24] Song H, Liu C, Zhu H, Kong F, Lu B, Xu J, Wang J and Zhao F 2013 Improved thermoelectric performance of free-standing PEDOT:PSS/ Bi_2Te_3 films with low thermal conductivity *J. Electron. Mater.* **42** 1268–74
- [25] He M, Ge J, Lin Z, Feng X, Wang X, Lu H, Yang Y and Qiu F 2012 Thermopower enhancement in conducting polymer nanocomposites via carrier energy scattering at the organic–inorganic semiconductor interface *Energy Environ. Sci.* **5** 8351
- [26] Dun C, Hewitt C A, Huang H, Xu J, Zhou C, Huang W, Cui Y, Zhou W, Jiang Q and Carroll D L 2015 Flexible n-type thermoelectric films based on Cu-doped Bi_2Se_3 nanoplate and polyvinylidene fluoride composite with decoupled Seebeck coefficient and electrical conductivity *Nano Energy* **18** 306–14
- [27] Kim C, Hong J and Park J W 2019 Synthesis and thermoelectric properties of selenium nanoparticles coated with PEDOT:PSS *Polymers* **11** 1052
- [28] Kim S *et al* 2017 Synthesis and thermoelectric characterization of bulk type tellurium nanowire/polymer nanocomposite *J. Mater. Sci.* **52** 12724–33
- [29] Kim S, Ryu S H, Kwon Y T, Lim Y R, Park K R, Song Y and Choa Y H 2017 Synthesis and thermoelectric characterization of high density Ag_2Te nanowire/PMMA nanocomposites *Mater. Chem. Phys.* **190** 187–93
- [30] Meng Q, Qiu Y, Cai K, Ding Y, Wang M, Pu H, Yao Q, Chen L and He J 2019 High performance and flexible polyvinylpyrrolidone/ $\text{Ag}/\text{Ag}_2\text{Te}$ ternary composite film for thermoelectric power generator *ACS Appl. Mater. Interfaces* **11** 33254–62
- [31] Wei K and Nolas G S 2018 Enhanced thermoelectric properties of polymer/inorganic bulk composites through EG treatment and spark plasma sintering processing *Scr. Mater.* **150** 70–73
- [32] Li Y, Zhao Q, Wang Y G and Bi K 2011 Synthesis and characterization of Bi_2Te_3 /polyaniline composites *Mater. Sci. Semicond. Process.* **14** 219–22
- [33] Zhao X B, Hu S H, Zhao M J and Zhu T J 2002 Thermoelectric properties of $\text{Bi}_{0.5}\text{Sb}_{1.5}\text{Te}_3$ /polyaniline hybrids prepared by mechanical blending *Mater. Lett.* **52** 147–9
- [34] Zheng B, Liu Y, Zhan B, Lin Y, Lan J and Yang X 2014 Enhanced thermoelectric properties of BiCuSeO /polyaniline composites *J. Electron. Mater.* **43** 3695–700
- [35] Ao W Q, Wang L, Li J Q, Pan F and Wu C N 2011 Synthesis and characterization of polythiophene/ Bi_2Te_3 nanocomposite thermoelectric material *J. Electron. Mater.* **40** 2027–32
- [36] Kshirsagar A S, Hiragond C, Dey A, More P V and Khanna P K 2019 Band engineered I/III/V–VI binary metal selenide/MWCNT/PANI nanocomposites for potential room temperature thermoelectric applications *ACS Appl. Energy Mater.* **2** 2680–91
- [37] Chatterjee K, Suresh A, Ganguly S, Kargupta K and Banerjee D 2009 Synthesis and characterization of an electro-deposited polyaniline-bismuth telluride nanocomposite—a novel thermoelectric material *Mater. Charact.* **60** 1597–601
- [38] Wang Y, Zhang S M and Deng Y 2016 Flexible low-grade energy utilization devices based on high-performance thermoelectric polyaniline/tellurium nanorod hybrid films *J. Mater. Chem. A* **4** 3554–9
- [39] Meng C Z, Liu C H and Fan S S 2010 A promising approach to enhanced thermoelectric properties using carbon nanotube networks *Adv. Mater.* **22** 535
- [40] See K C, Feser J P, Chen C E, Majumdar A, Urban J J and Segalman R A 2010 Water-processable polymer-nanocrystal hybrids for thermoelectric *Nano Lett.* **10** 4664
- [41] Wang Y Y, Cai K F, Yin J L, An B J, Du Y and Yao X 2011 *In situ* fabrication and thermoelectric properties of PbTe -polyaniline composite nanostructures *J. Nanopart. Res.* **13** 533–9
- [42] Wang Y Y, Cai K F, Yin J L, Dua Y and Yao X 2012 One-pot fabrication and thermoelectric properties of Ag_2Te -polyaniline core-shell nanostructures *Mater. Chem. Phys.* **133** 808–12
- [43] Yin S, Lu W, Wu R, Fan W, Guo C Y and Chen G 2020 Poly(3,4-ethylenedioxythiophene)/ Te /single-walled carbon nanotube composites with high thermoelectric performance promoted by electropolymerization *ACS Appl. Mater. Interfaces* **12** 3547–53
- [44] Choi J, Lee J Y, Lee S S, Park C R and Kim H 2016 High-performance thermoelectric paper based on double carrier-filtering processes at nanowire heterojunctions *Adv. Energy Mater.* **6** 1502181
- [45] Bae E J, Kang Y H, Lee C and Cho S Y 2017 Engineered nanocarbon mixing for enhancing thermoelectric properties of telluride-PEDOT:PSS nanocomposite *J. Mater. Chem. A* **5** 17867–73
- [46] Yee S K, Coates N E, Majumdar A, Urban J J and Segalman R A 2013 Thermoelectric power factor optimization in PEDOT:PSS tellurium nanowire hybrid composites *Phys. Chem. Chem. Phys.* **15** 4024
- [47] Wang L, Zhang Z, Liu Y, Wang B, Fang L, Qiu J, Zhang K and Wang S 2018 Exceptional thermoelectric properties of flexible organic–inorganic hybrids with monodispersed and periodic nanophase *Nat. Commun.* **9** 3817
- [48] Nunna R *et al* 2017 Ultrahigh thermoelectric performance in Cu_2Se -based hybrid materials with highly dispersed molecular CNTs *Energy Environ. Sci.* **10** 1928–35

- [49] Zhang T, Li K, Li C, Ma S, Hng H H and Wei L 2017 Mechanically durable and flexible thermoelectric films from PEDOT:PSS/PVA/Bi_{0.5}Sb_{1.5}Te₃ nanocomposites *Adv. Electron. Mater.* **3** 1600554
- [50] He M, Qiua F and Lin Z 2013 Towards high-performance polymer-based thermoelectric materials *Energy Environ. Sci.* **6** 1352–61
- [51] Thongkham W, Lertsatitthanakorn C, Jiramitmongkon K, Tantisanisom K, Boonkoom T, Jitpukdee M, Sinthiptharakoon K, Klamchuen A, Liangruksa M and Khanchaitit P 2019 Self-assembled three-dimensional Bi₂Te₃ nanowire–PEDOT:PSS hybrid nanofilm network for ubiquitous thermoelectrics *ACS Appl. Mater. Interfaces* **11** 6624–33
- [52] Du Y, Cai K F, Chen S, Cizek P and Lin T 2014 Facile preparation and thermoelectric properties of Bi₂Te₃ based alloy nanosheet/PEDOT:PSS composite films *ACS Appl. Mater. Interfaces* **6** 5735–43
- [53] Dresselhaus M S, Chen G, Tang M Y, Yang R, Lee H, Wang D, Ren Z, Fleurial J P and Gogna P 2007 New directions for low-dimensional thermoelectric materials *Adv. Mater.* **19** 1043–53
- [54] Zaia E W, Sahu A, Zhou P, Gordon M P, Forster J D, Aloni S, Liu Y S, Guo J and Urban J J 2016 Carrier scattering at alloy nanointerfaces enhances power factor in PEDOT:PSS hybrid thermoelectric *Nano Lett.* **5** 3352–9
- [55] Byeon D *et al* 2019 Discovery of colossal Seebeck effect in metallic Cu₂Se *Nat. Commun.* **10** 72
- [56] Sun Y, Xi L, Yang J, Wu L, Shi X, Chen L, Snyder J, Yange J and Zhang W 2017 The ‘electron crystal’ behavior in copper chalcogenides Cu₂X (X = Se, S) *J. Mater. Chem. A* **5** 5098–105
- [57] Dun C, Hewitt C A, Huang H, Xu J, Montgomery D S, Nie W, Jiang Q and Carroll D L 2015 Layered Bi₂Se₃ nanoplate/polyvinylidene fluoride composite based n-type thermoelectric fabrics *ACS Appl. Mater. Interfaces* **13** 7054–9
- [58] Tanaka Y *et al* 2012 Evolution of electronic structure upon Cu doping in the topological insulator Bi₂Se₃ *Phys. Rev. B* **85** 125111
- [59] Brahlek M, Koirala N, Salehi M, Bansal N and Oh S 2014 Emergence of decoupled surface transport channels in bulk insulating Bi₂Se₃ thin films *Phys. Rev. Lett.* **113** 026801
- [60] Martin C, Craciun V, Miller K H, Uzakbauly B, Buvaev S, Berger H, Hebard A F and Tanner D B 2013 Bulk Fermi surface and electronic properties of Cu_{0.07}Bi₂Se₃ *Phys. Rev. B* **87** 201201(R)
- [61] Xu Q, Qu S, Ming C, Qiu P, Yao Q, Zhu C, Wei T R, He J, Shi X and Chena L 2020 Conformal organic-inorganic semiconductor composites for flexible thermoelectric *Energy Environ. Sci.* **13** 511–8
- [62] Kumar A, Battabyal M, Chauhan A, Suresh G, Gopalan R, Ravi K N V and Satapathy D K 2019 Charge transport mechanism and thermoelectric behavior in Te:(PEDOT:PSS) polymer composites *Mater. Res. Express* **6** 115302
- [63] Finefrock S W, Zhu X, Sun Y and Wu Y 2015 Flexible prototype thermoelectric devices based on Ag₂Te and PEDOT:PSS coated nylon fiber *Nanoscale* **7** 5598–602
- [64] Jao Y-T, Li Y-C, Xie Y and Lin Z-H 2017 A self-powered temperature sensor based on silver telluride nanowires *ECS J. Solid State Sci. Technol.* **6** N3055–7

Enhanced thermoelectric performance of template based nanostructured polyaniline

Shilpa Maity, Subhra Rakshit, Sukhen Das, and Krishanu Chatterjee

Citation: [AIP Conference Proceedings](#) **1832**, 110053 (2017); doi: 10.1063/1.4980677

View online: <http://dx.doi.org/10.1063/1.4980677>

View Table of Contents: <http://aip.scitation.org/toc/apc/1832/1>

Published by the [American Institute of Physics](#)

Enhanced Thermoelectric Performance Of Template Based Nanostructured Polyaniline

Shilpa Maity¹, Subhra Rakshit², Sukhen Das¹, Krishanu Chatterjee^{2*}

¹Department of Physics, Jadavpur University, Kolkata, India 700032

²Department of Physics, Techno India University, Kolkata, India 700091

*Corresponding Author's Email – itskrishanu@gmail.com

Abstract: Nanostructured polyaniline doped with organic dopant has been synthesized employing a template based in-situ polymerization. Spectral analysis of the sample shows a more ordered structure. The transport properties are carried out for thermoelectric applications which shows that the template based synthesis plays an important role to influence the electrical transport properties of PANI. This template based synthesis of nanostructured PANI is proposed for enhancement of figure of merit through an increase in the electrical conductivity and thermoelectric power and decrease in thermal conductivity. Compared to the earlier works the figure of merit evaluated is much higher.

Keywords: Conducting polymer; Thermoelectric Power; Power Factor; Thermal Conductivity; Figure of Merit.

PACS: 72.80.Le

INTRODUCTION

Conducting polymers (CP), since their discovery, open up a new trend of research. With the advent, these polymers have influenced a vast number of growing new technologies [1–2]. Recently, synthesis of nanopolymer has attracted researchers in the area of thermoelectricity due to their high value of electrical conductivity to thermal conductivity ratio compared to that of inorganic materials [3]. Among the CPs, polyaniline (PANI) is thought to be a potential candidate to be used as thermoelectric (TE) material due to its simple and reversible doping/dedoping chemistry, changeable electrical conductivity, environmental stability and ease of processing [4]. The process of synthesis greatly influences the transport properties of PANI. Till date different technique has been employed for the synthesis and enhancement of transport properties of PANI. Doped nanostructured PANI shows better performance as thermoelectric material due to decrease of the torsional angle suggesting a greater conjugation [4]. In addition the ordering of the molecular backbone chain is an effective way for the enhancement of thermoelectric performance [5]. In this study, PANI has been synthesized employing a template based in-situ polymerization and the template used is mesoporous silica. This template based synthesis is the reason for the ordering of the molecular backbone chain which in turn enhances the power factor at and near room

temperatures. The value of the thermal conductivity is also found to be very low and hence the figure of merit is found to be enhanced.

EXPERIMENTAL

Sulfosalicylic acid (SSA), ammonium peroxydisulfate (APS) and aniline were purchased from Merck Chemicals. Tetraethylorthosilicate (TEOS) was purchased from E-Merck, Germany. Cetyltrimethylammonium bromide (CTAB) and Hydrofluoric acid (HF) were purchased from Loba Chemie, India. Water was purchased from Hydrolab. All the chemicals were of analytical reagent grade and are used without further purification. The mesoporous silica (MCM 48) has been synthesized as reported in literature [6]. PANI is synthesized using template-based oxidative polymerization of aniline in an aqueous solution of SSA, using APS as oxidant and MCM 48 as a template. In a typical procedure aniline was dissolved in an aqueous solution containing SSA and mesoporous silica. The solution was stirred and heated to boiling and then cooled to room temperature. A pre-cooled aqueous solution of APS used as oxidant was mixed drop-wise to start the oxidation, and the reaction mixture was stirred for 6 h. Throughout the reaction time the temperature of the reaction mixture was kept between 0 and 5°C. A dark green precipitate was formed, indicating PANI emeraldine salt, which was recovered from the reaction vessel by filtration.

The precipitate was washed with ethanol and water several times to remove any of the oxidant present, until the filtered water became colourless. It was rinsed with SSA to compensate for the loss of dopant and again washed with water. Finally the prepared sample was vacuum dried at 60 °C for 24 h. The dried sample was immersed in HF solution for 24 hours for the removal of MCM 48 and then filtered. Finally it was again dried at 60 °C for 24 h.

CHARACTERIZATION

The synthesized sample was structurally characterized by powder x-ray diffraction (XRD), fourier transform infrared (FTIR) and UV-Vis spectrum. Morphology of the prepared samples was studied by field emission scanning electron microscopy (FESEM) and transmission electron microscopy (TEM). The prepared sample was pressed at room temperature under 2 tons pressure and cut into small rectangular piece for measurement of the electrical transport properties. The variations of the electrical conductivity (σ) as well as the thermoelectric power (S) with temperature were carried out in the range 290 – 420 K. The electrical conductivity of the sample was measured by four probe method using a four probe set up. For the measurement of thermoelectric power, an auxiliary heater was placed at one end of the sample holder to establish a temperature difference, while the corresponding potential drop was measured by a Hewlett Packard data acquisition system. Room-temperature thermal conductivity (κ) measurements were carried out for the prepared samples using a Hot Disk thermal constants analyser.

RESULTS AND DISCUSSIONS

Fourier transform infrared (FTIR) spectra of the samples are shown in figure 1. Distinct peaks of conducting PANI are observed from the spectra and are indicated in the figure. It is observed that the numbers of benzoid units (1578 cm^{-1}) are more than quinoid one (1494 cm^{-1}) which is a signature of more ordered molecular arrangement of PANI which is also reflected from the electrical and the thermoelectric power results. Inset of figure 1 shows the XRD pattern of nanostructured PANI. The three broad peaks at 15° , 20° , and 25° for pure PANI are observed from the figure, which are due to the repeat unit of PANI chain, the periodic perpendicular to the polymer backbone chain and the periodic parallel to the polymer backbone chain respectively. The observation of peak sharpening is related to the monodistribution of the periodicity of the repeat unit of the PANI chain, and ordering of the molecular arrangement of the PANI chain perpendicular and parallel to the polymer backbone chain respectively.

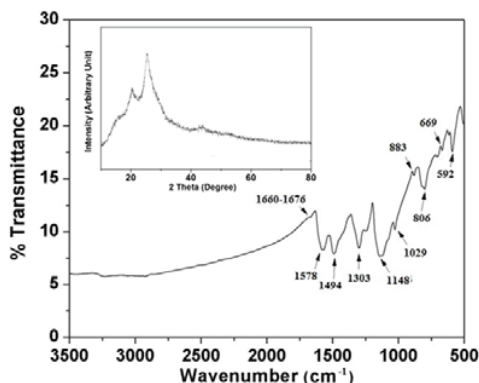


FIGURE 1. FTIR Spectra of the prepared sample. Inset shows the XRD spectra of the prepared sample.

Figure 2 shows the UV-vis spectra of the polymerized sample used to explore the electronic states of PANI which indicates the characteristic bands. The UV-vis spectra of the polymerized sample (inset 1b) shows indicates a greater extent of doping as inferred from the absence of the broad band around 634 nm in the spectrum [7]. This also signifies an ordered molecular arrangement of PANI.

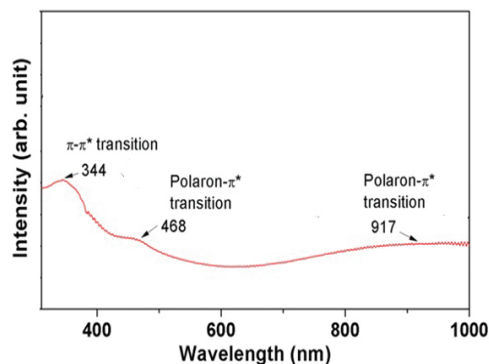


FIGURE 2. UV-Vis spectra of the prepared sample.

Microscopic images of the template based nanostructured PANI are shown in figure 3. The prepared samples show very ordered structure which is in consistent with the XRD and the FTIR analysis. It is noteworthy that this type of ordered structure of polyaniline is reported for the first time. This ordered structure is mainly attributed to the mesoporous silica which gives a directional growth of PANI. The enhancement of electrical conductivity is in tune with this ordered structure. Figure 4 shows the temperature variation of the σ , S and P of the prepared sample. The value of σ decreases with temperature but the decrease is nonlinear. This non-linear variation of the σ with temperature mainly attributed to the metallic

conduction with a tunnelling or hopping mechanism operative for the carrier between the nanorods which are formed during deposition as is seen from the microscopic images. At higher temperatures, predominance of metallic conduction is attributed to the complete delocalization of charge carriers.

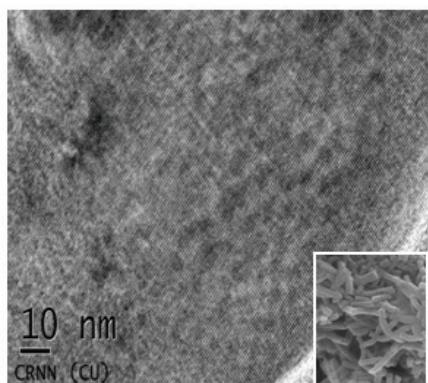


FIGURE 3. TEM image of the prepared sample. Inset shows the FESEM image of the prepared sample.

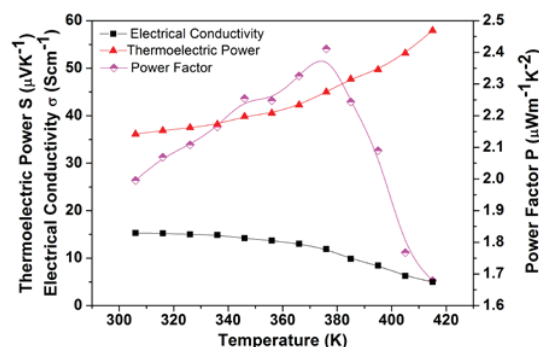


FIGURE 4. Temperature variation of electrical conductivity, thermoelectric power and power factor of the prepared sample.

It is noteworthy that unlike the bulk materials increase of σ does not dominate the increase of the S . This increase in the thermoelectric power is very much surprising. The increase in the grain boundaries due to the template based synthesis probably results in the enhancement of the electron energy filtering effects by allowing high energy carriers to pass while blocking cold energy carriers. Further the ordering of the molecular arrangement increases the effective degree of delocalization and also reduces the π - π interaction conjugated defects in the polymer backbone decreasing the carrier hopping barrier in PANI matrix. The power factor reaches a maximum value of $2.41 (\mu\text{Wm}^{-1}\text{K}^{-1})$ at 376 K and then it starts decreasing.

The value of κ at room temperature is $0.1009 \text{ Wm}^{-1}\text{K}^{-1}$, which is lower than recently reported values for polymer based thermoelectric materials. This low value of κ is attributed to the selective scattering of phonons by the nanointerfaces of PANI. The ZT value as evaluated in this work comes out to be 0.0061. Interestingly, this value though lower than inorganic TE materials, it still higher than that of the polymer based bulk nanostructured TE materials. To the best of our knowledge the figure of merit (ZT) value evaluated for PANI 2 is more than the all other reported value in literature. This may be attributed to the ordered molecular arrangement as has been perceived from the TEM images and confirmed from the FTIR data.

CONCLUSION

To the best of author's knowledge template based nanostructured PANI has been synthesised for the first time. spectral analysis shows formation of an ordered structure which is in tune with the microscopic images. Consequently, there is a reduction in the π - π conjugation defect in the backbone of PANI chain. Interestingly the structural and spectral studies confirms each other. As a result of this structural ordering the electrical conductivity and thermoelectric power increases. Due to the scattering of phonons the value of thermal conductivity is found to be very low. The ZT value comes out to be 0.0061, which is among the best for polymer based thermoelectric materials. Thus the template based synthesis is an effective way for ordering the molecular structure of PANI which in turn enhance the transport parameters.

ACKNOWLEDGEMENT

The authors gratefully acknowledge the Department of Science and Technology, India for financial support.

REFERENCES

1. B.J.Feldman, P. Burgmayer and R.W. Marray. *J. Am. Chem. Soc.* **107**, 872 (1985)
2. J.Gao, J.M.Sansiena, and H.L.Wang, *Synth. Met.* **135**, 809 (2003).
3. K.Chatterjee, A.Suresh, S.Ganguly, K.Kargupta and D.Banerjee, *Mater. Charac.* **60**, 1597 (2009).
4. K.Chatterjee, M.Mitra, S.Ganguly, K.Kargupta and D.Banerjee, *J Appl. Polym. Sci.* 39920 (2013).
5. Q.Yao, L.Chen, W.Zhang, S.Liufu and X.Chen, *ACS Nano*, **4**, 2445 (2010.)
6. B.Boote, H.Subramanian and K.T. Ranjit, *Chem. Commun.*, 4543 (2007).
7. F.Yakuphanoglu, and B.F. Şuenkal, *J. Phys. Chem. C*, **111**, 1840 (2007).

SEMINAR ATTENDED



The Indian Science Congress Association

14, Dr. Biresh Guha Street,
Kolkata – 700 017


Paper Presentation Certificate

This is to certify that Prof./Dr./Shri/Smt. Shilpa Maity
.....of..... Techno India University.
has presented a Paper (Oral/Poster) entitled..... Synthesis of Zinc Incorporated
..... Polyaniline – rGO Nano....in the Section of.....
.....“MATERIAL SCIENCE”.....during
the 103rd Indian Science Congress held at University of Mysore, Mysuru from
January 3 to 7, 2016.

His/Her Membership Number is..... SLM 3012.....

Date..... 05-01-2016.....

Office Seal


Sectional President
(Signature)



7th Vidyasagar - Satyendranath Bose National Workshop 2016

on

Theory and Application of Advanced Materials (TAAM 2016)



Organized by

Department of Physics & Technophysics, Vidyasagar University, Midnapore
(UGC SAP & DST FIST Sponsored Department)

Sponsored by

Theoretical Physics Seminar Circuit of SNBNCBS, Kolkata,
DST & UGC, New Delhi

This is to certify that ...*Shilpa Maity*.....
of ...*Dept. of Physics, Jadavpur University*.....
has participated / presented a paper entitled...*Template based synthesis of Polyaniline....*
...*and its enhanced thermoelectric performance*..... in the 7th Vidyasagar
- Satyendranath Bose National Workshop 2016 on Theory and Application of Advanced Materials
(TAAM 2016)' held at Vidyasagar University, Midnapore, W.B. during March 15-17, 2016.

Prof. Radha Raman Pal
Convener, TAAM 2016 & HOD
Dept. of Physics and Technophysics
VU, Midnapore

Prof. B.C. Patra
Dean, Faculty of Science
VU, Midnapore





Recent Trend in Composite Material 2016

Technical Education Quality Improvement Programme - II (TEQIP - II)

Sponsored One Day Seminar - August 18, 2016

Mechanical Engineering Department, Jadavpur University, Kolkata

This is to certify that SHILPA MAITY

Participated / ~~Presented Paper~~ / ~~Delivered~~ Invited Talk in the Seminar of
RECENT TREND IN COMPOSITE MATEIRAL on **18th August, 2016** in the
Machanical Engineering Department under TEQIP - JU program.

Sebanik Ray

Co-ordinator

Dr. Shilpa Maity

Nodal Officer, R&D
TEQIP II - JU

Sybil

Co-ordinator, TEQIP II - JU



आत्मदीपो भव

UGC SPONSORED NATIONAL SEMINAR ON



FRONTIERS IN MODERN PHYSICS

21 & 22 November, 2016

Organised by
DEPARTMENT OF PHYSICS JOGAMAYA DEVI COLLEGE
92, Shyamaprasad Mukherjee Road, Kolkata-700 026

In Collaboration with
Centre for Interdisciplinary Research and Education
404B, Jodhpur Park, Kolkata-700 068

Certified that SM. SHILPA MAITY.....of

JADAVPUR UNIVERSITY.....

has participated / presented a paper the seminar.

Ballari Chakrabarti 22/11/16

BALLARI CHAKRABARTI / RUMA BASU

Convenors

Suchismita Bandyopadhyay 22.11.16

Principal / Teacher-in-charge

International Conference on
EMERGING TRENDS IN CHEMICAL SCIENCES (ETCS-2018)



DEPARTMENT OF CHEMISTRY, DIBRUGARH UNIVERSITY
Dibrugarh, Assam, India.



Shilpa Maity

This is to certify that Prof./Dr./Mr./Ms.....
of.....**Jadavpur University**.....attended/presented research paper

(Invited lecture/Oral/Poster) in the International Conference "Emerging Trends in
Chemical Sciences" held during 26 -28 February, 2018.

(P. Das)
Convener

(S. Konwer)
Co-Convener

(A. Baruah)
Co-Convener

61st DAE Solid State Physics Symposium

*Sponsored by Board of Research in Nuclear Sciences
Department of Atomic Energy, Government of India*

Certificate of Participation

This is to certify that

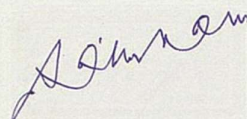
Shilpa Maity

of

Jadavpur University, Kolkata

*has presented a paper and participated in this symposium
held in KIIT University, Bhubaneswar*

between 26 and 30 December, 2016



REG-514

Dated: 30 December 2016

Prof. Saibal Basu

Convener, DAE SSPS 2016 &
Head, Solid State Physics Division
Bhabha Atomic Research Centre, Mumbai

AWARDS AND ACHIEVEMENTS



**Association of Indian Universities, New Delhi
&
Central University of Jharkhand, Ranchi
ANVESHAN - 2018**



Student Research Convention (Eastern Zone)

Certificate

This is to certify that Mr/Ms/Dr Shelpha Maity
S/o / Daughter of Shri Susanta Kumar Maity enrolled in Ph.D
Department / Faculty of Physics of
Jadavpur University / Institute participated in
Eastern Zone Student Research Convention held at Central University of Jharkhand, Ranchi during February 18-19, 2019.
His / Her Proposal / project entitled Natural Plant Resin Gum - - for the Nature
under the category of Basic Sciences and secured First position.


Dr. Amarendra Pani

Joint Director & Head Research
Association of Indian Universities, , New Delhi


Dr. Ajai Singh

Zonal Co-ordinator
Central University of Jharkhand


Prof. Nand Kr. Yadav 'Indu'

Vice-Chancellor
Central University of Jharkhand



ANVESHAN

National Student Research Convention

March 12-14, 2019

Certificate

This is to Certify that Mr / Ms / Dr. Shilpa Maity

affiliated with Jadavpur University, Kolkata


_____ participated in **Anveshan: National Student Research Convention** organized by **Association of Indian Universities, New Delhi** and hosted by **Ganpat University, Gujarat** during March 12-14, 2019.

His/Her research project titled Natural plant resin gum acacia based multifunctional nano- device for heavy metal detection and remediation: "From the nature, for the nature"

_____ under the category of **Basic Sciences** has won **SECOND PRIZE**.


Dr. Amarendra Pani
Chief Convener

Director(I/c), Research
Association of Indian Universities, New Delhi


Dr. Satyen Parikh
Anveshan Coordinator
Dean, Faculty of Computer Applications
Ganpat University


Dr. Mahendra Sharma
Director General
Ganpat University

